1 May 2009 | $10

Science

MESSENGER's
Second Mercury Flyby

AAAS

Gene expression and function analysis sample and assay technologies by QIAGEN

Enjoy first-time success

Rely on QIAGEN's manual and automated workflow solutions for:

- **Sample collection and disruption**
- **RNA stabilization and purification**
- **Real-time PCR and RT-PCR and gene expression assays**
- **RNAi and gene silencing**
- **miRNA purification and assays**
- **Methylation analysis in epigenetics research**
- **Protein sample preparation and assays**

Making improvements in life possible — www.qiagen.com

QIAGEN®

Sample & Assay Technologies

GEPart03095 1 WW

Part of IBC's
Drug Discovery & Development Week

August 3-5, 2009
World Trade Center Boston/Seaport Hotel
Boston, MA USA

The Next Wave of Antibody Therapeutics

Practical Strategies Generating Exciting Preclinical and Clinical Results

focus on

- Antibody-Drug Conjugates
- Improving Potency and Efficacy
- Combinations of Antibody Drugs
- Bi/Multi-Specific Antibody Drugs
- Pharmacodynamic Biomarkers of Antibodies

Conference Keynote

Quantitative Prediction of Anti-tumor Antibody Macro and Microdistribution

K. Dane Wittrup, Ph.D.
J.R. Mares Professor of Chemical Engineering and Bioengineering
Massachusetts Institute of Technology

Post-Conference Workshop

Understanding and Exploiting the Role of Cancer Stem Cells in Drug Development

- Anti-DLL4 antibody and Notch signaling
- Biologic targeting IL-3R
- Novel target Mab for solid tumors
- Wnt and Hedgehog pathways

Plenary Keynote

Global Pharma Innovator: Daiichi Sankyo's Challenge to Build a Competitive Pharmaceutical Company in the Global Market

Takashi Shoda
President and CEO
Daiichi Sankyo Co., Ltd., *Japan*

Organized by
ibc Life Sciences
an informa business

www.drugdisc.com/Antibody

Register Today
Use Priority Code
D9201ASA

Biacore systems

from inspiration ...to publication

Highest quality, information-rich interaction data from Biacore™ systems deepen your understanding of molecular mechanisms and interaction pathways and enable you to add function to structure.

Select the perfect solution for your application and draw conclusions with confidence – from the company that continues to set the standard for label-free protein interaction analysis.

For further information or register to have one of our scientific experts contact you, please visit **www.gelifesciences.com/biacore-science**

Biacore T100
unmatched performance

Biacore X100
ready to run research system

Biacore Flexchip
array-based comparative profiling

imagination at work

© 2009 General Electric Company – All rights reserved.
GE Healthcare Biacore AB, a General Electric Company.

EDITORIAL

567 Science in the White House
John P. Holdren

NEWS OF THE WEEK

572 As Swine Flu Circles Globe, Scientists Grapple With Basic Questions

574 Hundreds Gather for Rally to Defend Animal Research

575 Africans' Deep Genetic Roots Reveal Their Evolutionary Story
>> Science *Express Research Article by S. A. Tishkoff* et al.

576 Obama Courts a Smitten Audience at the National Academy

576 Study Changes Cosmic Ray–Climate Link

577 From *Science*'s Online Daily News Site

578 'Protein' in 80-Million-Year-Old Fossil Bolsters Controversial *T. rex* Claim
>> *Report p. 626*

579 IOM Panel Backs Public Disclosure of Drug Company Payments

579 From the *Science* Policy Blog

NEWS FOCUS

ORIGINS
580 On the Origin of the Immune System
>> Science *Podcast*

583 Newsmaker Interview: Defying Skeptics, Richard Scheller Thinks Genentech Will Thrive

584 Herschel Will Open a New Vista on Infant Stars and Galaxies …

584 … While Planck Dusts the Skies for the Fingerprints of Inflation

587 Corn-Based Ethanol Flunks Key Test

588 American Association of Physical Anthropologists Meeting
Civilization's Cost: The Decline and Fall of Human Health
Of Tools and Tubers
Reproductive Fate Versus Environment

LETTERS

590 Iraq Study Failed Replication Test
M. Spagat
Iraq Study Response Lacks Objectivity
F. Checchi
Confronting Racism
A. J. M. Dijker
Response
K. Kawakami et al.

592 CORRECTIONS AND CLARIFICATIONS

BOOKS *ET AL.*

593 Blue Gold: World Water Wars
S. Bozzo, Director
Legacy of the Great Aletsch
N. Brandestini and S. Ellington, Directors
Onze Kost [Our Coast]
I. van Ditshuyzen, Director

POLICY FORUM

594 Reducing the Risks of the Wildlife Trade
K. F. Smith et al.

PERSPECTIVES

596 Alexander von Humboldt and the General Physics of the Earth
S. T. Jackson

597 Magnetic Twisters on Mercury
K.-H. Glassmeier
>> *Reports pp. 606 and 610*

598 A Circadian Loop asSIRTs Itself
H. Wijnen
>> *Reports pp. 651 and 654*

599 The Geographic Footprint of Glacier Change
G. Balco
>> *Report p. 622*

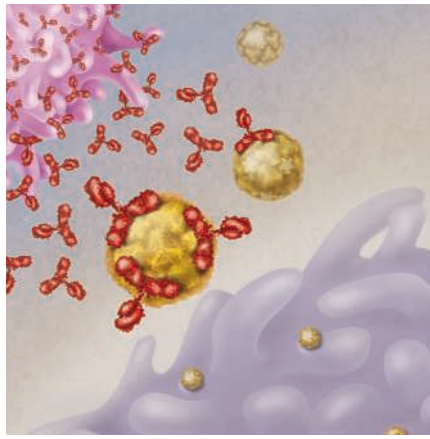

page 580

page 593

601 A Glassy State of Supersolid Helium
J. Saunders
>> *Reports pp. 631 and 632*

602 Complicated Supercomplexes
D. M. Livingston

603 Avoiding Unintended Toxicity
T. E. Golde and T. L. Kukar
>> *Report p. 639*

CONTENTS continued >>

COVER

A mosaic of images collected as the MESSENGER spacecraft viewed Mercury obliquely on approach on 6 October 2008. The Rembrandt impact basin, 715 kilometers in diameter, is seen at the center as night falls across its eastern edge. Results from the flyby are discussed in four Reports beginning on page 606 and a Perspective on page 597.

Image: NASA/Johns Hopkins University Applied Physics Laboratory/Arizona State University/Carnegie Institution of Washington

DEPARTMENTS

565 This Week in *Science*
568 Editors' Choice
570 *Science* Staff
571 Random Samples
663 New Products
664 *Science* Careers

Published by AAAS

BREVIA

605 Neural Mechanisms of a Genome-Wide Supported Psychosis Variant
C. Esslinger et al.
A genetic polymorphism associated with schizophrenia conveys a risk for abnormal connectivity between brain regions.

REPORTS

606 MESSENGER Observations of Magnetic Reconnection in Mercury's Magnetosphere
J. A. Slavin et al.
Mercury's magnetosphere responds more strongly to the influence of the Sun's magnetic field than does Earth's magnetosphere.
>> *Perspective p. 597*

610 MESSENGER Observations of Mercury's Exosphere: Detection of Magnesium and Distribution of Constituents
W. E. McClintock et al.
High-resolution observations of Mercury's exosphere reveal different spatial distributions of magnesium, calcium, and sodium.
>> *Perspective p. 597*

613 The Evolution of Mercury's Crust: A Global Perspective from MESSENGER
B. W. Denevi et al.
Data from the Mariner 10 and MESSENGER flybys imply that a substantial fraction of Mercury's surface is volcanic in origin.

618 Evolution of the Rembrandt Impact Basin on Mercury
T. R. Watters et al.
This basin, showing a unique pattern of radial and concentric tectonic features, represents an intermediate stage of filling by volcanic plains.

622 High-Frequency Holocene Glacier Fluctuations in New Zealand Differ from the Northern Signature
J. M. Schaefer et al.
The patterns of glacial advances and retreats in New Zealand during the Holocene contrast markedly with those of the Northern Hemisphere.
>> *Perspective p. 599*

626 Biomolecular Characterization and Protein Sequences of the Campanian Hadrosaur *B. canadensis*
M. H. Schweitzer et al.
Analysis of well-preserved tissues from an 80-million-year-old hadrosaur support the dinosaur-bird relationship.
>> *News story p. 578*

631 A Gross-Pitaevskii Treatment for Supersolid Helium
P. W. Anderson

632 Evidence for a Superglass State in Solid ^{4}He
B. Hunt et al.
A new theoretical argument and a study of the temperature-dependent relaxation dynamics of helium show that defects may play an important role in describing its supersolid behavior.
>> *Perspective p. 601*

636 Competition for Light Causes Plant Biodiversity Loss After Eutrophication
Y. Hautier et al.
A few species take advantage of fertilizer to grow fast, shade out competitors, and reduce the number of species in grassland.

639 γ-Secretase Heterogeneity in the Aph1 Subunit: Relevance for Alzheimer's Disease
L. Serneels et al.
Targeted knockout of only part of the γ-secretase complex lessens toxicity and still improves disease phenotypes.
>> *Perspective p. 603*

643 Burst Spiking of a Single Cortical Neuron Modifies Global Brain State
C. T. Li et al.
Stimulation of a single nerve cell triggers a switch between slow wave and rapid eye movement sleep.

646 Self-Control in Decision-Making Involves Modulation of the vmPFC Valuation System
T. A. Hare et al.
The neural circuitry underlying choice and self-control is revealed by modeling and brain imaging.

649 Exchange of Genetic Material Between Cells in Plant Tissue Grafts
S. Stegemann and R. Bock
Plant genes can transfer between cells and across graft junctions, possibly explaining horizontal gene transfer.

651 Circadian Clock Feedback Cycle Through NAMPT-Mediated NAD$^+$ Biosynthesis
K. M. Ramsey et al.

654 Circadian Control of the NAD$^+$ Salvage Pathway by CLOCK-SIRT1
Y. Nakahata et al.
A transcriptional-enzymatic feedback loop controls interactions between metabolism and circadian rhythms in mouse cells.
>> *Perspective p. 598*

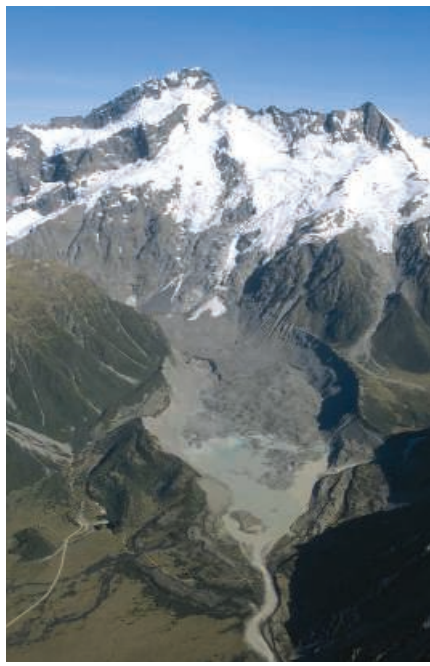

page 599 & 622

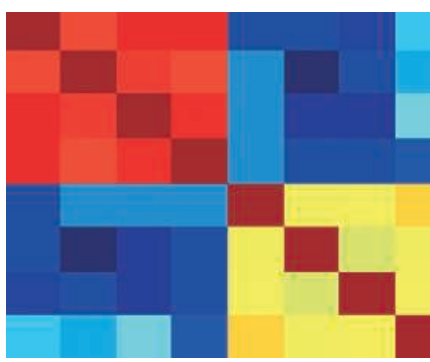

page 659

657 A Cytidine Deaminase Edits C to U in Transfer RNAs in Archaea
L. Randau et al.
A nonconventional cytosine is edited out to allow a functional transfer RNA structure to form.

659 A Yeast Hybrid Provides Insight into the Evolution of Gene Expression Regulation
I. Tirosh et al.
Gene expression between species of yeast may diverge, but recombination rewires their offspring into vigorous hybrids.

Published by AAAS

SCIENCEONLINE

SCIENCEXPRESS
www.sciencexpress.org

The Genetic Structure and History of Africans and African Americans
S. A. Tishkoff et al.

A genetic study illuminates population history, as well as the relationships among and the origin of major language families.
10.1126/science.1172257
>> *News story p. 575;* Science *Podcast*

Abscisic Acid Inhibits Type 2C Protein Phosphatases via the PYR/PYL Family of START Proteins
S.-Y. Park et al.
10.1126/science.1173041

Regulators of PP2C Phosphatase Activity Function as Abscisic Acid Sensors
Y. Ma et al.

Links between two ancient multimember protein families signal responses to the plant hormone abscisic acid.
10.1126/science.1172408

Dispersion of the Excitations of Fractional Quantum Hall States
I. V. Kukushkin et al.

The dispersion of excitations in a buried two-dimensional electron system can now be probed.
10.1126/science.1171472

Superconductivity at the Two-Dimensional Limit
S. Qin et al.

Superconductivity persists in lead films down to just two monolayers thick.
10.1126/science.1170775

SCIENCENOW
www.sciencenow.org
Highlights From Our Daily News Coverage

China Falls Short on Olympic Cleanup
Attempt to control emissions did little to curb pollution, study finds.

Presto, Instant Sunglasses!
A lightning-fast chemical provides glare protection in a split second.

Artificial Blood Vessels Prove Effective
Tubes made from a patient's own cells show promise for kidney dialysis.

SCIENCESIGNALING
www.sciencesignaling.org
The Signal Transduction Knowledge Environment

EDITORIAL GUIDE: Omic Empiricism
D. B. Searls

Omics researchers might do well to consider the duality between empiricism and rationalism.

RESEARCH ARTICLE: $G\alpha_{i1}$ and $G\alpha_{i3}$ Are Required for Epidermal Growth Factor–Mediated Activation of the Akt-mTORC1 Pathway
C. Cao et al.

Two members of the $G\alpha_i$ family of G proteins form complexes with EGFR and the adaptor protein Gab1 to mediate activation of Akt.

RESEARCH ARTICLE: Ligand Binding to LRP1 Transactivates Trk Receptors by a Src Family Kinase–Dependent Pathway
Y. Shi et al.

Trk receptor–mediated neurite outgrowth is triggered by distinct ligands that activate LRP1.

RESEARCH ARTICLE: Neurotransmitters Drive Combinatorial Multistate Postsynaptic Density Networks
M. P. Coba et al.

Analysis of protein phosphorylation patterns provides insight into the organization of molecular networks at the postsynaptic density.

PERSPECTIVE: Nontraditional Signaling Mechanisms of Lipoprotein Receptors
G. W. Rebeck

Lipoprotein receptors can trigger calcium-dependent kinase activation, gene transcription, or TrkA receptor–dependent signaling.

REVIEW: Signaling by Gasotransmitters
A. K. Mustafa et al.

Nitric oxide, carbon monoxide, and hydrogen sulfide act as messengers in the cardiovascular, immune, and nervous systems.

PRESENTATION: Mechanobiology of the Skeleton
C. H. Turner et al.

Mechanical force induces osteogenesis by repressing the production of sclerostin, an inhibitor of Wnt signaling.

SCIENCECAREERS
www.sciencecareers.org/career_magazine
Free Career Resources for Scientists

Taken for Granted: The Burning Question of Lab Safety
B. L. Benderly

After the death of a lab worker, experts warn that many academic labs are unsafe.

For Med Students, Research Training Opportunities Abound
L. S. Chiu

Specialized programs, plus adding research to the curriculum, give medical students a taste of research.

A Chemistry Career on the Fast Track
E. Pain

Romanian chemist Mihail Barboiu keeps several projects going at several institutions.

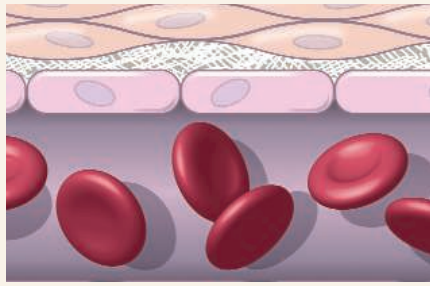

SCIENCESIGNALING
Gasotransmitters elicit vasorelaxation.

SCIENCECAREERS
Safety in academic labs.

SCIENCEPODCAST
www.sciencemag.org/multimedia/podcast
Free Weekly Show

Download the 1 May *Science* Podcast to hear about the evolutionary history of Africans and African Americans, the origins of the immune system, and more.

ORIGINSBLOG
blogs.sciencemag.org/origins
A History of Beginnings

SCIENCEINSIDER
blogs.sciencemag.org/scienceinsider
Science Policy News and Analysis

SCIENCE (ISSN 0036-8075) is published weekly on Friday, except the last week in December, by the American Association for the Advancement of Science, 1200 New York Avenue, NW, Washington, DC 20005. Periodicals Mail postage (publication No. 484460) paid at Washington, DC, and additional mailing offices. Copyright © 2009 by the American Association for the Advancement of Science. The title SCIENCE is a registered trademark of the AAAS. Domestic individual membership and subscription (51 issues): $146 ($74 allocated to subscription). Domestic institutional subscription (51 issues): $835; Foreign postage extra: Mexico, Caribbean (surface mail) $55; other countries (air assist delivery) $85. First class, airmail, student, and emeritus rates on request. Canadian rates with GST available upon request, GST #1254 88122. Publications Mail Agreement Number 1069624. **Printed in the U.S.A.**

Change of address: Allow 4 weeks, giving old and new addresses and 8-digit account number. **Postmaster:** Send change of address to AAAS, P.O. Box 96178, Washington, DC 20090–6178. **Single-copy sales:** $10.00 current issue, $15.00 back issue prepaid includes surface postage; bulk rates on request. **Authorization to photocopy** material for internal or personal use under circumstances not falling within the fair use provisions of the Copyright Act is granted by AAAS to libraries and other users registered with the Copyright Clearance Center (CCC) Transactional Reporting Service, provided that $20.00 per article is paid directly to CCC, 222 Rosewood Drive, Danvers, MA 01923. The identification code for *Science* is 0036-8075. *Science* is indexed in the *Reader's Guide to Periodical Literature* and in several specialized indexes.

AAAS
ADVANCING SCIENCE, SERVING SOCIETY

CREDITS: (*SCIENCE CAREERS*) PHOTODISC; (*SCIENCE SIGNALING*) CHRIS BICKEL

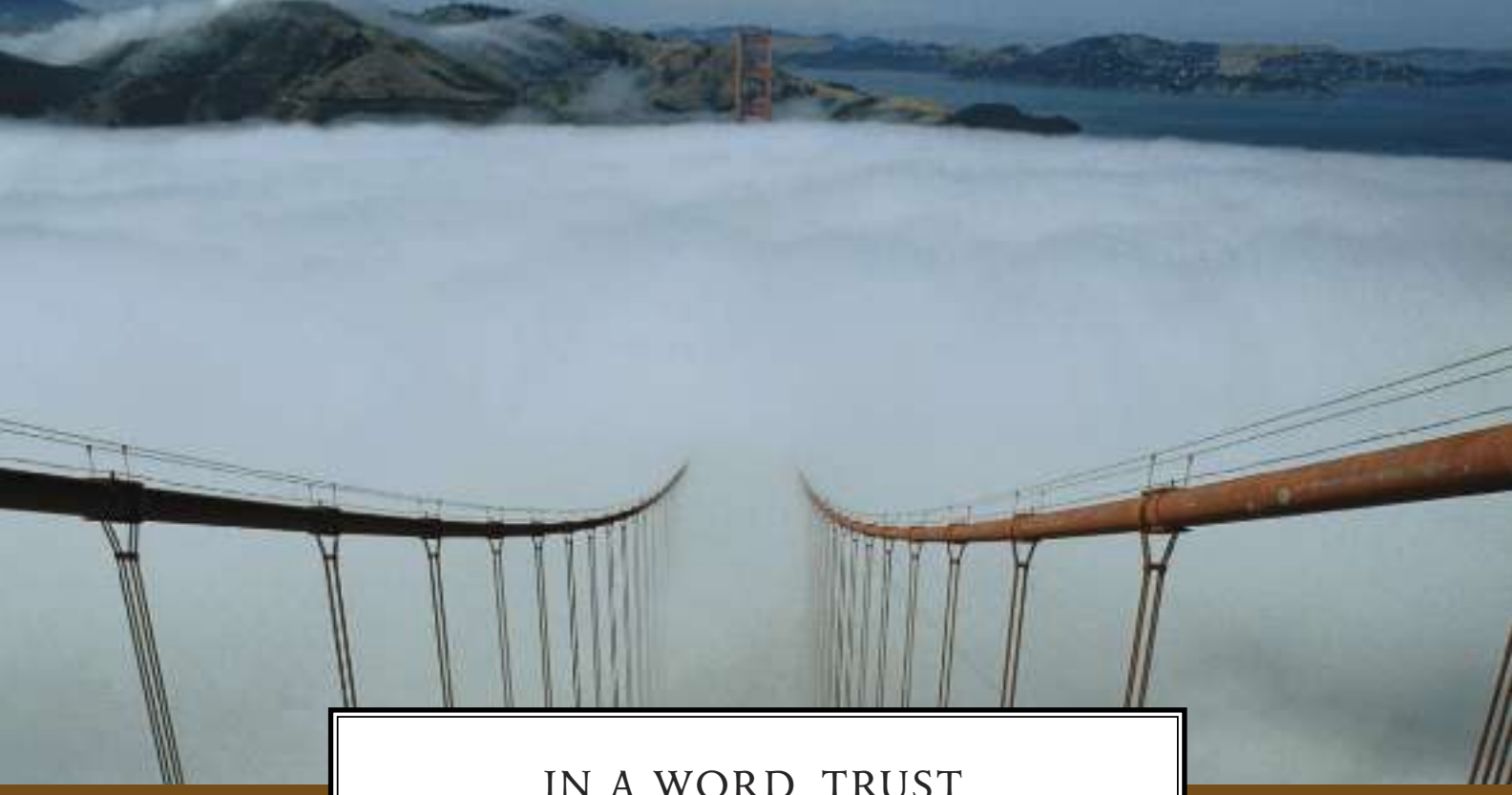

IN A WORD, TRUST.

T4 DNA Ligase

New England Biolabs is dedicated to providing our customers with guaranteed enzyme performance. Our recombinant T4 DNA Ligase is the most extensively used ligase for cloning experiments and other applications, including sample preparation and next generation sequencing. It is available at exceptional value, and an even greater value when purchased in large quantities for high throughput technologies. For cohesive, blunt, simple or complex reactions, make T4 DNA Ligase from NEB your first choice.

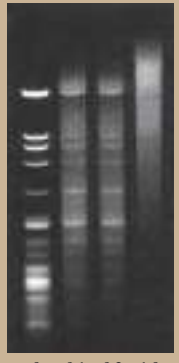

Ligation of blunt-ended HaeIII fragments of Lambda DNA using various amounts of T4 DNA Ligase (400,000 cohesive end units/ml) in a 20 µl reaction volume. Reactions were incubated for 30 minutes at 16°C.

Ligation of HindIII fragments (4-base overhang) of Lambda DNA using 1 cohesive end unit (1µl of 1:400 dilution) of T4 DNA Ligase. Reactions were incubated at 25°C.

Advantages:

Quality - Highly pure enzyme with no lot-to-lot variation

Convenience - Choose original T4 DNA Ligase or the Quick Ligation Kit to meet the demands of a variety of reaction conditions

Flexibility - Active at room temperature or 16°C; reaction times run from 5 minutes to overnight

Robustness - Active in a variety of reaction buffers

T4 DNA Ligase* RR
Regular Concentration **M0202S/L**
For standard cloning reactions

High Concentration **M0202T/M**
For large or difficult constructs

Quick Ligation™ Kit* RR **M2200S/L**
For ligation of cohesive or blunt-end DNA fragments in 5 minutes at room temperature

RR = Recombinant
*NEB ligase products are BSA-free

For more information regarding customization and OEM opportunities, please contact **oem@neb.com**

New England Biolabs, Inc. is an ISO 9001 certified company

NEW ENGLAND BioLabs® Inc.
enabling technologies in the life sciences

EDITED BY STELLA HURTLEY

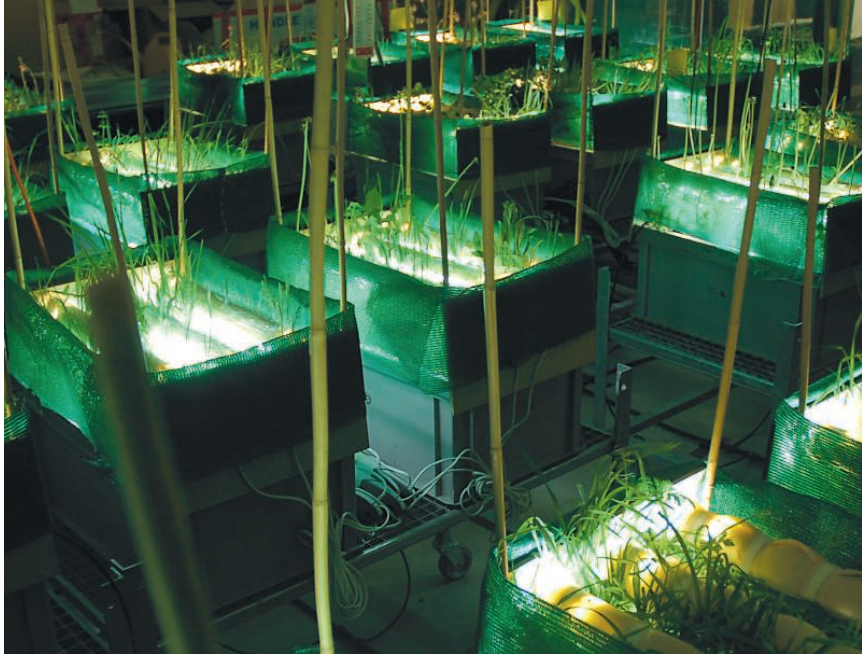

<< Shedding Light on a Problem

Human activities—mainly the application of fertilizers to farmland—have increased the availability of nutrients in terrestrial and aquatic ecosystems. In grasslands, nutrient enrichment reduces plant species diversity, but the mechanisms underlying this loss of biodiversity remain unclear. **Hautier *et al.*** (p. 636) use an experimental manipulation, addition of supplementary light to the grassland understory, which supports the idea that competition for light is the major mechanism of plant diversity loss.

MESSENGER from Mercury

The spacecraft MESSENGER passed by Mercury in October 2008, in what was the second of three flybys before it settles into the planet's orbit in 2011. Another spacecraft visited Mercury in the mid-1970s, which mapped 45% of the planet's surface. Now, after MESSENGER, only 10% of Mercury's surface remains to be imaged up close. **Denevi *et al.*** (p. 613) use this near-global data to look at the mechanisms that shaped Mercury's crust, which likely formed by eruption of magmas of different compositions over a long period of time. Like the Moon, Mercury's surface is dotted with impact craters. **Watters *et al.*** (p. 618) describe a well-preserved impact basin, Rembrandt, which is second in size to the largest known basin, Caloris. Unlike Caloris, Rembrandt is not completely filled by material of volcanic origin, preserving clues to its formation and evolution. It displays unique patterns of tectonic deformation, some of which result from Mercury's contraction as its interior cooled over time. Mercury's exosphere and magnetosphere were also observed (see the Perspective by **Glassmeier**). Magnetic reconnection is a process whereby the interplanetary magnetic field lines join the magnetospheric field lines and transfer energy from the solar wind into the magnetosphere. **Slavin *et al.*** (p. 606) report observations of intense magnetic reconnection 10 times as intense as that of Earth. **McClintock *et al.*** (p. 610) describe simultaneous, high-resolution measurements of Mg, Ca, and Na in Mercury's exosphere, which may shed light on the processes that create and maintain the exosphere.

Vive La Différence

How closely do climate changes in the Northern and Southern Hemispheres resemble each other? Much discussion has concentrated on the Holocene, the warm period of the past 11,500 years in which we now live, which represents a baseline to which contemporary climate change can be compared. **Schaefer *et al.*** (p. 622; see the Perspective by **Balco**) present a chronology of glacial movement over the last 7000 years in New Zealand, which they compare to similar records from the Northern Hemisphere. Clear differences are observed between the histories of glaciers in the opposing hemispheres, which may be owing to regional controls. Thus, neither of two popular arguments—that the hemispheres change in-phase or that they change in an anti-phased manner—appear to be correct.

The Birds and the Dinosaurs

The extent to which primary tissues are preserved in ancient fossils remains controversial. **Schweitzer *et al.*** (p. 626; see the news story by **Service**) describe well-preserved tissues and primary collagen sequences from the femur of an 80-million-year-old hadrosaur. The fossil preserved structures resembling primary bone tissues and vessels. Both extracts and tissue pieces were analyzed in multiple laboratories by mass spectrometry, which revealed ancient collagen sequences that support a close relation between birds and dinosaurs.

Glasslike Supersolid

Recent experiments with solid helium confined to the ring of a torsional oscillator at extremely low temperatures have been interpreted in terms of an exotic supersolid phase—a crystalline solid that somehow flows like a superfluid. However, behavioral differences between samples have raised many questions (see the Perspective by **Saunders**). **Hunt *et al.*** (p. 632) present a comprehensive study of the relaxation dynamics of the torsional oscillator system as a function of time and temperature. The data provides evidence for a "supersolid glass," where glassy behavior of crystal dislocations and superfluidity can coexist. In a separate theoretical study, **Anderson** (p. 631) argues that supersolidity ought to be a ground state for all bose solids, but that defects in the sample may mask the supersolid signature.

Tactical Target

Intramembrane proteolysis by the γ-secretase complex is important during development and in the pathology of Alzheimer's disease. γ-Secretase has usually been considered as a homogeneous activity. **Serneels *et al.*** (p. 639, published online 19 March; see the Perspective by **Golde and Kukar**) now show that the Aph1B component of the γ-secretase complex is responsible for the generation of long β-amyloid species involved in Alzheimer's disease. In a mouse model of Alzheimer's disease, full knockout of Aph1B improved disease phenotypes, without the sort of toxicity previously observed when targeting γ-secretase more generally.

Single-Cell Brain Switching

Different behavioral states of an animal are characterized by distinct patterns of global brain activity. For example, slow-wave sleep is associated with membrane potential transitions in cortical neurons and high-amplitude, low-frequency

Continued on page 566

CREDITS (TOP TO BOTTOM): YANN HAUTIER; MARY HIGBY SCHWEITZER (NCSU, MEAS) AND ZHIYONG SUO (MSU, ICAL)

Published by AAAS

Coming Fourth Quarter 2009

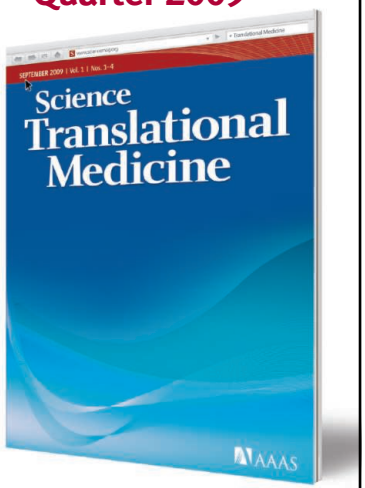

Integrating medicine and science

AAAS, publisher of the world's leading general science journal, *Science*, is launching the new weekly journal, *Science Translational Medicine*, in the fourth quarter of 2009.

The journal's mission is to facilitate communication and cooperation among basic and preclinical researchers, physician scientists, regulators, policy makers, industry, and funding agencies in order to improve health around the world. It will present original, science-based peer-reviewed research that successfully moves the field closer to helping patients. Perspectives and reviews from basic and clinical viewpoints along with discussions about research funding and regulatory issues will be included.

With *Science Translational Medicine*, you can expect the same level of breakthrough research that is the hallmark of the journal *Science*. The journal is edited by Katrina L. Kelner, Ph.D. Elias A. Zerhouni, M.D., heads an international advisory group of clinician scientists and other experts.

The editors are now accepting manuscripts. Be one of the first to be considered for publication in the inaugural issue! **www.sciencemag.org/marketing/stm/papers.dtl**

For information contact the editors at **scitranslmededitors@aaas.org** For information on site licenses and subscriptions to print, please contact **sciencemedicine@aaas.org**.

Science Translational Medicine AAAS

www.ScienceTranslationalMedicine.org

Continued from page 565

local field potential and electroencephalogram signals. In contrast, during rapid–eye-movement sleep and wakefulness, low-amplitude, high-frequency cortical activity dominates with neuronal membrane potentials fluctuating around a depolarized level. **Li *et al.*** (p. 643) asked whether action potentials in a single neuron can change global network activity. In a series of in vivo single-cell stimulation experiments, using intracellular stimulation via a whole-cell patch pipette, a brief episode of intracellular stimulation switched brain states.

Dieter's Dilemma

The ability to exercise self-control is central to human success and well-being. However, little is known about the neurobiological underpinnings of self-control and how or why these neural mechanisms might differ between successful and unsuccessful decision-makers. **Hare *et al.*** (p. 646) used brain imaging in a dieting population undergoing real-life decisions between a healthy or a tempting, yet nutritionally inferior, choice of food. Activity in the ventromedial prefrontal cortex correlated with the value of the stimulus, termed goal value. Importantly, this activity integrated both health and taste values in individuals who were able to exert self-control in their choices, while reflecting only taste in those unable to exert self-control.

Hard Graft

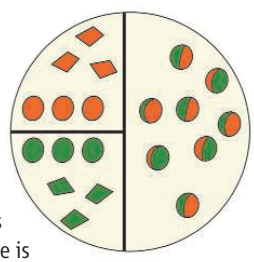

In plants, it is not clear whether heritable changes can be induced by tissue grafting—for example, when one plant is grafted onto a different root stock. **Stegemann and Bock** (p. 649) now show that genetic material is transferred between plants across graft junctions. This suggests that eukaryotic cells can indeed exchange genetic information, and in this way, grafting allows genes to cross species barriers. Although the exchange is limited to the site around the graft, the finding blurs the boundary between natural gene transfer and genetic engineering techniques and suggests that natural grafting may serve as a mechanism of horizontal gene transfer during evolution.

Circadian Oscillations

The 24-hour day-night cycle plays an important role in mammalian physiology and behavior and, as most travelers are well aware, there is an intimate link between our in-built circadian clocks and metabolic rhythms. This link is in part forged by the protein deacetylase SIRT1, which regulates the clock's molecular circuitry. SIRT1 uses as a cofactor the cellular metabolite NAD^+, which is synthesized through a salvage pathway that includes the enzyme nicotinamide phosphoribosyltransferase (NAMPT) (see the Perspective by **Wijnen**). **Ramsey *et al.*** (p. 651; published online 19 March) and **Nakahata *et al.*** (p. 654, published online 12 March) now show that NAMPT and NAD^+ levels oscillate during the daily 24-hour cycle and that this oscillation is regulated by the circadian clock. Furthermore, the oscillations in NAD^+ modulate the activity of SIRT1 feeding back into the circadian clock.

Edited Information Flow

RNA is generally a faithful mirror of the information encoded in DNA. However, posttranscriptional RNA editing is a widespread phenomenon that can result in a translated protein differing from its gene code. A class of deaminase enzymes related to human APOBEC (apolipoprotein B editing complex protein) edit adenosines in eukaryotes. **Randau *et al.*** (p. 657) have discovered an addition to this enzyme family in prokaryotes that edits cytosine to uridine at the highly conserved and structurally critical position 8 in the majority of transfer RNAs of the hyperthermophilic archaebacterium *Methanopyrus kandleri*.

Gene Expression in Hybrids

A large proportion of genes differ in their expression patterns between closely related species, and this divergence is believed to be an important driver of phenotypic evolution. However, little is known about the genetic basis of this divergence. **Tirosh *et al.*** (p. 659) use allele-specific expression profiling of two yeast species and their hybrid to identify which genes diverged in expression owing to changes in their genomic loci (cis) and which genes diverged owing to changes in their regulators (trans). The data can be used to explain the distinct gene expression pattern observed in the hybrid.

CREDIT: STEGEMANN AND BOCK

John P. Holdren is President Obama's science advisor and until recently was a professor at Harvard University and director of the Woods Hole Research Center, Falmouth, MA.

Science in the White House

THE U.S. PRESIDENT'S SCIENCE ADVISOR—OFFICIALLY, THE ASSISTANT TO THE PRESIDENT FOR Science and Technology (S&T)—has the daunting task of providing accurate and timely input to the president, the vice president, and their senior advisors on the full range of S&T topics that bear on the policy challenges facing the nation, from economic recovery to national security to environmental sustainability. Besides these "S&T for policy" responsibilities, moreover, "policy for S&T" must be attended to: helping craft the S&T budgets for the executive-branch departments and agencies that support much of the country's R&D; partnering with the Domestic Policy Council and the Department of Education in efforts to strengthen science, technology, engineering, and mathematics (STEM) education; enhancing the capabilities and diversity of the science and engineering workforce; ensuring coordination and cooperation among the numerous governmental S&T initiatives that involve multiple agencies; advancing appropriate forms of international S&T cooperation; promoting openness, transparency, and scientific integrity in the conduct of the nation's S&T business; and more.

This wide array of responsibilities far exceeds the capabilities of any one person, of course. Fulfilling them requires the joint efforts of the White House Office of Science and Technology Policy (OSTP), which is directed by the science advisor and, at full strength, has some 60 staff members, including four Senate-confirmed associate directors; the President's Council of Advisors on Science and Technology (PCAST), a group coordinated by OSTP that will include about 20 senior figures from the business, academic, and nongovernmental organizations who advise the White House; and the National Science and Technology Council, which is chaired by the president and includes the heads of all of the executive-branch departments, agencies, and offices with substantial S&T roles. Adequately addressing all of the demands that arise in the White House in the domains of S&T for policy and policy for S&T also requires intensive engagement of the wider science, engineering, and innovation communities (as emphasized by President Clinton's second-term science advisor, Neal Lane, on this page last month). Much of that engagement is facilitated by the U.S. National Academies, the American Association for the Advancement of Science, and other science and engineering professional societies, but it also entails a good deal of reaching out—by the science advisor, PCAST, and the OSTP staff—to individual scientists and engineers for their input.

I see the top S&T priorities for the Obama administration in terms of four practical challenges and four cross-cutting foundations of success in addressing all of them. The practical challenges are: bringing S&T more fully to bear on driving economic recovery, job creation, and growth; driving the energy-technology innovation needed to reduce energy imports and climate-change risks while creating green jobs and competitive new businesses; applying advances in biomedical science and information technology together to help Americans live longer, healthier lives with reduced health care costs; and ensuring that we have the defense, homeland security, and national intelligence technologies needed to protect our troops, citizens, and national interests, and to verify the old and new arms control and nonproliferation agreements that are likewise essential to our security.

The cross-cutting foundations of success are: increasing the capacities and output of our country's fundamental research institutions, including our great research universities and major public and private laboratories and research centers; strengthening STEM education at every level, from precollege to postgraduate to lifelong learning; improving and protecting the information, communication, and transportation infrastructures that are essential to our commerce, science, and security alike; and maintaining and vigorously exploiting a cutting-edge set of capabilities in space, which must be understood not just as grand adventure and focus for expanding our knowledge of how the universe works, but also as a driver of innovation and a linchpin of communications, geopositioning technology, intelligence gathering, and Earth observation.

It is a lot to get done. But led by a president who deeply grasps the importance of S&T to our national goals and who is putting scientists, engineers, and innovators back into the center of what the executive branch does, "Yes, we can."

– John P. Holdren

10.1126/science.1174783

CREDITS: (TOP) MARTHA STEWART; (RIGHT) JUPITERIMAGES

Published by AAAS

EDITED BY GILBERT CHIN AND JAKE YESTON

ASTRONOMY

A Stellar Future Ahead?

Barnard 68 is a dark molecular cloud about 400 light years away from Earth. It contains mostly molecular hydrogen mixed with other molecules and dust grains in such high concentrations as to render it completely opaque at optical wavelengths. Stars are thought to be born in dark, cold places such as this. Yet Barnard 28 is still starless; before a star can form within the core, it needs to contract under the force of gravity for a period sufficient to ignite nuclear fusion. There is contradictory evidence as to whether Barnard 68 is still stable or already in a very early phase of gravitational collapse. Burkert and Alves now argue that Barnard 68, far from being a stable, isolated molecular cloud, is colliding with another, smaller cloud, as suggested by its asymmetric and distorted shape. Their numerical simulations of the collision imply that signs of an impending gravitational collapse can already be seen in Barnard 68, and the cloud should condense into a Sun-like star within the next 200,000 years. — MJC

Astrophys. J. **695**, 1308 (2009).

PSYCHOLOGY

Learning Control at an Early Age

Adults who try to master a second language often never attain the degree of fluency with which they converse in their mother tongue. In contrast, children usually fare considerably better, and it is not uncommon for the descendants of immigrants to display proficiency in the parental language as well as that of their peers. Even more impressively, infants exposed to two languages from birth assort two distinct vocabularies and sentence structures while reaching milestones in language production as quickly as their monolingual compatriots.

Kovács and Mehler demonstrate that cognitive control, which is inferred to be needed for switching between language representations, develops more rapidly in 7-month-old infants that have grown up in a bilingual, rather than monolingual, household. Both sets of infants learned at the same rate to associate auditory cues with the visual reward of a gaily-colored puppet shown either to their left or their right, but only the children of parents with different mother tongues (in Trieste, most frequently Italian and Slovene) were able to inhibit the learned response when the reward location was switched and to shift their anticipatory gaze to the other side. — GJC

Proc. Natl. Acad. Sci. U.S.A. **106**, 6556 (2009).

CELL BIOLOGY

Signals of Stress

Two papers have identified a signaling function for ribonucleases in stress. During times of stress, protein synthesis is inhibited via phosphorylation of eukaryotic translation initiation factor 2A (eIF2A). Yamasaki *et al*. focused on observations that translational arrest can occur in cells that express a mutant eIF2A that lacks the phosphorylation site. They found that cells exposed to oxidative stress accumulated cleavage products of transfer RNA (tRNA). Angiogenin is a secreted ribonuclease that has been implicated in tumorigenesis because it promotes the formation of blood vessels, and the authors found that depleting cells of angiogenin inhibited the stress-induced cleavage of tRNA. Thus, stressed cells may signal their neighbors by secreting angiogenin.

Yeast cells also cleave tRNA when exposed to oxidative stress, and Thompson and Parker have identified Rny1 as the ribonuclease responsible. Rny1 was released from the vacuole into the cytoplasm in response to oxidative stress, and overexpression of Rny1 caused apoptosis (cell death) in yeast. Nevertheless, Rny1 must do more than cleave tRNAs, because mutants that lacked catalytic activity could still promote cell death. Intriguingly, the human ortholog of Rny1, RNASET2, has a tumor-suppressing activity that is independent of its catalytic activity. Thus, it appears that release of Rny1 from the vacuole (analogous to the apoptotic release of cytochrome c from mitochondria) both causes cleavage of cytoplasmic tRNAs and affects signaling pathways controlling cell death. — LBR

J. Cell Biol. **185**, 35; 43 (2009).

APPLIED PHYSICS

Quantum Phone Calls

Certain conversations or transactions are meant to be private. Yet despite the encryption of digital communication in one form or another, information theory presents a loophole whereby such encrypted messages can be compromised, if only in principle (in practice it may be extremely difficult to do so). Quantum mechanics closes that loophole altogether. Sharing quantum mechanically–entangled photons can provide a secure key with which to encrypt and send a message, safe in the

CREDITS (TOP TO BOTTOM): ESO; ALAN LANGUS/LANGUAGE COGNITION AND DEVELOPMENT LAB/INTERNATIONAL SCHOOL OF ADVANCED STUDIES

Published by AAAS

knowledge that the message cannot be opened by an eavesdropper, at least not without alerting you to the breach. Chen *et al.* demonstrate a quantum key distribution protocol in a real-world application scenario, with the quantum key distributed over a network consisting of three stations linked by 20 km of commercial optical fiber. The generated keys can be used immediately in the context of encrypted real-time telephone conversations between the separated stations. With such a demonstration, quantum privacy in your own home may not be a too distant prospect. — ISO

Opt. Express **17**, 6540 (2009).

BIOMEDICINE

Becoming Androgen-Independent

Signaling pathways comprising many proteins translate extracellular signals into phenotypic responses via selective regulation of gene expression. Transcription factors interpret the signals and, in concert with situational cofactors, manipulate an appropriate combination of genes. In prostate cells, the androgen receptor is a transcription factor that promotes distinct gene expression patterns in order to regulate proliferation, differentiation, and cell survival. Xu *et al.* show that the E3 ubiquitin ligase RNF6 can modulate the gene expression output patterns of the androgen receptor by atypical polyubiquitination of the receptor. Prostate

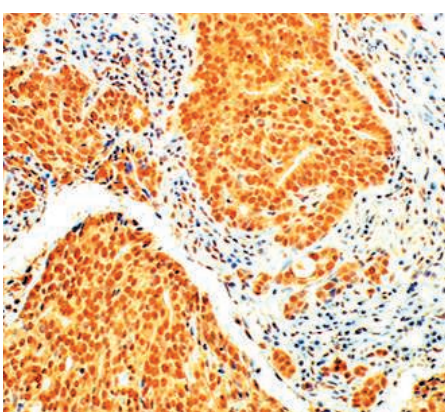

cancer is a leading cause of death in men, and current androgen-ablation therapies provide only a temporary solution because resistance develops rapidly. The authors found that RNF6 (brown in the image) was up-regulated in hormone-refractory prostate cancer cells and was required for their growth, suggesting RNF6 as a potential drug target for the treatment of prostate cancer. — HP*

Cancer Cell **15**, 270 (2009).

CREDIT: XU *ET AL.*, *CANCER CELL* 15, 270 (2009)

*Helen Pickersgill is a locum editor in *Science*'s editorial department.

CHEMISTRY

Acid Analysis

Acids catalyze a wide range of chemical reactions by lending a proton to stabilize a particular intermediate structure. As Macht *et al.* show, however, the sensitivity of chemical rates to catalytic acid strength can vary in a subtle and at times surprising manner as a consequence of the reaction mechanism. The authors specifically compared the rate dependence of three reactions—dehydrations of 1- and 2-butanol and isomerization of hexane to 2-methylpentane—to the varied acid strengths of a range of solid acid polyoxometalate and zeolite catalysts. The overall barriers to reaction increased from 2-butanol dehydration to the alkyl isomerization, with 1-butanol dehydration effectively in the middle of the range. However, both dehydrations evidenced the same sensitivity to acid strength, whereas the alkyl isomerization sensitivity was roughly three times higher. To account for this result, the authors suggest that the concentrated charge distributions in the dehydration transition states are stabilized to some extent by conjugate base charge on the catalyst—an effect enhanced as acid strength drops—and so the overall impact of catalyst acidity is reduced. Conversely, the significance of this electrostatic stabilizing interaction is diminished for the more diffuse charge distribution in the isomerization transition state, resulting in a more pronounced barrier dependence on acid strength. — JSY

J. Am. Chem. Soc. **131**, 10.1021/ja900829x (2009).

SYSTEMS BIOLOGY

Ex Vivo Treatment

Although laboratory experiments are usually designed on the basis of pure populations of cells, responses within an organism often rely on heterogeneous populations. This is certainly true of tumor-infiltrating lymphocytes (TILs), which are used in adoptive cell transfer for the treatment of metastatic melanoma. Oved *et al.* used computational approaches to characterize—according to a panel of cell surface markers—TIL populations isolated from 91 human patients and to predict their reactivity to melanoma cells. No single marker could accurately predict the anti-tumor reactivity of the entire population; however, a set of population-based markers predicted the anti-tumor reactivity of the population (as defined by levels of interferon-γ produced) with 89% accuracy. The authors then took 12 non-reactive TIL populations from four other patients and succeeded in manipulating the frequencies of subpopulations in order to convert the populations into a reactive state—hopefully a step toward less toxic tumor therapy in vivo. — BJ

Mol. Syst. Biol. **5**, 10.1038/msb.2009.15 (2009).

CALL FOR PAPERS

Submit your research now to be one of the first to be considered for publication in the **inaugural issue** of

Science Translational Medicine!

Science Translational Medicine, to be published online weekly beginning in the fourth quarter 2009, focuses on the conversion of basic biomedical research into practical applications, thus bridging the research-to-application gap.

The editors of ***Science Translational Medicine*** are accepting manuscripts for review in the following areas: cancer, cardiovascular disease, metabolism/diabetes/obesity, neuroscience/neurology/psychiatry, immunology/vaccines, infectious diseases, policy, behavior, bioengineering, physics, chemical genomics/drug discovery, imaging, applied physical sciences, medical nanotechnology, drug delivery, biomarkers, gene therapy/regenerative medicine, toxicology and pharmacokinetics, data mining, cell culture, animal and human studies, medical informatics, and other interdisciplinary approaches to medicine.

» **Katrina L. Kelner, Ph.D.**
Editor
American Association for the Advancement of Science

» **Elias A. Zerhouni, M.D.**
Chief Scientific Adviser
Senior Fellow, Global Health Program, Bill & Melinda Gates Foundation
Former Director, National Institutes of Health

Review the call for papers and information for authors, and submit your research at http://sciencemag.org/marketing/stm/papers.dtl

Recommend a subscription to your library: www.sciencemag.org/cgi/recommend_subscription

For more information, contact Editor Katrina Kelner, Ph.D. at scitranslmededitors@aaas.org

Science Translational Medicine
AAAS

Integrating Medicine and Science

www.ScienceTranslationalMedicine.org

www.sciencemag.org

Science

1200 New York Avenue, NW
Washington, DC 20005
Editorial: 202-326-6550, FAX 202-289-7562
News: 202-326-6581, FAX 202-371-9227
Bateman House, 82-88 Hills Road
Cambridge, UK CB2 1LQ
+44 (0) 1223 326500, FAX +44 (0) 1223 326501

Subscription Services For change of address, missing issues, new orders and renewals, and payment questions: 866-434-AAAS (2227) or 202-326-6417, FAX 202-842-1065. Mailing addresses: AAAS, P.O. Box 96178, Washington, DC 20090-6178 or AAAS Member Services, 1200 New York Avenue, NW, Washington, DC 20005

Institutional Site Licenses please call 202-326-6755 for any questions or information

Reprints: Author Inquiries 800-635-7181
Commercial Inquiries 803-359-4578

Permissions 202-326-7074, FAX 202-682-0816

Member Benefits AAAS/Barnes&Noble.com bookstore www.aaas.org/bn; AAAS Online Store www.apisource.com/aaas/ code MKB6; AAAS Travels: Betchart Expeditions 800-252-4910; Apple Store www.apple/eppstore/aaas; Bank of America MasterCard 1-800-833-6262 priority code FAA3YU; Cold Spring Harbor Laboratory Press Publications www.cshlpress.com/affiliates/aaas.htm; GEICO Auto Insurance www.geico.com/landingpage/go51.htm?logo=17624; Hertz 800-654-2200 CDP#343457; Office Depot https://bsd.officedepot.com/portalLogin.do; Seabury & Smith Life Insurance 800-424-9883; Subaru VIP Program 202-326-6417; VIP Moving Services www.vipmayflower.com/domestic/index.html; Other Benefits: AAAS Member Services 202-326-6417 or www.aaasmember.org.

science_editors@aaas.org	(for general editorial queries)
science_letters@aaas.org	(for queries about letters)
science_reviews@aaas.org	(for returning manuscript reviews)
science_bookrevs@aaas.org	(for book review queries)

Published by the American Association for the Advancement of Science (AAAS), *Science* serves its readers as a forum for the presentation and discussion of important issues related to the advancement of science, including the presentation of minority or conflicting points of view, rather than by publishing only material on which a consensus has been reached. Accordingly, all articles published in *Science*—including editorials, news and comment, and book reviews—are signed and reflect the individual views of the authors and not official points of view adopted by AAAS or the institutions with which the authors are affiliated.

AAAS was founded in 1848 and incorporated in 1874. Its mission is to advance science, engineering, and innovation throughout the world for the benefit of all people. The goals of the association are to: enhance communication among scientists, engineers, and the public; promote and defend the integrity of science and its use; strengthen support for the science and technology enterprise; provide a voice for science on societal issues; promote the responsible use of science in public policy; strengthen and diversify the science and technology workforce; foster education in science and technology for everyone; increase public engagement with science and technology; and advance international cooperation in science.

Information for Authors
See pages 807 and 808 of the 6 February 2009 issue or access www.sciencemag.org/about/authors

EDITOR-IN-CHIEF **Bruce Alberts**
EXECUTIVE EDITOR **Monica M. Bradford**
NEWS EDITOR **Colin Norman**
MANAGING EDITOR, RESEARCH JOURNALS **Katrina L. Kelner**
DEPUTY EDITORS **R. Brooks Hanson, Barbara R. Jasny, Andrew M. Sugden**

Editorial **senior editor/perspectives** Lisa D. Chong; **senior editors** Gilbert J. Chin, Pamela J. Hines, Paula A. Kiberstis (Boston), Marc S. Lavine (Toronto), Beverly A. Purnell, L. Bryan Ray, Guy Riddihough, H. Jesse Smith, Phillip D. Szuromi (Tennessee), Valda Vinson; **associate editors** Kristen L. Mueller, Jake S. Yeston, Laura M. Zahn; **online editor** Stewart Wills; **associate online editors** Robert Frederick, Tara S. Marathe; **web content developer** Martyn Green; **book review editor** Sherman J. Suter; **associate letters editor** Jennifer Sills; **editorial manager** Cara Tate; **senior copy editors** Jeffrey E. Cook, Cynthia Howe, Harry Jach, Barbara P. Ordway, Trista Wagoner; **copy editors** Chris Filiatreau, Lauren Kmec; **editorial coordinators** Carolyn Kyle, Beverly Shields; **publications assistants** Ramatoulaye Diop, Carlos L. Durham, Joi S. Granger, Jeffrey Hearn, Lisa Johnson, Scott Miller, Jerry Richardson, Jennifer A. Seibert, Brian White, Anita Wynn; **editorial assistants** Emily Guise, Michael Hicks, Patricia M. Moore; **executive assistant** Sylvia S. Kihara; **administrative support** Maryrose Madrid

News **deputy news editors** Robert Coontz, Eliot Marshall, Jeffrey Mervis, Leslie Roberts; **contributing editors** Elizabeth Culotta, Polly Shulman; **news writers** Yudhijit Bhattacharjee, Adrian Cho, Jennifer Couzin, David Grimm, Constance Holden, Jocelyn Kaiser, Richard A. Kerr, Eli Kintisch, Andrew Lawler (New England), Greg Miller, Elizabeth Pennisi, Robert F. Service (Pacific NW), Erik Stokstad; **intern** Jackie D. Grom; **contributing correspondents** Dan Charles, Jon Cohen (San Diego, CA), Daniel Ferber, Ann Gibbons, Robert Koenig, Mitch Leslie, Charles C. Mann, Virginia Morell, Evelyn Strauss, Gary Taubes; **copy editors** Linda B. Felaco, Melvin Gatling, Melissa Raimondi; **administrative support** Scherraine Mack, Fannie Groom; **bureaus** New England: 207-549-7755, San Diego, CA: 760-942-3252, FAX 760-942-4979, Pacific Northwest: 503-963-1940

Production director James Landry; **senior manager** Wendy K. Shank; **assistant manager** Rebecca Doshi; **senior specialists** Steve Forrester, Chris Redwood; **specialist** Anthony Rosen; **Preflight director** David M. Tompkins; **manager** Marcus Spiegler; **specialist** Jason Hillman

Art director Yael Kats; **associate art director** Laura Creveling; **illustrators** Chris Bickel, Katharine Sutliff; **senior art associates** Holly Bishop, Preston Huey, Nayomi Kevitiyagala; **art associate** Jessica Newfield; **photo editor** Leslie Blizard

***Science* International**

Europe (science@science-int.co.uk) **editorial: international managing editor** Andrew M. Sugden; **senior editor/perspectives** Julia Fahrenkamp-Uppenbrink; **senior editors** Caroline Ash, Stella M. Hurtley, Ian S. Osborne, Peter Stern; **associate editor** Maria Cruz; **locum editor** Helen Pickersgill; **editorial support** Deborah Dennison, Rachel Roberts, Alice Whaley; **administrative support** John Cannell, Janet Clements; **news: europe news editor** John Travis; **deputy news editor** Daniel Clery; **contributing correspondents** Michael Balter (Paris), John Bohannon (Vienna), Martin Enserink (Amsterdam and Paris), Gretchen Vogel (Berlin); **intern** Claire Thomas

Asia Japan Office: Asca Corporation, Eiko Ishioka, Fusako Tamura, 1-8-13, Hirano-cho, Chuo-ku, Osaka-shi, Osaka, 541-0046 Japan; +81 (0) 6 6202 6272, FAX +81 (0) 6 6202 6271; asca@os.gulf.or.jp; **asia news editor** Richard Stone (Beijing: rstone@aaas.org); **contributing correspondents** Dennis Normile (Japan: +81 (0) 3 3391 0630, FAX +81 (0) 3 5936 3531; dnormile@gol.com); Hao Xin (China: +86 (0) 10 6307 4439 or 6307 3676, FAX +86 (0) 10 6307 4358; cindyhao@gmail.com); Pallava Bagla (South Asia: +91 (0) 11 2271 2896; pbagla@vsnl.com)

EXECUTIVE PUBLISHER **Alan I. Leshner**
PUBLISHER **Beth Rosner**

Fulfillment Systems and Operations (membership@aaas.org); **director** Waylon Butler; **senior systems analyst** Jonny Blaker; **customer service supervisor** Pat Butler; **specialists** Latoya Casteel, LaVonda Crawford, Vicki Linton, April Marshall; **data entry supervisor** Cynthia Johnson; **specialists** Eintou Bowden, Tarrika Hill, William Jones

Business Operations and Administration director Deborah Rivera-Wienhold; **assistant director, business operations** Randy Yi; **manager, business analysis** Michael LoBue; **manager, business operations** Jessica Tierney; **financial analysts** Priti Pamnani, Celeste Troxler; **rights and permissions: administrator** Emilie David; **associate** Elizabeth Sandler; **marketing director** Ian King; **marketing manager** Allison Pritchard; **marketing associates** Aimee Aponte, Alison Chandler, Mary Ellen Crowley, Julianne Wielga, Wendy Wise; **marketing executive** Jennifer Reeves; **marketing/member services executive** Linda Rusk; **director, site licensing** Tom Ryan; **director, corporate relations** Eileen Bernadette Moran; **publisher relations, eresources specialist** Kiki Forsythe; **senior publisher relations specialist** Catherine Holland; **publisher relations, east coast** Phillip Smith; **publisher relations, west coast** Philip Tsolakidis; **fulfillment supervisor** Iquo Edim; **fulfillment coordinator** Laura Clemens; **electronic media: manager** Lizabeth Harman; **project manager** Trista Snyder; **assistant manager** Lisa Stanford; **senior production specialists** Christopher Coleman, Walter Jones; **production specialists** Nichele Johnston, Kimberly Oster

Advertising director, worldwide ad sales Bill Moran

Product (science_advertising@aaas.org); **midwest/west coast/w. canada** Rick Bongiovanni: 330-405-7080, FAX 330-405-7081; **east coast/e. canada** Laurie Faraday: 508-747-9395, FAX 617-507-8189; **uk/europe/asia** Roger Goncalves: TEL/FAX +41 43 243 1358; **japan** Mashy Yoshikawa: +81 (0) 3 3235 5961, FAX +81 (0) 3 3235 5852; **senior traffic associate** Deiandra Simms

Commercial Editor Sean Sanders: 202-326-6430

Project Director, Outreach Brianna Blaser

Classified (advertise@sciencecareers.org); **u.s.: sales manager** Daryl Anderson: 202-326-6543; **inside sales representative** Tina Burks: 202-326-6577; **key account manager/midwest** Joribah Able; **east coast** Alexis Fleming: 202-326-6578; **west/south central** Nicholas Hintibidze: 202-326-6533; **sales coordinators** Rohan Edmonson, Shirley Young; **international: sales manager** Tracy Holmes: +44 (0) 1223 326525, FAX +44 (0) 1223 326532; **sales** Susanne Kharraz, Dan Pennington, Alex Palmer; **sales assistant** Louise Moore; **japan** Mashy Yoshikawa: +81 (0) 3 3235 5961, FAX +81 (0) 3 3235 5852; **advertising support manager** Karen Foote: 202-326-6740; **advertising production operations manager** Deborah Tompkins; **senior production specialist/graphic designer** Amy Hardcastle; **senior production specialist** Robert Buck; **senior traffic associate** Christine Hall; **publications assistant** Mary Lagnaoui

AAAS Board of Directors **retiring president, chair** James J. McCarthy; **president** Peter C. Agre; **president-elect** Alice Huang; **treasurer** David E. Shaw; **chief executive officer** Alan I. Leshner; **board** Alice Gast, Linda P. B. Katehi, Nancy Knowlton, Cherry A. Murray, Julia M. Phillips, Thomas D. Pollard, David S. Sabatini, Thomas A. Woolsey

AAAS
ADVANCING SCIENCE, SERVING SOCIETY

SENIOR EDITORIAL BOARD

John I. Brauman, *Chair, Stanford Univ.*
Richard Losick, *Harvard Univ.*
Robert May, *Univ. of Oxford*
Marcia McNutt, *Monterey Bay Aquarium Research Inst.*
Linda Partridge, *Univ. College London*
Vera C. Rubin, *Carnegie Institution*
Christopher R. Somerville, *Univ. of California, Berkeley*

BOARD OF REVIEWING EDITORS

Joanna Aizenberg, *Harvard Univ.*
Sonia Altizer, *Univ. of Georgia*
David Altshuler, *Broad Institute*
Arturo Alvarez-Buylla, *Univ. of California, San Francisco*
Richard Amasino, *Univ. of Wisconsin, Madison*
Angelika Amon, *MIT*
Meinrat O. Andreae, *Max Planck Inst., Mainz*
Kristi S. Anseth, *Univ. of Colorado*
John A. Bargh, *Yale Univ.*
Cornelia I. Bargmann, *Rockefeller Univ.*
Ben Barres, *Stanford Medical School*
Marisa Bartolomei, *Univ. of Penn. School of Med.*
Facundo Batista, *London Research Inst.*
Ray H. Baughman, *Univ. of Texas, Dallas*
Stephen J. Benkovic, *Penn State Univ.*
Ton Bisseling, *Wageningen Univ.*
Mina Bissell, *Lawrence Berkeley National Lab*
Peer Bork, *EMBL*
Robert W. Boyd, *Univ. of Rochester*
Paul M. Brakefield, *Leiden Univ.*
Stephen Buratowski, *Harvard Medical School*
Joseph A. Burns, *Cornell Univ.*
William P. Butz, *Population Reference Bureau*
Mats Carlsson, *Univ. of Oslo*
Peter Carmeliet, *Univ. of Leuven, VIB*
Mildred Cho, *Stanford Univ.*
David Clapham, *Children's Hospital, Boston*
David Clary, *Oxford University*
J. M. Claverie, *CNRS, Marseille*
Jonathan D. Cohen, *Princeton Univ.*
Andrew Cossins, *Univ. of Liverpool*
Robert H. Crabtree, *Yale Univ.*
Wolfgang Cramer, *Potsdam Inst. for Climate Impact Research*
F. Fleming Crim, *Univ. of Wisconsin*
William Cumberland, *Univ. of California, Los Angeles*
Jeff L. Dangl, *Univ. of North Carolina*
Stanislas Dehaene, *Collège de France*
Edward DeLong, *MIT*
Emmanouil T. Dermitzakis, *Wellcome Trust Sanger Inst.*
Robert Desimone, *MIT*
Claude Desplan, *New York Univ.*
Dennis Discher, *Univ. of Pennsylvania*
Scott C. Doney, *Woods Hole Oceanographic Inst.*
W. Ford Doolittle, *Dalhousie Univ.*
Jennifer A. Doudna, *Univ. of California, Berkeley*
Julian Downward, *Cancer Research UK*
Denis Duboule, *Univ. of Geneva/EPFL Lausanne*
Christopher Dye, *WHO*
Gerhard Ertl, *Fritz-Haber-Institut, Berlin*
Mark Estelle, *Indiana Univ.*
Barry Everitt, *Univ. of Cambridge*
Paul G. Falkowski, *Rutgers Univ.*
Ernst Fehr, *Univ. of Zurich*
Tom Fenchel, *Univ. of Copenhagen*
Alain Fischer, *INSERM*
Scott E. Fraser, *Cal Tech*
Chris D. Frith, *Univ. College London*
Wulfram Gerstner, *EPFL Lausanne*
Charles Godfray, *Univ. of Oxford*
Diane Griffin, *Johns Hopkins Bloomberg School of Public Health*
Christian Haass, *Ludwig Maximilians Univ.*
Niels Hansen, *Technical Univ. of Denmark*
Dennis L. Hartmann, *Univ. of Washington*
Chris Hawkesworth, *Univ. of Bristol*
Martin Heimann, *Max Planck Inst., Jena*
James A. Hendler, *Rensselaer Polytechnic Inst.*
Ray Hilborn, *Univ. of Washington*
Kei Hirose, *Tokyo Inst. of Technology*
Ove Hoegh-Guldberg, *Univ. of Queensland*
Brigid L. M. Hogan, *Duke Univ. Medical Center*
Ronald R. Hoy, *Cornell Univ.*
Olli Ikkala, *Helsinki Univ. of Technology*
Meyer B. Jackson, *Univ. of Wisconsin Med. School*
Stephen Jackson, *Univ. of Cambridge*
Steven Jacobsen, *Univ. of California, Los Angeles*
Peter Jonas, *Universität Freiburg*
Barbara B. Kahn, *Harvard Medical School*
Daniel Kahne, *Harvard Univ.*
Gerard Karsenty, *Columbia Univ. College of P&S*
Bernhard Keimer, *Max Planck Inst., Stuttgart*
Elizabeth A. Kellog, *Univ. of Missouri, St. Louis*
Hanna Kokko, *Univ. of Helsinki*
Alan B. Krueger, *Princeton Univ.*
Lee Kump, *Penn State Univ.*
Mitchell A. Lazar, *Univ. of Pennsylvania*
David Lazer, *Harvard Univ.*
Virginia Lee, *Univ. of Pennsylvania*
Olle Lindvall, *Univ. Hospital, Lund*
Marcia C. Linn, *Univ. of California, Berkeley*
John Lis, *Cornell Univ.*
Richard Losick, *Harvard Univ.*
Ke Lu, *Chinese Acad. of Sciences*
Andrew P. MacKenzie, *Univ. of St Andrews*
Raul Madariaga, *École Normale Supérieure, Paris*
Anne Magurran, *Univ. of St Andrews*
Charles Marshall, *Harvard Univ.*
Virginia Miller, *Washington Univ.*
Yasushi Miyashita, *Univ. of Tokyo*
Richard Morris, *Univ. of Edinburgh*
Edvard Moser, *Norwegian Univ. of Science and Technology*
Naoto Nagaosa, *Univ. of Tokyo*
James Nelson, *Stanford Univ. School of Med.*
Timothy W. Nilsen, *Case Western Reserve Univ.*
Roeland Nolte, *Univ. of Nijmegen*
Helga Nowotny, *European Research Advisory Board*
Eric N. Olson, *Univ. of Texas, SW*
Stuart H. Orkin, *Dana-Farber Cancer Inst.*
Erin O'Shea, *Harvard Univ.*
Elinor Ostrom, *Indiana Univ.*
Jonathan T. Overpeck, *Univ. of Arizona*
John Pendry, *Imperial College*
Simon Phillpot, *Univ. of Florida*
Philippe Poulin, *CNRS*
Mary Power, *Univ. of California, Berkeley*
Molly Przeworski, *Univ. of Chicago*
Colin Renfrew, *Univ. of Cambridge*
Trevor Robbins, *Univ. of Cambridge*
Barbara A. Romanowicz, *Univ. of California, Berkeley*
Edward M. Rubin, *Lawrence Berkeley National Lab*
Shimon Sakaguchi, *Kyoto Univ.*
Jürgen Sandkühler, *Medical Univ. of Vienna*
David W. Schindler, *Univ. of Alberta*
Georg Schulz, *Albert-Ludwigs-Universität*
Paul Schulze-Lefert, *Max Planck Inst., Cologne*
Christine Seidman, *Harvard Medical School*
Terrence J. Sejnowski, *The Salk Institute*
Richard J. Shavelson, *Stanford Univ.*
David Sibley, *Washington Univ.*
Joseph Silk, *Univ. of Oxford*
Montgomery Slatkin, *Univ. of California, Berkeley*
Davor Solter, *Inst. of Medical Biology, Singapore*
Joan Steitz, *Yale Univ.*
Elsbeth Stern, *ETH Zürich*
Jerome Strauss, *Virginia Commonwealth Univ.*
Jurg Tschopp, *Univ. of Lausanne*
Derek van der Kooy, *Univ. of Toronto*
Bert Vogelstein, *Johns Hopkins Univ.*
Ulrich H. von Andrian, *Harvard Medical School*
Bruce D. Walker, *Harvard Medical School*
Christopher A. Walsh, *Harvard Medical School*
Graham Warren, *Yale Univ. School of Med.*
Colin Watts, *Univ. of Dundee*
Detlef Weigel, *Max Planck Inst., Tübingen*
Jonathan Weissman, *Univ. of California, San Francisco*
Sue Wessler, *Univ. of Georgia*
Ellen D. Williams, *Univ. of Maryland*
Ian A. Wilson, *The Scripps Res. Inst.*
Jerry Workman, *Stowers Inst. for Medical Research*
Xiaoliang Sunney Xie, *Harvard Univ.*
John R. Yates III, *The Scripps Res. Inst.*
Jan Zaanen, *Leiden Univ.*
Huda Zoghbi, *Baylor College of Medicine*
Maria Zuber, *MIT*

BOOK REVIEW BOARD

John Aldrich, *Duke Univ.*
David Bloom, *Harvard Univ.*
Angela Creager, *Princeton Univ.*
Richard Shweder, *Univ. of Chicago*
Ed Wasserman, *DuPont*
Lewis Wolpert, *Univ. College London*

Banking on Twins

Researchers in the United Kingdom are aiming to set up the world's largest twin registry.

"We've been developing TwinBank for about a year," says behavioral geneticist Robert Plomin of the Institute of Psychiatry in London, who is working with genetic epidemiologist Timothy Spector of King's College London.

A pilot study funded by the U.K.'s National Health Service, which has birth records for more than 600,000 twins, estimates that at least 300,000 pairs would agree to participate, Plomin says. That would outnumber all the world's other twin registries combined. Determining whether twins are monozygotic (identical) or dizygotic (fraternal) "would add tremendous value" in studying genetic and environmental contributions to health, he says.

Plomin and Spector are currently casting around for funding. The Medical Research Council decided it couldn't afford the project. The pair estimate that it will cost £12 million to get DNA from 300,000 pairs born since 1920.

"The U.K. TwinBank would expand greatly the number of traits and conditions for which such studies could be done," says Jaakko Kaprio, a leader of the Finnish Twin Cohort Studies at the University of Helsinki. For example, it would yield insights into why rare genetically influenced diseases sometimes hit only one in a pair of identical twins. "Finding enough [identical] pairs truly discordant for a trait" is difficult even when there are several tens of thousands of twin pairs in a study, Kaprio says.

Eight-Legged Zombies

A test of spiders' resistance to drowning has uncovered an unsuspected survival mechanism. While timing how long spiders could survive in vials of water, arachnologist Julien Pétillon and his graduate student at France's Université de Rennes 1 left some apparently dead spiders in the lab to dry. But upon their return several hours later, some of the arachnids were up and moving again.

To learn more, the researchers collected 360 wolf spiders from two salt marsh species and one forest species and submerged them in saltwater for up to 48 hours, checking on them every 2 hours. Spiders from two species drowned, but 70% of the salt-marsh–dwelling *Arctosa fulvolineata* fell into a "coma" and survived up to 40 hours of submersion, the researchers reported online 22 April in *Biology Letters*. The adaptation allows them to survive during high tide, Pétillon says. The spiders take about 2 hours to recover.

Several underwater comalike states have been observed in marine animals, such as blue crabs and shrimp, in oxygen-poor waters, but this is a first for a terrestrial organism, Pétillon says. It's an "interesting and unexpected adaptation," says physiological ecologist Kenneth Prestwich of the College of the Holy Cross in Worcester, Massachusetts. Just how the spiders do it remains to be discovered.

Winners in Medicine

Two big medical prizes were announced last week, honoring discoveries in immunology and research on muscular dystrophy.

Ralph Steinman of the Rockefeller University in New York City; Charles Dinarello of the University of Colorado, Denver; and Bruce Beutler of The Scripps Research Institute in San Diego, California, shared the $500,000 Albany Medical Center Prize for advancing knowledge of the human immune system. Steinman is honored for his 1973 discovery of the dendritic cell, a type of white blood cell that alerts T-cells to mount an immune response against harmful invaders. Dinarello and Beutler are cited for work uncovering the role of cytokines—signaling proteins—in inflammation, which has led to therapies for a number of ailments.

Molecular physiologist Kevin Campbell of the University of Iowa, Iowa City, and geneticist Louis Kunkel of Harvard Medical School in Boston, are sharing this year's $250,000 March of Dimes Prize for identifying genes and proteins involved in muscular dystrophy. Their work has led to the development of diagnostic tools and therapies for nine forms of muscular dystrophy and related muscle-wasting disorders.

Onward and Upward

Indian scientists have made major strides both in quality and productivity since 2000, according to the latest figures from the ScienceWatch tracking service (www.sciencewatch.com). The number of papers produced by Indian scientists was more or less stagnant from 1985 to 2000 but jumped from 17,000 in 2001 to 27,000 in 2007 (see chart). Citation rates are also rising across the board—more than doubling, for example, in biology and biochemistry. The biggest gains have come in the physical sciences, especially materials science. Nobuko Miyairi, a consultant at Thomson Reuters, which publishes ScienceWatch, calls it "noteworthy" that Indian science is "fairly well balanced between life sciences and physical sciences," because most of the rest of Asia "tends to be more heavily focused on … physical sciences."

ANNUAL INDIAN PAPER OUTPUT

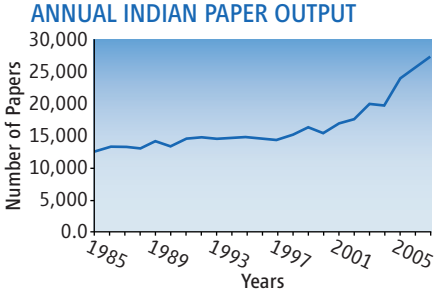

CREDITS (LEFT TO RIGHT): JOHN LAMB/GETTY IMAGES; SONIA DOURLOT; SOURCE: THOMSON REUTERS NATIONAL SCIENCE INDICATORS

Published by AAAS

Obama lays out his science plans 576

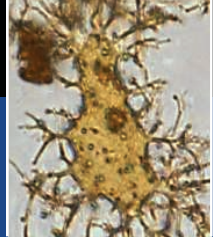

Dinosaur proteins 578

Covering all bases. Mexico City, the hardest hit locale, has taken extra precautionary measures to slow swine flu's spread.

INFECTIOUS DISEASES

As Swine Flu Circles Globe, Scientists Grapple With Basic Questions

On 27 April, 6 days after the U.S. Centers for Disease Control and Prevention (CDC) first reported an unusual swine flu outbreak in humans, international agencies were still struggling to determine how serious a threat the virus posed. "Every new strain of the flu virus is unique," CDC acting Director Richard Besser said at a press conference, "and until the outbreak has progressed, you don't know what it is going to do."

Shortly after CDC rang the alarm bell on 21 April in a *Morbidity and Mortality Weekly Report* dispatch about two cases of swine flu in southern California, scientists and health officials around the world went on alert, concerned that this never-before-seen virus could lead to a killer pandemic. They quickly determined the genetic sequence of the virus, linked the U.S. cases to an apparently much larger outbreak in Mexico, and began fashioning international and local responses.

"On the bright side, this event was widely expected," says Julio Frenk, the former secretary of health in Mexico who now heads Harvard School of Public Health in Boston. In the wake of outbreaks of avian influenza, "there have been good efforts to prepare."

But others say the world hasn't done nearly enough over the past 10 years to prepare for a pandemic. They worry that most countries will find themselves without access to vaccines or antiviral drugs, which could become especially dangerous if the virus causes severe disease in many people—which is still uncertain—or evolves to do so. Some also question why the disease wasn't recognized as an international emergency several weeks earlier, which might have offered a chance to stop it at the source instead of battling it around the planet.

Much confusion surrounds the origins of the virus, why it seems to cause severe disease in Mexico and not elsewhere, and the overall threat it poses to the world. "Right now, there's more unknown than there is known," says microbiologist Francis Plummer, who heads the National Microbiology Laboratory in Winnipeg, part of the Public Health Agency of Canada (PHAC) and a key player in unraveling the Mexican link.

By 28 April, Mexico had connected this swine flu to 152 deaths (most of which have yet to be confirmed). But in the United States and Canada, "it doesn't seem to be anything different than seasonal flu," says Plummer. Solving that riddle will require tests on the suspected cases in Mexico, which totaled nearly 2000, to see whether they indeed are swine flu. But CDC and PHAC—the only two labs that initially had all the reagents necessary to test for the virus—had confirmed a mere two dozen cases as the new H1N1 at the time. Each had scientists in Mexico helping officials build the capacity to do the tests themselves.

As to the virus's spread, newspaper headlines seem to speak volumes. But what's needed to predict spread, says epidemiologist and disease modeler Ira Longini of the University of Washington, Seattle, is an estimate of the virus's basic reproductive number, or R_0, a variable that denotes the number of new infections caused by each infected person. Longini and others are trying to get their hands on as much data as they can from the first outbreak clusters to make that estimate.

The outbreak's discovery underscores the axiom that luck comes to those who are prepared. Although Mexico began to experience an unusually high number of hospitalizations with respiratory problems in late March, no special investigation took place, in part because the cases overlapped with the end of flu season. The disease also spared young children and the elderly, the two groups most vulnerable to severe cases of flu, which some researchers say should have triggered suspicions that an altogether new pathogen was responsible. The answer came when two respiratory cases, both of which

Online
sciencemag.org
For continuing coverage of the epidemic, go to *Science*'s policy blog, http://blogs.sciencemag.org/scienceinsider/

CREDIT: ALFREDO ESTRELLA/AFP/GETTY IMAGES

Published by AAAS

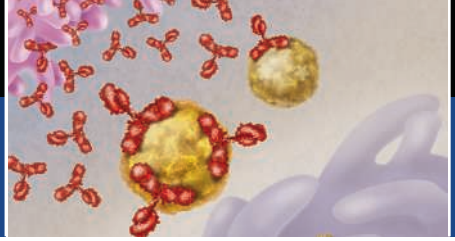

The origin of the immune system

580

The carbon footprint of corn ethanol

587

looked like run-of-the-mill flu, came to the lab at the Naval Health Research Center (NHRC) in San Diego, California, which is conducting sophisticated tests for influenza as part of other studies.

Most people who have the flu never see a doctor, and the virus is rarely analyzed. But the Navy is developing better influenza diagnostics along with CDC's Border Infectious Disease Surveillance project and the Department of Defense's Global Emerging Infections Surveillance and Response System. The standard rapid test for influenza determines whether the virus is strain A or B. The tests under development analyze specific subtypes based on two proteins on the viral surface, hemagglutinin (H) and neuraminidase (N). When the naval lab could not subtype two patient samples, they rushed the samples to CDC, which had determined by 17 April that both were from a novel H1N1 swine flu virus.

Despite the crush of activity since CDC first identified this H1N1, we are still "making decisions with incomplete information," Besser said. Part of the problem is that swine flu infections of humans have rarely been documented. Virologist Christopher Olsen of the University of Wisconsin, Madison, School of Veterinary Medicine co-authored a study in 2007 that found only 50 cases in the biomedical literature dating back to 1958. During the past 12 years, several new influenza genotypes surfaced in swine, making for "a very confusing picture," says Olsen.

Researchers would like to know whether a virus must mutate to move from pigs to humans and whether, as is the case with bird flu in humans, a specific mutation makes it more virulent. "There is a feeling that once you know the sequence, you know everything about a virus, and you really don't," says virologist Robert Webster of St. Jude Children's Research Hospital in Memphis, Tennessee.

CDC and PHAC have found that the current H1N1 combines pieces of influenza from North American swine and avian viruses, with human and swine sequences from Europe and Asia. "It's really a grand old mix-up," says Webster.

Webster and Olsen also emphasize that just because the first cases surfaced in Mexico, the outbreak did not necessarily originate there. The pig that transmitted the virus may have been imported into the country, or the first transmission to a human may have occurred elsewhere.

Early on, CDC began to brew a "seed" strain for a possible vaccine against swine H1N1, and by 27 April the World Health Organization in Geneva, Switzerland, was already talking to vaccine manufacturers. One key problem is that the world's influenza vaccine production capacity—which still relies on growing the vaccine virus in chicken eggs—is limited to some 400 million vaccine doses a year and is impossible to expand quickly. Manufacturing swine flu vaccine would thus come at the expense of seasonal vaccine production, says retired pharma executive and flu vaccine expert David Fedson, and might lead to higher mortality and morbidity from the three seasonal strains.

For now, WHO says manufacturers should continue preparing vaccine for the 2009–10 flu season. But that could change if swine flu proves particularly severe. "We're in a casino now, and we're placing our bets," says Fedson.

As to drugs, many countries began stockpiling oseltamivir after avian influenza put the pandemic threat on the political agenda in 2003. Individual governments, mostly in Western countries, have at least 220 million treatment courses in stock, says Martina Rupp, a spokesperson for Roche, the main producer of Tamiflu. Roche could ramp up its production capacity to some 400 million treatment courses annually fairly rapidly, she says; in addition, there are at least 10 generic manufacturers, four of them working under license from Roche, that produce oseltamivir. But the drug's complex manufacturing process makes it too pricey for many poor nations, says Fedson.

Déjà vu. A hospital worker in Singapore, a country hit hard by SARS in 2003, stands ready to assess patients with respiratory illnesses.

From pigs to people. Swine flu has occasionally jumped the species barrier before but was never known to transmit easily between humans.

Both CDC and WHO have made clear that the careful plans developed over the past 5 years to squelch pandemics at their source don't play a role at all now because the virus is already too widely dispersed. In papers published in 2005 in *Science* and *Nature*, scientists concluded that it might be possible to stop a budding pandemic locally by aggressive, targeted use of antivirals and measures such as shutting down transport and schools. WHO had stashed away some 5 million treatment courses of oseltamivir that could be used to that end.

The scenario might have worked for swine flu, says Longini—if it had been tried much earlier. "There were 800 or 900 [suspected] cases before it hit the global radar screen; that's way beyond a containable outbreak," Longini says.

Why it took so long to garner attention has many scientists puzzled. John Brownstein, the director of HealthMap, one of several systems set up recently to provide the world with real-time information about suspicious disease activity by having software scour news sources around the globe, says the first reports about a respiratory illness appeared in a Mexican newspaper on 1 April. "But there were 300 outbreaks at the same time, so what made this one different?" Brownstein asks. "We have to go back and see if there was a signature that we should have picked up here."

–JON COHEN AND MARTIN ENSERINK

CREDITS (TOP TO BOTTOM): PHOTOS.COM; VIVEK PRAKASH/REUTERS/LANDOV

Published by AAAS

SCIENCE AND SOCIETY

Hundreds Gather for Rally to Defend Animal Research

LOS ANGELES, CALIFORNIA—Last week marked what some hope will be a turning point in the clash of wills between proponents of biomedical research and animal-rights extremists, who've ratcheted up their attacks on researchers in the United States in recent years. On 20 April, a Los Angeles County grand jury arraigned two animal-rights activists on 10 felony charges each, including stalking and threatening two researchers at the University of California, Los Angeles (UCLA). The following day, the Federal Bureau of Investigation added an animal-rights activist—Daniel Andreas San Diego—to its Most Wanted Terrorists list for his alleged role in bombing two San Francisco–area office buildings in 2003. This is the first time a domestic terrorist has been added to the list that includes the likes of Osama bin Laden. And on 22 April, hundreds of people turned out for a pro-research rally on the UCLA campus.

It's too early to tell whether these events will help diminish the recent spate of attacks on researchers at UCLA (*Science*, 21 December 2007, p. 1856) and elsewhere (*Science*, 8 August 2008, p. 755). Since 2006, animal-rights extremists have claimed responsibility for at least 10 acts of arson, attempted arson, and other vandalism at UCLA. Researchers there report being intimidated by death threats and harassed at their homes by people in masks who show up in the middle of the night.

Although no charges have been filed in any of the arson or attempted-arson cases, the indictments announced last week charge Linda Faith Greene, 61, and Kevin Richard Olliff, 22, with stalking and threatening UCLA researchers Lynn Fairbanks and Dario Ringach. That announcement follows the arrest on 22 February of four activists in connection with incidents targeting researchers at the University of California campuses in Santa Cruz and Berkeley. The FBI alleges the four violated the Animal Enterprise Terrorism Act, a 2006 law that carries penalties of up to 5 years in prison for using force, violence, or threats to interfere with research or other activities involving animals. "The message has now been sent pretty clearly that law enforcement is invested in this, that they're expending resources to stop the violence," says Frankie Trull, president of the Foundation for Biomedical Research in Washington, D.C.

A visible police presence may have helped discourage any bad behavior last Wednesday when proponents and opponents of animal research gathered at UCLA. In the morning, several dozen animal-rights advocates set up shop on a street corner bordering UCLA's medical campus, carrying posters with images of bloody animals and slogans decrying animal experimentation as torture and fraud. Several protesters said they oppose animal experimentation, period. Others saw shades of gray but harbored doubts about whether lab animals are treated as humanely as possible, whether the benefits to human medicine are as great as scientists say, and whether researchers are doing too many redundant experiments or trying hard enough to find alternatives. The recent firebombings and other violence have distracted attention from such questions and made it harder for nonviolent activists to get their message out, said 3rd-year UCLA law student Jill Ryther, a member of the campus Animal Law Society. Those tactics "are giving animal-rights activists a bad name," she said.

Meanwhile, a much larger crowd assembled as part of the Pro-Test rally organized by UCLA neuroscientist J. David Jentsch, who woke up the night of 7 March to find his car in flames. With the help of British pro-research activist Tom Holder, Jentsch modeled the rally on protests at the University of Oxford that were widely credited with helping to turn the tide of public opinion against animal-rights activists. Pro-Testers carried homemade signs with slogans such as "Science saves lives" and "Stop bombing us." The group marched to the science quad for a series of short talks. Fairbanks, the first researcher targeted in the recent string of incidents at UCLA, said she spoke not as a researcher but as the mother of a son who had juvenile diabetes. "Animal research saved my son's life," she said. "It's not true when they say it doesn't work."

Others offered refutations to claims made by animal-rights activists—that animal research is unnecessarily cruel, that it's unregulated, and that it reveals nothing that couldn't be learned from tissue culture experiments, computer modeling, and other methods. The public's limited understanding of these issues has been exploited by extremists to justify their actions, said John Young, the director of comparative medicine at Cedars-Sinai Medical Center in Los Angeles and chair of the board of the pro-research group Americans for Medical Progress. He urged scientists to speak up. "The public wants to hear our story," he said.

Jentsch and Holder said the turnout exceeded their expectations. Jentsch hopes the Pro-Testers sent a strong message to the public as well as those behind the attacks: "I think putting our faces on what we do humanizes the effort and makes it harder to write obscene things in the middle of the night and to brutalize people."

–GREG MILLER

Speaking out. Biomedical researchers and supporters took to the streets at UCLA last week.

CREDIT: REED SAXON/AP PHOTO

Read more detailed coverage of the rally on *Science*Insider at http://is.gd/v8MV.

Published by AAAS

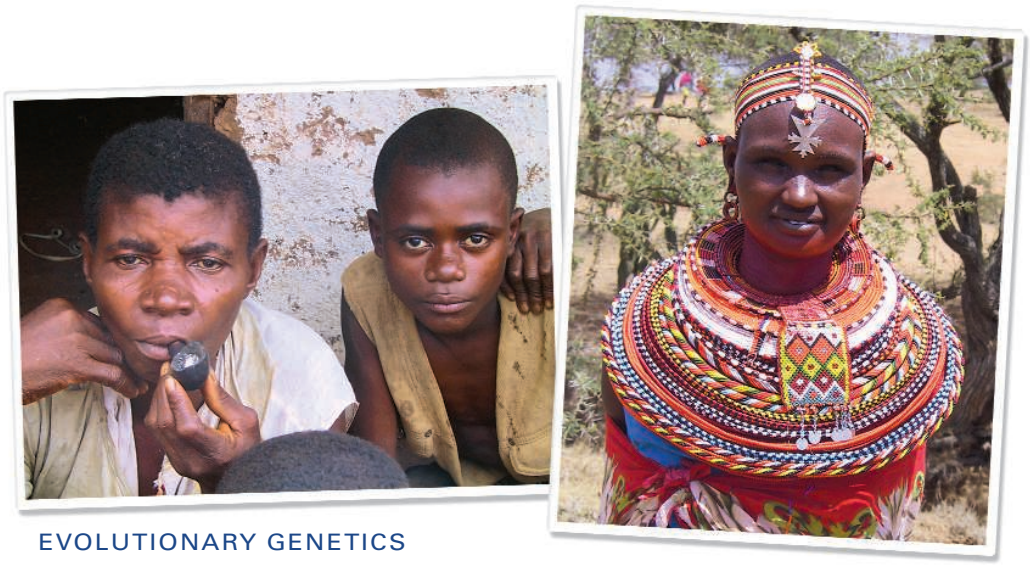

Distant cousins. These pygmies from Cameroon (*left*) are not closely related to this Samburu woman, whose ancestors migrated to Kenya in the past 1500 years.

CREDITS (LEFT TO RIGHT): EVAN LEACH; SARA TISHKOFF

EVOLUTIONARY GENETICS

Africans' Deep Genetic Roots Reveal Their Evolutionary Story

Africa is the birthplace of modern humans, and so our species has lived longest—200,000 years—on that continent. As a result, Africans have had more time to accumulate changes in their DNA than humans elsewhere. But until now, researchers have barely scratched the surface of the rich diversity in Africans' nuclear DNA. Most genetic studies of Africans and African-Americans are based on data from just a few gene lineages, or on genomewide scans of a handful of the diverse African groups. "Africans have been the most completely neglected and underrepresented genetically of any continental group, because the most diverse groups are often remote," says evolutionary geneticist Sarah Tishkoff of the University of Pennsylvania. "Hunter-gatherers don't usually get to clinics."

Now, in the largest study ever of African genetic diversity, an international team of researchers led by Tishkoff has analyzed nuclear DNA collected over a decade from 113 populations of Africans from across the continent. In a report published online in *Science* (www.sciencemag.org/cgi/content/abstract/1172257) this week, the team has found that Africans are descended from 14 ancestral populations, which often correlate with language and cultural groups. They found that all hunter-gatherers and pygmies in Africa today shared ancestors 35,000 years ago and that East Africa was the source of the great migration that populated the rest of the world. They also found that African-American individuals, on average, have mixed ancestry from all over western Africa, which will make it difficult to trace roots to specific ethnic groups.

"Wow! This data gives us raw material for understanding human evolution that we have never had before," says geneticist Jeffrey Long of the University of Michigan (UM) Medical School in Ann Arbor. Adds geneticist Noah Rosenberg, also of UM, "It's a treasure trove of information."

Tishkoff and a team of European and African collaborators, in particular postdoc Floyd Reed, now at the Max Planck Institute for Evolutionary Biology in Plön, Germany, began collecting blood from far-flung tribes in Africa more than a decade ago. They drove off-road to visit peoples as diverse as the pygmies of Cameroon and hunter-gatherers in Tanzania. They set up centrifuges wherever they could find generators, survived a car crash, and spent years negotiating permits to collect blood ethically. "It was no small feat to get these samples," says Tishkoff.

They ended up with blood from 3194 Africans from 113 populations. Working with additional collaborators, they genotyped the samples for a panel of 1327 well-known markers used to map genetic diseases in diverse populations. They then used various statistical methods to sort the DNA into closely related clusters and to trace patterns of inheritance. They also compared markers in Africans with those from 98 African-Americans, 21 Yemenites, and 952 individuals from around the world.

In many cases, the team found that ethnic, cultural, and linguistic differences reflected real genetic differences, which is "reassuring," says paleoanthropologist Stanley Ambrose of the University of Illinois, Urbana-Champaign. For example, the hunter-gatherers spread throughout Africa, including the Sandawe and Hadza of Tanzania and the Khoisan speakers of southern Africa, shared common ancestors. All three of these groups speak click languages, which incorporate strong "click" consonants, some similar to the click used to urge a horse to speed up. The click-speakers and other hunter-gatherers from throughout Africa are all descendants of one protohunter-gatherer group that split apart more than 35,000 years ago, says Tishkoff. She also traces the origins of pygmies to that group, which suggests that pygmies may originally have been click-speakers.

The team found that San bushmen of southern Africa were among a handful of groups with the most diverse nuclear DNA, confirming mitochondrial and Y chromosome studies that suggested the ancestors of the San led a major migration throughout Africa, spreading out from their ancient homeland. The data also confirm earlier research indicating that the source population for the out-of-Africa migration of modern humans came from east Africa near the Red Sea.

The team focused on another migration as well: the exodus of slaves from Africa, sampling DNA from African-Americans in four U.S. states. These people inherited, on average, 71% of their DNA from ancestors who came from all over western Africa, 8% from other parts of Africa, and 13% from Europeans. This suggests that most African-Americans had ancestors from all over Africa, which will make it difficult to pinpoint their origins to specific ethnic groups, as ancestry-tracing kits now purport to do. The data will be important for "studies that seek to map disease genes in African-Americans," says Rosenberg.

Overall, the paper is "a monumental synthesis," says Ambrose, and the data, which will be posted on Tishkoff's Web site, are likely to be used by both biomedical and evolutionary researchers. "To understand the population genetics of any human population, we really need to understand Africa first," says geneticist Jonathan Pritchard of the University of Chicago in Illinois. "It is sure to be an important paper and an important data set."

Tishkoff herself says "there are still gaps in our knowledge." She hopes to "help people designing biomedical research," specifically to see how differences in DNA affect how people respond to disease and drugs. Treatments for AIDS, malaria, and tuberculosis can be life-threatening for some people, says Tishkoff, and the key to more effective treatments may be in their genes.

–ANN GIBBONS

Published by AAAS

U.S. SCIENCE POLICY

Obama Courts a Smitten Audience at the National Academy

Only once before has a newly elected president—John F. Kennedy in 1961—traveled the 10 blocks from the White House to the National Academy of Sciences (NAS) to explain his policies on science and innovation to the nation's most prestigious scientific organization. On Monday, President Barack Obama made the trip, and the symbolism was as important as the message: Many of the promises Obama made—to increase research spending, achieve energy independence, improve science education, and remove ideology from science decision-making—were not new, but having the president himself deliver them made all the difference.

Celebrating science. NAS President Ralph Cicerone (*left*) and John Holdren welcome the president to the academy.

"This is a major deal," said NAS President Ralph Cicerone, still slightly awestruck half an hour after Obama had finished his 38-minute speech (www.nas.edu), shaken hands with front-row dignitaries, and headed back to the White House to greet a collegiate women's basketball team. "He understands how innovation works, and he has a wonderful way of explaining it to the public. The speech was inspiring and credible. We are extremely lucky to have him in the White House."

The crowd, which began queuing up at 6 a.m., was already on his side long before presidential science adviser John Holdren introduced his boss at 9:12 a.m. But Obama clinched the deal by appealing both to their sense of duty—"I want to challenge you to use your love and knowledge of science to spark [a] sense of wonder and excitement in a new generation"—and their desire for more support—"We will devote more than 3% of our GDP to research and development, … the largest commitment to scientific research and innovation in American history."

"Wow. Three percent has sort of been the Holy Grail for research funding," says Charles Vest, president of the National Academy of Engineering. "It depends on so many things, including the denominator, and it's not really an end in itself. But it's a heck of a good place to start."

Five countries are above that level, according to the *Science and Engineering Indicators 2008* report from the National Science Foundation (NSF), with the United States at 2.6% in 2006. The report warns that the ratio is affected by many factors outside the government's control, from the amount of industrial spending to the health of the global economy, and that "meeting any specific ratio [is] an elusive policy goal." Even within the government, the puzzle has many pieces: U.S. spending on defense, which is mostly applied research, far exceeds levels in any other country, for example. Speaking briefly after the meeting, Holdren said that no date has been set for reaching or exceeding 3%.

In announcing the target, Obama said his

CLIMATE CHANGE

Study Challenges Cosmic Ray–Climate Link

If rising levels of greenhouse gases aren't pushing up global temperatures, as contrarians argue, what else could be? The leading alternative has been a fickle sun, and the sun's most likely—or most heavily promoted—agent of change has been cosmic rays. Now scientists have published the first comprehensive modeling of how the sun might indirectly thin cloud cover and thus warm the planet. It suggests that cosmic rays are not up to the task by two orders of magnitude. "It's a really good first study," says modeler Dominick Spracklen of the University of Leeds, U.K., but "the first attempt is always going to be uncertain. There's going to be debate."

Until now, the debate over cosmic rays and climate has dwelt more on wavy lines on graphs than on state-of-the-art global modeling. In 1997, physicists Henrik Svensmark and Eigil Friis-Christensen of the Technical University of Denmark in Copenhagen reported that the extent of Earth's cloud cover seemed to vary in step with galactic cosmic rays—high-energy charged particles from outer space—striking Earth's atmosphere. The more cosmic rays, the more cloud cover screened out the warming rays of the sun and counteracted greenhouse warming.

Such correlation does not prove causation, everyone agreed. Some experts disputed the existence of a correlation in the first place, and the consensus reports of the Intergovernmental Panel on Climate Change saw no substantial role for the sun in 20th century climate change. But debate rolled on, in part because researchers had been discussing a plausible physical mechanism since the 1950s. The sun's magnetic field fends off cosmic rays, they noted; lowered solar activity weakens that shield, increasing the flux of cosmic rays streaking into Earth's atmosphere. The cosmic rays ionize more gas molecules, which go on to form 1-nanometer-diameter particles that then grow to become the starter particles for cloud droplets, so-called cloud condensation nuclei (CCN). And the more cloud droplets, the denser and more pervasive the sun-shielding clouds.

Although this chain of causation no doubt exists, no one could say whether it is strong enough to make any difference in global climate. So modelers Jeffrey Pierce and Peter Adams of Carnegie Mellon University in Pittsburgh, Pennsylvania, simulated the chain in a global atmospheric computer model of the sort used to model climate. Their model also incorporated the relevant microscale physical processes, from gas ionization to CCN formation. They ran simulations with cosmic-ray fluxes typical of maxima and minima in the 11-year solar cycle, which also happened to approximate the 20% range of cosmic-ray variation across the 20th century.

As Pierce and Adams report in a paper in press in *Geophysical Research Letters*, their model showed that changes in cosmic rays are two orders of magnitude too feeble to cause

CREDIT: KEVIN DIETSCH/UPI/LANDOV

Published by AAAS

benchmark was the Apollo program of the 1960s, as the U.S. responded to the Soviet Union's launching of Sputnik. "That was the high-water mark of America's investment in research and development," Obama recalled, "… and it is time for us to lead once again."

One way to do that, he said, is to double the budgets for NSF, the Office of Science at the Department of Energy (DOE), and the National Institute of Standards and Technology as part of a boost in spending for the physical sciences. Another initiative would double spending on cancer research at the National Institutes of Health. He also made official his Administration's support for DOE's new Advanced Research Projects Agency-Energy, which was created in 2007 and received $400 million in the recent stimulus package.

Although he praised the president's overall message, Lennard Fisk, a former head of the academies' Space Studies Board and of NASA's science program, said it is ironic that Obama is invoking memories of the space race at the same time NASA, which needs billions of dollars more to carry out all the scientific missions on its books, isn't one of the agencies whose budgets the Administration has pledged to double. "What type of space program does he envision?" asked Fisk, an astrophysicist at the University of Michigan, Ann Arbor. "It was fine in its day, but we don't need another Apollo program."

The sole new effort unveiled by the president was a joint education initiative at NSF and DOE to stimulate interest in energy research. NSF Director Arden Bement said that the two agencies would be spending "hundreds of millions of dollars a year" on efforts to entice students to pursue careers in clean energy and to educate the public about the challenges of moving from fossil fuels to renewable sources of energy. The money will go for classroom and laboratory activities at levels ranging from elementary school through graduate training, as well as for informal education. Bement said the initiative, dubbed RE-ENERGYSE in a White House press release, will tap into the 2-year stimulus funding for NSF and DOE along with regular agency budgets in this and subsequent years. He said other agencies may also participate.

The biggest applause line of Obama's speech had nothing to do with money. But it is the reason why so many academy members have welcomed his election. Referring to the actions of his predecessor, Obama promised that "under this Administration, the days of science taking a back seat to ideology are over." Toward that end, he also announced the rest of the members of the President's Council of Advisors on Science and Technology (www.ostp.gov). The 20-member council, co-chaired by Holdren, Harold Varmus, and Eric Lander, wasted no time getting down to business, convening in private only minutes after Obama hit the road. **–JEFFREY MERVIS**

No response? Clouds in a model do not block more sunlight when cosmic rays increase.

CREDITS (TOP TO BOTTOM): CYTOGRAFT TISSUE ENGINEERING; GENTOOGEEK.ORG

the changes in clouds. "I'm feeling fairly confident that other models will also show the change in CCN is very weak," Pierce adds. "It's possible the models are missing something important; it just doesn't seem likely."

The reason cosmic-ray variations don't make themselves felt up the chain, at least in the model, seems to be the daunting matter of millionfold growth. Once a tiny amount of, say, sulfuric acid vapor condenses onto a cosmic-ray–induced ion to form a 1-nanometer particle, a million times more vapor must condense on it within its lifetime of less than a week before it grows large enough to trigger cloud drop formation. All the while, other growing particles are competing for the scarce vapor and gobbling up smaller particles that they collide with. Make only a few ion-nucleated particles, and they are not enough to matter; make a lot, and there's too little vapor to go around, so few particles grow large enough.

Other modelers have just started to run global simulations of atmospheric particle formation, provoking a range of reactions. "We see a very similar thing" in our model, says Jan Kazil of the University of Colorado, Boulder. "Cosmic-ray variations have only a small effect on the clouds in our model."

But Fangqun Yu of the University at Albany in New York says he disagrees with the Carnegie Mellon researchers "because of problems in their simulations." Among other problems, Yu suspects that in simulating only two rates of new particle formation via ionization—very high and much lower—Pierce and Adams may have missed a "sweet spot" production rate in between, at which just enough but not too many particles are produced. Testing the Goldilocks hypothesis will take more modeling and observations.

–RICHARD A. KERR

ScienceNOW.org

From *Science*'s Online Daily News Site

China Falls Short on Olympic Cleanup. The Chinese government went to great lengths to reduce air pollution in Beijing in advance of the Olympic Games. But a new analysis in *Geophysical Research Letters* suggests that the country achieved only mediocre results. The problem? Officials didn't take the weather into account. http://tinyurl.com/chjzyo

Artificial Blood Vessels Prove Effective. Scientists report in *The Lancet* that artificial blood vessels made using a person's own skin cells work well in patients receiving kidney dialysis. The new blood vessels mark the first vascular grafts to be derived entirely from a patient's own tissues, which lowers the odds of a harmful immune reaction. Down the road, engineered grafts may also prove useful in treating patients with circulatory problems in their legs and coronary arteries. http://tinyurl.com/d333v6

Presto, Instant Sunglasses! Researchers report in the *Journal of the American Chemical Society* that they have developed a material that almost instantaneously changes from clear to dark blue when exposed to ultraviolet light, and it just as quickly reverts to clear when the light is turned off. The new material, one of a class called photochromics, could be useful in optical data storage as well as in superfancy sunglasses. http://tinyurl.com/dj2x45

"Shall We Dance?" Pond scum may seem like a mass of ungraceful goop, but look closer: That gunk could be in the midst of an elegant minuet. According to new research in *Physical Review Letters*, tiny colonies of the common algae *Volvox* can whirl each other around for hours like ballroom dancers, driven by the rhythm of tiny, tail-like structures called flagella. The findings could shed light on how interaction between primitive organisms evolved. http://tinyurl.com/djrme4

Read the full postings, comments, and more on **sciencenow.sciencemag.org**.

Published by AAAS

Dino score. *Brachylophosaurus* is preserved as more than stone, if new analysis is correct.

PALEONTOLOGY

'Protein' in 80-Million-Year-Old Fossil Bolsters Controversial *T. rex* Claim

A controversial finding that protein fragments can be recovered from dinosaur fossils has been replicated for the first time. Two years ago, Mary Schweitzer, a paleontologist at North Carolina State University in Raleigh, and colleagues stunned the paleontology community when they reported discovering intact protein fragments in a fossil from a *Tyrannosaurus rex* that died 68 million years ago. The claim has remained contentious, because proteins in tissue normally degrade quickly after an animal dies. On page 626, however, Schweitzer and colleagues report finding an even larger number of protein fragments from an 80-million-year-old fossil from a duck-billed dinosaur, or hadrosaur, known as *Brachylophosaurus canadensis*.

"This will either be nothing or the biggest revolution in paleontology ever," says Tom Kaye, a paleontologist at the Burke Museum in Seattle, Washington, and a critic of the original *T. rex* study. If the finding holds up, agrees Matthew Collins, an archaeologist and protein mass spectrometry expert at the University of York in the United Kingdom, "that would transform the way we do paleontology," turning it into a discipline like genetics and molecular biology, built on molecular data.

Similar hopes followed the original *T. rex* study. That paper (*Science*, 13 April 2007, p. 280) reported recovering collagen from a *T. rex* fossil unearthed in Montana and from a fossilized mastodon as much as 600,000 years old. Collagen, the principal protein in connective tissue, is rarely found in fossils more than a few hundred thousand years old. The paper reported that antibodies to collagen bound to the recovered material that had been chemically stripped of its minerals to leave behind what appeared to be soft tissue. When this material was run through a mass spectrometer, which identifies the sequence of amino acids in protein fragments, the sequences resembled those in collagen from birds, supporting fossil evidence that birds are descended from dinosaurs.

Outsiders, however, raised several concerns. At the top of the list was the mass spectrometry data. The technique chops proteins into small snippets and then weighs them. By comparing the masses with those of known protein fragments, researchers can work out the amino acid sequences in the original protein fragments. But for some fragments in the samples, the mass signature was barely visible above the noise, lowering the statistical confidence in their proper identification. Kaye also suggested in July 2008 in *PloS ONE* that the proteins could have come from bacterial contamination (*Science*, 1 August 2008, p. 623).

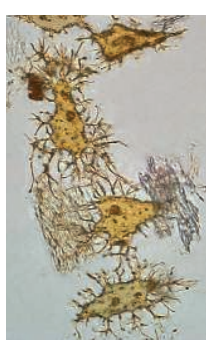

Real thing? Material from fossil resembles bone cells.

In a pair of technical comments in *Science*, Schweitzer and John Asara, a mass spectrometrist at Harvard Medical School (HMS) in Boston who was part of Schweitzer's team, defended the mass spec results and laid out a further case for why they thought the fossil proteins weren't from bacterial contaminants. They also posted all of their mass spec data in a public database, after critics complained that they couldn't evaluate the data without access to the complete data set. "It has been a stressful time," says Schweitzer of the back and forth.

But Schweitzer has welcomed the skepticism. Last November, she invited about a dozen of her staunchest critics to a meeting in Raleigh to go over the latest data. "Everyone discussed the ideas," says Collins. "But at the end of the meeting, there were still the skeptics" calling for more control studies, independent verification, and better mass spec results, Collins says.

The new paper "did a pretty good job in addressing the issues raised previously," says William Stetler-Stevenson, a biochemist who specializes in studying proteins such as collagen, laminin, and elastin that are found in the extracellular matrix and bone, and who is not affiliated with Schweitzer's collaboration. For starters, Schweitzer's team went to great lengths to avoid contamination, says Martin McIntosh, a biostatistician at the Fred Hutchinson Cancer Research Center in Seattle, Washington, and critic of the original *T. rex* paper. During excavation, the researchers used sterilized instruments to expose the bone and immediately placed their samples in sealed jars.

Schweitzer then took some of the samples back to her lab and used chemicals to dissolve away the minerals, leaving behind what looks like a network of soft, transparent vessels, cells, and extracellular matrix. Other bone samples were sent to Raghu Kalluri, a biochemist at HMS, who carried out his own demineralization procedure and analysis. Both groups then independently performed biochemical and antibody-binding studies that showed evidence of collagen as well as laminin and elastin, two proteins found in blood vessels.

Schweitzer also sent some of her demineralized extracts to Asara, who further processed them and tested them on a mass spectrometer more sensitive than the one used for the *T. rex* study. Asara's group identified eight collagen fragments. Asara sent some of the processed material to William Lane, another mass spec expert at Harvard University, who confirmed the presence of three of the collagen fragments. A later analysis of the purported hadrosaur collagen sequences found them more closely related to the samples from *T. rex* and to collagen from birds than to collagen from reptiles or other organisms.

"This proves the first [*T. rex*] study was not a one-hit wonder," Asara says. Perhaps, McIntosh says. "I'm not saying it's true. But I cannot right now make a plausible argument that it's not true." He adds: "The door is closing on plausible alternatives."

–ROBERT F. SERVICE

CREDITS (TOP TO BOTTOM): © JULIUS T. CSOTONYI (CSOTONYI.COM), "LEONARDO" ™ GREAT PLAINS DINOSAUR MUSEUM; MARY HIGBY SCHWEITZER (NCSU, MEAS) AND ZHIYONG SUO (MSU, ICAL)

Published by AAAS

CONFLICTS OF INTEREST

IOM Panel Backs Public Disclosure Of Drug Company Payments

The best way to damp down concerns about doctors' and researchers' financial conflicts of interest is to require full disclosure, according to an expert report that adds its voice to a growing chorus. A panel of the National Academies' Institute of Medicine (IOM) says faculty members at medical institutions should be required to report all industry money they receive from outside their institution—no matter how small the amount—to special committees that would keep track of the data and manage conflicts. Such payments would also have to be reported publicly by the companies.

"If [institutions] don't get their act together, they're really inviting the legislators to step in."

—BERNARD LO, UCSF

The policy recommended by IOM would be far more intrusive than current U.S. rules, which require National Institutes of Health (NIH) grantees to report to their own institutions outside income of more than $10,000 per year. But IOM's mostly voluntary plan has an important selling point, some say: It could head off more-intrusive federal regulations.

Panel members agreed that some action is called for. "Many relationships between researchers and industry are very constructive, but it has to be overseen and kept in bounds," says panel chair Bernard Lo, a bioethicist at the University of California, San Francisco (UCSF).

IOM decided to undertake the study 2 years ago amid growing concerns that academic researchers who took drug company payments were withholding data from publication or otherwise biasing results. (Funding for the study came from NIH, IOM, and several foundations.) Similar concerns resulted in a ban on all such payments to intramural scientists at NIH, Lo notes. More recently, as part of an ongoing investigation, Senator Chuck Grassley (R–IA) has identified several psychiatrists who allegedly failed to disclose hundreds of thousands of dollars in consulting income.

Disclosure is "a critical but limited first step" toward addressing conflicts of interest, the IOM panel concludes.* It urges research and physician organizations to develop a standard reporting format. And it endorses a proposal similar to one from Grassley to require that drug and device companies report payments to physicians in a public database. Companies should also disclose money given to institutions, scientific societies, patient groups, and basic researchers, the report says, because their work can lead to clinical trials.

Three of the 17 panel members recommended that physicians and researchers themselves also be required to publicly report their financial ties with companies, including stock. But the others disagreed partly because they felt it would be expensive, could intrude on privacy, and would not add much to the company database.

As a rule, the report says, institutions should ensure that if a significant conflict exists, a researcher "may not conduct research with human participants" unless his or her role is essential to the research. The report also recommends that institutions ban faculty members from accepting drug company gifts, serving as a spokesperson for a company, and authoring articles ghostwritten by industry.

Many of these steps have been recommended in past reports from the Association of American Medical Colleges (AAMC), which has also endorsed the company payments database. But not all schools have followed AAMC's advice. "We give a pretty clear warning," Lo says. "If the [institutions] don't get their act together, they're really inviting the legislators to step in. That, he warns, could lead to "very, very blunt" regulations and "a risk that valuable relationships will be curtailed in ways that will hurt patients."

–JOCELYN KAISER

*Conflicts of Interest in Medical Research, Education, and Practice, National Academies, www.iom.edu/CMS/3740/47464/65721.aspx

CREDIT: COURTESY OF UNIVERSITY OF CALIFORNIA, SAN FRANCISCO

ScienceInsider

From the *Science* Policy Blog

The Department of Health and Human Services (HHS) has decided to maintain **limits on travel** by National Institutes of Health (NIH) staff established during the Bush Administration. Scientists at the Bethesda, Maryland, NIH campus are unhappy about the continued restrictions, which HHS brass say are needed because of tight budgets. "We should be allowed to spend our money the way we think is best," says Samuel Cushman, a 30-year NIH veteran. The limits come as NIH rushes to spend more than $10 billion in stimulus funding, the majority of which will go to research grants and construction.

Astronauts, lawyers, and scientists met last week at the University of Nebraska to begin to hash out an international framework for dealing with **asteroids heading toward Earth**. One proposal under consideration was a body that would advise the United Nations on threats.

British scientists who had been hoping for a £1 billion stimulus were disappointed when there was no increase for research in the **U.K. government's new budget** announced last week. Researchers have been hoping for one along the lines of the $21 billion boost U.S. scientists have received. The budget did feature a bonanza of climate-related funding increases, however, in keeping with the government's commitment to reduce greenhouse gas emissions, including £525 million for offshore wind projects, £435 million for energy efficiency, and £405 million to encourage low-carbon energy and advanced green manufacturing.

Elsewhere … A new tally of **Iraqi deaths** during the Iraq war by that nation's government puts the figure at 87,215. That deepens questions about a 2006 *Lancet* study that estimated the number at roughly 600,000. … The U.S. Smithsonian National Museum of American History is highlighting **Lincoln's scientific bona fides** as part of an exhibit marking the president's 200th birthday.

For the full postings and more, go to **blogs.sciencemag.org/scienceinsider.**

Published by AAAS

On the Origin of The Immune System

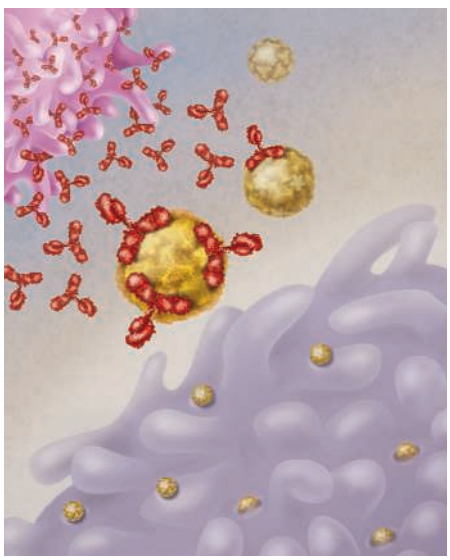

IT WAS A DRAMATIC MOMENT IN THE MOST dramatic confrontation so far between science educators and scientists determined to keep evolution in the classroom and advocates of the quasi-religious theory known as intelligent design (ID). In 2005, Lehigh University biochemist Michael Behe sat on a witness stand in Dover, Pennsylvania, as lawyer Eric Rothschild quizzed him about the claim in Behe's pro-ID book, *Darwin's Black Box*, that "We can look high or we can look low in books or in journals, but the result is the same. The scientific literature has no answers to the question of the origin of the immune system."

When Behe reiterated that belief, Rothschild was ready. He began piling in front of the witness a large stack of recent journal articles, books, and book chapters, all relating research on the evolutionary origins of immunity, and asking Behe several times what he thought about the various publications. The biochemist admitted that he hadn't read much of the material, but he wouldn't budge from his position.

"So these are not good enough?" Rothschild asked at one point.

"They're wonderful articles. … They simply just don't address the question that I pose," Behe responded.

The judge, John E. Jones, found Behe's responses revealing. Behe "was presented with 58 peer-reviewed publications, nine books, and several immunology textbook chapters about the evolution of the immune system; however, he simply insisted that this was still not sufficient evidence of evolution," the judge wrote in his decision. Jones concluded that ID proponents set "a scientifically unreasonable burden of proof for the theory of evolution." Score one for evolution, which is now taught without competition from ID in Dover schools.

It is fitting that studies of the origins of immunity provided a strong defense for the ideas first set forth by Charles Darwin 150 years ago. Darwin's elaboration of diversification and natural selection as organizing principles of life inspired early immunologists, helping them see that humans and pathogens are locked in their own survival-of-the-fittest battle. His theory also helped researchers realize that some of our immune defenses depend on a system of diversity coupled with selection among proteins.

As this newfound evolutionary mindset shaped immunological thinking near the turn of the 19th century, researchers also began to speculate about how our complex system of defenses arose. After decades of research, modern immunologists now think that single-celled organisms must have started by harnessing toxic peptides and gene-disabling molecules to thwart invading microbes—these weapons are still found in the simplest eukaryotes and more complex animals. And then when multicellular creatures evolved, they were able to devote specialized cells to tasks such as engulfing bacteria and viruses.

Today, an ancient set of defensive mechanisms based upon protein receptors that recognize common features of dangerous pathogens has become hard-wired into the genome of every animal. (Plants have their own, parallel system.) Considered the first line of defense in animals, this "innate" immunity involves cells and molecules that rush to the site of an infection. Comparative studies of earthworms, sea squirts, sponges, and more suggest that this inflammatory response dates back to the origin of multicellularity.

In what has been called the "big bang of immunology," most vertebrates later evolved a second form of immunity, in which white blood cells exquisitely targeted to a specific pathogen are rallied and then maintained in the body as an immune memory. This "adaptive" arm seemed to have appeared out of nowhere some 450 million years ago and may be the serendipitous outcome of invading DNA introduced by a virus or microbe infecting a fishlike creature.

It may seem ironic that an infectious agent endowed vertebrates with the keys to a new microbial defense, but it illustrates that microbes have shaped the evolution of animals for millennia. Indeed, a few researchers now suggest that immune systems evolved as much to manage and exploit beneficial microbes as to fend off nasty ones. "It's a paradigm shift in immunology," says Thomas Bosch of Christian Albrechts University Kiel in Germany. Finding proof for such a radical change in thinking will be challenging, but scientists should soon have a more detailed view of immune evolution as they decipher the genomes of more invertebrates and vertebrates and tally up the defensive weapons shared by the various branches of life.

Darwinian immunology

It was only shortly after *On the Origin of Species* was published in 1859 that infectious diseases were discovered and became a compelling example of a Darwinian struggle—humans pitted against pathogens—notes science historian Alfred Tauber of Boston University. To understand that contest, immunology emerged in the late 19th century as the science of host defense. Soon, scientists were fighting over the importance of two competing defense mechanisms: the humoral system of antibodies in the blood versus mobile amoebalike cells known as phagocytes. German biologist Paul Ehrlich and others championed the former; Russian Elie Metchnikoff, an embryologist, lobbied for the latter.

Darwin's ideas permeated Metchnikoff's formulation, says Tauber. The Russian maintained that phagocytes evolved first as nutritive cells—eating and delivering food to cells in animals without a gut—and were eventually enlisted to eat deleterious bacteria as well. In 1882, he observed that phagocytes within a starfish enveloped and digested foreign bodies, including bacteria.

As the field of immunology matured, it embraced both Metchnikoff and the humoralists, as researchers realized that the phagocytes complemented the defense offered by blood factors.

THE YEAR OF DARWIN

This essay is the fifth in a monthly series. For more on evolutionary topics online, see the Origins blog at **blogs.sciencemag.org/origins.** For more on the immune system, listen to a podcast by author John Travis at **www.sciencemag.org/multimedia/podcast.**

CREDITS (TOP TO BOTTOM): KATHARINE SUTLIFF/*SCIENCE*; WIKIPEDIA/GEORGE RICHMOD, FROM ORIGINS, RICHARD LEAKEY AND ROBERT LEWIN

Published by AAAS

In 1908, the embryologist even shared a Nobel Prize with Ehrlich.

A half-century later, another major intellectual advance within immunology bore the fingerprints of Darwin. Darwin's theory of evolution held that a large amount of variation exists among individuals in a species and that species can adapt to new circumstances because evolution weeds out the less fit, favoring variants that improve reproduction and survival. Immunologist Frank Macfarlane Burnet drew heavily on this concept in developing his theory about how the body forms its antibodies, the pathogen-binding molecules secreted by lymphocytes called B cells, according to science historian Arthur Silverstein of Johns Hopkins University School of Medicine in Baltimore, Maryland.

While other immunologists focused on how antibodies might evolve to better target a pathogen, undergoing their own kind of natural selection, Burnet proposed that the lymphocyte was the key evolutionary player being selected within the body. Those white blood cells making antibodies that react to the body's own tissues would be deleted, whereas one whose antibodies recognized a pathogen would survive and indeed be stimulated to expand greatly in number.

"It is a Darwinian theory," notes Tauber. "You have enormous variation and then selection." This process, what Burnet called clonal selection, lets the body tailor its response to a particular pathogen. Moreover, some of the selected lymphocytes stick around, providing a "memory" that helps the immune system thwart the same invader even faster if it comes again.

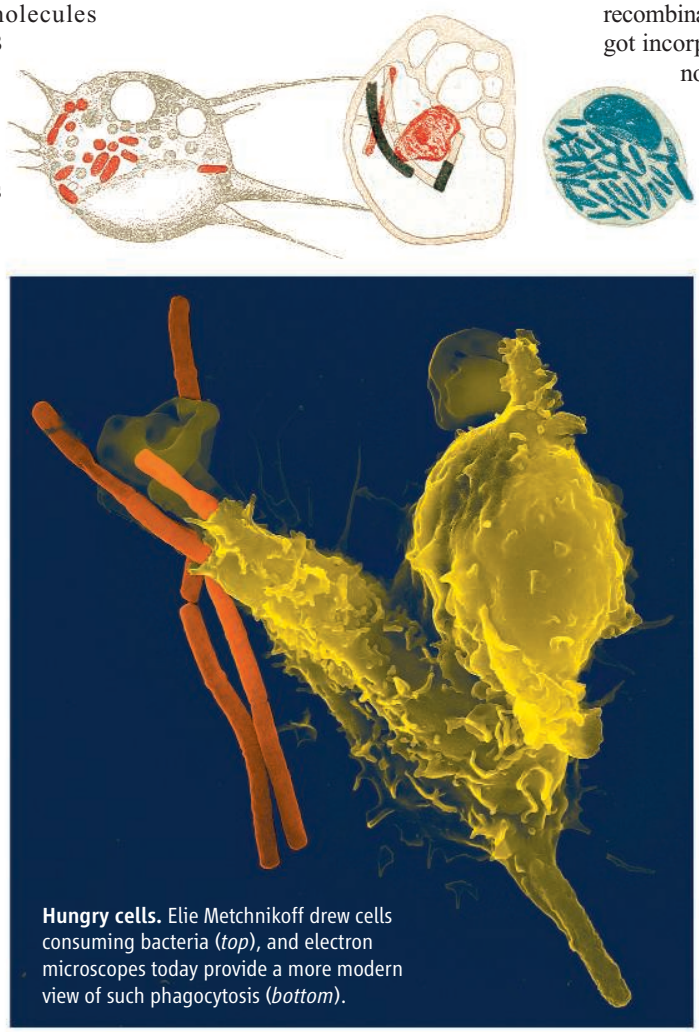

Hungry cells. Elie Metchnikoff drew cells consuming bacteria (*top*), and electron microscopes today provide a more modern view of such phagocytosis (*bottom*).

CREDITS (TOP TO BOTTOM): E. METCHNIKOFF/IMMUNITÄT BEI INFEKTIONSKRANKHEITEN (VERLAG VON GUSTAV FISCHER, JENA, 1902)/S. H. E. KAUFMAN, MAX PLANCK INSTITUTE FOR INFECTION BIOLOGY, BERLIN; V. BRINKMANN, *PLOS PATHOGENS*, 1(3), NOVEMBER 2005

Understanding the big bang

Clonal selection theory didn't answer all the mysteries about antibody formation. Although Burnet's idea assumed a large variation in preexisting antibodies, immunologists in the 1960s and '70s realized that animals could generate distinct antibodies to almost any protein or other molecular feature of a microbe. In fact, the vertebrate immune system could raise antibodies specific even to humanmade molecules not found in nature. Given the prevailing dogma that behind every protein there was a specific gene, immunologists were at a loss to explain this phenomenon, which became known as the generation of diversity, or GOD, problem.

In the late 1970s, in work that would earn him a Nobel Prize, Susumu Tonegawa of the Massachusetts Institute of Technology in Cambridge demonstrated that B cells can produce such a vast array of antibodies thanks to a complicated process called VDJ recombination. A maturing B cell starts with dozens to hundreds of three classes of gene segments—the V's, D's, and J's—and as it develops, the cell excises all but one of each class. The surviving V, D, and J then get stitched together into a DNA sequence that encodes an antibody unique to each mature B cell. (The other key player in the adaptive system, the T cell, also bypasses the one gene–one protein hurdle and similarly recombines gene segments to create distinct cell-surface receptors for pathogens.)

The elucidation of VDJ recombination gradually exposed immunology's big bang, recalls David Schatz of the Yale School of Medicine. By 1990, he and other colleagues then working in David Baltimore's lab at the Whitehead Institute for Biomedical Research in Cambridge had identified two genes essential to VDJ recombination, *RAG1* and *RAG2* (for recombination-activating genes). Sharks and all the other jawed vertebrates with adaptive immunity have these genes, but all the evidence at the time indicated that hagfish, lampreys, and invertebrates didn't. So, where did *RAG1* and *RAG2* come from?

Several clues, including that the two genes are located immediately next to each other, prompted Schatz and his colleagues to wonder whether the pair had once been part of a DNA recombination system in fungi or viruses that got incorporated into vertebrates. As immunologists teased out what the proteins encoded by the two did, they realized the molecules are the scissors and knitting needles that cut out all but one V, D, and J and stitch those remaining three gene segments together.

In 1995, Craig Thompson, then at the University of Chicago in Illinois, formally proposed that the DNA now encoding *RAG1* and *RAG2* was once a mobile genetic element called a transposon. Transposons can cut themselves out of one DNA sequence and stick themselves back in another, so immunologists could envision those skills being co-opted to recombine V, D, and J gene segments. In this "transposon hypothesis," Thompson suggested that at some point after jawed and jawless vertebrates split into two branches, about 450 million years ago, a transposon invaded the former lineage, perhaps brought in by a virus that infected a germ cell. Boom—the enzymes that would ultimately provide adaptive immunity, by creating diverse antibodies and T cell receptors, were now in place and could mutate into that new role.

Many research teams began trying to verify the transposon hypothesis. In 1998, for example, Schatz's team and one led by Martin Gellert of the National Institute of Diabetes and Digestive and Kidney Diseases in Bethesda, Maryland, independently showed that the enzymes encoded by *RAG1* and *RAG2* could, in addition to cutting out DNA sequences, actually insert one stretch of DNA into another. In a commentary in *Nature*, immunologist Ronald Plasterk of the Netherlands Cancer Institute in Amsterdam expressed the awe of many at this solid evi-

Published by AAAS

dence of the transposon hypothesis. "We may owe our existence to one transposition event that occurred 450 million years ago," he wrote.

At the Dover trial, much of the research literature piled in front of Behe detailed the increasing evidence for this transposon hypothesis. Although those papers satisfied the judge and show why the hypothesis is widely accepted, a major surprise since the Dover verdict suggests that this transposon invasion took place even earlier.

In 2006, a team led by Jonathan Rast of the University of Toronto in Canada and Sebastian Fugmann of the National Institute on Aging in Bethesda, Maryland, analyzed the genome of the purple sea urchin and found genes that closely resemble *RAG1* and *RAG2*, the first time they've been uncovered in invertebrates. Their existence in the urchin suggests that the transposon with these enzymes invaded animals far earlier than had been thought but was lost in most lineages except for jawed vertebrates, which adapted them to perform VDJ recombination. That's an easier version of the story for some immunologists to swallow, as it allows more time for mutations to deactivate the jumping ability of a transposon and convert its DNA to a new job. "There was never a big bang of immunology," suggests Bosch.

Thompson and others aren't so ready to defuse the explosive hypothesis, however. The *RAG1-RAG2* transposon may have entered sea urchins and vertebrates independently, they stress. The role of *RAG1* and *RAG2* in sea urchins remains unknown, and Rast agrees that the timing of the transposon invasion responsible for adaptive immunity won't be nailed down until more invertebrate genomes are deciphered over the next few years. "The basic idea of an immune 'big bang' in the vertebrates has led to a variety of oversimplifications and conceptual problems," says Rast. "Whatever the actual evolutionary pathway that led to the very complex vertebrate adaptive system, it was surely a gradual progression that co-opted many preexisting immune mechanisms."

First line of defense

Researchers have also made progress understanding the origins of innate immunity, encouraged by the recent appreciation that these defenses can be as sophisticated and effective as the adaptive arm. After all, about 90% of animal species have no adaptive immunity, yet they thrive, with many living for decades, in a world of microbes.

At the heart of this protection are proteins, called Toll-like receptors (TLRs), on cells of the innate immune system. Over the past decade, it has become clear that TLRs are the long-sought cell-surface receptors that recognize common microbial features such as bacterial wall components or the distinctive DNA sequences of a virus. This role could date back to the earliest multicellular organisms, as humans and some of the most evolutionarily primitive animals share TLRs and the molecules involved in the TLR signaling cascade.

> "Whatever the actual evolutionary pathway that led to the very complex vertebrate adaptive [immune] system, it was surely a gradual progression that co-opted many preexisting immune mechanisms."
>
> —Jonathan Rast, University of Toronto

The sea urchin genome revealed more than 200 TLR genes, for example, and in 2006, a group headed by Werner E. G. Müller of the University of Mainz in Germany reported that sponges also encode these microbial sensors. And plant disease-resistance proteins that recognize bacteria, viruses, and fungi include portions that structurally resemble TLRs, hinting that ancestors of these microbial sensors were on patrol long before plants and animals diverged.

As additional genomes reveal their secrets, evolutionary biologists should ultimately sort out which creatures have which immune molecules. Making sense of that data may demand conceptual breakthroughs in understanding the purpose of our immune defenses. Many immunologists accustomed to studying people, mammals, or other vertebrates assume that the adaptive immune system emerged because it allowed these more complex animals to deal with more complex microbial threats. And Thompson, now scientific director at the Abramson Family Cancer Research Institute in Philadelphia, Pennsylvania, thinks the key advantage is that the adaptive response conserves scarce resources by quickly fine-tuning the otherwise all-out assault mounted by the innate immune system. "Specificity gives you the advantage of being able to use the least amount of an immune system," he says.

Still, some invertebrate biologists aren't convinced that their colleagues have nailed down the selective advantage of the adaptive immune system. "It's very hard to say what is the benefit," says Bosch. He predicts one important line of future inquiry in the evolutionary study of immunology will be how immune systems have helped organisms adapt to their specific environments or ecological niches.

Bosch also cites the growing realization that animals harbor within their bodies a world of microbes that are crucial to development, nutrition, and more; by some estimates, humans are 90% bacterial cells. Immunologists, says Bosch, need to shift their thinking "from bacteria make you sick to bacteria make you healthy." Such a shift may ultimately force a reconsideration of the roots of the immune system. Did the innate and adaptive arms truly evolve to keep out harmful organisms? Or instead, are one or both more like bouncers at a nightclub, honed for the more subtle task of allowing the right microbes in and kicking the less desirable ones out? If another evolution-versus-ID trial ever takes place, biologists addressing this provocative question will no doubt have added to the impressive stack of literature on how our immune system arose. **–JOHN TRAVIS**

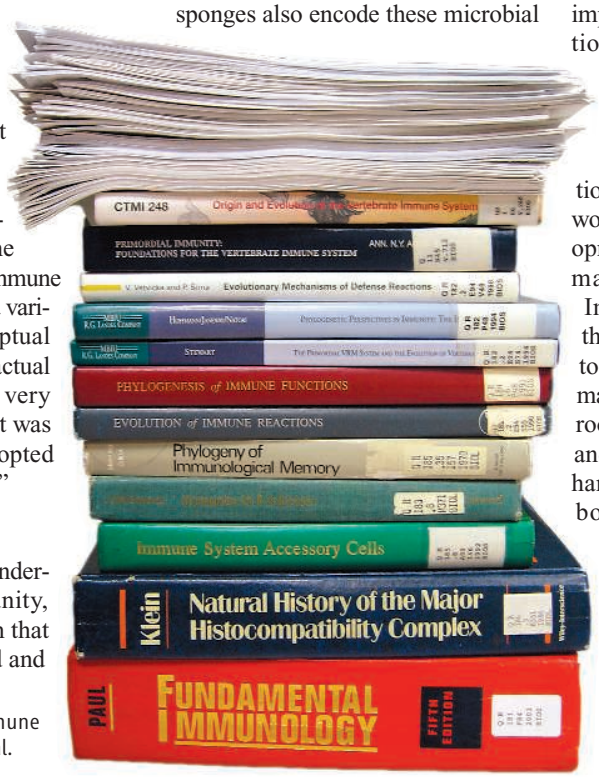

Exhibit A. This stack of evolutionary immune research literature was used in the Dover trial.

CREDIT: NICK MATZKE/NATIONAL CENTER FOR SCIENCE EDUCATION

Published by AAAS

CREDIT: PHOTO COURTESY OF GENENTECH

Minister of culture. Richard Scheller says he can preserve Genentech's culture of innovation under Roche.

NEWSMAKER INTERVIEW

Defying Skeptics, Richard Scheller Thinks Genentech Will Thrive

At the end of March, Swiss drugmaker Roche achieved its long-sought acquisition of Genentech, the pioneering biotechnology company in South San Francisco, California. Long before the deal was official, biotech analysts, former Genentech employees, and others bemoaned what they saw as the end of an era. Surely the buttoned-down pharmaceutical behemoth would crush the famously innovative culture at Genentech, where scientists have relished their freedom to pursue pet projects in basic science and the laid-back work environment, which among other niceties features Friday night "hohos," or keg parties. People inside and outside Genentech credit its culture for its success as the first biotech company (it was founded in 1976) and one of the most profitable.

Richard Scheller, Genentech's new executive vice president for research and early development, says his number-one job is to prove the naysayers wrong. He will run Genentech as an independent research center, Roche announced on 14 April. Formerly a neuroscientist at Stanford University in Palo Alto, California, Scheller joined Genentech in 2001 and served as its executive vice president for research and chief scientific officer prior to the merger. Finally allowed to speak publicly, he spoke with *Science* last week about what the merger will (and mostly won't) mean for research at Genentech. His comments have been edited for brevity. **–GREG MILLER**

Q: Can you explain how Genentech will operate independently?

R.S.: I will report directly to the CEO of Roche and will operate independently here in South San Francisco a group of folks who do the research and clinical trials through phase II. We have complete decision-making authority over which projects we work on, how long we work on them, when to propose to move them forward, et cetera. The idea is, we'll be able to maintain the independence we had when Genentech was a publicly traded company.

Q: Are you saying nothing will change?

R.S.: No. If anything, now that phase I and II clinical development will also report to me, I think the research group will be even closer to the earlier stages of clinical development, which is absolutely critical. The first stages of clinical development are really more like basic science, attempting to obtain proof of concept for your hypothesis in man. [In] phase III, you're attempting to replicate the data on a larger number of patients. That's more of a logistical task. That part is best left to the global Roche development group. Our goal will be to hand them molecules that are ready for this final stage of clinical development.

Q: Many people saw Arthur Levinson as personifying the science-first culture of Genentech. What will be the impact of his departure as Genentech CEO?

R.S.: Art will remain on our scientific advisory board. He will come to research-review meetings. He will be chair of the board of Genentech. Art will still have a strong presence here, but he will not have the role [in daily operations] he had as CEO.

Q: How do you plan to maintain the famous Genentech culture?

R.S.: By making sure that scientists continue to have time to work on their own projects that aren't translational, that aren't governed in any specific way, and that scientists have time to think and imagine and invent, not just do routine things.

Q: Is that all there is to it?

R.S.: Coming up with a compensation system that's motivating to employees will be extremely important. And the ability to publish. The ability for scientists to develop their own international reputation, where they're not prevented from publishing or they only publish in the patent literature, for example, is something that will continue. We will continue to have a postdoc program. We have 120 postdocs at Genentech. The goal is for people to come and do interesting science and publish papers. There's no requirement that any of the work be translational. That keeps young and exciting people coming in to Genentech.

Q: Will the merger affect your ability to attract and retain top talent?

R.S.: I hope not. Time will tell. Since the bid for the merger was announced, Morgan Sheng joined us from MIT [Massachusetts Institute of Technology]. Morgan knew the bid would likely be successful and still decided to leave his position as a professor at MIT and a Howard Hughes investigator to move across the country to run neuroscience for Genentech. I think that's a pretty good sign.

Q: Why the push in neuroscience when so many disorders have proven frustratingly difficult to treat?

R.S.: It's a little bit ironic. When I came to Genentech, all work in neuroscience [here] was … being dismantled. I didn't believe at the time there was enough insight into the cellular and molecular basis of neurological disorders … to make an impact there. Two things have happened: Now we have a world-class small-molecule drug-discovery group. And we've learned enough about neuroscience—from finishing the genome to all that we've learned about ion channels and signal transduction and development—to think more rationally about diseases. It's not going to be easy, but in our opinion, it's time to get really, really serious about neuroscience.

Published by AAAS

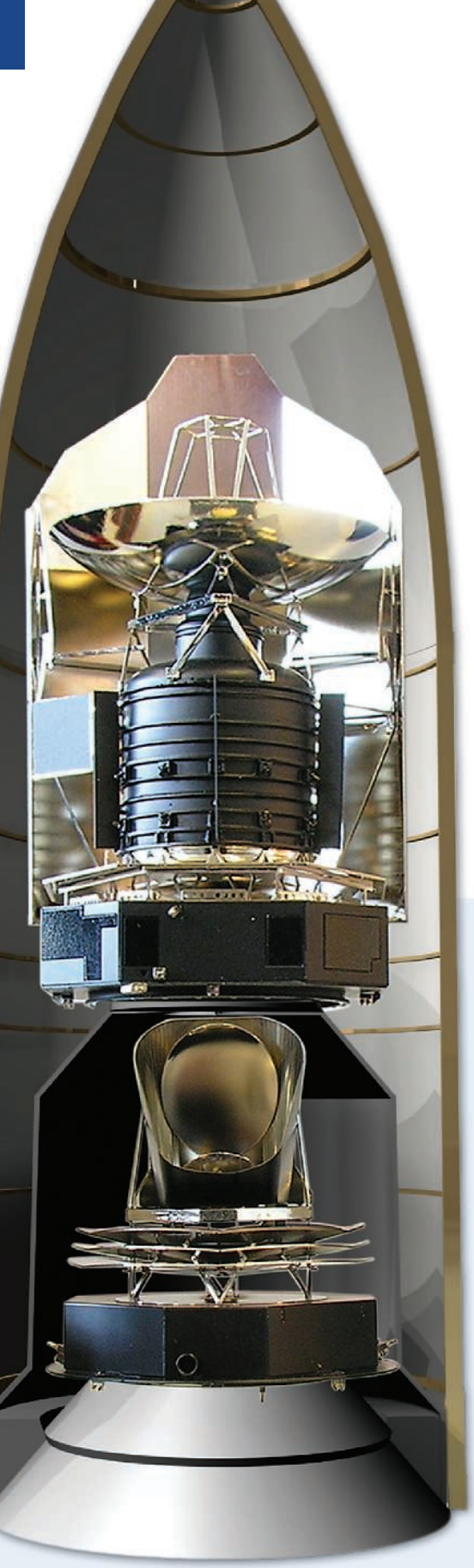

Bunkmates. Named for astronomer William Herschel, the Herschel telescope will ride atop the Planck satellite, named for physicist Max Planck.

CREDIT: ESA/GUARNIERO

ASTRONOMY

Herschel Will Open a New Vista On Infant Stars and Galaxies …

With the biggest mirror yet flown in space, Europe's new observatory will peer through a new wavelength window at the cool regions of the universe

Over the years, astronomers have scoured most of the electromagnetic spectrum, from long-wavelength radio waves to very high-energy gamma rays, for information about the universe and its denizens. Later this month, Europe's Herschel Space Observatory will start to fill one of the remaining gaps: a region of the far infrared and submillimeter radiation with wavelengths between 200 and 850 micrometers. Researchers are keen to peer through this unseen window because they hope to see stars and galaxies in their formative years, periods during which they are obscured by gas and dust at other wavelengths. "Herschel gives us a picture of the cold universe, the dusty universe. Galaxy and star formation generate most energy here," says astrophysicist Michael Rowan-Robinson of Imperial College London.

For the first part of its journey into space, Herschel will have company. The European Space Agency (ESA) will launch the €1 billion observatory together with Planck—a mission to map the cosmic microwave background radiation in unprecedented detail (see below)—on board a European Ariane 5 rocket. Although their scientific missions are very different, the two probes were managed as a single project by the same industrial team and have similar final destinations, around the Lagrangian point L2.

Lagrangian points are gravitational wells in the sun-Earth system. L2 lies on the night side of Earth, 1.5 million kilometers farther from the sun—a place far from interfering signals from Earth, where spacecraft can hover without using too much fuel (see figure, p. 585). Planck will settle into an orbit around L2 roughly 2 months after launch; Herschel will arrive more than a month later and take up a wider orbit. "It's an ingenious place to put such missions," says Rowan-Robinson.

…While Planck Dusts the Skies For the Fingerprints of Inflation

The newborn universe supposedly expanded faster than the speed of light. The Planck satellite might prove it

The big bang: The universe bursts into existence, an infinitely dense and hot soup of subatomic particles and radiation. In a fraction of a nanosecond, it doubles its size again and again, in a faster-than-light growth spurt known as inflation. That bizarre, hypothetical stretching evens out the universe but also sets off ripples in space and time called gravitational waves, which 13.7 billion years later should have left traces in the afterglow of the big bang, the cosmic microwave background (CMB). The 400 researchers working with the European Space Agency's (ESA's) Planck satellite hope to spot those traces—subtle patterns in the polarization of the microwaves called "B modes"—before anyone else does.

"The next Nobel Prize [for CMB studies] will go to the experiment that detects these modes," predicts Nazzareno Mandolesi, a Planck team member from the Institute of Spatial Astrophysics and Physical Cosmology in Bologna, Italy. "That will prove without a doubt that inflation happened."

The CMB has been a scientific treasure trove. Its accidental discovery in 1964 bolstered the then-controversial notion of the big bang and netted a Nobel Prize 14 years later. In 1992, NASA's Cosmic Background Explorer (COBE) spacecraft measured the spectrum of the microwaves and from its shape confirmed that the universe emerged in a single instant. COBE also detected tiny variations in the radiation's temperature across the sky. Those advances won a Nobel in 2006.

Sixteen years in the planning, the €700 million Planck satellite will be the third to study the CMB. The second was NASA's Wilkinson Microwave Anisotropy Probe (WMAP), which in 2003 charted in detail the temperature variations COBE had glimpsed.

Published by AAAS

Astronomers studying infrared and submillimeter wavelengths have a tough time: Earth's atmosphere blocks such photons, and warm objects emit infrared radiation that swamps astronomical signals. Scientists have had some success putting telescopes in very high, dry places, but the real breakthrough came with the Infrared Astronomical Satellite, launched in 1983. ESA's Infrared Space Observatory followed in 1995, and then NASA's Spitzer Space Telescope in 2003 and Japan's AKARI in 2006.

"These were extremely powerful and successful missions, but they were limited by the need to have very cold instruments and telescopes," says Matt Griffin of the University of Wales, Cardiff, a principal investigator of one of Herschel's detectors. To damp down infrared signals from the spacecraft, those probes used liquid helium to cool their detectors and mirrors. But it takes a lot of helium to cool a large mirror, and it is heavy stuff to loft into space. Hence, none of the earlier missions had mirrors larger than 1 meter, a limitation that restricted their ability to resolve distant objects.

"Herschel is a different kind of mission," says Rowan-Robinson. Its wavelength range of 60 to 670 micrometers covers much of the gap between earlier infrared missions (up to about 200 micrometers) and ground-based submillimeter telescopes (850 micrometers and above). Not only is Herschel venturing into unexplored terrain, but it also carries the biggest mirror yet to fly in space, 3.5 meters across. To make such a size work, "we had to take the mirror out of the cryostat," says Göran Pilbratt, ESA's project scientist for Herschel. Once that was done, "we were constrained by the size of the rocket," he says. The huge reflector boosts angular resolution and sensitivity, allowing Herschel to see fainter objects, but leaving it at the slightly warmer ambient temperature of space adds noise. "Most of the power falling on the detectors comes from the telescope, not the sky," says Pilbratt, and this signal has to be removed in later processing.

Herschel had a long gestation. The idea for such a mission arose in a workshop on submillimeter astronomy in 1982. When ESA announced a call for proposals for its Horizon 2000 science program later that year, some participants in the workshop put together a proposal. By 1986, the mission, then known as the Far Infrared Space Telescope (FIRST), was selected as one of Horizon 2000's four cornerstone projects, but it was the last of the four. ESA's science directorate, with a limited budget, had to work through three other large and complex missions before Herschel got its chance. "We had an opportunity to develop our instruments and get better detectors. They improved by an order of magnitude over the years," says Thijs de Graauw, one of FIRST's originators and now director of the Atacama Large Millimeter/submillimeter Array (ALMA) in Chile.

One challenge was to develop detectors for Herschel's range of wavelengths. Astronomers working in the infrared have benefited from the military, which likes to spot warm things on the ground from space and has developed sensitive infrared detectors. At Herschel's slightly longer wavelengths, "there's been nothing done by anyone other than astronomers," says Pilbratt. It's also an awkward middle ▶

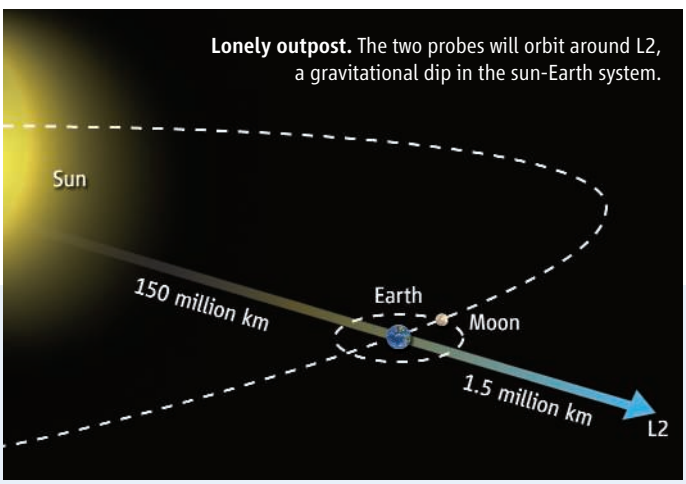

Lonely outpost. The two probes will orbit around L2, a gravitational dip in the sun-Earth system.

SOURCE: ESA; CREDITS: JUPITERIMAGES

Those variations arose from the sloshing of matter and radiation in the early universe. With the data, researchers nailed down the makeup of the universe: 4% ordinary matter; 23% mysterious dark matter, whose gravity holds the galaxies together; and 73% space-stretching dark energy, which is speeding up the expansion of the universe.

Planck will chart the temperature variations in CMB with 10 times WMAP's sensitivity and three times its angular resolution. The microwaves are also polarized so that the electric fields in waves coming from any particular spot in the sky wiggle in a definite direction—just as ordinary light waves reflected from a pond are polarized so they oscillate horizontally as they zip into your eye. WMAP sketched the polarization of the CMB; Planck will render it in great detail.

Still, Planck may not be the sure-fire winner that COBE and WMAP were, some researchers say. "If it works as it should, then at the minimum, Planck will do very good science," says David Spergel, a cosmologist at Princeton University and a member of the WMAP team. But there's no guarantee that Planck will spot something completely new, Spergel says: "That's what happens when you're the third satellite."

Planck will be far more sophisticated than its predecessors. WMAP sampled microwaves at five frequencies; Planck will monitor nine of them over a range 12 times wider. WMAP cooled its detectors by exposing them to the frigidity of space; some of Planck's detectors must be cooled to within a fraction of a degree of absolute zero with a liquid-helium refrigerator. As WMAP did, Planck will circle the sun in synchrony with Earth, hovering at the so-called second Lagrange point, or L2 (see figure, above). There it will spin, scanning its microwave eyes across the sky and amassing in 18 months more than 100 billion measurements.

At the least, Planck should make superior measurements of the part-in-100,000 temperature variations. These variations reflect differences in the density of the primordial universe, irregularities that seeded the formation of the galaxies. With their stronger gravity, the denser regions drew in more matter, both dark and ordinary. Simultaneously, radiation pushed against the gathering ordinary matter, causing the matter to rebound. That jostling is encoded in the temperature variations, which is why WMAP could measure the relative amounts of dark and ordinary matter in the universe.

Planck should be able to nail down another key piece of information: the distribution of the original density variations. These variations can be broken down into longer and shorter wavelike undulations, much as a musical chord can be broken into individual notes. The relative strength of longer and shorter wavelength variations can be described by a single number called a spectral index, a cosmological parameter perhaps more important than any that WMAP measured, says Joseph Silk, a cosmologist at the University of Oxford, U.K., who works on Planck. "Planck is going to [measure] it much, much better than WMAP," he says. "It's going to be beautiful."

But the prize quarry for Planck researchers is the B modes. These features are swirls in the CMB polarization mapped across the ▶

Published by AAAS

Stellar nursery. Herschel will seek out embryonic galaxies burning bright with star formation, as in this artist's impression.

ground between optics and radio electronics: Two of Herschel's detectors take an optics approach, whereas the third relies on radio techniques. The radio detector, known as HIFI, is a "remarkable achievement," says Pilbratt. "Ten years ago, there was nothing like what you see in HIFI today."

The mirror also had problems along the way. The plans originally called for it to be made of lightweight carbon fiber, but it proved difficult to build one large enough out of that material. A NASA team produced a prototype but had to pull out of developing it because of funding constraints. The managers decided to switch to silicon carbide, which ESA researchers had been experimenting with as a backup.

With its huge telescope, Herschel will be able to peer through gas and dust to construct a history of star formation from the early years of the universe to today. Griffin says the distant galaxies seen by the likes of the Hubble Space Telescope are already grown up. Hubble "doesn't see the ones in formation, behind the dust and gas," he says. "We don't know how many of them there are," adds De Graauw. Such star-forming galaxies emit radiation mostly in the cool infrared, and Herschel's wavelength range lets it spy on regions cooler than earlier satellites could. Herschel will be able to count the number of these distant galaxies in six different wavelength bands, charting their evolution. "We'll be able to say what's going on in these galaxies … [and] say how a galaxy like our own evolved into what it is today," says Pilbratt.

Closer to home, Herschel will study in detail the life cycle of stars—how old first-generation stars explode, seeding the interstellar medium with heavy elements that then form part of the next generation of stars. "It's an ecosystem in balance," says Griffin. "We can get a handle on all parts of the cycle. The chemistry and physics is not well understood." De Graauw hopes researchers will find the trigger for star formation. "What starts the early ones—those without heavy atoms—is still a riddle," he says.

Aside from the formation of galaxies and stars, astronomers also hope to use Herschel to study comets, asteroids, and planetary atmospheres in our solar system and how debris disks around stars form into planets. "It's a very good general-purpose observatory," says Griffin. But Herschel had better not wait too long to make an impact, because another major general-purpose observatory will soon be snapping at its heels. ALMA, an array of 66 giant dishes under construction in Chile, will be producing science in just a few years and will cover wavelengths ranging from about 1 centimeter down to 300 micrometers. Says De Graauw: "There's quite an overlap. Herschel's going to be just in time."

–DANIEL CLERY

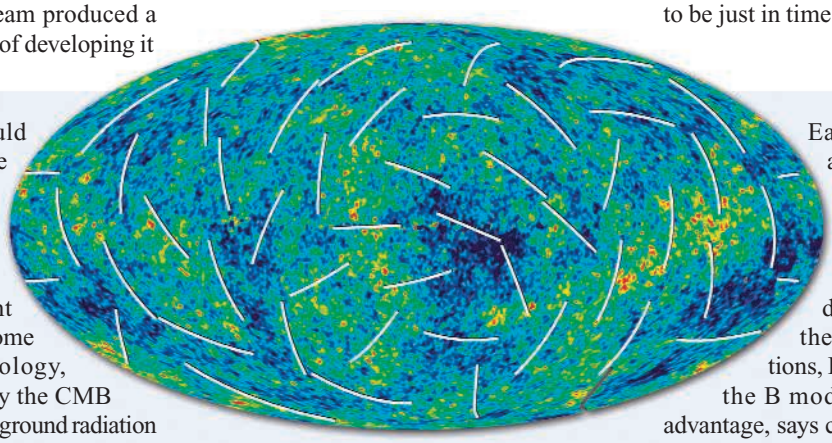

Soon in HD. Planck will improve on WMAP's maps of temperature (colors) and polarization (lines).

sky, and spotting them would essentially clinch the case for the mind-bending theory of inflation.

The notion that the universe briefly expanded at faster than light speed might seem absurd, but it solves some thorny problems in cosmology, including a big one posed by the CMB itself. The temperature of background radiation is almost exactly the same—2.725 kelvin—all over the sky. That's perplexing because the distant reaches of the universe in opposite directions are so far apart that not even light has had time to travel between them. So they could not have interacted and should have no reason to have reached so nearly the same temperature. Inflation solves this problem by positing that opposite ends of the universe were cheek-by-jowl until the sudden expansion pulled them very far apart.

Although inflation fits the facts so far, researchers do not yet have direct proof that it occurred. The B modes would provide that. Current theory predicts that inflation should have generated gravitational waves and that those waves should have left lingering swirls in the polarization of the CMB.

Unfortunately, theory doesn't guarantee that the swirls will be strong enough for Planck to detect. Even if they are, Planck will have to sift through the effects created by our galaxy, which can also generate swirling polarization patterns. Planck's sensitivity to higher frequencies should help it identify such "foregrounds." Planck will also have to beat out ground-based and balloon experiments searching for the B modes. Such small-scale efforts stole some of WMAP's thunder by precisely measuring the temperature variations first (*Science*, 28 April 2000, p. 595).

In principle, a spacecraft should have an edge over any instrument staring up through Earth's microwave-emitting atmosphere, says Alan Kogut, an astrophysicist at NASA's Goddard Space Flight Center in Greenbelt, Maryland. But Planck was designed primarily to study the CMB temperature variations, Kogut says, not to search for the B modes. Still, Planck has one advantage, says cosmologist John Carlstrom of the University of Chicago in Illinois. Mapping the whole sky, Planck will be able to look for the largest swirls. Ground-based experiments will be more sensitive to smaller ones. "Each has its niche where it offers more than the other," Carlstrom says.

The future of CMB space missions may depend on Planck's and its rivals' at least glimpsing the B modes. Researchers are already planning more-sensitive spacecraft, but "if we do not find that signal, then I do not know how strong the argument will be to go that next step," says Jan Tauber, Planck project scientist at ESA in Noordwijk, Netherlands. Among CMB studies, Planck should be either a very good satellite or a great one. If it's not a great one, it might also be the last of them.

–ADRIAN CHO

CREDITS: NASA/ESA/STSCI (G. BACON); NASA/WMAP

Published by AAAS

BIOFUELS

Corn-Based Ethanol Flunks Key Test

In setting state rules for low-carbon fuels, California officials have calculated that corn ethanol is worse than gasoline

A California regulatory agency charged with reducing greenhouse emissions from the state's cars has embraced a controversial approach for determining the true environmental impact of alternative transportation fuels. Its analysis could have broad implications for the future of corn-based ethanol or other fuels grown on U.S. cropland.

Last week, the California Air Resources Board (CARB) adopted a low-carbon fuel standard that requires greater use of fuels that cause lower greenhouse emissions, compared with gasoline (see graph). Corn-based ethanol doesn't meet that test and won't benefit from the new standard, CARB says, because diverting corn into ethanol production increases deforestation and the clearing of grasslands.

The biofuels industry has attacked the board's methodology, as well as similar conclusions in a regulation drafted last year by the U.S. Environmental Protection Agency (EPA) that is under review by the Obama Administration. Matt Hartwig, a spokesperson for the Renewable Fuels Association in Washington, D.C., says the California regulation will "have a tremendously chilling effect on future investment."

But such a pullback would please Timothy Searchinger, a biofuel critic at Princeton University. Searchinger says that much of the claimed environmental benefit from biofuels depends on "an accounting error. They treat land as free."

The debate was once confined to the pages of scientific publications. For example, Searchinger has found that corn ethanol produces twice the greenhouse gas emissions of gasoline, for every mile driven, once emissions from land conversion are counted (*Science*, 29 February 2008, p. 1238). Searchinger used a global model of agriculture to calculate the effects of increasing ethanol production. (About one-quarter of this year's U.S. corn crop will be turned into ethanol.) The model indicates that if U.S. farmers devote more land to growing corn for ethanol, food prices would increase, leading farmers around the world to convert grasslands and forests into crops. That shift, in turn, would release large amounts of greenhouse gases.

But other researchers expect farmers and agribusinesses to respond to higher food prices in less destructive ways. They foresee innovations that increase yields on existing land.

Government efforts to promote alternative fuels are now drawing regulators into the crossfire. California's new low-carbon fuel standard will require a 10% reduction in greenhouse gas emissions from the average liter of transportation fuel by 2020. To calculate that reduction, CARB's staff measured the "carbon intensity" of alternative fuels, including likely emissions from the ripple effects of biofuel production on global agriculture. At the federal level, a 2007 law requires EPA to calculate the "life cycle greenhouse gas emissions" of renewable fuels, to make sure they meet minimum standards.

CARB relied on a model, developed by researchers at Purdue University, that concluded that corn-based ethanol produces slightly greater greenhouse emissions than does gasoline, with about 30% of those emissions occurring as farmers clear land for crops.

EPA has not yet released its studies, but some who have been briefed on them say the agency anticipates an even larger area of the world's forest and grassland being converted into food and ethanol production. Ethanol receives a better overall grade, however, because EPA assumes that current ethanol refineries are more efficient.

The analyses have infuriated biofuel advocates, who last week condemned the board's methodology as unfair, artificial, and lacking any real-world data. More than 100 scientists, many of them involved in biofuel research, have told CARB that the science of estimating emissions from land conversion is "far too limited and uncertain" to use in regulations. In Congress, a dozen farm-state senators want EPA to halt any effort to calculate the greenhouse effects of land-use change caused by biofuels. "It defies common sense that EPA would publish a proposed rulemaking with harmful conclusions for biofuels based on incomplete science and inaccurate assumptions," said Senator Charles Grassley (R–IA) in March.

CARB, for now, is sticking to its guns. "We feel that our recommended value [for greenhouse emissions from land-use change] is very reasonable," said CARB staffer Wes Ingram. However, the board promised a full review of the issue in January 2011, 1 year before the regulation takes effect.

Searchinger, for one, thinks that CARB's estimate is too low. He points out that CARB's model predicts that higher prices would lead to less food produced globally, which he says probably means more hunger. Efforts to avoid that fate would increase greenhouse emissions, he says.

Bruce Babcock, an economist at Iowa State University in Ames who is working with EPA, says broader consideration of land-use decisions could spark new controversies. The best way to reduce the clearing of land for crops, says Babcock, would be to impose a tax on meat consumption. "If we all turned into vegetarians, we could get by on one-tenth of the land," he says. **–DAN CHARLES**

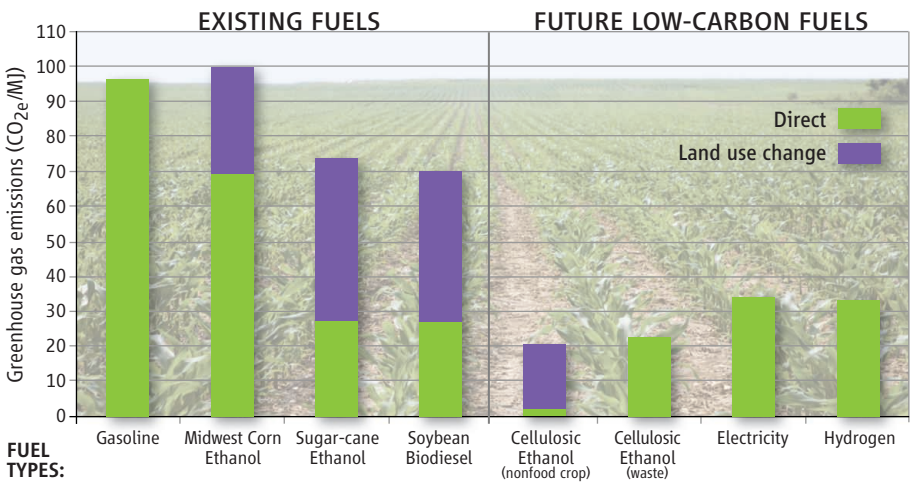

Degrees of green. California officials say today's ethanol is no better than gasoline, but they're banking on cleaner biofuels by 2020.

CREDITS: ADAPTED FROM CALIFORNIA AIR RESOURCES BOARD; (IMAGE) PHOTOS.COM

Published by AAAS

Civilization's Cost: The Decline and Fall of Human Health

When humans were freed from searching for food from dawn to dusk, they finally had time to build cities, create art, and even muse about the gods. Agriculture and cities made human life better, right? Wrong, say archaeologists who presented stunning new evidence that most people's health deteriorated over the past 3000 years. "We document a general decline in health across Europe and the Mediterranean," says bioarchaeologist Clark Spencer Larsen of Ohio State University in Columbus. He's a coinvestigator of the European Global History of Health Project, an ambitious new effort to study the health of Europeans during the past 10,000 years.

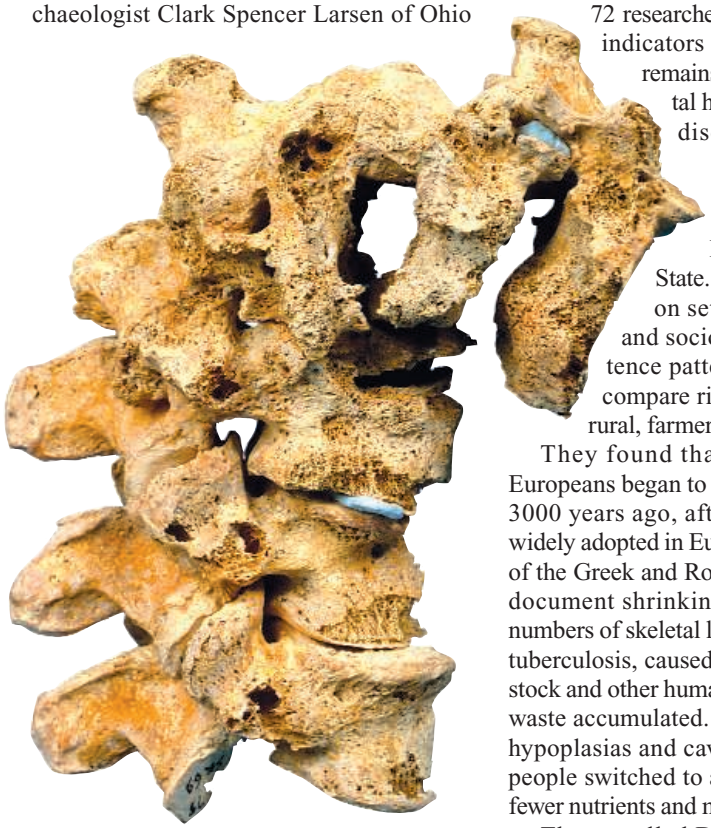

Bad back. The rise in tuberculosis in the Middle Ages left its mark on the spine of this English skeleton.

Most bioarchaeology studies tend to tell the tale of illness and death of people from a single site, such as a burial pit for plague victims or an ancient cemetery. Larsen's project is one of the first—and the largest—to try to reveal broad trends by assembling standardized data from large samples. In a series of posters, the team presented the first analysis of data on 11,000 individuals who lived from 3000 years ago until 200 years ago throughout Europe and the Mediterranean. "This is a real tour de force," says bioarchaeologist George Armelagos of Emory University in Atlanta, after reviewing the posters.

The project has taken 8 years and $1.2 million to organize so far. The goal was to pool 72 researchers' data on standardized indicators of health from skeletal remains, including stature, dental health, degenerative joint disease, anemia, trauma, and the isotopic signatures of what they ate, says project leader Richard Steckel of Ohio State. They also gathered data on settlement size, latitude, and socioeconomic and subsistence patterns so that they could compare rich and poor, urban and rural, farmers and hunter-gatherers.

They found that the health of many Europeans began to worsen markedly about 3000 years ago, after agriculture became widely adopted in Europe and during the rise of the Greek and Roman civilizations. They document shrinking stature and growing numbers of skeletal lesions from leprosy and tuberculosis, caused by living close to livestock and other humans in settlements where waste accumulated. The numbers of dental hypoplasias and cavities also increased as people switched to a grain-based diet with fewer nutrients and more sugars.

The so-called Dark Ages were indeed grim for many people who suffered from more cavities, tooth loss, rickets, scurvy, and bone infections than had their ancestors living in hunter-gatherer cultures. People became shorter over time, with males shrinking from an average of 173 centimeters in 400 B.C.E., for example, to 166 centimeters in the 17th century—a sure sign that children who were not members of the elite were eating less nutritious food or suffering from disease.

Why would people want to settle in towns or cities if it made them sick? One answer is that settlers suffered less bone trauma than nomadic hunter-gatherers, suggesting to Steckel that they might have felt safer in villages and, later, towns where an emerging elite punished violent behavior—but also controlled access to food.

The social and political inequities in urban centers meant that for nonelites, moving into cities was "almost a death sentence" for centuries, notes Armelagos. In the Middle Ages, people in the countryside were generally taller than people in cities.

After a long, slow decline through the Middle Ages, health began to improve in the mid-19th century. Stature increased, probably because of several factors: The little Ice Age ended and food production rose, and better trade networks, sanitation, and medicine developed, says Steckel. But take heed: Overall health and stature in the United States has been declining slightly since the 1950s, possibly because obese Americans eat a poor-quality diet, not unlike early farmers whose diet was less diverse and nutritious than that of hunter-gatherers. By understanding how disease and malnutrition spread in the past, researchers hope to apply those lessons in the future. "Our goal is to understand the health context for what we have today," says Larsen. **–A.G.**

Of Tools and Tubers

If tools make the man, then sharp, durable tools make an even handier man or woman. That knowledge was not lost on our ancestors as early as 2 million years ago, according to a new analysis of stone tools and bones left behind near Lake Victoria in Kenya. At the Paleoanthropology Society gathering, which met concurrently with the larger meeting, researchers reported that at this early date humans purposely selected the highest-quality stone and transported it more than 13 kilometers to an animal butchery site. A collaborating team also reported that these early humans, presumably *Homo habilis* or early *H. erectus*, used tools not only to deflesh carcasses but also to slice tuberous roots, possibly a key part of their diet.

These tools, found at the site of Kanjera South in Kenya, are not the oldest known, which date back to 2.6 million years ago in Ethiopia. But they are "the first evidence that [early humans] were not just using tools to eat

CREDIT: CHARLOTTE ROBERTS

Published by AAAS

Reproductive Fate Versus Environment

Women's fertility is determined in large part at birth. They are born with their total number of ovarian follicles, for example, which normally influences the age at which menopause begins. But in the 1990s, researchers proposed that if a child's energy is depleted by malnutrition, disease, or other factors, he or she would be less fertile as an adult. By using the natural experiment of migration, researchers demonstrated in a talk how differences during childhood do indeed alter the course of reproduction in adult women.

Biological anthropologist Gillian Bentley of Durham University in the United Kingdom and colleagues compared levels of reproductive hormones in 250 Bangladeshi women, including women who migrated from Sylhet, Bangladesh, to London; women who stayed in Sylhet; and Bangladeshi women born in London. In the first stage of their study, Bentley and Alejandra Núñez-de la Mora of Durham University found that women who migrated from Bangladesh as children had higher levels of the hormone progesterone in their saliva than women who lived in Sylhet, but less than women born in London. This had a direct effect on fecundity: Migrant women in London had an 11% higher rate of ovulation during their lives than did women in Sylhet, the team reported in 2007. "We're beginning to see how the ovaries get feedback from the environment" to determine how many eggs are allowed to mature, says anthropologist Benjamin Campbell of the University of Wisconsin, Milwaukee.

The team has now studied 900 women between the ages of 35 and 60 to see if the onset of menopause varies between migrants and women in Sylhet. Bentley presented preliminary results from their measurement of hormones that regulate the maturation of ovarian follicles and are indirect indices of how many ova they can still produce. Her team found that women who migrated as adults had higher levels of inhibin B and anti-Müllerian hormone in their blood than women in Sylhet did but less than women born in London. This suggests that migrants enter menopause later than did women who stayed in Bangladesh but earlier than did those born in London. "The adult migrants seem to be sensitive to improved conditions," says Bentley.

The group is trying to find out which environmental factors in Bangladesh lower growing girls' fertility. All the Bangladeshi women in the study came from middle-class, land-owning families, who grew up with adequate calories. However, girls growing up in Bangladesh were probably exposed to more infectious diseases, including parasitic worms, during crucial developmental years. So, they may have had to make tradeoffs among using energy to grow, to maintain their bodies, or to maximize their reproductive potential as adults. Bentley plans to test that idea next year when her team returns to Bangladesh to see if girls there suffer from more diseases than do those in London. "In other words," says Bentley, "where you spend your childhood influences adult reproductive function." **–A.G.**

Fertile soil? Bangladeshi women who live in London are more fertile than those in Bangladesh.

meat but to process plants, and possibly woodworking," observes paleoanthropologist Alison Brooks of George Washington University in Washington, D.C. "This shows dietary diversity and the investment of energy to have the best tools to enhance that diversity."

Paleoanthropologists Thomas Plummer of Queens College in New York City and David Braun of the University of Cape Town in South Africa found that one-third of the stone tools at Kanjera were made of durable stone, such as quartzite and rhyolite, that came from at least 13 kilometers away. The team tested the stone for durability and ease of flaking and found that the imported stone kept a sharp edge far longer than did the site's local limestone. "This suggests [early humans] are being selective and that the quality of the lithics is important. Otherwise, why transport it?" says Plummer.

To find out just what early *Homo* was doing with the tools, Plummer enlisted archaeologist Cristina Lemorini of the University of Rome, "La Sapienza." She studied replicas of the Kanjera tools, made with the same kinds of stone, that modern Hadza hunter-gatherers of Tanzania had used to butcher animals, process wild tubers, cut grass, and work wood. Then, using confocal and metallographic microscopes, she compared patterns of wear on the edges of the Kanjera tools with those on the replicas. She reported that the ancient tools had telltale signs of being used to process plant materials, such as cutting grass, and the distinct striations made by sediment as tools were used to clean and section fibrous tubers. She also saw patterns consistent with defleshing carcasses and woodworking, possibly to make wooden tools.

Thirst quencher. Hadza hunter-gatherers dig tubers for water.

Researchers have proposed before that early humans relied on tuberous root vegetables as an important fallback food (*Science*, 7 October 2005, p. 46), but they lacked direct evidence and so have failed to convince skeptics. In a separate talk at the meeting, anthropologist Margaret Schoeninger of the University of California, San Diego, offered a new reason why tubers might have been important: as a source of water.

In a study of the Hadza, Schoeninger found that they chewed tuberous roots such as panjuko and makaritakos. But they didn't swallow the fibrous wad, which would yield few calories. Instead, they spit it out, apparently after sucking the liquid out of the tubers, which are 80% water. Schoeninger suggests that tubers were portable canteens as well as a fallback food. "Tubers could have provided much-needed water as our ancestors moved into open, more seasonal environments," she says. One test of this idea would be to see if other hunter-gatherers also quench their thirst with starchy tubers, says Brooks. For now, it seems that sharp tools helped humans develop two distinct dietary tastes, for meat—and root vegetables. **–ANN GIBBONS**

CREDITS (TOP TO BOTTOM): ALEJANDRA NÚÑEZ-DE LA MORA; ALYSSA CRITTENDEN

Published by AAAS

Water worries
593

von Humboldt's scientific legacy
596

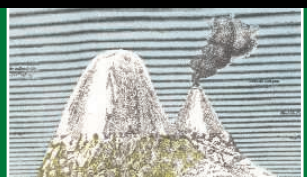

LETTERS

edited by Jennifer Sills

Civilian casualties. A U.S. medic holds an injured Iraqi boy in the 28th Combat Support hospital in Baghdad. Controversy continues over a 2006 report recording the number of Iraq war violent deaths.

Iraq Study Failed Replication Test

J. BOHANNON, IN HIS NEWS OF THE WEEK STORY "AUTHOR OF IRAQI deaths study sanctioned" (6 March, p. 1278), quotes Les Roberts, a coauthor of the controversial *Lancet* survey (*1*) that estimated 601,000 violent deaths during the first 3.3 years of the Iraq war. Roberts emphasizes that the key to verifying the study's findings lies in replication.

The *Lancet* survey has already failed a replication test (*2*): The World Health Organization (WHO) published the results of its Iraq Family Health Survey (IFHS) in 2008 (*3*). This was a rigorous, well-supervised, and much larger survey than the *Lancet* study, and it estimated 151,000 violent deaths, compared with 601,000 violent deaths estimated by the *Lancet* survey for almost precisely the same time period. The IFHS ground activities are documented on the IFHS Web site (*4*), which provides the questionnaire in English and Arabic, along with extensive information on the sample design and the field work. In contrast, the lead author of the *Lancet* survey has just been censured by the American Association for Public Opinion Research for repeatedly refusing to disclose the corresponding information for his survey (*5*). In fact, the rigor of the ground activities for the *Lancet* survey was so lax that the U.S.-based authors, who never entered Iraq at any stage of the study, only discovered that the field workers had implemented an incorrect and unethical data entry form after the field work had been completely finished (*6*).

MICHAEL SPAGAT

Department of Economics, Royal Holloway College, University of London, Egham, Surrey TW20 0EX, UK. E-mail: M.Spagat@rhul.ac.uk

References

1. G. Burnham *et al.*, *Lancet* **368**, 9545 (2006).
2. J. Bohannon, *Science* **319**, 5861 (2008).
3. Iraq Family Health Survey Study Group, *New Engl. J. Med.* **358**, 5 (2008).
4. WHO Country Office in Iraq, Iraq Family Health Survey (www.emro.who.int/iraq/ifhs.htm).
5. Executive Council, American Association for Public Opinion Research (www.aapor.org/uploads/AAPOR_Press_Releases/BurhnamDetailWebsite.pdf).
6. Johns Hopkins School of Public Health, Public Health News Center, "Review completed of 2006 Iraq mortality study" (www.jhsph.edu/publichealthnews/press_releases/2009/iraq_review.html).

Iraq Study Response Lacks Objectivity

IF THE OBJECT OF GILBERT BURNHAM *ET AL.*'S study (*1*) had been a risk factor for cardiovascular disease instead of the health effects of the Iraq war, scientists might have objectively and systematically reviewed the strengths and weaknesses of each study and, if warranted, attempted to obtain stronger evidence. Instead, the tone and content of scientific discourse and media reporting around Iraq mortality has achieved little beyond casting a shadow of irrational suspicion over Burnham *et al.*'s estimates ("Author of Iraqi deaths study sanctioned," J. Bohannon, News of the Week, 6 March, p. 1278), which may be subject to important biases, but are far from implausible. This is a disservice to the Iraqi people, all the more given the scarcity of data on population health in Iraq. Indeed, the main aim of some critics seems to have been to disprove Burnham *et al.*'s alarmingly high estimates at all costs (*2*–*4*), rather than to generate better data.

Accurate estimation of Iraqi civilian deaths following the 2003 invasion is of utmost importance. Aside from an undisciplined, unconstructive dispute over one study, science and civil society have done shockingly little to achieve this aim.

FRANCESCO CHECCHI

Department of Infectious and Tropical Diseases, London School of Hygiene and Tropical Medicine, London WC1 E7HT, UK. E-mail: francesco.checchi@lshtm.ac.uk

References and Notes

1. G. Burnham *et al.*, *Lancet* **368**, 9545 (2006).
2. H. Dardagan, J. Dougherty, J. Sloboda, "Reality checks: Some responses to the latest *Lancet* estimates" (Iraq Body Count, 2006); www.iraqbodycount.org/analysis/beyond/reality-checks/.
3. N. F. Johnson, M. Spagat, S. Gourley, J.-P. Onnela, G. Reinert, *J. Peace Res.* **45**, 653 (2008).
4. D. Kane, "*Lancet* on Iraqi Mortality" (2009); http://lancetiraq.blogspot.com/.
5. Conflict of interest: I was advised by Gilbert Burnham during my Master's studies at the Johns Hopkins University School of Hygiene and Public Health, and have previously collaborated with Les Roberts (a co-author of the study in question).

Letters to the Editor

Letters (~300 words) discuss material published in *Science* in the previous 3 months or issues of general interest. They can be submitted through the Web (www.submit2science.org) or by regular mail (1200 New York Ave., NW, Washington, DC 20005, USA). Letters are not acknowledged upon receipt, nor are authors generally consulted before publication. Whether published in full or in part, letters are subject to editing for clarity and space.

Confronting Racism

IN THEIR REPORT ("MISPREDICTING AFFECTIVE and behavioral responses to racism," 9 January, p. 276), K. Kawakami *et al.* showed that non-black research participants (termed "experiencers") did not respond particularly negatively when they heard a white person make a racist comment about a black person. In contrast, other participants required to

CREDIT: DAMIR SAGOLJ/REUTERS/LANDOV

Published by AAAS

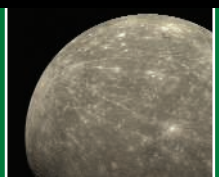

Hello Mercury

597

Glacier dynamics

599

forecast what their responses would be in this situation ("forecasters") predicted relatively more emotional distress and social rejection in response to the racist comment. I would like to offer my interpretation of their findings.

Experiencers may have reported not their initial reaction, but an emotional state resulting from their efforts to cope with a stressful situation. Especially in unfocused interpersonal situations (e.g., in a waiting room or elevator), tolerant or egalitarian people attempt to cope with their automatic responses to others perceived as deviant by controlling and concealing these responses. This process tends to result in heightened self-consciousness, tension, and awkwardness, which may not be visible in self-reported emotions (*1*). Hearing the racist remark could considerably add to the experienced stress and perhaps the resulting regulatory efforts. Hence, experiencers may not be as indifferent to the racist comment as they seemed, and forecasters may not have been as inaccurate as suggested by Kawakami *et al*.

Furthermore, experiencers may not have confronted the person who made the remark because they feared retaliation or the return of the victim. Kawakami *et al*. found that reported distress in relation to the racist comment was positively related with seeking contact with the black victim, evidence that experiencers may have been motivated by protective tendencies.

In modern Western society, tolerant and generally caring individuals are trained to look the other way when confronted with deviance, and hence may feel overwhelmed when confronted with racist or other hurtful acts. To combat this, we should work to provide people with effective coping strategies rather than making them more aware of their apparent failure to predict their own emotional reactions.

ANTON J. M. DIJKER

Faculty of Health, Medicine, and Life Sciences, Maastricht University, Post Office Box 616, 6200 MD Maastricht, Netherlands. E-mail: a.dijker@gvo.unimaas.nl

Reference

1. A. J. M. Dijker, W. Koomen, *Stigmatization, Tolerance, and Repair: An Integrative Psychological Analysis of Responses to Deviance* (Cambridge Univ. Press, Cambridge, 2007).

Response

DIJKER PROPOSES THAT AFTER BEING EXPOSED to a racist comment, people may feel uncertain and overwhelmed, spurring emotion regulation processes that lead them to report feeling unperturbed. Recent findings on implicit prejudice, however, suggest that because the majority of people hold negative nonconscious attitudes toward blacks (*1*, *2*), they would not be upset by a negative racist act. Nonetheless, it is difficult to rule out the possibility in our studies that witnessing racism provoked a brief flash of intense distress that was subsequently inhibited. Even so, any initial distress (if it

Published by AAAS

existed) had disappeared without a trace by the time participants reported their feelings, just moments after they heard the comment, and whatever initial distress was experienced did not deter participants from choosing to work with the person who made the racist comment (compared to a "no comment" control condition). Indeed, research on affective forecasting suggests that people are often able to come to terms with an upsetting situation within seconds of the event in a largely automatic fashion (*3*). Although it is important to test the possibility that people regulate their initial emotional responses upon hearing a racist comment (*4*), in the absence of such evidence, it is more parsimonious to assume that little distress was experienced than to posit that distress appeared and then disappeared.

Dijker also notes that people sometimes fail to confront racism because of potential costs, such as a fear of retaliation. Although we agree that such costs can reduce willingness to confront racism in daily life, for methodological reasons this explanation does not readily apply to our context, which allowed participants to express their disapproval indirectly. In our procedure, privately reporting distress on an anonymous emotion survey did not carry obvious costs and thus should not be influenced by fear of retaliation. Furthermore, the fact that lower levels of reported distress accounted for participants' tendency to select the white over the black partner is inconsistent with the notion that this choice was driven by a fear of retaliation. If fear of retaliation led participants to select the white partner, higher levels of upset would be expected to predict selection of the white over the black partner, but we found just the opposite.

We wholeheartedly agree with Dijker about the importance of discovering new interventions to ease the burden of prejudice. However, we do not agree with his assumption that making people aware of their tacit acceptance of racism may hurt—not help—these efforts. Indeed, many current models of prejudice reduction propose that awareness of one's biases is a critical first step to addressing the problem (*5*, *6*).

KERRY KAWAKAMI,[1] ELIZABETH DUNN,[2] FRANCINE KARMALI,[1] JOHN F. DOVIDIO[3]

[1]Department of Psychology, York University, Toronto, ON M3J 1P3, Canada. [2]Department of Psychology, University of British Columbia, Vancouver, BC V6T 1Z4, Canada. [3]Department of Psychology, Yale University, New Haven, CT 06520–8205, USA.

References

1. J. F. Dovidio, K. Kawakami, N. Smoak, S. L. Gaertner, in *Implicit Measures of Attitudes*, R. Petty, R. Fazio, P. Brinol, Eds. (Psychology Press, New York, 2009), pp. 165–192.
2. A. G. Greenwald, D. E. McGhee, J. K. L. Schwartz, *J. Personal. Soc. Psychol.* **74**, 1464 (1998).
3. T. D. Wilson, T. Wheatley, J. Kurtz, E. W. Dunn, D. T. Gilbert, *Personal. Soc. Psychol. Bull.* **30**, 340 (2004).
4. K. Kawakami, *Science* Podcast, 9 January 2009.
5. P. G. Devine, M. J. Monteith, in *Affect, Cognition, and Stereotyping: Interactive Processes in Group Perception*, D. Mackie, D. Hamilton, Eds. (Academic Press, San Diego, CA, 1993), pp. 317–344.
6. M. J. Monteith, L. Ashburn-Nardo, C. I. Voils, A. M. Czopp, *J. Personal. Soc. Psychol.* **83**, 1029 (2002).

CORRECTIONS AND CLARIFICATIONS

Editors' Choice: "One shell fits all" (23 January, p. 438). The image accompanying the text was mislabeled. The image shows voids in the cancellous interior of the turtle shell that contain hematopoietic cells.

Perspectives: "Ex uno plura" by S. Feau and S. P. Schoenberger (23 January, p. 466). Emma Teixeiro's name was misspelled both in the first paragraph and in reference 2.

Call for Papers

Science Signaling

Science Signaling, from the publisher of ***Science***, AAAS, features top-notch, peer-reviewed, original research. The journal publishes leading-edge findings in cellular regulation including:

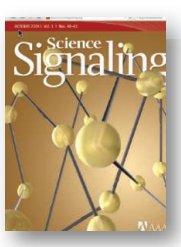

- Molecular Biology
- Development
- Immunology
- Neuroscience
- Microbiology
- Pharmacology
- Biochemistry
- Cell Biology
- Bioinformatics
- Systems Biology
- Physiology and Medicine

Subscribing to ***Science Signaling*** ensures that you and your lab have the latest cell signal resources. To subscribe go to **http://pubs.aaas.org/pub7/pub7_setup.asp.**

Submit your research at: www.sciencesignaling.org/about/help/research.dtl

Science Signaling
AAAS
www.sciencesignaling.org

Published by AAAS

FILM: ENVIRONMENT

Three Takes on People and Water

The 17th annual Environmental Film Festival in the Nation's Capital offered Washington, D.C., viewers a very wide range of topics. Many showings examined environmental issues (Ian Connacher's *Addicted to Plastic*) or celebrated nature (Dereck and Beverly Joubert's *Eye of the Leopard*). Others—such as Richard Rifkind and Carole Rifkind's *Naturally Obsessed: The Making of a Scientist* (screened at AAAS headquarters) and David Conover's *Cracking the Ocean Code* (on Craig Venter's global voyage)—highlighted the pursuit of research. The oceans and their (often-threatened) life were the focus of a series of films that also included a 1929 adaptation of Jules Verne's *The Mysterious Island* starring Lionel Barrymore. Several screenings were world or U.S. premieres, and the organizers arranged a retrospective of 12 movies by Werner Herzog. Short descriptions of all 135 films are still available at www.dcenvironmentalfilmfest.org/films.php. Here we consider three that explore aspects of people's relations with water.

Blue Gold: World Water Wars. Sam Bozzo, Director. Purple Turtle Films, Canada, 2008. 90 minutes. DVD, $24.95, C$34.95. www.bluegold-worldwaterwars.com.

Sam Bozzo's award-winning *Blue Gold* addresses an important topic. Many in the developed world (certainly in the United States) take water for granted in the same way that they take the air they breathe for granted. However, as the film makes clear, water is increasingly being treated as a commodity, like oil, and people are losing the rights to it within their own countries and for their own land.

Bozzo begins by presenting basic facts and answering fundamental questions such as why the water cycle we learned about in elementary school isn't enough to keep our water supplies stable. The film paints a grim picture of the politics surrounding the exploitation of water resources. From Grenoble to Atlanta, government representatives have been accused of taking bribes to support the privatization of water supplies. The World Bank has made such privatization a condition for debt relief. Violence has broken out, as in Cochabamba, Bolivia, where even the rainwater was privatized.

The movie is not without flaws. It is fairly one-sided, and, in covering a lot of ground, it makes some sweeping generalizations. Nonetheless, it is packed with verifiable stories and facts.

In a postscreening discussion, Bozzo explained that he had originally planned a sequel to *The Man Who Fell to Earth* (which is about an alien race trying to get Earth's water). For background, he read Maude Barlow and Tony Clarke's *Blue Gold: The Fight to Stop the Corporate Theft of the World's Water*. Horrified about the lack of coverage of the situation, he gave up fiction and turned to documentary. **–Barbara R. Jasny**

CREDITS: (TOP TO BOTTOM) STEVE ELLINGTON & NICK BRANDESTINI; PURPLE TURTLE FILMS; LEO ERKEN; *ONZE KUST*/IDTV DOCS

Legacy of the Great Aletsch. Nick Brandestini and Steve Ellington, Directors. Switzerland, 2008. 52 minutes. www.aletschfilm.com.

Nearly 23 km long and reaching a thickness of almost 1000 m, the Great Aletsch is the largest glacier in the Alps. In the past 150 years, it has retreated some 3 km and its surface fallen by more than 100 m. But the effects and threats of climate change form only one of the strands Brandestini and Ellington weave around their descent of the glacier (beginning from the highest railway station in Europe). Martin Nellen (their mountain guide) and Art Furrer (a renowned freestyle skier turned hotelier) recount personal experiences and describe the glacier and the influences it has had on them and other local residents—such as traditional fears that the purgatorial souls of the dead emerge at night to trod the surface of the ice. Additional perspectives and memories are provided by a geologist (who has reconstructed previous waxing and waning of the glacier), a Pro Natura naturalist, a hydroelectrical engineer, a glacial pilot, a Greenpeace activist, students, and tourists.

The film contains many striking images of the spectacular landscapes of Switzerland's Jungfrau-Aletsch-Bietschhorn region (a UNESCO World Heritage site). Viewers may, however, find themselves more fascinated by the stories of people who live with these mountains. **–Sherman J. Suter**

Onze Kost [Our Coast]. Ireen van Ditshuyzen, Director. IDTV-DITS, Netherlands, 2005. 78 minutes. DVD, €25. www.idtvdocs.nl.

The Dutch have long toiled to reclaim and protect their lands from the sea. They remember drowned villages, shifting islands, and disasters such as the floods of 1953. Thus, it is no surprise that proposals to cut notches in seashore dunes or adopt other practices of dynamic coastal management lead to heated discussions. *Onze Kust* is the result of a seven-year project that documentary film–maker Ireen van Ditshuyzen embarked on after controversy arose in her own neighborhood. Piotr Kukla's cinematography presents the beauty of beaches, dunes, grasses, and waves. Coastal dwellers and workers recall their experiences and fears. Citizens clash with policymakers at public hearings. The film mixes these scenes with historical footage to explore how the Dutch live with their coast. It offers multiple perspectives on such questions as how hard should people try to resist the sea and how can the goals of nature conservation and coastal protection be reconciled. (The film, without English subtitles, can be viewed at http://player.omroep.nl/?aflid=2337934.) **–Sherman J. Suter**

10.1126/science.1175002

Published by AAAS

ECOLOGY

Reducing the Risks of the Wildlife Trade

Importation of wildlife into the United States, most with scant identification, brings an increased threat of disease and introduction of invasive species.

Katherine F. Smith,[1,2]* Michael Behrens,[3] Lisa M. Schloegel,[2,4] Nina Marano,[5] Stas Burgiel,[6] Peter Daszak[2]*

The magnitude of the international wildlife trade is immense, with estimates of billions of live animals and animal products traded globally each year (*1*, *2*). This trade has facilitated the introduction of species to new regions, where they compete with native species for resources, alter ecosystems, damage infrastructure, and destroy crops (*1*, *3*). It has also led to the introduction of pathogens that threaten public health, agricultural production, and biodiversity (*1*, *4*).

The 2003 outbreak of monkeypox virus in the United States illustrates the public health risks associated with live wildlife importation. Human infections resulted from contact with pet prairie dogs infected with monkeypox by African rodents imported for the pet trade (*5*–*7*). The monkeypox outbreak resulted in 72 human cases (*8*). The Centers for Disease Control and Prevention (CDC) and Food and Drug Administration issued regulations that, by November 2003, restricted both domestic trade in, and importation of, African rodents.

Nearly all government initiatives to regulate live wildlife imports have been reactive, focusing on detecting and preventing the spread of nonnative species already established (*9*) or initiated as an urgent response to an emerging public health issue (*10*). Current regulations are inadequate to accurately assess the diversity of wildlife imported or the risk they pose as invasive species or hosts of harmful pathogens. We obtained and analyzed all Law Enforcement Management Information System (LEMIS) shipment records gathered by the U.S. Fish and Wildlife Service (USFWS) for live wildlife imports and exports for the period 2000–06 (*11*). Whereas shipment data allow us to quantify the origin, source (wild versus captive), purpose, and diversity of taxonomic groups in the U.S. wildlife trade (*11*), the number of individuals in each shipment reveals the extraordinary magnitude of wildlife traded by the country. Over half a million shipments of wildlife containing >1.48 billion live animals have been imported by the United States since 2000 (see figure, top left). The number of shipments has increased significantly over this time, although the number of individuals shipped has not. With each shipment representing a potentially different origin, this suggests a growing threat. The majority (92%) of imports were designated for commercial purposes, largely the pet trade. Nearly 80% of shipments contained animals from wild populations, the majority of which have no mandatory testing for pathogens before or after shipment. Over 69% of live animal imports originated in Southeast Asia, which is considered a hotspot for emerging zoonotic diseases (*12*) (table S1). Cnidarians (e.g., coral) and fish, respectively, made up the greatest proportion of imported shipments and individual animals, although all major taxonomic groups were imported (see figure, bottom).

Despite mandated labeling of imported animals to species (50 Code of Federal Regulations 14) (*13*), the majority of shipment records did not contain the appropriate level of taxonomic information (see figure, top right), and almost one-third (31.1%) of imported shipments were identified with commonly used labels such as "marine fish," "live invertebrate," or "non-CITES" (that is, not subject to the Convention on International Trade in Endangered Species of Wild Fauna and Flora

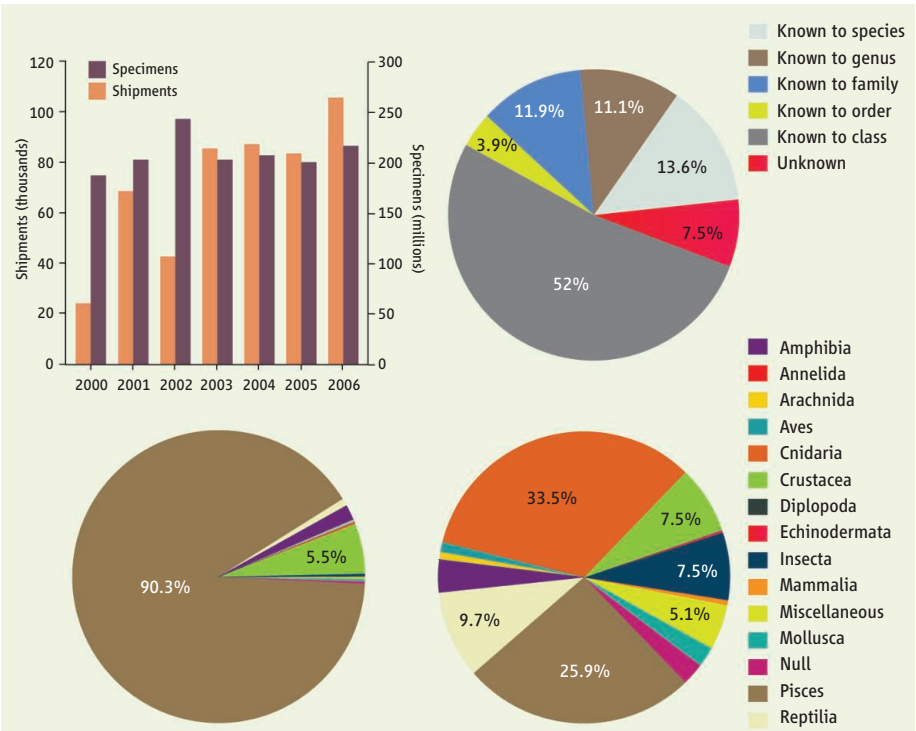

Imported wildlife. (**Top, left**) Numbers of shipments and individual live wildlife specimens imported into the United States, for the period 2000–06 (*11*). Annual shipments have increased significantly over the period of the study ($R^2 = 0.76$, $F_{1,5} = 16.216$, $P = 0.010$). (**Top, right**) Percentage of live wildlife shipments imported for the period 2000–06 that were identified to a given taxonomic level. (**Bottom, left and right**) Percentage of live animal specimens (left) and shipments (right) depicted by taxonomic class or phylum, imported into the United States for the period 2000–06. LEMIS records place marine and freshwater fishes under the label "Pisces." Null refers to a shipment with no taxonomic information.

[1]Brown University, Ecology and Evolutionary Biology, Providence, RI 02912, USA. [2]Wildlife Trust, New York, NY 10001, USA. [3]Pacific Lutheran University, Biology, Tacoma, WA 98447, USA. [4]Kingston University, School of Life Sciences, Surrey, KT1 2EE, UK. [5]Centers for Disease Control and Prevention, Atlanta, GA 30333, USA. [6]Global Invasive Species Programme, Alexandria, VA 22301, USA.

*Authors for correspondence. E-mail: katherine_smith@brown.edu and daszak@wildlifetrust.org

Published by AAAS

or CITES). USFWS is charged with record-keeping of live wildlife imports at U.S. ports of entry [Endangered Species Act, 16 USC 1538(e)]. Port officers have the authority to detain or refuse shipments if the required documentation is missing or incomplete. The poor reporting of taxonomic status we find in the LEMIS database suggests a need to tighten protocols and makes it impossible to fully assess the biological diversity of wildlife entering the United States.

There is currently no coordinated national strategy, legislative authority, or funding devoted to oversight of the live wildlife trade. Scientific risk analysis of imported taxa, at the level of genus or species, would provide a considerable advance in assessing the threat that imported wildlife pose as invasive species or pathogen reservoirs. However, this is impossible given the current state of record-keeping. Correcting this problem would be a major first step toward risk analysis and reduction.

Risk analysis, as defined by the Convention on Biological Diversity (CBD), involves assessing the consequences of introduction, the likelihood of establishment of nonnative species, and the identification of measures to reduce or manage these risks, taking into account socioeconomic and cultural considerations (*14*). Effective risk analysis would require participation from all stakeholders, including the pet industry, and would need to be quantitative, to incorporate recently published data, and to include cost-benefit analyses of the economic and social benefits of wildlife ownership and trade. Findings could be used to rank threat levels for imported taxa and to prioritize those requiring more research or regulation, such as an importation ban.

Risk analysis based on the CBD definition would add balance to the Nonnative Wildlife Invasion Prevention Act (H.R. 669), the most recent proposal to improve U.S. regulation of wildlife importation. In its current form, H.R. 669 does not consider the economic benefits of wildlife trade. We argue that it should. H.R. 669 requires evaluation of the threat imported wildlife species pose as invasive species or carriers of known pathogens before importation. It proposes creation of lists of species "approved" or "unapproved" for import. Although the Act recognizes that there are species for which adequate scientific and commercial evidence is not yet available to make an evaluation of import risk, it does not stipulate how such species should be handled. For these species, we propose that H.R 669 should require their temporary placement on a "gray list." These gray-listed species should receive priority funding for risk analysis. It is currently impossible to know the proportion of species that would be on such a gray list. Until we begin evaluating the species proposed for import, it will not be clear which have adequate information for risk analysis and which do not.

Realistically, scientific information on the environmental, health, and economic impacts of many species in the trade is likely to be minimal. To support fair commerce we propose that, until scientific findings are released, gray-listed species that have been previously imported should be provisionally approved, whereas newly proposed species should be restricted. This would enable a flexible approach to the management of these species as additional information is collected.

H.R. 669 could be used immediately to deal with many traded species that have been fully researched by the scientific community. For example, some imported amphibians are reservoirs of a fungus (*Batrachochytrium dendrobatidis*) that causes chytridiomycosis, a lethal disease to many amphibians, and the cause of recent extinctions (*15*). There is excellent science identifying amphibian species that are likely carriers (*16*), which could be used to conduct adequate risk analysis.

To further reduce the risk of pathogen introduction via the wildlife trade, we believe measures should include third-party screening of selected species for high-priority diseases before importation—a measure not covered by H.R. 669. Screening would be improved by the development and/or validation of testing tools [e.g., MassTag PCR (multiple tag–based DNA amplification with the polymerase chain reaction), viral and panmicrobial microarrays, and high-throughput sequencing]. On an international scale, implementation should include groups that monitor or control the spread of nonnative hosts and pathogens to new regions such as the Invasive Species Specialist Group, Global Invasive Species Information Network, Food and Agriculture Organization of the United Nations, World Health Organization, Office International des Épizooties (OIE), nongovernmental organizations specializing in biodiversity conservation and health and others—perhaps working through a single intergovernmental agency.

Implementation of these measures can occur in a way that supports the healthy trade of wildlife, rather than acting as an economic hindrance to trade stakeholders. It could use the OIE's approach, which provides incentives (the declaration of disease-free status) to trading nations. This would likely promote ex situ captive-breeding of frequently traded animals, reducing pressure on wild populations and the risk of disease introduction.

Voluntary measures to reduce risk have been proposed. CDC's "Healthy Pets, Healthy People" Web site advises pet owners about zoonotic diseases associated with some wildlife (www.cdc.gov/healthypets). The Pet Industry Joint Advisory Council (www.pijac.org) promotes a National Reptile Improvement Plan, encouraging importers to screen animals for ticks. Such voluntary regulatory measures are a useful, but not a complete, solution and they need to include trade stakeholders, and to be independently assessed to determine success.

Collectively, risk analysis on wildlife species in trade, preborder pathogen screening, and voluntary support should go a long way to reducing costs associated with species invasion [estimated at $120 billion per year in the United States (*17*)] and to protect public, environmental, and animal health.

References and Notes

1. Defenders of Wildlife, *Broken Screens: The Regulation of Live Animal Imports in the United States* (Defenders of Wildlife, Washington, DC, 2007).
2. W. B. Karesh, R. A. Cook, E. L. Bennett, J. Newcomb, *Emerg. Infect. Dis.* **11**, 1000 (2005).
3. P. M. Vitousek, C. M. D'Antonio, L. L. Loope, R. Westbrooks, *Am. Sci.* **84**, 468 (1996).
4. P. Daszak, A. A. Cunningham, A. D. Hyatt, *Science* **287**, 443 (2000).
5. C. L. Hutson *et al.*, *Am. J. Trop. Med. Hyg.* **76**, 757 (2007).
6. K. D. Reed *et al.*, *N. Engl. J. Med.* **350**, 342 (2004).
7. D. B. Di Giulio, P. B. Eckburg, *Lancet Infect. Dis.* **4**, 15 (2004).
8. Centers for Disease Control and Prevention, *MMWR Morb. Mortal. Wkly. Rep.* **52**, 561 (2003).
9. A. J. Fowler, D. M. Lodge, J. F. Hsia, *Front. Ecol. Environ* **5**, 353 (2007).
10. Food and Drug Administration, "Joint order of the Centers for Disease Control and Prevention and the Food and Drug Administration, Department of Health and Human Services." *Fed. Regist.* **68**, 36566 (2003).
11. Further information is available in the supporting material on *Science* Online.
12. K. E. Jones *et al.*, *Nature* **451**, 990 (2008).
13. USFWS Permits, www.fws.gov/permits/ltr/ltr.shtml.
14. M. De Poorter *et al.*, *In-Depth Review of Ongoing Work on Alien Species That Threaten Ecosystems, Habitats or Species. Addendum: A Preliminary Report of Expert Workshop on Best Practices For Pre-Import Screening of Live Animals in International Trade*, 9 to 11 April 2008, South Bend, IN (Ninth CBD, U.N. Environment Programme, New York, 2008); www.cbd.int/doc/meetings/cop/cop-09/information/cop-09-inf-32-add1-en.pdf.
15. L. M. Schloegel *et al.*, *EcoHealth* **3**, 35(2006).
16. L. M. Schloegel *et al.*, *Biol. Conserv.*, in press.
17. D. Pimentel *et al.*, *Ecol. Econ.* **52**, 273 (2005).

18. Supported by the Cestone Foundation, the Eppley Foundation, a National Science Foundation Human and Social Dynamics "Agents of Change" award (BCS–0826779), the New York Community Trust, the Rockefeller Foundation, the Smith Fellowship Program, the Switzer Foundation, and the V. Kann Rasmussen Foundation. We thank G. Townsend of USFWS for help compiling LEMIS data. Opinions expressed by the authors do not necessarily reflect the opinions of the Centers for Disease Control and Prevention.

Supporting Online Material

www.sciencemag.org/cgi/content/full/324/5927/594/DC1

10.1126/science.1174460

Published by AAAS

HISTORY OF SCIENCE

Alexander von Humboldt and the General Physics of the Earth

In the early 19th century, Alexander von Humboldt laid the foundations for today's Earth system sciences.

Stephen T. Jackson

As scientists are celebrating the 200th anniversary of Charles Darwin's birth and the 150th anniversary of the publication of his *On the Origin of Species*, Darwin's ideas continue to shape and enrich the sciences (*1*). 6 May 2009 marks the 150th anniversary of the death of another 19th-century figure—Alexander von Humboldt—whose scientific legacy also flourishes in the 21st century. Humboldt helped create the intellectual world Darwin inhabited, and his writings inspired Darwin to embark on *H.M.S. Beagle*. More pertinent to our time, Humboldt established the foundation for the Earth system sciences: the integrated system of knowledge on which human society may depend in the face of global climate change.

Like Darwin, Humboldt undertook a major voyage that would shape his ideas and thinking. Humboldt spent 5 years (1799 to 1804) with botanist Aimé Bonpland exploring Venezuela, the northern Andes, and central Mexico, with visits to Tenerife, Cuba, and the United States. They collected botanical, zoological, geological, and ethnological specimens, made extensive atmospheric and geophysical measurements, and recorded the geographic location of their thousands of specimens and tens of thousands of measurements. Humboldt spent the next 22 years and most of his inherited fortune in Paris, preparing and publishing 45 volumes of a never-finished report on his travels.

Of these volumes, the first was a slim work entitled *Essay on the Geography of Plants* (*2*, *3*). The modest title belies the intellectual richness within. In the text and accompanying color plate (see the figure), Humboldt lays out a vision of a comprehensive "general physics of the Earth" aimed at nothing less than a synthesis of atmospheric, oceanic, geological, ecological, and cultural phenomena across the globe. Humboldt's obsession with geographically referenced measurements and collections was central to his vision. He recognized that spatial arrays of observations could be aggregated to reveal patterns that would in turn reveal underlying processes—such as the distribution of incident radiation, the transport of heat and materials in winds and ocean currents, the influence of temperature on plant form, and the effect of latitude and continentality on mountain snowline.

Intellectual riches. The central portion of Humboldt's *Physical Tableau of the Andes and Neighboring Countries*, published as part of (*2*, *3*), shows Chimborazo in profile, with vegetation zones, plant species, and snowline depicted at appropriate elevations. In the original, the profile is flanked on both sides by tables describing elevational patterns in temperature, humidity, light refraction and intensity, agriculture, fauna, and other physical, chemical, and biological features.

He expanded this vision in the succeeding years, establishing international cooperative networks of meteorological and geomagnetic measurement stations, inventing isotherms and other graphical devices to portray spatial patterns, and noting that plant form is often better predicted by local environment than by taxonomic affinity (a paradox resolved by Darwin). Humboldt's genius lay in his geographical vision, and in his intuition that Earth's land surface, oceans, atmosphere, and inhabitants form an integrated whole, with linkages among the various components (*4*, *5*). Humboldt's general physics of the Earth envisioned climate as a major control of Earth-surface phenomena, with vegetation serving as both an index of climate and a proximal control of microclimate, animal habitat, and cultural practices (*6*–*8*).

Humboldt's dream of systematic observational arrays across the globe took hold in the 19th century. Throughout the century, countless Humboldt-inspired explorations were launched, each involving systematic measurement and mapping of physical, biological, and often cultural features of landscapes and oceans (*8*–*10*). These surveys were relentlessly inductive, typically producing detailed descriptive reports with little integration within or among the component entities. However, for a few intellectually nimble participants—including Charles Darwin, T. H. Huxley, Matthew Maury, Asa Gray, C. Hart Merriam, and Peter Kropotkin—these explorations provided data and experience that spurred the development of biogeography, ecology, oceanography, and other environmental sciences (*11*).

Botany Department and Program in Ecology, University of Wyoming, Laramie, WY 82071, USA. E-mail: jackson@uwyo.edu

CREDIT: REPRODUCED FROM AN ORIGINAL COPY IN THE NATURAL HISTORY MUSEUM, PARIS

Published by AAAS

Unfortunately, the conceptual unification among the sciences of the Earth that Humboldt sought never developed in the century following his death. Disciplinary specialization played a large role in eclipsing Humboldt's integration, as did 20th-century trends toward reductionism, experimentalism, and fine-scale processes in many disciplines.

A new incarnation of Humboldt's general physics of the Earth began to emerge with the plate tectonics revolution in the 1960s. Drawing on Humboldtian spatial arrays of observations, this theory provided a unified explanatory framework for disparate geophysical, geological, paleontological, and biogeographic phenomena.

Today, a second, even broader manifestation of Humboldt's vision aspires to understand the interactions and feedbacks among the components of the Earth system, encompassing the lithosphere, atmosphere, hydrosphere, cryosphere, and biosphere as well as human societies and economies. This effort is often referred to as Earth system science, but it could just as well be designated "general physics of the Earth," using the early-19th century definition of physics as the study of the material world and its phenomena (which we now call science).

Global environmental change may be the greatest challenge faced by human societies since the advent of agriculture. Humboldt advocated for science that spoke to human needs and concerns (*5*). It is fitting that on the 150th anniversary of his death, we recognize his role in fostering the sciences that speak to the most profound human concerns—sustainability of human societies and the ecosystems on which they depend.

References and Notes

1. P. J. Bowler, *Science* **323**, 223 (2009).
2. A. de Humboldt, *Essai sur la géographie des plantes* (Levrault, Schell & Co., Paris, 1807).
3. An English translation of (*2*) is currently in press at the University of Chicago Press, Chicago.
4. A. de Humboldt, *Personal Narrative of Travels to the Equinoctial Regions of the New Continent, During the Years 1799-1804, by Alexander de Humboldt and Aime Bonpland; with Maps, Plans, &c.* (Longman, Hurst, Rees, Orme, & Brown, London, 1814 to 1829), vols. 1 to 7.
5. A. von Humboldt, *Cosmos: A Sketch of the Physical Description of the Universe* (Johns Hopkins Univ. Press, Baltimore, 1997), vol. 1.
6. M. Nicolson, *Hist. Sci.* **25,** 167 (1987).
7. M. Nicolson, in *Romanticism and the Sciences*, A. Cunningham, N. Jardine, Eds. (Cambridge Univ. Press, Cambridge, 1990), p. 169.
8. M. Dettelbach, in *Cultures of Natural History*, N. Jardine *et al.*, Eds. (Cambridge Univ. Press, Cambridge, 1996), p. 287.
9. S. F. Cannon, *Science in Culture: The Early Victorian Period* (Dawson, New York, 1978).
10. W. H. Goetzmann, *New Lands, New Men: America and the Second Great Age of Discovery* (Viking, New York, 1986).
11. P. J. Bowler, *The Norton History of the Environmental Sciences* (Norton, New York, 1993).

10.1126/science.1171659

PLANETARY SCIENCE

Magnetic Twisters on Mercury

Observations of Mercury during the recent MESSENGER spacecraft flybys reveal a complex magnetosphere.

Karl-Heinz Glassmeier

Mercury is an enigmatic planet. Located closest to the Sun and without an atmosphere, it has only a weak planetary magnetic field to help it withstand the solar wind. The recent flybys of the MESSENGER spacecraft confirm the existence of the Hermean magnetosphere (*1*, *2*), discovered 35 years ago by the Mariner 10 mission (*3*). This magnetosphere is rather small, with the magnetopause (the boundary between the interplanetary medium and the magnetospheric plasma) located as close as 1700 km above the planet surface. Not much is known about the structure and dynamics of the Hermean magnetosphere, and it is here where the observations by MESSENGER are shedding new light. Reports on the discovery of magnesium in the exosphere of Mercury by McClintock *et al.* on page 610 of this issue (*4*) and the detection of flux transfer events by Slavin *et al.* on page 606 (*2*) demonstrate that Mercury is directly exposed to the harsh conditions of the interplanetary medium.

Flux transfer events are regions of localized magnetic flux transfer due to transient magnetic reconnection at the magnetopause (*5*, *6*). Magnetic reconnection is the process that converts magnetic energy into kinetic energy and is one of the most fundamental processes in astrophysical plasmas. Reconnection occurs in regions of strong magnetic shear. Through pairs of magnetic flux tubes, a topological connection between the interplanetary and planetary magnetic field can be achieved. During MESSENGER's second flyby, the interplanetary magnetic field was pointing southward, antiparallel to the Hermean planetary magnetic field. The magnetopause is thus highly sheared—optimum conditions for reconnection. The magnetopause would usually separate the interplanetary magnetic field from the planetary field. Mass and energy flow across the boundary would thus be vastly reduced. During flux transfer events, however, the magnetopause is perforated at multiple points and the magnetosphere opens up, exposing the planet to the interplanetary medium (see the figure).

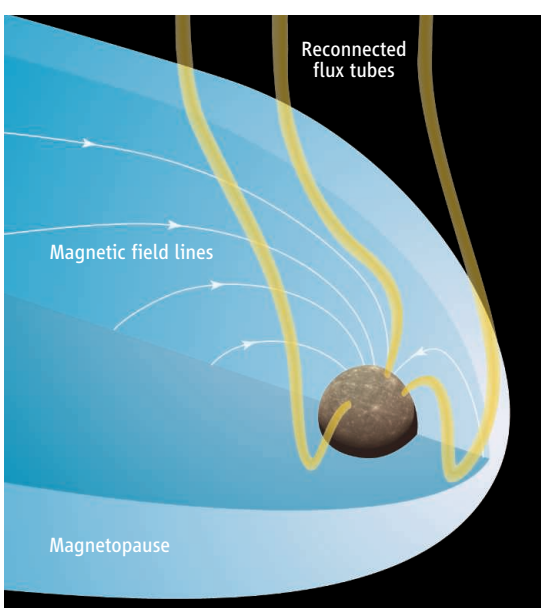

Magnetic twisters. As a result of dayside local magnetic reconnection, bundles of magnetic field lines penetrate the magnetopause, are convected tailward by the solar wind, plough through the magnetosphere, and interact with the planetary surface.

PHOTO CREDIT: NASA/JOHNS HOPKINS UNIVERSITY APPLIED PHYSICS LABORATORY

Institute of Geophysics and Extraterrestrial Physics, Technical University of Braunschweig, Braunschweig, and Max Planck Institute for Solar System Research, Katlenburg-Lindau, Germany. E-mail: kh.glassmeier@tu-bs.de

It is such a perforated magnetopause that is described by Slavin *et al.* Of extreme interest is the large size of the observed flux transfer events. At around 900 km in diameter, they are comparable to the overall scale of the Hermean magnetosphere. These events also have a short lifetime, indicating a fast and efficient transformation of magnetic into kinetic energy. During magnetic reconnection events, interplanetary magnetic field lines are connected to

Published by AAAS

Mercury's planetary field lines. The flux transfer events can be viewed as magnetic flux tubes or magnetic twisters dancing on the magnetopause, rooted deep in the magnetosphere or planetary interior, and are carried out into the interplanetary medium by the solar wind flow. In the terrestrial magnetosphere, flux transfer events cause plasma convection at their ionospheric foot point and transient auroral events (*7*). The corresponding processes in the Hermean magnetosphere are unknown.

Somehow, the electric currents associated with the reconnected flux tubes need to be closed, either within the magnetosphere or in the upper surface layers of Mercury. But the very nature of this closure will have implications for the flux tube dynamics. Much like a tornado in Earth's atmosphere interacts with the ground, the magnetic twisters on Mercury due to the flux transfer events interact with the planet surface. The observations of McClintock *et al.* are very important in this respect. Intensive emissions from Mercury's neutral exosphere reveal the existence of sodium, calcium, and magnesium in the exosphere. This material is sputtered off by energetic electrons hitting the surface. High-energy electrons are produced by various dynamic processes within the magnetospheric plasma. Flux transfer events are one of them. The observed north-south enhancement of sodium by McClintock *et al.* (*4*) could be a result of magnetospheric plasma dynamics induced by flux transfer events. And particles released at the surface will be picked up by the magnetospheric plasma, like cometary ions are picked up by the solar wind (*8*). This mass loading causes modifications of the plasma's dynamics. A picture of a strongly mutually dependent system emerges.

Slavin *et al.* also observed magnetic reconnection activity in the magnetotail of Mercury, as is observed at Earth during magnetospheric substorm events (*9*). A substorm is the major dynamic process in the terrestrial magnetosphere. The new perspective afforded by these latest observations is that flux transfer events are a real competitor to tail reconnection. In the much larger terrestrial magnetosphere, a substorm requires a growth phase (*9*), during which the magnetotail is magnetically charged up before it collapses. At Mercury, the dynamics are much faster, and dayside flux transfer and nightside magnetotail reconnection are more entangled with each other.

Mercury's strong coupling to its local interplanetary environment is intriguing and poses new opportunities for our geological and geophysical understanding of this and other planets (*10*, *11*). The magnetosphere is to Mercury what the troposphere is to Earth, with magnetospheric processes determining the weather in the planetary environment. Here, exogenic geological processes formed the surface of Mercury over the past eons. Mercury is a unique plasma laboratory, still hiding most of its secrets yet to be unravelled by the present MESSENGER mission and the future European-Japanese BepiColombo mission (*12*). Mercury is indeed an enigmatic planet!

References

1. J. A. Slavin *et al.*, *Science* **321**, 85 (2008).
2. J. A. Slavin *et al.*, *Science* **324**, 606 (2009).
3. N. F. Ness *et al.*, *Science* **185**, 151 (1974).
4. W. E. McClintock *et al.*, *Science* **324**, 610 (2009).
5. G. Haerendel *et al.*, *J. Geophys. Res.* **83**, 3195 (1978).
6. C. T. Russell, R. C. Elphic, *Space Sci. Rev.* **22**, 681, (1978).
7. P. E. Sandholt, C. J. Farrugia, *J. Geophys. Res.* **112**, A04203, 10.1029/2006JA011952 (2007).
8. K. Szegö *et al.*, *Space Sci. Rev.* **94**, 429 (2000).
9. V. Angelopoulos *et al.*, *Science* **321**, 931 (2008).
10. S. Orsini *et al.*, *Space Sci. Rev.* **132**, 551 (2007).
11. K. H. Glassmeier, H. U. Auster, U. Motschmann, *Geophys. Res. Lett.* **34**, L22201, 10.1029/2007GL031662 (2007).
12. A. Milillo *et al.*, *Planet. Space Sci.*, 10.1016/j.pss.2008.06.005 (2009).

10.1126/science.1173770

CIRCADIAN RHYTHMS

A Circadian Loop asSIRTs Itself

The oscillating biosynthesis of NAD$^+$ constitutes a feedback loop that integrates the mammalian circadian clock with metabolism.

Herman Wijnen

Daily time keeping in many organisms depends on internal circadian clocks that temporally organize biological functions relative to each other as well as the environment. These clocks generate rhythms in physiology and behavior by using circuits of gene expression that are organized in negative-feedback loops (*1*). Two studies in this issue, by Nakahata *et al.* (*2*) on page 654 and Ramsey *et al.* (*3*) on page 651, propose the addition of a new negative-feedback loop to this circuitry that involves the metabolite nicotinamide adenine dinucleotide (NAD$^+$) and the protein SIRTUIN1 (SIRT1). The new loop suggests connections between the circadian clock and SIRT1-dependent functions associated with cell survival, development, inflammation, and metabolism.

In the mammalian clock, a central role is played by the heterodimeric transcription complex CLOCK-BMAL1, which induces the expression of a number of genes, including those encoding the PERIOD (PER) and CRYPTOCHROME (CRY) proteins that directly repress CLOCK-BMAL1 activity, as well as REV-ERB and ROR nuclear receptors that control *Bmal1* expression. The new negative-feedback loop identified by Nakahata *et al.* and Ramsey *et al.* involves the CLOCK-BMAL1–controlled gene nicotinamide phosphoribosyltransferase (*Nampt*), its metabolite NAD$^+$, and SIRT1 (which represses CLOCK-BMAL1 activity in a NAD$^+$-dependent manner) (see the figure).

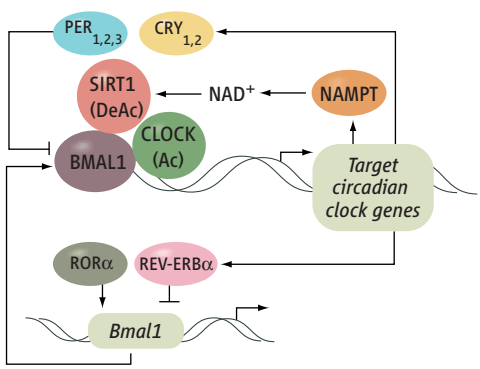

The NAMPT-SIRT1 circadian loop. Mammalian circadian clock circuits are shown as two loops of gene expression that feed back on the CLOCK-BMAL1 transcription complex. NAD$^+$ metabolism integrates into this network through the circadian control of *Nampt*, which encodes the rate-limiting enzyme in NAD$^+$ biosynthesis. NAD$^+$ regulates SIRT1 deacetylase activity (DeAc), which alters CLOCK-BMAL1–dependent transcription. CLOCK also acts as an acetyl transferase (Ac).

A key step in the new time-keeping loop is the transcriptional regulation of *Nampt* by CLOCK-BMAL1. *Nampt* encodes an enzyme that produces nicotinamide mononucleotide from nicotinamide and 5′-phosphoribosyl 1-pyrophosphatase, a rate-limiting step in NAD$^+$ biosynthesis. Nakahata *et al.* and Ramsey *et al.* found that *Nampt* transcript levels peak at about the same time as known CLOCK-BMAL1–regulated transcripts, and NAMPT protein oscillates with a somewhat

Department of Biology, University of Virginia, Charlottesville, VA 22904, USA. E-mail: hw9u@virginia.edu

Published by AAAS

later phase. *Nampt* expression decreased in response to mutations in *Clock* and *Bmal1*, but increased when both *Cry1* and *Cry2* were mutated. Moreover, the *Nampt* gene contains a number of cis-regulatory elements with perfect and near-perfect matches to the consensus binding site for CLOCK-BMAL1. Indeed, *Nampt* regulatory elements bind to CLOCK-BMAL1 in vivo. Another element in the new loop is the circadian oscillation of NAD^+. Apart from connecting glycolysis and the citric acid cycle to oxidative phosphorylation, NAD^+ is a substrate for sirtuin histone deacetylases (*4*). Sirtuins, present in all domains of life, were first identified in budding yeast where they contribute to DNA silencing, genomic integrity, and progression of the cell division cycle. NAD^+ levels show clock-dependent oscillations in mouse liver and fibroblasts that roughly match the reported phase of SIRT1 deacetylase activity (*5*). Nakahata *et al*. and Ramsey *et al*. found that these NAD^+ rhythms are disrupted by mutations in circadian clock genes and by the NAMPT inhibitor FK866.

The loop is closed by feedback of SIRT1 on CLOCK-BMAL1–dependent transcription. SIRT1 is a component of CLOCK-BMAL1 transcription complexes and affects the expression of clock genes (*5*, *6*). SIRT1 has now been detected at cis-acting sites in the clock-controlled genes *Dbp*, *Per2*, and *Nampt* (*2*, *3*, *5*), and proposed to act as a negative transcriptional regulator in this context. Nakahata *et al*. and Ramsey *et al*. found that SIRT1 overexpression or its activation by resveratrol repressed the *Per2* promoter, whereas the SIRT1 inhibitors nicotinamide and Ex-527 had the opposite effect. Furthermore, the *Nampt* inhibitor FK866 not only depressed NAD^+ production, but also modulated circadian expression of *Dbp* and *Per2*, and reversed SIRT1-dependent repression of the *Per2* promoter.

SIRT1 and its homologs function in heterochromatin formation and transcriptional repression through the deacetylation of histones H3 and H4 (*4*). Deacetylation of histone H3 at the *Dbp* promoter responds to SIRT1 and its inhibitors nicotinamide and splitomycin (*5*). Histones are, however, not the only relevant target for deacetylation by SIRT1. Both BMAL1 and PER2 are deacetylated by SIRT1 (*5*, *6*), and Nakahata *et al.* found that FK866 increased BMAL1 acetylation. In addition, CLOCK shows acetyltransferase activity toward histone H3 and BMAL1 (*7*, *8*). Complexes containing both CLOCK-BMAL1 and SIRT1 may, therefore, have dynamically balanced acetyltransferase and deacetylase activities that differentially affect promoter activity via multiple substrates.

By associating with CLOCK-BMAL1, SIRT1 could affect the daily timing of molecular, cellular, metabolic, endocrine, physiological, and behavioral functions. Conversely, SIRT1 plays an important role in cell survival, development, inflammation, and metabolism, and the circadian control of SIRT1 deacetylase activity may be reflected in these functions. Interestingly, the nuclear receptor peroxisome proliferator-activated receptor–γ (PPAR-γ) and the nuclear receptor cofactor PPAR-γ coactivator 1α (PGC1α), which control energy metabolism, not only exhibit circadian expression, but also affect the expression of clock genes (*9*–*11*). Moreover, SIRT1 and its activator resveratrol promote deacetylation and the activity of PGC-1α in association with glucose homeostasis in the liver and mitochondrial function in muscle and brown fat (*12*, *13*). Furthermore, in white adipose tissue, SIRT1 binds and represses PPAR-γ in association with mobilization of fat stores during food deprivation (*14*). Unraveling how these mechanisms incorporate interactions between the circadian clock and SIRT1 may help yield insights into the etiology of metabolic diseases and aging.

References and Notes

1. H. Wijnen, M. W. Young, *Annu. Rev. Genet.* **40**, 409 (2006).
2. Y. Nakahata, S. Sahar, G. Astarita, M. Kaluzova, P. Sassone-Corsi, *Science* **324**, 654 (2009); published online 12 March 2009 (10.1126/science.1170803).
3. K. M. Ramsey *et al.*, *Science* **324**, 651 (2009); published online 19 March 2009 (10.1126/science.1171641).
4. S. Michan, D. Sinclair, *Biochem. J.* **404**, 1 (2007).
5. Y. Nakahata *et al.*, *Cell* **134**, 329 (2008).
6. G. Asher *et al.*, *Cell* **134**, 317 (2008).
7. M. Doi, J. Hirayama, P. Sassone-Corsi, *Cell* **125**, 497 (2006).
8. J. Hirayama *et al.*, *Nature* **450**, 1086 (2007).
9. X. Yang *et al.*, *Cell* **126**, 801 (2006).
10. N. Wang *et al.*, *Cell Metab.* **8**, 482 (2008).
11. C. Liu, S. Li, T. Liu, J. Borjigin, J. D. Lin, *Nature* **447**, 477 (2007).
12. J. T. Rodgers *et al.*, *Nature* **434**, 113 (2005).
13. M. Lagouge *et al.*, *Cell* **127**, 1109 (2006).
14. F. Picard *et al.*, *Nature* **429**, 771 (2004).

15. This work was supported by NIH grant R01 GM78839.

10.1126/science.1174132

CLIMATE

The Geographic Footprint of Glacier Change

Greg Balco

Glacier advances and retreats over the past 10,000 years illustrate the complexity of climate dynamics.

Alpine glaciers leave spectacular records of climate change. Lakes, moraines, and other landforms shaped by past glacier advances and retreats dominate the foreground of nearly all mountain landscapes. These glacial deposits are rich records of past climate that are widespread, obvious, and easily accessible. In many regions without sedimentary or ice-core records, they are the only record of climate before instrumental records began. A report on page 622 of this issue by Schaefer *et al.* highlights the value of these glacial records in understanding past climate dynamics while also revealing their complexity (*1*).

Most glacier records for the Holocene (the past 10,000 years) show several prominent advances at intervals of 1000 to 2000 years. Interpretations of these records have aimed to test hypotheses about past climate by determining whether glacier advances in widely separated regions were synchronous or asynchronous. Simultaneous advance of mountain glaciers worldwide would favor a hypothesis in which changes in solar irradiance warm or cool the Earth as a whole (*2*). In contrast, out-of-phase advances of Northern and Southern Hemisphere glaciers would favor a scenario in which reduced deep-ocean ventilation and associated heat transport in the Northern Hemisphere are balanced by increased ventilation in the Southern Hemisphere (*3*).

So far, none of these tests have proven conclusive, mainly because the uncertainty of dating techniques for glacial deposits is comparable to the time scale of the climate processes in question. However, two advances in glacier chronology have made progress on this problem.

The first has been a focused search of recently deglaciated glacier forelands for organic material—wood and peat—that grew at a time when glaciers were less extensive and that survived erosion by later glacier advances (*4*). Before this effort, most researchers only dated moraines that formed when glaciers were larger than present. Radiocarbon dating

Berkeley Geochronology Center, Berkeley, CA 94709, USA. E-mail: balcs@bgc.org

Published by AAAS

of the preserved wood and peat has now revealed times when glaciers were smaller than at present, and filled in the missing half of the existing chronologies.

The second has been the advent of increasingly precise and numerous cosmogenic-nuclide exposure ages on glacial moraines. Moraines are formed of rock quarried at glacier beds; this material is not exposed to the surface cosmic-ray flux until deposited at the glacier margin. Thus, the concentration in a moraine boulder of certain rare isotopes produced only by cosmic-ray interactions dates the glacier advance that formed the moraine. The key advantage of this method over radiocarbon dating is the sheer number of boulders available: Nearly any Holocene moraine is covered with potential samples.

Schaefer *et al.* exploit this advantage, as well as an array of analytical improvements, to generate an unusually large data set of unusually precise exposure ages from Holocene glacial moraines in New Zealand. But the greatest value of their data set arises from comparison to radiocarbon-dated preglacial wood from Northern Hemisphere sites. Because ice-free periods recorded by the radiocarbon-dated wood are long compared with the uncertainty in the exposure ages, one can now state with high confidence whether or not glaciers in New Zealand were large when glaciers in the Alps were small.

This is important because it should make it possible to rigorously test whether Holocene glacier advances were synchronous or asynchronous. Schaefer *et al.* come to the unexpected conclusion that neither hypothesis explains the full data set: Sometimes glaciers in New Zealand were larger than at present when those in the Alps were smaller, but at other times both appear to have advanced simultaneously. The answer to the question "were Holocene glacier advances in the Northern and Southern Hemispheres in phase, or out of phase?" turns out to be "no."

This answer satisfies advocates of neither hypothesis. Instead, it highlights the challenge—and the opportunity—of better reconciling paleoclimate data, such as glacier advances and retreats, with advances in glacier modeling and modern climate dynamics.

The geographically sparse nature of paleoclimate data naturally leads to the idea that global-scale phenomena can be identified by correlating widely separated paleoclimate records; both hypotheses about Holocene climate discussed above proceed from this premise. Yet, a central concept of modern climate dynamics is that climate variability is expressed in complex regional patterns, such as the El Nino–Southern Oscillation, the Pacific Decadal Oscillation, and others. If this was also true in the past—as there is no reason to doubt—then past glacier changes were regionally patterned at a geographic scale that may well be smaller than the spacing of the paleoclimate data.

In addition, glaciers are reservoirs for many years of snow accumulation. This can add to their value as a climate proxy, because they should filter out year-to-year variability to reveal trends. On the other hand, this "memory" effect also smoothes short-term stochastic variability (which is always present even in a steady climate) into longer-period changes in glacier length. Glacier models driven by random year-to-year variability in precipitation and temperature, but no change in the mean climate, can mimic the centennial to millennial spacing of large advances seen in Holocene moraine records.

These ideas pose two challenges in interpreting the chronology of past glacier change. First, one must disprove the null hypothesis: Can the timing and magnitude of observed past glacier changes in a particular region be explained by stochastic variability inherent in a steady climate, or is a change in the mean climate required (*5*)? Second, if one has established that a glacier advance requires a substantial change in mean climate, one must determine the regional "footprint" of that change and compare it to that inferred from modern instrumental climate records, or simulated by climate models, for a particular climate-change scenario (*6*).

Glacier models and modern climate dynamics can also help to decide which—and how many—glaciers to study. Existing studies of past glacier change have focused on glaciers that left particularly spectacular geologic records, but these glaciers may not be the best ones for answering questions about past climate. Future studies should use model simulations and the modern observational record to identify those glaciers that are most sensitive to certain climate parameters and to explore what spatial density of glacier change records is needed to understand the relationship between past and present patterns of regional climate variability.

Advance and retreat. A series of concentric moraines in front of the terminus of the Kluane Glacier in Alaska's St. Elias Mountains record advances and retreats of this glacier during the past several thousand years. The photo shown here was taken on 10 August 1961. In 1973, Denton and Karlen showed that moraines in this region of Alaska had similar ages as others in Scandinavia and proposed that glaciers worldwide had advanced and retreated together in response to changes in solar irradiance (*2*). Subsequent research, including the report in this issue by Schaefer *et al.*, has neither proved nor disproved this hypothesis but rather has revealed the complexity of past climate changes and the response of glaciers to these changes.

CREDIT: AUSTIN POST/COURTESY OF THE GEOPHYSICAL INSTITUTE/UNIVERSITY OF ALASKA FAIRBANKS

References

1. J. M. Schaefer *et al.*, *Science* **324**, 622 (2009).
2. G. Denton, W. Karlen, *Quatern. Res.* **3**, 155 (1973).
3. W. S. Broecker, *Paleoceanography* **13**, 119 (1998).
4. A. Hormes, J. Beer, C. Schlucter, *Geog. Ann.* **88**, 281 (2006).
5. B. K. Reichert, L. Bengtsson, J. Oerlemans, *J. Climate* **15**, 3069 (2002).
6. S. Rupper, G. Roe, *J. Climate* **21**, 5384 (2008).

10.1126/science.1172468

Published by AAAS

PHYSICS

A Glassy State of Supersolid Helium

Disorder and defects appear to play an important role in the formation of a supersolid from helium-4 atoms.

John Saunders

Superfluid helium is best known for its ability to flow without resistance. Superfluids also differ from ordinary fluids in that they fail to respond to a slow steady rotation (*1*). The atoms in a superfluid are in the same quantum state, so they move coherently and cannot gradually "spin up," as does water in a rotated container. An intriguing question is whether a supersolid—formed by applying pressure to a superfluid—could combine these remarkable properties, quantum coherence and dissipationless mass flow of atoms, in a solid that still has structural order and rigidity (*1*–*4*).

In an ordinary classical crystal, all atomic motion is frozen out at absolute zero, but solid helium-4 is a quantum solid; each atom is highly delocalized in a quantum probability cloud around its equilibrium position, and as a result, atoms on neighboring sites can exchange positions and move through the solid. In 2004, Kim and Chan (*5*) claimed to have observed supersolidity in solid helium-4. This discovery was followed by experimental and theoretical studies suggesting that disordered glassy solids play a key role in creating the putative supersolid state.

Two reports in this issue address the origin and effects of this disorder. On page 632, Hunt *et al.* (*6*) report their observation of the onset of remarkable ultraslow dynamics on cooling samples of solid helium, which constitutes new evidence for glass-like behavior. They reveal a subtle interplay between this glassiness and the observed supersolid-like mechanical responses. On page 631, Anderson (*7*) argues that the supersolid will still occur in a pristine crystal, but coupling to disordered regions near dislocations enhances the supersolid response. His bold hypothesis is that every solid composed of bosons will have a supersolid ground state.

In extensive experiments by Chan and others (*8*, *9*), solid helium-4 is grown in a cylinder or annulus, which acts as the "bob" of a torsion pendulum that oscillates (twists) about its axis on resonance at acoustic frequencies (typically hundreds of hertz) (see the figure, panel A). Upon cooling below an onset temperature, the solid partially decouples from the oscillation, so the torsional pendulum, referred to as a torsional oscillator (TO), appears to have a "missing moment of inertia" (MMI) (*10*), which is detected by a small change in frequency. However, this MMI signature depends on sample quality and geometry and varies greatly, from around 0.04% to 20%, which suggests that disorder may also play a role in how the supersolid forms. Smaller variations in its temperature onset (from 80 to 300 mK) from sample to sample are also observed.

Theoretical studies show that such amorphous structures constitute a "superglass" (*11*, *12*). However, in experiments, the MMI survives even in the best-quality crystalline samples. These samples will inevitably be permeated by a network of dislocations and may contain grain boundaries. Although simulations show that both such defects support supersolidity (*13*), their density is expected to be too small to account for the measured MMI.

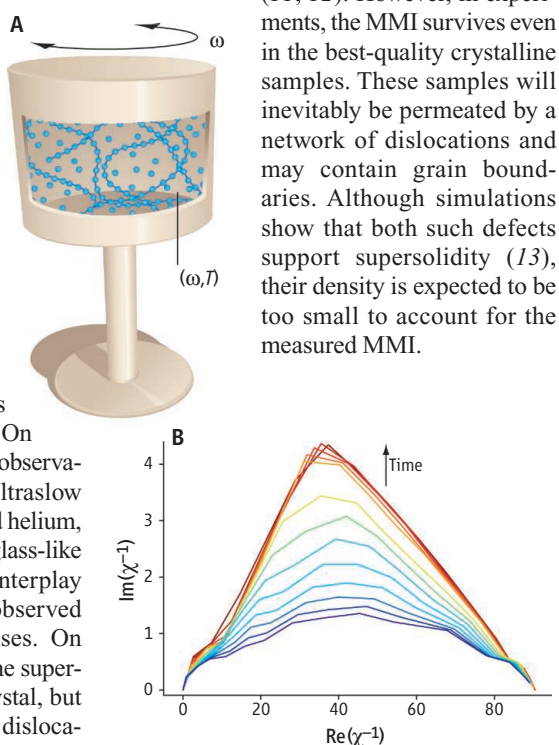

A supersolid response. (**A**) Experiments probe how solid helium-4, permeated with dislocations, responds when its container is oscillated at frequency ω. (**B**) The response of the solid to oscillation is captured by the function $\chi(\omega,T)$. Small shifts in resonance frequency correspond to the real part of χ^{-1}, $\mathrm{Re}(\chi^{-1})$; increases in resonance width correspond to the imaginary part, $\mathrm{Im}(\chi^{-1})$. The contour of $\mathrm{Im}(\chi^{-1})$ versus $\mathrm{Re}(\chi^{-1})$ in arbitrary units, based on measurements at different temperatures, provides a fingerprint of the solid's response.

Obtaining incontrovertible experimental proof of the supersolid state is challenging. In steady-rotation experiments on superfluid liquid helium-4, the MMI unambiguously demonstrates quantum coherence. The superfluid fraction tends to unity well below the transition. However, the TO experiments on solid helium-4 involve jiggling the sample at finite frequency, and the observed MMI is rather small in the highest-quality crystals. Hunt *et al.* carefully discuss how measurements of small changes in the oscillator's frequency and energy dissipation reflect the real imaginary parts of the complex number that represents the rotational susceptibility, whose temperature dependence characterizes the system. Such analysis can help to identify responses from processes unrelated to forming a supersolid, such as viscoelasticity (which has a temperature-dependent relaxation time) and atoms in a glassy state tunneling between sites.

Solid helium-4 indeed has a viscoelastic character; transverse sound measurements show a freezing of motion of the dislocation network upon lowering the temperature, which closely mimics the MMI seen in TO experiments (*14*). Andreev has shown that tunneling of atoms between two levels in glassy solid helium can also give rise to MMI (*15*). Even if the ground state of the system is supersolid, it is predicted to be reached by cooling through a vortex liquid state, which has a different signature in the rotational susceptibility (*16*).

The rotational susceptibility contour reported by Hunt *et al.* (see the figure, panel B) is stretched along the real axis. The observed frequency shifts are much greater than the shifts predicted by a model of glass-like or viscoelastic relaxation and are consistent with the presence of a supersolid state. Furthermore, thermal cycling experiments reveal an ultraslow evolution of the fingerprint. The time scale of this starts to grow rapidly below 60 to 70 mK, and reaches 5000 s at 20 mK. Previous observations of hysteretic response (*17*) are consistent with such slow dynamics. Hunt *et al.* suggest the onset of an exotic superglass phase as one possibility.

The movement of helium atoms between sites has been seen by nuclear magnetic resonance in fermionic solid helium-3

Department of Physics, Royal Holloway, University of London, Egham, Surrey TW20 0EX, UK. E-mail: j.saunders@rhul.ac.uk

CREDIT: ADAPTED BY P. HUEY/SCIENCE

Published by AAAS

(*18*). However, the theoretical consensus (*19*, *20*) is that such motion does not alone lead to the supersolid state in the bosonic helium-4 crystal. A version of Heisenberg's uncertainty principle requires that a macroscopic quantum state with definite phase must undergo fluctuations in particle number (*21*). This requirement can be accommodated by mobile defects or some other departure from the simple picture of an ideal crystal. In the original theoretical scenario, some fraction of atomic sites were spontaneously empty (mobile zero-point vacancies, or ZPVs), creating a homogeneous but incommensurate ground state, one with some lattice sites unfilled by atoms. The realization of this possibility in solid helium-4 is hotly disputed (*20*, *22*).

However, Anderson argues that the strongly correlated ground state of a boson crystal is indeed incommensurate. The supersolid transition temperature will be governed by Bose-Einstein condensation of the dilute gas of ZPVs. In his picture, the ZPVs are coupled to a cloud of vacancies around dislocations or other defects such as grain boundaries or surfaces, which enhance the fraction of supersolid present.

It seems that incipient glassy regions, dislocation cores, and the putative incommensurate crystal may all contribute to a supersolid MMI. In two-dimensional films of helium-4, the superfluid stiffness is controlled by the presence of thermally excited vortex-antivortex pairs. By contrast, solid helium-4 inevitably contains frozen-in line defects (dislocations) that intriguingly may both contribute to the supersolidity and also destroy it through their thermal motion. Might it be that steady, as opposed to oscillatory, supersolid flow at finite temperature is impossible?

In future studies, we can expect attempts to measure the rotational susceptibility and excitations of better-characterized samples. The emerging confluence of the physics of glasses and supersolidity in a quantum crystal is exciting. A quantum solid of Bose particles is perhaps the simplest strongly correlated system in nature, and the imperative to unlock its secrets is compelling.

References

1. A. J. Leggett, *Phys. Rev. Lett.* **25**, 1543 (1970).
2. L. Reatto, *Phys. Rev.* **183**, 334 (1969).
3. A. F. Andreev, I. M. Lifshitz, *Sov. Phys. JETP* **29**, 1107 (1969).
4. G. V. Chester, *Phys. Rev. A* **2**, 256 (1970).
5. E. Kim, M. H. W. Chan, *Science* **305**, 1941 (2004); published online 2 September 2004 (10.1126/science.1101501).
6. B. Hunt *et al.*, *Science* **324**, 632 (2009).
7. P. W. Anderson, *Science* **324**, 631 (2009).
8. M. H. W. Chan, *Science* **319**, 1207 (2008).
9. S. Balibar, F. Caupin, *J. Phys. Cond. Matter* **20**, 173201 (2008).
10. P. Phillips, A. V. Balatsky, *Science* **316**, 1435 (2007).
11. M. Boninsegni, N. Prokof'ev, B. Svistunov, *Phys. Rev. Lett.* **96**, 105301 (2006).
12. G. Biroli, C. Chamon, F. Zamponi, *Phys. Rev. B* **78**, 224306 (2008).
13. L. Pollet *et al.*, *Phys. Rev. Lett.* **101**, 097202 (2008).
14. J. Day, J. R. Beamish, *Nature* **450**, 853 (2007).
15. A. F. Andreev, *JETP Lett.* **85**, 585 (2007).
16. P. W. Anderson, *Nat. Phys.* **3**, 160 (2007).
17. Y. Aoki, M. C. Keiderling, H. Kojima, *Phys. Rev. Lett.* **100**, 215303 (2008).
18. R. A. Guyer, R. C. Richardson, L. I. Zane, *Rev. Mod. Phys.* **43**, 532 (1971).
19. D. M. Ceperley, B. Bernu, *Phys. Rev. Lett.* **93**, 155303 (2004).
20. N. Prokof'ev, *Adv. Phys.* **56**, 381 (2007).
21. P. W. Anderson, *Rev. Mod. Phys.* **38**, 298 (1966).
22. D. Galli, L. Reatto, *J. Phys. Soc. Jpn.* **77**, 111010 (2008).

10.1126/science.1172973

CANCER

Complicated Supercomplexes

Molecular details of how proteins interact to repair DNA breaks reveal complexities that underlie their tumor-suppressive effects in different cancers.

David M. Livingston

In the world of genome repair analysis, much attention has been focused on the mechanism underlying error-free repair of DNA double-strand breaks. This process, which involves homologous recombination–based repair, warrants close attention, not least because failure to repair double-strand breaks can be lethal. Similarly, disorderly repair can result in loss of chromosomal integrity and spur tumor development. Three recent studies emphasize the complex nature of the suspected link between the homologous recombination mechanism in mammalian cells and the suppression of cancer.

In mammalian cells, a double-strand break elicits a series of events, many triggered by activation of the kinase ataxia telangiectasia mutated (ATM). ATM subsequently phosphorylates multiple participants in homologous recombination, including the protein BRCA1/p220, which interacts with BRCA2 and its partner, the Rad51 strand-insertion recombinase (*1*). *BRCA1* and *BRCA2* are also high-penetrance suppressors of breast and ovarian cancer. Indeed, *BRCA1* appears to largely suppress breast and ovarian cancer, while *BRCA2* also performs this role for cancers in other organs, such as prostate, male breast, and pancreas (*2*).

Numerous structure-function analyses of BRCA1 and BRCA2 suggest that their homologous recombination function contributes to their role in tumor suppression (*3*). Moreover, certain BRCA1-interacting proteins with roles in homologous recombination (including ATM, PALB2, BACH1/BRIP1, NBS1, and Rad 50) also act as breast cancer suppressors (*3*). Together, this evidence implies that mounting a homologous recombination response represents an important defense against the development of breast and ovarian cancer.

A polypeptide called partner and localizer of BRCA2 (PALB2) associates with BRCA2 (*4*) and has recently attracted considerable scrutiny and clinical attention. Like *BRCA2*, *PALB2* is a breast cancer suppressor gene, although the phenotype associated with *PALB2* mutations is less penetrant than that associated with mutations in *BRCA1* or *BRCA2* (*5*–*7*). In addition, PALB2 is tightly bound to the amino terminus of BRCA2; it, too, participates in DNA repair and, like BRCA2, it is defective in a subtype of Fanconi's anemia (*8*, *9*). PALB2 conveys BRCA2 to stable binding sites in chromatin. Indeed, BRCA2 cannot function in homologous recombination or elicit tumor-suppressor effects in breast cancer without PALB2 (*4*). Furthermore, both PALB2 and BRCA2 are concentrated, along with BRCA1 and other DNA damage response proteins, at focal genomic sites containing double-strand breaks. BRCA1 conveys BRCA2 to double-strand breaks or, at least, stabilizes its localization at these sites (whereas BRCA1 is conveyed there by another mechanism) (*10*). Despite these findings, little has been known of how PALB2 becomes localized at these structures or of the role it plays once concentrated there.

Some of these mysteries have now been unraveled by Zhang *et al.* (*11*) and Sy *et al.* (*12*). Both groups have found that PALB2 binds to BRCA1 and that this interaction is the biochemical basis for the long-known interaction between BRCA1 and BRCA2 (*1*). These

Dana-Farber Cancer Institute, Departments of Genetics and Medicine, Harvard Medical School, Boston, MA 02115, USA. E-mail: david_livingston@dfci.harvard.edu

Published by AAAS

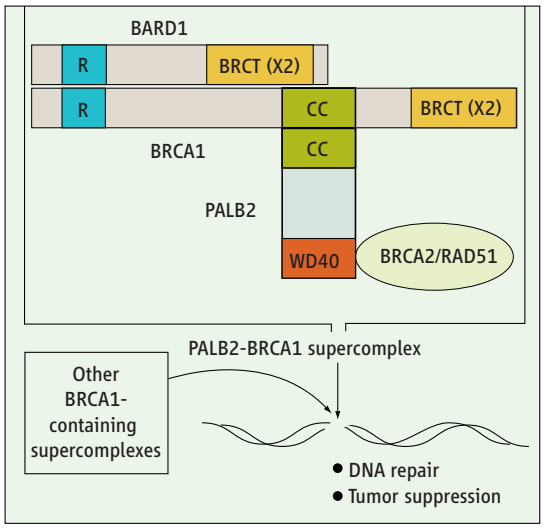

Intricate machinery. BRCA1 and its partner BARD1 both contain RING (R) and paired BRCT motifs, constitute an E3 ubiquitin ligase, and interact through specific coiled coil (CC) domains with PALB2. The carboxyl terminal segment of PALB2, which is rich in WD40 motifs, interacts with the extreme amino terminus of BRCA2 (which independently associates with RAD51). This supercomplex, likely together with other BRCA1 supercomplexes (*10*), supports homologous recombination and elements of BRCA1/2-driven tumor suppression.

studies have also revealed that the BRCA1-PALB2 interaction is grounded in the physical interaction of unique coiled-coil domains (see the figure), that BRCA1 is responsible for the concentration of PALB2 at focal sites containing double-strand breaks, and that a specific BRCA1-PALB2 interaction is required for cells to carry out homologous recombination-based repair after the introduction of double-strand breaks. Thus, not only is PALB2 a BRCA2-binding protein that facilitates its partner's double-strand break repair function, it is also the source of a long-sought link between the homologous recombination functions of BRCA1 and BRCA2. In addition, Sy *et al.* (*12*) suggest, based on clinically relevant BRCA1 missense mutations, that the interaction of BRCA1 and PALB2 is required for the former to perform its tumor-suppressor function in breast cancer. This is in keeping with the knowledge that PALB2 is a breast cancer suppression gene (*5*) and the view that defective homologous recombination underlies at least part of the tumor-suppressor function of BRCA1 and BRCA2 in breast cancer.

There are also new clinical findings on PALB2. Jones *et al.* report that, among 96 patients with familial pancreatic cancer, 3 harbored stop codon–generating germline *PALB2* mutations (*13*). Familial pancreatic cancer has long been known to arise from germline BRCA2 mutations (*14*). Thus, it is satisfying to find that PALB2, which is required for the docking of BRCA2 in chromatin and for its homologous recombination function, is, likewise, an exocrine pancreas tumor-suppressing protein.

These new observations come amid growing interest in the contrasting pathobiology of BRCA1 and BRCA2. While both are breast and ovarian tumor-suppressing genes, their lack of function is associated with the development of contrasting molecular pathological subtypes of breast cancer. In addition, the repertoire of *BRCA1*- and *BRCA2*-affected tissues differs considerably. Only *BRCA2* is responsible for disease in tissues other than the breast and ovary.

Although PALB2 is defective in the FANC-N subtype of Fanconi's anemia, and is a breast and a pancreatic cancer gene product, BRCA1, which also interacts with and depends on PALB2 for its homologous recombination function, is neither a pancreatic cancer nor a Fanconi's anemia protein. These seemingly disconnected phenomena likely reflect limited knowledge of the full range of BRCA1, PALB2, and BRCA2 functions and the mechanisms that underlie them. Thus, understanding why BRCA1 interacts with three different Fanconi's anemia proteins, is required for homologous recombination, and is not a Fanconi's anemia gene product, and/or why BRCA1 and BRCA2 are interacting homologous recombination proteins but exert qualitatively different organ-specific tumor-suppressor effects, might shed light on why *BRCA1* and *BRCA2* are breast and ovarian cancer suppressors at all.

References

1. J. Chen *et al.*, *Mol. Cell* **2**, 317 (1998).
2. P. M. Campeau, W. D. Foulkes, M. D. Tischkowitz, *Hum. Genet.* **124**, 31 (2008).
3. T. Walsh, M.-C. King, *Cancer Cell* **11**, 103 (2007).
4. B. Xia *et al.*, *Mol. Cell* **22**, 719 (2006).
5. H. Erkko *et al.*, *Nature* **446**, 316 (2007).
6. N. Rahman *et al.*, *Nat. Genet.* **39**, 165 (2007).
7. M. Tischkowitz *et al.*, *Proc. Natl. Acad. Sci. U.S.A.* **104**, 6788 (2007).
8. B. Xia *et al.*, *Nat. Genet.* **39**, 159 (2007).
9. S. Reid *et al.*, *Nat. Genet.* **39**, 162 (2007).
10. R. A. Greenberg *et al.*, *Genes Dev* **20**, 34 (2006).
11. F. Zhang *et al.*, *Curr. Biol.* 19, 524 (2009).
12. S. Sy, M. Huen, J. Chen, *Proc. Natl. Acad. Sci. U.S.A.* 10.1073/pnas.0811159106 (2009).
13. S. Jones *et al.*, *Science* **324**, 217 (2009).
14. M.Goggins *et al.*, *Cancer Res.* **56**, 5360 (1996).

10.1126/science.1174839

MEDICINE

Avoiding Unintended Toxicity

Todd E. Golde and Thomas L. Kukar

Drugs that inhibit a distinct form of γ-secretase may be useful in treating Alzheimer's disease without causing harmful side effects.

Amyloid-β protein (Aβ) deposition in the brain is one of the pathological hallmarks of Alzheimer's disease. Considerable data support the concept that the aggregation and accumulation of Aβ in the brain trigger a complex pathological cascade that ultimately results in neuronal dysfunction and neurodegeneration (*1*). Thus, therapies for Alzheimer's disease have focused mainly on preventing or slowing Aβ aggregation, neutralizing toxic Aβ aggregates, or clearing and breaking up these aggregates (*2*). On page 639 of this issue, Serneels *et al.* (*3*) report a theoretically safe approach to decrease Aβ production and thereby slow Aβ aggregation.

Aβ is an internal region within the amyloid-β protein precursor (APP). When the *APP* gene was cloned in 1987, the position of Aβ indicated that to be generated, APP had to be cut twice, at Aβ's amino terminus and carboxyl terminus. But the carboxyl terminus lies within the transmembrane domain of APP, and at that time it was heretical to propose that a protease could cut a peptide within a lipid bilayer. Thus, dogma held that Aβ was only produced in a disease state where membrane damage occurred, exposing the peptide to classic proteases. But 5 years later, Aβ was shown to be a normal, secreted, proteolytic product of APP (*4, 5*), indicating that intramembrane proteolysis is a normal physiologic event. Moreover, because proteases are often good drug targets, it was assumed that the

Mayo Clinic, College of Medicine, Department of Neuroscience, Mayo Clinic Florida, 4500 San Pablo Road, Jacksonville, FL 32224, USA. E-mail: tgolde@mayo.edu; kukar.thomas@mayo.edu

Published by AAAS

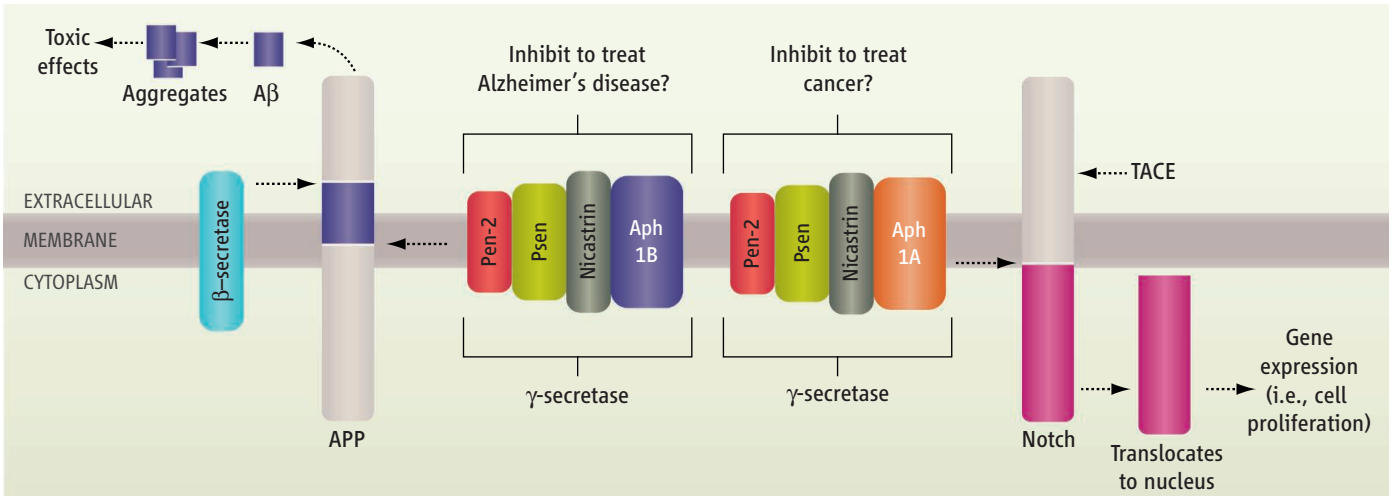

Targeted inhibitors Blocking a specific γ-secretase (containing Aph1B or Aph1A) might allow treatment of Alzheimer's disease or cancer without altering the normal functions of other γ-secretases. Psen, presenilin; TACE, tumor necrosis factor–α converting enzyme.

proteases generating Aβ would be rapidly identified; small-molecule inhibitors of these proteases would follow, and be successfully tested in the clinic.

By 1999, both proteases that sequentially cleave APP to generate Aβ—β-secretase [also called β-site of APP cleaving enzyme (BACE1) or Memapsin 2] and γ-secretase—were definitively identified (see the figure). Though β-secretase—a type 1 membrane protein with homology to classic aspartyl protease—is an excellent theoretical target, as it is the rate-limiting enzyme in Aβ production, it has proved to be a challenging pharmacologic target. Small-molecule β-secretase inhibitors that can penetrate the blood-brain barrier have been hard to identify, though one has entered early-phase human trials (*6*). γ-Secretase turned out to be a multisubunit aspartyl protease capable of cleaving within the lipid bilayer. The presenilin 1 or 2 proteins form the catalytic core of γ-secretase, and three accessory proteins form the γ-secretase complex: Aph1, Nicastrin, and Pen-2 (*7*). Numerous brain-penetrant γ-secretase inhibitors have been identified; however, target-based toxicity has been a major obstacle for their clinical development. γ-Secretase cleaves not only APP but also numerous other type 1 transmembrane proteins; for example, its cleavage of the protein Notch1 is critical for Notch signaling , which controls processes such as cell growth, differentiation, and proliferation (*8*). The absence of presenilin is lethal in mouse embryos. Moreover, treatment of mice with nonselective γ-secretase inhibitors leads to a variety of toxicities related to Notch inhibition, including rapid gastrointestinal, skin, and immune system abnormalities.

In contrast to a single enzymatic entity as originally envisioned, γ-secretase complexes are heterogeneous. In humans, two presenilin genes (*PS1* and *PS2*), along with Aph1 isoforms A (which can be alternatively spliced to a long and short form) and B, can produce up to six different γ-secretase complexes (*9*). The situation in rodents is even more complex due to the presence of the *Aph1C* gene that most likely arose from duplication of *Aph1B*. The physiological role of these different γ-secretase complexes and how they process substrates are largely unknown. The absence of Aph1A is embryonic lethal in the mouse, probably due to inhibition of Notch signaling. However, mice lacking both Aph1B and C develop normally without obvious defects.

Serneels *et al*. show that selective removal of Aph1B and C in a mouse model of Alzheimer's disease decreases Aβ plaque formation, improves behavioral deficits, and, importantly, shows no side effects from Notch impairment. They also demonstrate that γ-secretase complexes containing Aph1A or B produce different ratios of Aβ species, which may be related to different conformations of the enzyme. The major implication of this work is that specific inhibition of Aph1B γ-secretase complexes in the brain may be a useful strategy to lower Aβ production while avoiding Notch-related side-effects.

Other strategies are being pursued to decrease Aβ production while avoiding Notch toxicity. At least two γ-secretase inhibitors that block Aβ production but spare Notch have advanced to clinical trials, but the mechanisms by which they avoid impairing Notch are unknown (*10*). Another approach is the use of γ-secretase modulators that shift cleavage away from the more toxic $A\beta_{42}$ isoform to the shorter, less toxic fragments (*11*). The recent discovery that some γ-secretase modulators (such as flurizan, the first γ-secretase modulator to be evaluated in humans) bind to APP instead of γ-secretase, suggests a way to avoid Notch toxicity and develop more potent and efficacious γ-secretase modulators (*12*). Another way to reduce toxicity is to administer dexamethasone together with a γ-secretase inhibitor, a treatment that blocks gastrointestinal toxicity of the γ-secretase inhibitor in mice (*13*).

Serneels *et al.* provide new evidence that targeting specific γ-secretase complexes may decrease Aβ without Notch toxicity, as the study indicates that the Aph1B γ-secretase complex is conformationally distinct from the Aph1A complex. The realization that γ-secretase inhibitors may be useful as therapies beyond Alzheimer's disease, such as in various cancers (*14*), provides an additional incentive to characterize the biology of the different γ-secretase complexes and develop drugs to inhibit or modulate their activity.

References

1. J. Hardy, D. J. Selkoe, *Science* **297**, 353 (2002).
2. T. E. Golde, *J. Neurochem.* **99**, 689 (2006).
3. L. Serneels *et al.*, *Science* **324**, 639 (2009); published online 19 March 2009 (10.1126/science.1171176).
4. M. Shoji *et al.*, *Science* **258**, 126 (1992).
5. C. Haass *et al.*, *Nature* **359**, 322 (1992).
6. A. K. Ghosh, S. Gemma, J. Tang, *Neurotherapeutics* **5**, 399 (2008).
7. B. De Strooper, *Neuron* **38**, 9 (2003).
8. B. De Strooper *et al.*, *Nature* **398**, 518 (1999).
9. K. Shirotani *et al.*, *J. Biol. Chem.* **279**, 41340 (2004).
10. S. C. Mayer *et al.*, *J. Med. Chem.* **51**, 7348 (2008).
11. S. Weggen *et al.*, *Nature* **414**, 212 (2001).
12. T. L. Kukar *et al.*, *Nature* **453**, 925 (2008).
13. P. J. Real *et al.*, *Nat. Med.* **15**, 50 (2009).
14. P. Rizzo *et al.*, *Oncogene* **27**, 5124 (2008).

10.1126/science.1174267

Published by AAAS

Neural Mechanisms of a Genome-Wide Supported Psychosis Variant

Christine Esslinger,[1]* Henrik Walter,[2,3]* Peter Kirsch,[1]* Susanne Erk,[3] Knut Schnell,[2,3] Claudia Arnold,[3] Leila Haddad,[1] Daniela Mier,[1] Carola Opitz von Boberfeld,[3] Kyeon Raab,[1] Stephanie H. Witt,[4] Marcella Rietschel,[4] Sven Cichon,[5] Andreas Meyer-Lindenberg[1]†

For over a century, disturbed interactions between brain areas have been proposed to underlie schizophrenia (*1*). Extensive work in patients (*1*, *2*) has demonstrated abnormal coupling between structures implicated in schizophrenia, dorsolateral prefrontal cortex (DLPFC) and hippocampal formation (HF), but the relevance for heritable risk was unclear. Through genome-wide association study and followup, a single nucleotide polymorphism (SNP) in *ZNF804A*, rs1344706, was recently found to be associated (*3*) with psychosis, affording an opportunity to establish neurogenetic risk mechanisms.

In 115 healthy genotyped German participants, we used functional magnetic resonance imaging (fMRI) and a well-validated executive cognition probe, the n-back task, related to heritable schizophrenia risk, DLPFC and HF activity, and candidate gene variation (*4*) [see (*5*) for task details and table S1 for sample description]. We studied task-related regional activation of DLPFC and HF and coupling between these structures. For this, we used "functional connectivity" (*2*), an established method that measures correlation between fMRI time series: two regions are functionally connected if their activities are significantly correlated. Although the robustness of this measure has not been formally established [but see (*6*)] and it is not directly indicative of structural or causal connections, functional connectivity has been used successfully to delineate the functional anatomy in health and schizophrenia (*2*) and the impact of genetic variation (*4*). Because rs1344706 has also been implicated in bipolar disorder (*3*), we also used an emotional face-matching task that shows altered activation and connectivity of amygdala linked to neuroticism and genetic risk for mood disorder (*4*). Cognitive probes were used as strong activators of neural systems to investigate genotype effects (a reverse genetics approach) (*4*). Rs1344706 effects on activation and connectivity were mapped across the brain by using the general linear model; because this entails multiple tests, we followed procedures shown to exert strong control of type I error in imaging genetics (*7*).

Regional brain activation was not significantly related to genotype [see (*5*) for result details], but connectivity of the most activated DLPFC locale was strongly altered (Fig. 1, A to C): In risk-allele carriers, connectivity both within DLPFC (same side) and to contralateral DLPFC was reduced. Conversely, the HF was uncoupled from DLPFC in non–risk-allele homozygotes but showed dose-dependent increased connectivity in risk-allele carriers. Lastly, the risk allele predicted extensive increases of connectivity from amygdala (Fig. 1D and table S2), including to hippocampus, orbitofrontal cortex, and medial prefrontal cortex. Rs1344706 genotype had no impact on performance [reaction time and percentage of correct answers (table S1)], and we did not find correlations between behavior and connectivity (*5*) (table S3), indicating that genetic variation is more penetrant on the neurobiological (imaging) phenotype level, as expected for intermediate phenotypes (*4*).

Because rs1344706 was associated with schizophrenia at a genome-wide level (*3*) and we used procedures that strongly control type I error (*7*), our findings establish dysconnectivity as a core neurogenetic mechanism, where reduced DLPFC connectivity could contribute to disturbed executive function (*1*) and increased coupling with HF to deficient interactions between prefrontal and limbic structures (*2*). Because amygdala connectivity is not implicated in genetic risk for schizophrenia (*6*), the observed effects on limbic connectivity might relate to bipolar disorder, where increased connectivity of amygdala has been observed and could contribute to emotional instability. More generally, our findings show that rs1344706, or genetic variant(s) in linkage disequilibrium (i.e., variants that are nonrandomly related), is functional in human brain. The molecular changes leading up to altered neural systems function remain to be elucidated. We speculate that, because genetic variation in dopaminergic and glutamatergic neurotransmission affects DLPFC or HF connectivity (*4*), examination of ZNF804A in those neurotransmitter cascades is warranted, as is its role in white matter development and plasticity. Lastly, our findings validate the intermediate phenotype strategy in psychiatry by showing that mechanisms underlying genetic findings supported by genome-wide association are highly penetrant in brain, agree with the pathophysiology of overt disease, and mirror candidate gene effects (*4*). Confirming a century-old conjecture by combining genetics with imaging, we find that altered connectivity emerges as part of the core neurogenetic architecture of schizophrenia and possibly bipolar disorder, identifying novel potential therapeutic targets.

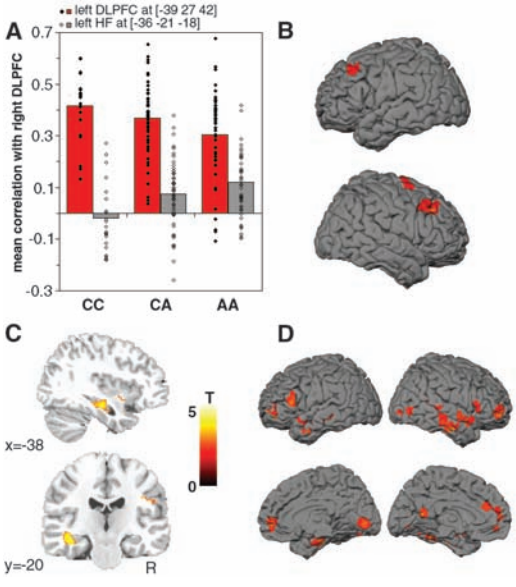

Fig. 1. (**A** to **C**) Altered functional coupling of the right DLPFC in rs1344706 risk-allele carriers. (**A**) Correlation coefficients (columns represent mean of Fisher *z*-transformed coefficients) reflecting connectivity with right DLPFC by genotype: connectivity with left DLPFC [at (–39 27 42)] shown as red columns and solid diamonds, connectivity with left HF [at (–36 –21 –18)] as gray columns and open diamonds. (**B**) Frontal brain regions where genotype predicts reduced connectivity with right DLPFC. (**C**) Brain regions in temporal lobe where genotype predicts increased correlation with right DLPFC. Thresholded for display at $P < 0.005$ within a cluster of more than 20 contiguous voxels. (**D**) Increased functional coupling of right amygdala in rs1344706 risk-allele carriers. Voxels significant at $P < 0.05$, false discovery rate corrected for multiple testing, are displayed.

References and Notes

1. K. E. Stephan, T. Baldeweg, K. J. Friston, *Biol. Psychiatry* **59**, 929 (2006).
2. A. S. Meyer-Lindenberg *et al.*, *Arch. Gen. Psychiatry* **62**, 379 (2005).
3. M. C. O'Donovan *et al.*, *Nat. Genet.* **40**, 1053 (2008).
4. A. Meyer-Lindenberg, D. R. Weinberger, *Nat. Rev. Neurosci.* **7**, 818 (2006).
5. Materials and methods are available as supporting material on *Science* Online.
6. R. Rasetti *et al.*, *Am. J. Psychiatry* **166**, 216 (2009).
7. A. Meyer-Lindenberg *et al.*, *Neuroimage* **40**, 655 (2008).
8. Funding was provided by Bundesministerium für Bildung und Forschung (Nationales Genomforschungsnetz plus MooDs) and Deutsche Forschungsgemeinschaft (SFB 636-B7). We thank T. Paul, B. Newport, D. Gass, O. Grimm, and C. Sauer for data acquisition; T. Demirakca and M. Ruf for technical support; and T. Schulze and M. Nöthen for helpful discussion.

Supporting Online Material

www.sciencemag.org/cgi/content/full/324/5927/605/DC1
Materials and Methods
Tables S1 to S3
References

28 October 2008; accepted 12 February 2009
10.1126/science.1167768

[1]Department of Psychiatry and Psychotherapy, Central Institute of Mental Health, University of Heidelberg, J5, 68159 Mannheim, Germany. [2]Division of Medical Psychology, University of Bonn, 53105 Bonn, Germany. [3]Department of Psychiatry and Psychotherapy, University of Bonn, 53105 Bonn, Germany. [4]Department of Genetic Epidemiology in Psychiatry, Central Institute of Mental Health, University of Heidelberg, J5, 68159 Mannheim, Germany. [5]Department of Genomics, Life and Brain Center and Institute of Human Genetics, University of Bonn, 53105 Bonn, Germany.

*These authors contributed equally to this work.
†To whom correspondence should be addressed. E-mail: a.meyer-lindenberg@zi-mannheim.de

MESSENGER Observations of Magnetic Reconnection in Mercury's Magnetosphere

James A. Slavin,[1]* Mario H. Acuña,[2]† Brian J. Anderson,[3] Daniel N. Baker,[4] Mehdi Benna,[2,5] Scott A. Boardsen,[1,5] George Gloeckler,[6,7] Robert E. Gold,[3] George C. Ho,[3] Haje Korth,[3] Stamatios M. Krimigis,[3,8] Ralph L. McNutt Jr.,[3] Jim M. Raines,[6] Menelaos Sarantos,[1] David Schriver,[9] Sean C. Solomon,[10] Pavel Trávníček,[9,11] Thomas H. Zurbuchen[6]

Solar wind energy transfer to planetary magnetospheres and ionospheres is controlled by magnetic reconnection, a process that determines the degree of connectivity between the interplanetary magnetic field (IMF) and a planet's magnetic field. During MESSENGER's second flyby of Mercury, a steady southward IMF was observed and the magnetopause was threaded by a strong magnetic field, indicating a reconnection rate ~10 times that typical at Earth. Moreover, a large flux transfer event was observed in the magnetosheath, and a plasmoid and multiple traveling compression regions were observed in Mercury's magnetotail, all products of reconnection. These observations indicate that Mercury's magnetosphere is much more responsive to IMF direction and dominated by the effects of reconnection than that of Earth or the other magnetized planets.

The two flybys of Mercury by the MErcury Surface, Space ENvironment, GEochemistry, and Ranging (MESSENGER) spacecraft have provided an opportunity to study a magnetosphere formed by solar wind interaction with a dipolar planetary magnetic field under solar wind conditions substantially different from those seen at Earth (*1*–*3*). When the interplanetary magnetic field (IMF) is brought into contact with the outer boundary of a magnetosphere [the magnetopause (MP)], and the angle between the two fields is between 90° and 270°, a magnetic X-line (also called a neutral line) will form, across which

[1]Heliophysics Science Division, NASA Goddard Space Flight Center, Greenbelt, MD 20771, USA. [2]Solar System Exploration Division, NASA Goddard Space Fight Center, Greenbelt, MD 20771, USA. [3]Johns Hopkins University Applied Physics Laboratory, Laurel, MD 20723, USA. [4]Laboratory for Atmospheric and Space Physics, University of Colorado, Boulder, CO 80303, USA. [5]Goddard Earth Science and Technology Center, University of Maryland, Baltimore County, Baltimore, MD 21228, USA. [6]Department of Astronomy, University of Maryland, College Park, MD 20742, USA. [7]Department of Atmospheric, Oceanic and Space Sciences, University of Michigan, Ann Arbor, MI 48109, USA. [8]Academy of Athens, Athens 11527, Greece. [9]Institute of Geophysics and Planetary Physics, University of California, Los Angeles, CA 90024, USA. [10]Department of Terrestrial Magnetism, Carnegie Institution of Washington, Washington, DC 20015, USA. [11]Astronomical Institute, Academy of Sciences of the Czech Republic, Prague 14131, Czech Republic.

*To whom correspondence should be addressed. E-mail: james.a.slavin@nasa.gov
†Deceased.

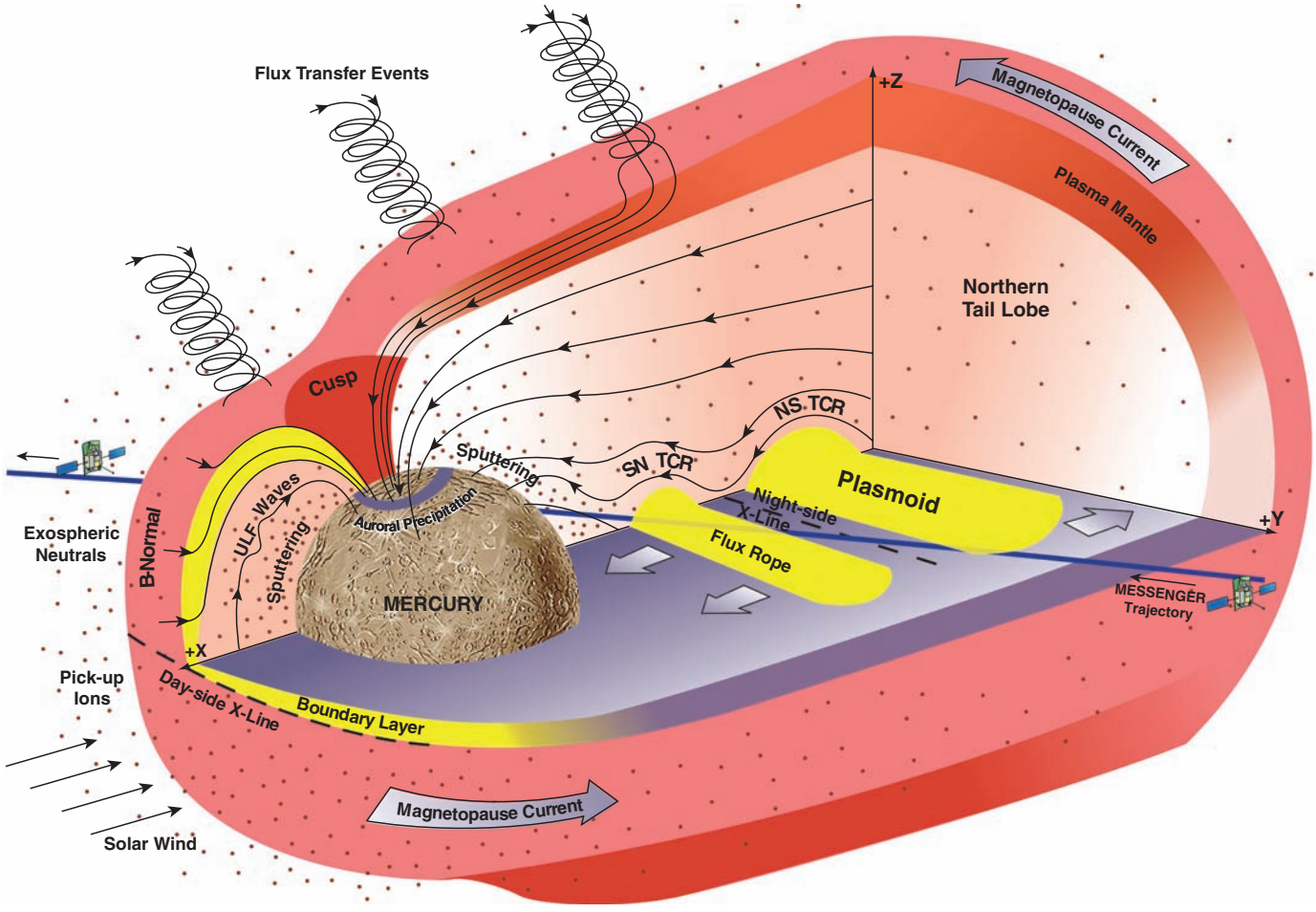

Fig. 1. Schematic of Mercury's magnetosphere under southward IMF conditions as observed by MESSENGER on 6 October 2008. Note the strong magnetic field normal to the dayside MP, the large FTEs, and the reconnection line in the near-tail region, leading to plasmoid ejection and sunward- (SN) and anti-sunward–moving (NS) TCRs. These features were not seen during MESSENGER's first Mercury flyby under northward IMF (*17*).

the flux tubes reconnect (*4*, *5*). This process of reconnection converts an interplanetary flux tube and a magnetospheric flux tube into two flux tubes, each with one end connected to the solar wind and the other rooted in the planet. This new magnetic field topology results in a magnetic field, B_N, normal to the MP (Fig. 1). Such magnetic field lines may be regarded as electrodynamic "brushes" that tap the $-v \times B_N$ electric field in the planetary frame of reference, where v is the solar wind flow velocity past the magnetosphere. In this manner, MP reconnection transfers solar wind energy into the magnetosphere, where, at Earth, it drives high-speed plasma flow, accelerates energetic charged particles, and powers magnetic storms.

Reconnection also occurs between the north and south lobes of planetary magnetotails (Fig. 1), especially after episodes of MP reconnection that increase the intensity of these tail magnetic fields (*6*). The circulation of plasma, magnetic flux, and energy from the X-line at the dayside MP to the nightside X-line in the cross-tail current layer and, later, back to the dayside magnetosphere constitutes the Dungey cycle that powers Earth-type magnetospheres (*4*).

Additional complexities are introduced when multiple X-lines form simultaneously at the MP or in the cross-tail current layer (*7*). The reconfiguration of the magnetic fields under these conditions produces magnetic flux ropes in addition to enhanced magnetic fields normal to the current sheet. These bundles of twisted magnetic flux are carried off by fast flow, comparable to the local Alfven speed, away from the X-lines. At the MP, such flux ropes are called flux transfer events (FTEs) (*8*). However, in planetary magnetotails they are usually called plasmoids when they are ejected tailward (*9*–*12*) or simply flux ropes when they are transported sunward back toward the planet (*13*). Numerical simulations of reconnection in Mercury's magnetosphere predict the formation of all of these types of flux ropes, as is the case at Earth (*14*). The signatures of these magnetic structures as they move over a spacecraft are strong functions of how close the probe passes to the center of the flux ropes. For their helical nature to be observed, it is necessary that the spacecraft pass relatively close to the central axis of the flux rope (*8*, *13*). Outside of the flux rope, magnetic field draping and compression result in readily observable perturbations known as traveling compression regions (TCRs) (*15*). The sense of the relative change in the north-south component of the tail lobe magnetic field that drapes over the flux ropes to form the TCR [north to south (NS) or south to north (SN)] indicates that the direction of motion of the underlying flux rope is anti-sunward or sunward, respectively. Although TCRs do not provide information on the internal structure of the flux ropes, they do signal the passage of these structures and provide estimates of their dimensions, location, and frequency of occurrence (*15*).

During the first MESSENGER flyby of Mercury on 14 January 2008, the IMF was generally northward and therefore unfavorable to reconnection between the IMF and the planetary magnetic field (*16*). Indeed, no evidence for magnetic reconnection between the IMF and the planetary magnetic field was observed except for some FTEs seen after brief southward excursions of the IMF when MESSENGER was outside the magnetosphere (*17*). Here we present measurements of magnetic reconnection and its effects on Mercury's magnetosphere, taken by the MESSENGER Magnetometer (MAG) (*18*)

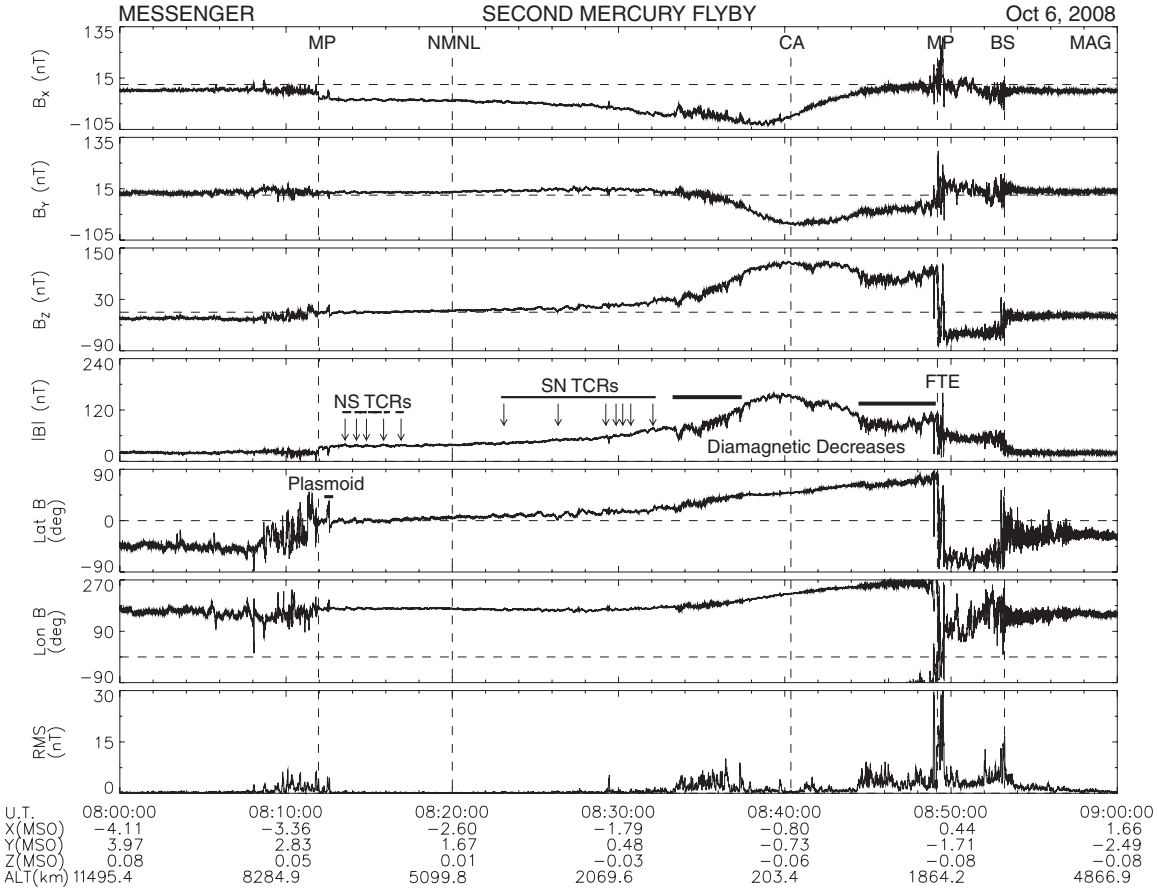

Fig. 2. Overview of magnetospheric measurements taken by the MAG during MESSENGER's second Mercury flyby. The magnetic field is displayed in the MSO coordinate system, defined as X_{MSO} directed from the center of the planet toward the Sun, Z_{MSO} normal to Mercury's orbital plane and positive toward the north celestial pole, and Y_{MSO} positive in the direction opposite to orbital motion. The longitude angle of the magnetic field is defined to be 0° toward the Sun and increases counterclockwise looking down from the north celestial pole. The magnetic field latitude angle is 90° when directed northward and 0° when it is in the X_{MSO}-Y_{MSO} plane. The root mean square (RMS) variance is calculated over 3-s intervals. CA was at an altitude of 199.4 km at 08:40:22 UTC, very near local midnight (00:04 local time).

during the spacecraft's second Mercury flyby on 6 October 2008.

MESSENGER's second flyby was, like the first, near-equatorial, but the spacecraft approached and entered the magnetosphere farther downstream than in the previous encounter (Fig. 1). The inbound and outbound bow shock crossings were at 07:19:25 and 08:53:13 UTC, respectively. The inbound and outbound MP crossings were at 08:11:57 and 08:49:11. When MESSENGER passed into Mercury's magnetotail (Fig. 2), there was a reduction in higher-frequency magnetic fluctuations, a rapid increase in magnetic field intensity, and a rotation in the orientation of the field to a near–anti-sunward orientation (that is, at a longitude angle near 180°), indicating that the spacecraft entered through the downstream MP into the south lobe of the magnetotail.

About 30 s after entering the tail, a large-amplitude NS variation in the magnetic field lasting 4 s, followed by a longer recovery back to $B_Z \sim 0$ [where X, Y, and Z are defined in the Mercury solar orbital (MSO) coordinate system (Figs. 1 and 2)], can be seen in the latitude angle of the field (Figs. 2 and 3A). This pattern is the signature of a plasmoid (*9*). High–time-resolution magnetic field measurements (Fig. 3A) show only a brief decrease in the total field magnitude just before and during the first half of the NS B_Z variation and only a weak B_Y enhancement, indicating only a shallow penetration into the plasmoid. After the plasmoid encounter, a series of five NS TCRs was observed between 08:13:30 and 08:17:00 UTC. The times between TCRs were ~0.1 to 1 min, and their durations were ~2 to 10 s (Figs. 2 and 3B). Remarkably, no energetic ions or electrons above 36 keV were measured by MESSENGER (*19*) in association with these tail reconnection events, in contrast to the impulsive energetic particle events reported by Mariner 10 during its first flyby, when the IMF was intermittently southward (*1*).

No further plasmoids or TCRs were observed until seven SN TCRs were observed between 08:23:06 and 08:32:04 UTC (Fig. 2). Like the earlier NS TCRs, these SN TCRs were identified on the basis of the compression in the total field and the correlated SN perturbation in the relative B_Z component (Fig. 3C). The times between the SN TCRs were comparable to those of the NS TCRs, but their individual durations were slightly shorter.

At Earth (*13*, *20*, *21*), Jupiter (*11*), and Saturn (*12*), plasmoids move down the tail with mean speeds of ~500 km/s. If a similar anti-sunward speed is assumed for the plasmoid observed by MESSENGER, then a diameter of ~0.8 R_M (where R_M is Mercury's radius, 2440 km) is implied. Relative to the dimensions of their respective magnetospheres, the plasmoids at Mercury and Earth appear similar in size, with diameters that are ~10% of the diameters of their magnetic tails. The transition from NS to SN TCRs observed by MESSENGER occurred near $X_{MSO} \sim -2.6\ R_M$ (Fig. 2), implying that this is the mean location of the near-Mercury neutral line (NMNL). At Earth, the corresponding near-Earth neutral line (NENL) distance is ~ –25 R_E (*21*). If the scaling factor of ~7 to 8 that has been found to map spatial structures in Mercury's magnetosphere to that of Earth (*1*) is applied, then the NMNL is about 20% closer to Mercury than would be expected on the basis of its Earth analog.

After measuring a peak magnetic field of ~158 nT near closest approach (CA), a region of depressed magnetic fields and strong fluctuations beginning at 08:44:26 UTC (Figs. 1 and 2) was traversed before the spacecraft crossed the MP and exited the magnetosphere. A similar region of depressed magnetic field intensity and large-amplitude fluctuations was observed adjacent to the dawn MP during the first flyby and attributed to the presence of a boundary layer with enhanced plasma pressure of unknown origins (*16*, *17*). Just inside the outbound MP during the second flyby, at a local time of ~08:48, the magnetic field magnitude was ~100 nT and the field was oriented primarily in the Z_{MSO} direction (Fig. 4A). When examined relative to the directions of minimum (B_1), intermediate (B_2), and maximum (B_3) variance (Fig. 4, B and C), the magnetic field variation across this outbound MP resembles a steepened rotational discontinuity with a strong component normal to the MP; that is, the mean magnetic field in the

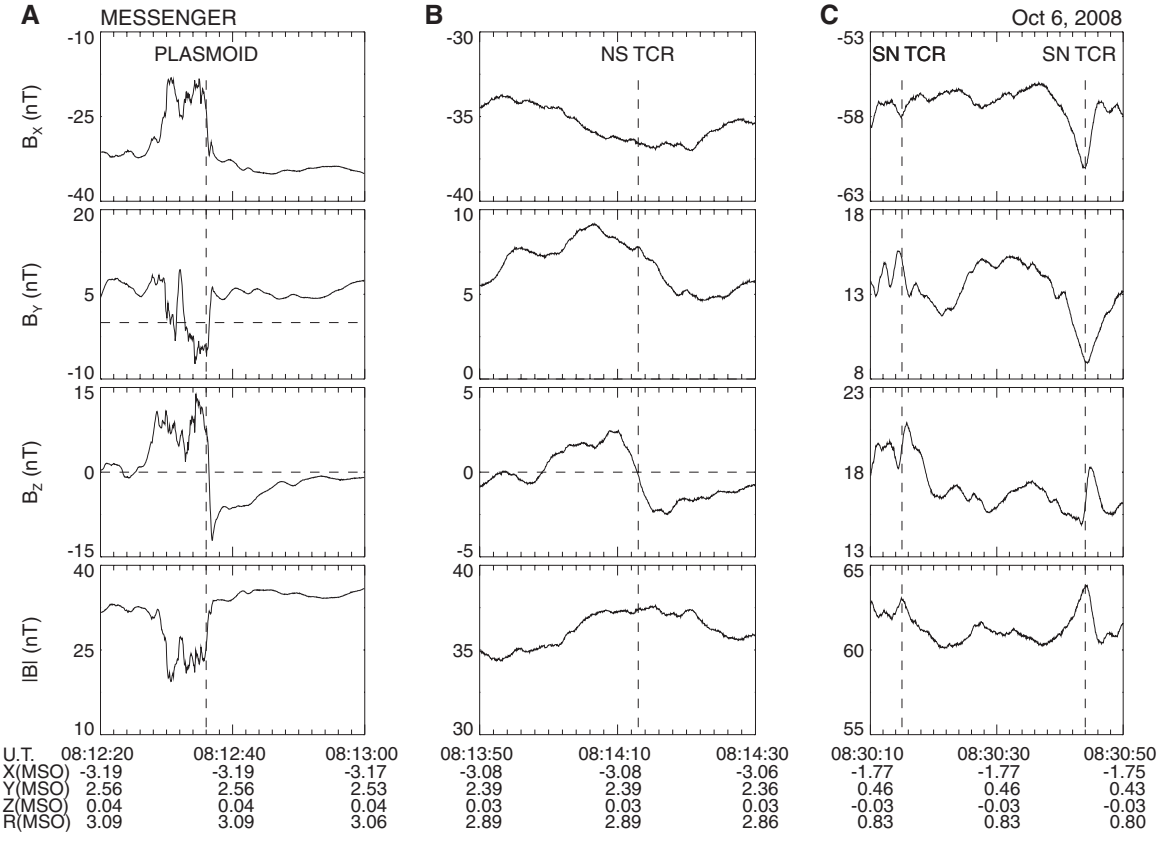

Fig. 3. Magnetic field observations of (**A**) a NS plasmoid 4 s in duration at $X_{MSO} \sim -3.2\ R_M$; (**B**) a NS TCR 8 s in duration at $X_{MSO} \sim -3.1\ R_M$; and (**C**) a pair of SN TCRs, each 2 s in duration and separated in time by ~30 s, at $X_{MSO} \sim -1.8\ R_M$.

minimum variance direction, B_1, was ~13 nT (Fig. 4B), and a large, ~180° rotation takes place in the plane of intermediate and maximum variance; i.e., B_2 and B_3 (Fig. 4C). These signatures are well known from studies of Earth's MP (*5*, *8*) and indicate that reconnection was taking place at an X-line located northward of the MESSENGER trajectory. In contrast, magnetic field measurements from the first MESSENGER flyby during northward IMF indicated that the structure of the dayside MP was a tangential discontinuity with a near-zero mean normal magnetic field (*17*).

The rate of reconnection is directly proportional to the ratio of the normal component of the magnetic field to the total field (*5*). Typical normal magnetic field components at Earth's MP for southward IMF are ~0.5 to 1 nT, and the ratio is ~1%. For the MP at Mercury, this ratio is 13 nT/100 nT = 13%, or about an order of magnitude greater than the typical value at Earth. Enhanced rates of MP reconnection at Mercury have been predicted because of the increase in interplanetary Alfven speed with decreasing distance to the Sun (*22*). Because MESSENGER crossed the MP just forward of the dawn terminator, it appears that the dayside X-line was at least 3 R_M long. For a magnetosheath flow of 300 km/s, the electric field potential applied to the magnetosphere equals 3 $R_M \times (v \times B_N)$ ~ 30 kV or a mean dawn-to-dusk internal electric field of ~2 mV/m. This electric field, along with the observed magnetic fields and magnetospheric dimensions, implies a Dungey cycle time (*23*) [time for plasma to drift from local noon to midnight in the polar cap or from the northern boundary of the tail down to the cross-tail current sheet] of ~2 min. The Dungey cycle time has been observed to determine the duration of magnetic substorms, and it ranges from ~1 month at Jupiter to ~1 week at Saturn (*24*) and ~1 hour at Earth (*4*).

Sixteen seconds after the outbound MP crossing, MESSENGER encountered the strongest magnetic field measured during the second flyby, 160 nT, in the core of an FTE ~3 s in duration (Fig. 4A). The helical topology is apparent in the bipolar B_X signature and the strong core field seen in the B_Y and B_Z components. However, the asymmetrical nature of the increase in magnetic field intensity relative to the central bipolar B_Y signature indicates that MESSENGER did not pass close to the central axis of this flux rope and that it was probably distorted by the force of the magnetosheath plasma flows (*8*). For a typical anti-sunward magnetosheath flow speed of ~300 km/s and the measured 3-s duration of the event, the size of this FTE is ~900 km or ~0.4 R_M. The diameter of this FTE is much greater than the ~30-km gyro-radius of a magnetosheath proton with a speed of 300 km/s in the 100-nT magnetic field just inside the MP. Relative to Mercury's magnetosphere, this FTE has a diameter equal to 28% of the 1.4-R_M mean distance from the center of the planet to the nose of the MP. By comparison, the FTEs observed by Mariner 10 (*25*) were only about 1 s in duration and similar in relative size to the FTEs observed at Earth, where they have typical diameters of ~1 R_E or about 9% of the average distance to the nose of the magnetosphere. The reason for the size difference between FTEs observed by Mariner 10 and MESSENGER is not clear, but the existence of large FTEs at Mercury supports predictions that solar wind kinetic scale lengths and the small dimensions of this magnetosphere will lead to a substantial increase in the size of FTEs at Mercury relative to those at Earth (*26*). Overall, these MESSENGER observations suggest that magnetic reconnection at the dayside MP is very intense compared with what is found at Earth and, as a result, Mercury's magnetosphere is probably much more sensitive to IMF intensity and direction than those of Earth

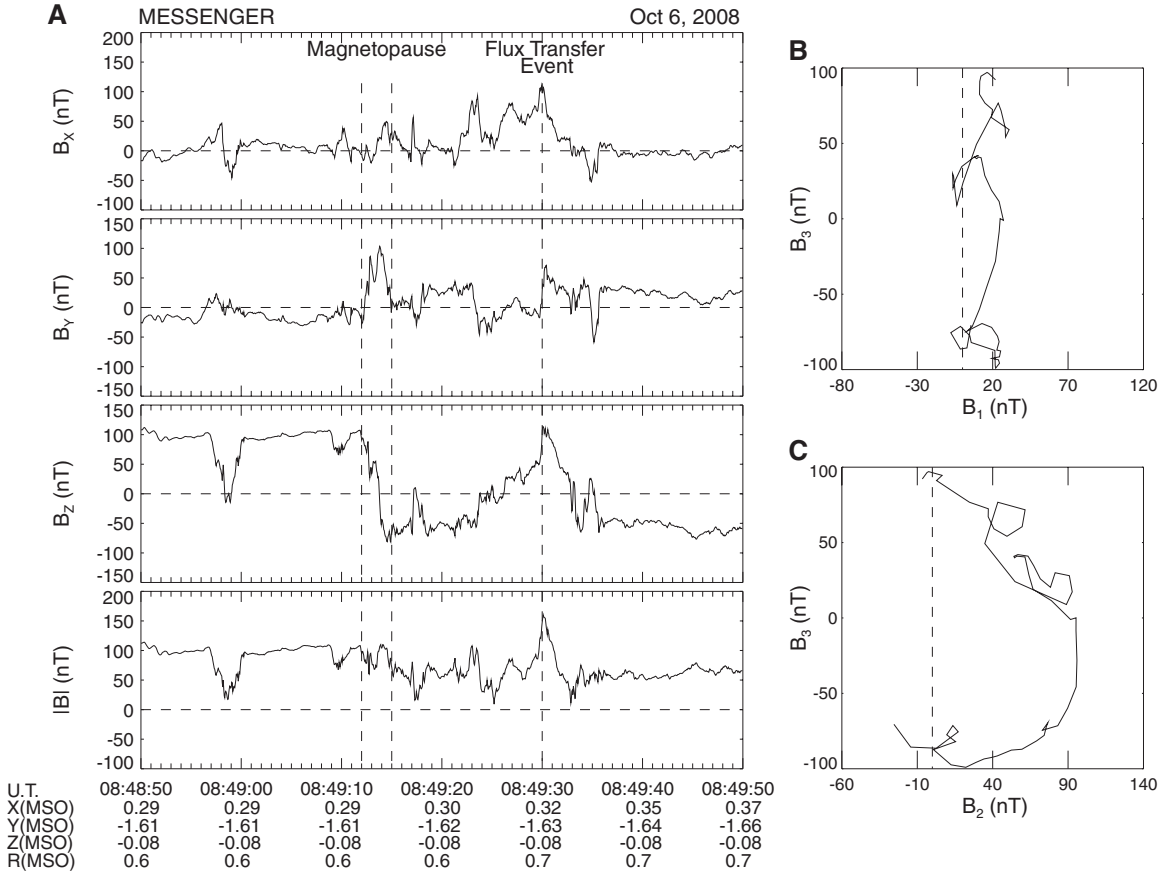

Fig. 4. (**A**) Magnetic field observations of the inner current sheet and MP boundary observed as MESSENGER exited the dawn-side magnetosphere. (**B**) Magnetic field measurements across the MP graphed in the plane of maximum and minimum variance. The minimum, intermediate, and maximum variance eigenvectors are B_1 = (0.95, 0.00, 0.30), B_2 = (–0.07, 0.97, 0.22), and B_3 = (–0.29, –0.23, 0.93), and the ratios of maximum to intermediate and intermediate to minimum eigenvalues are 9.2 and 4.2, respectively. (**C**) Magnetic field measurements across the MP graphed in the plane of maximum and intermediate variance.

and the other magnetized planets. The strong influence of the IMF on the magnetosphere should also serve to enhance the coupling between the solar wind and Mercury's surface-bounded exosphere (*27*).

References and Notes

1. C. T. Russell, D. N. Baker, J. A. Slavin, in *Mercury*, F. Vilas, C. R. Chapman, M. S. Matthews, Eds. (University of Arizona Press, Tucson, AZ, 1968), pp. 514–561.
2. M. Fujimoto *et al.*, *Space Sci. Rev.* **132**, 529 (2007).
3. W. Baumjohann *et al.*, *Adv. Space Res.* **38**, 604 (2006).
4. J. W. Dungey, *Phys. Rev. Lett.* **6**, 47 (1961).
5. B. U. O. Sonnerup *et al.*, *J. Geophys. Res.* **86**, 10049 (1981).
6. D. N. Baker, T. I. Pulkkinen, V. Angelopoulos, W. Baumjohann, R. L. McPherron, *J. Geophys. Res.* **101**, 12975 (1996).
7. L. C. Lee, Z. F. Fu, *Geophys. Res. Lett.* **12**, 105 (1985).
8. C. T. Russell, R. C. Elphic, *Space Sci. Rev.* **22**, 681 (1978).
9. E. W. Hones Jr. *et al.*, *Geophys. Res. Lett.* **11**, 5 (1984).
10. C. T. Russell, K. K. Khurana, D. E. Huddleston, M. G. Kivelson, *Science* **280**, 1061 (1998).
11. E. A. Kronberg, J. Woch, N. Krupp, A. Lagg, *J. Geophys. Res.* **113**, A10202 (2008).
12. C. M. Jackman *et al.*, *J. Geophys. Res.* **113**, A11213 (2008).
13. J. A. Slavin *et al.*, *J. Geophys. Res.* **108**, 1015 (2003).
14. A. Kidder, R. M. Winglee, E. M. Harnett, *J. Geophys. Res.* **113**, A09223 (2008).
15. J. A. Slavin *et al.*, *Geophys. Res. Lett.* **11**, 657 (1984).
16. B. J. Anderson *et al.*, *Science* **321**, 82 (2008).
17. J. A. Slavin *et al.*, *Science* **321**, 85 (2008).
18. B. J. Anderson *et al.*, *Space Sci. Rev.* **131**, 417 (2007).
19. R. E. Gold *et al.*, *Eos* **89** (fall meeting suppl.), abstr. U21A-0036 (2008).
20. A. Ieda *et al.*, *J. Geophys. Res.* **103**, 4453 (1998).
21. T. Nagai, H. J. Singer, T. Mukai, T. Yamamoto, S. Kokubun, *Adv. Space Res.* **25**, 1651 (2000).
22. J. A. Slavin, R. E. Holzer, *J. Geophys. Res.* **84**, 2076 (1979).
23. G. L. Siscoe, N. F. Ness, C. M. Yeates, *J. Geophys. Res.* **80**, 4359 (1975).
24. S. V. Badman, S. W. H. Cowley, *Ann. Geophys.* **25**, 941 (2007).
25. C. T. Russell, R. J. Walker, *J. Geophys. Res.* **90**, 11067 (1985).
26. M. M. Kuznetsova, L. M. Zeleny, *Proceedings of the Joint Varenna-Abastumani International School and Workshop on Plasma Astrophysics*, Sukhumi, USSR, 19 to 28 May 1986, SP-251 (European Space Agency, Noordwijk, Netherlands, 1986), pp. 137–146.
27. S. Orsini *et al.*, *Space Sci. Rev.* **132**, 551 (2007).

28. We deeply mourn the loss of our colleague and MESSENGER Co-Investigator Mario Acuña during the preparation of this manuscript; his many contributions to the MESSENGER mission and the space science community live on. We also thank all who contributed to the success of the first and second MESSENGER flybys of Mercury. Data visualization and graphics support by J. Feggans, C. Liebrecht, and M. Marosy are gratefully acknowledged. The MESSENGER project is supported by the NASA Discovery Program under contracts NAS5-97271 to the Johns Hopkins University Applied Physics Laboratory and NASW-00002 to the Carnegie Institution of Washington.

9 February 2009; accepted 3 April 2009
10.1126/science.1172011

MESSENGER Observations of Mercury's Exosphere: Detection of Magnesium and Distribution of Constituents

William E. McClintock,[1]* Ronald J. Vervack Jr.,[2] E. Todd Bradley,[3] Rosemary M. Killen,[4] Nelly Mouawad,[4] Ann L. Sprague,[5] Matthew H. Burger,[4] Sean C. Solomon,[6] Noam R. Izenberg[2]

Mercury is surrounded by a tenuous exosphere that is supplied primarily by the planet's surface materials and is known to contain sodium, potassium, and calcium. Observations by the Mercury Atmospheric and Surface Composition Spectrometer during MESSENGER's second Mercury flyby revealed the presence of neutral magnesium in the tail (anti-sunward) region of the exosphere, as well as differing spatial distributions of magnesium, calcium, and sodium atoms in both the tail and the nightside, near-planet exosphere. Analysis of these observations, supplemented by observations during the first Mercury flyby, as well as those by other MESSENGER instruments, suggests that the distinct spatial distributions arise from a combination of differences in source, transfer, and loss processes.

Whereas the interface between the planetary surface and external space environment is a classical, collision-dominated atmosphere for the three largest terrestrial planets, Mercury's interface is a tenuous, surface-bounded exosphere in which the constituent atoms and molecules travel on collisionless trajectories and are far more likely to impact the surface than to interact with each other. Mercury's exospheric properties are primarily determined by the interaction of the surface with the space environment. The planet's highly elliptical orbit and proximity to the Sun lead to strong seasonal variations in exospheric density distributions (*1*, *2*). In addition, Mercury's intrinsic magnetic field interacts with the interplanetary medium to modulate the spatial distribution and density of solar wind plasma and high-energy charged particles that impact and sputter materials from the planet's surface. This interaction leads to changes in exospheric densities that vary on time scales as short as a few hours (*3*). Impacts also supply both meteoritic and volatilized surface materials to the exosphere.

Constituents that have been detected in Mercury's exosphere include H and He, which were measured by the Mariner 10 Ultraviolet Spectrometer (*4*, *5*), and Na, K, and Ca, which were discovered with ground-based telescopes (*6*–*8*). Neutral species released from the surface with sufficient energy are accelerated by solar radiation pressure to form an extended, anti-sunward tail of neutral atoms, as demonstrated by ground-based observations of Mercury's Na tail (*9*–*11*). Here, we report observations of Mg, Ca, and Na in Mercury's exosphere and tail obtained with the Ultraviolet and Visible Spectrometer (UVVS) channel of the Mercury Atmospheric and Surface Composition Spectrometer (MASCS) (*12*) on 6 October 2008 during the second Mercury flyby of the MESSENGER spacecraft (*13*).

Observations made by the UVVS during the first Mercury flyby on 14 January 2008 revealed a distinct north-south asymmetry (25% brighter in the north) to the Na tail and a near-planet, nightside Ca distribution with a strong dawn-dusk asymmetry (10 times brighter toward the dawn) (*14*). To explore these structures further, observations during the second flyby included simultaneous measurements of both of these species as well as Mg, beginning in Mercury's tail approximately 8 R_M (R_M is Mercury's radius, 2440 km) anti-sunward of the planet, continuing through the nightside, near-planet exosphere, and ending near the dawn terminator. The observations were restricted to narrow wavelength ranges centered on the resonant emission lines of the neutral atoms at 285.2 nm (Mg), 422.7 nm (Ca), and 589.0 and 589.6 nm (Na D2 and D1 lines, respectively). These observations confirmed the persistence of Na and Ca structures seen in the first flyby and revealed Mg in Mercury's exosphere.

Observations of the D lines of Na began in the tail region ~56,000 km (23 R_M) behind the planet. At ~35,000 km from the planet, the UVVS switched observing programs to include the Mg and Ca resonance lines, which continued until the spacecraft was ~5000 km from the planet. Although the Na was clearly present from the beginning, the Ca and Mg emissions were detected with statistical significance only at distances less than 19,500 km (8 R_M).

During the tail observations the spacecraft rolled up and down about the Sun-Mercury line, scanning the UVVS 0.1° × 1.0° field of view across a plane defined by the Sun-Mercury line and Mercury's north pole. As the spacecraft rotated, spectra from Mg, Ca, and Na were recorded in rapid succession along nearly identical

[1]Laboratory for Atmospheric and Space Physics, University of Colorado, Boulder, CO 80303, USA. [2]Johns Hopkins University Applied Physics Laboratory, Laurel, MD 20723, USA. [3]Department of Physics, University of Central Florida, Orlando, FL 32816, USA. [4]Department of Astronomy, University of Maryland, College Park, MD 20742, USA. [5]Lunar and Planetary Laboratory, University of Arizona, Tucson, AZ 85721, USA. [6]Department of Terrestrial Magnetism, Carnegie Institution of Washington, Washington, DC 20015, USA.

*To whom correspondence should be addressed. E-mail: william.mcclintock@colorado.edu

lines of sight. The observations were designed to sweep the line-of-sight (LOS) intercept with the plane through a vertical distance bounded by ±3 R_M, which required the rotation angle to increase monotonically from ±5° to ±40° as the spacecraft approached the planet [see figure 1A in (*14*)]. Therefore, the UVVS LOS swept through larger angles as the tail observations progressed. In addition, the LOS often crossed Mercury's shadow, complicating density determinations because the observed resonance lines are excited by solar illumination, and atoms in the shadow region are not sunlit. The relative strength of the emission as a function of look direction, however, is a robust measurement because the UVVS effectively integrates from the spacecraft to infinity.

Mg emission (Fig. 1D) appears to be nearly uniformly distributed but shows evidence for a weak, double-lobed, north-south enhancement. Whereas Ca emission (Fig. 1E) peaks near the equatorial regions and declines toward higher latitudes, Na emission (Fig. 1F) exhibits a distinct high-latitude enhancement relative to the equatorial regions. Signals from both Mg and Ca are weaker than for Na; therefore, some of the variations seen in Fig. 1 result from detector count noise, which, after conversion to radiance, have one-standard-deviation values of 11, 9, and 75 rayleighs (R) for Mg, Ca, and Na, respectively. Although slight differences in viewing geometry do not allow for a direct comparison, Na tail observations from both MESSENGER flybys show an enhancement of emission at higher latitudes (Fig. 1G), a pattern noted in ground-based observations (*10*) and ascribed to variations in the solar-wind-sputtering source component of Na atoms. Because flybys 1 and 2 occurred at Mercury true anomaly 285.3° and 293.6°, respectively, differences in the exosphere resulting from seasonal variations are expected to be small.

Once the spacecraft entered Mercury's shadow, the UVVS carried out a "fantail" series of observations to explore the near-planet exosphere (Fig. 2, A and C). These began with the UVVS LOS pointed in Mercury's equatorial plane toward the dawn hemisphere. They continued as the spacecraft executed a 180° roll through north, and finished with the LOS pointed near the equatorial plane toward the dusk hemisphere. Immediately after the fantail, the UVVS LOS intersected the nightside surface of the planet. As the spacecraft passed through closest approach and began its outbound leg, it emerged from Mercury's shadow. Although the LOS still intersected the nightside surface, at least some part of the column between the spacecraft and surface was illuminated and resulted in measurable emission (Fig. 2, B and D). These observations continued until the LOS crossed the dawn terminator, at which point sunlight reflected from the bright dayside disk precluded exospheric observations.

As with the tail observations, both the fantail and near-terminator observations showed differing spatial distributions of the three constituents. Ca emission peaked near the dawn equator and monotonically declined during the rotation to the dusk direction. Na emission was weakest in the dawn direction, passed through a maximum near the north pole, and declined slightly toward dusk. In contrast, Mg emission remained more or less uniform throughout the fantail. During the near-terminator observations, all three species showed an increase in emission intensity as the illuminated column along the LOS increased as the spacecraft approached the dayside. Whereas the Ca and Mg emissions grew at a rate proportional to the illuminated column length, Na emission increased more rapidly.

The principal processes that liberate material from the surface and populate the exosphere include thermal desorption, photon-stimulated desorption, electron-stimulated desorption, meteoroid-impact vaporization, and ion sputtering (e.g., *15*). Ion sputtering followed by meteoroid-impact vaporization are the most energetic, and these processes, acting on regions of the surface near the terminator, likely provide the bulk of material observed in the tail region. Once species are lofted above the surface with an initial release velocity, their distributions are determined by gravity, radiation pressure, and photoionization followed by magnetic and electric field transport ending in either a rapid loss to the system along open magnetic field lines or a return to the surface. The relevant transport and ionization lifetimes (*16*, *17*) vary greatly for Mg, Ca, and Na (Table 1).

During flyby 2, the tail sweeps exhibited a brightness, uniform in the north-south direction, of 610 R at 56,000 km that increased as the inverse square of the distance from planet center. Near 22,000 km, where flyby 2 measurements first overlap those from flyby 1, radiance values of 3640 R (flyby 2) and 3420 R (flyby 1) were nearly identical, and the flux of Na escaping down the tail was ~6 × 10^{23} atoms s^{-1} at both encounters. That neutral Na can reach great distances is a consequence of its relatively long lifetime, coupled with intense radiation pressure. Atoms released from the surface with anti-sunward velocities as small as 1.4 km s^{-1}, corresponding to 0.23 electron volts (eV) of kinetic energy, are accelerated down the tail ~35 R_M, to a velocity of 8 km s^{-1}, in one ionization lifetime.

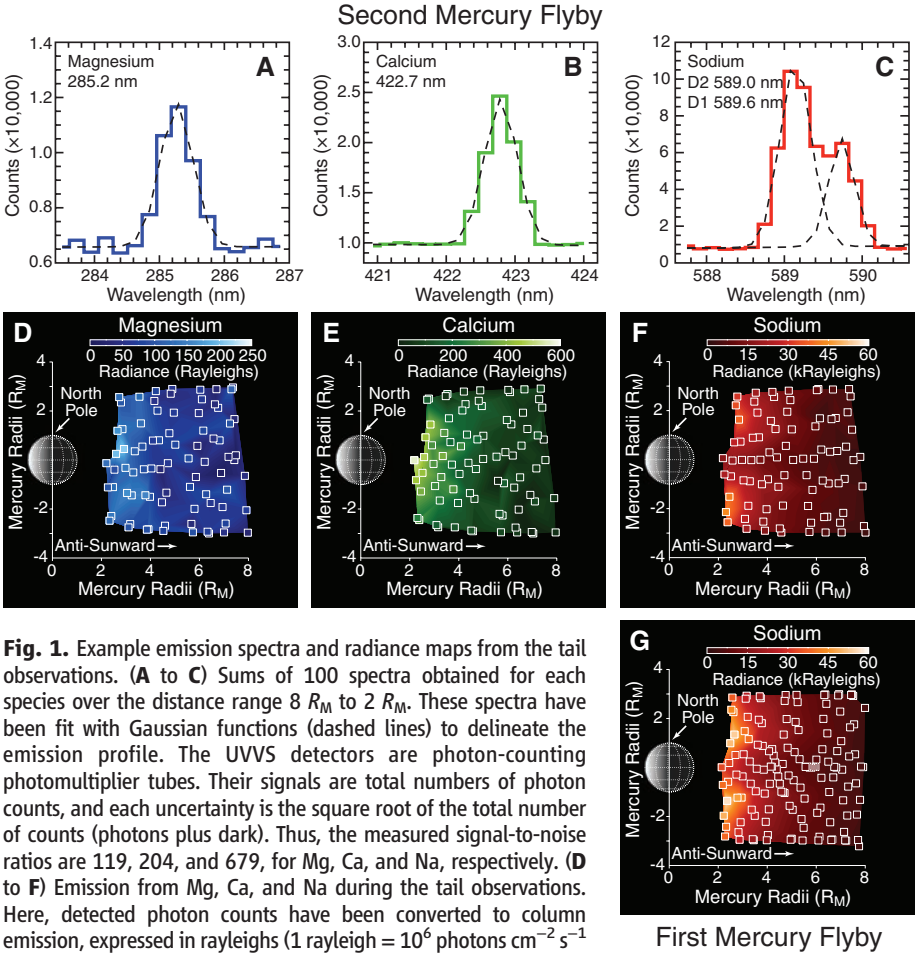

Fig. 1. Example emission spectra and radiance maps from the tail observations. (**A** to **C**) Sums of 100 spectra obtained for each species over the distance range 8 R_M to 2 R_M. These spectra have been fit with Gaussian functions (dashed lines) to delineate the emission profile. The UVVS detectors are photon-counting photomultiplier tubes. Their signals are total numbers of photon counts, and each uncertainty is the square root of the total number of counts (photons plus dark). Thus, the measured signal-to-noise ratios are 119, 204, and 679, for Mg, Ca, and Na, respectively. (**D** to **F**) Emission from Mg, Ca, and Na during the tail observations. Here, detected photon counts have been converted to column emission, expressed in rayleighs (1 rayleigh = 10^6 photons cm^{-2} s^{-1} emitted into 4π steradians), using instrument calibration coefficients, determined during ground tests (*12*). Individual observations (white squares) are overlaid on an image generated by projecting the observed LOS emissions onto a plane containing the Sun-Mercury line and the planet's north pole and interpolating to fill in regions not observed. (**G**) The Na tail emission from the first Mercury flyby, truncated at 2.1 R_M anti-sunward to match the spatial coverage obtained here.

Closer to the planet, the Na tail emissions observed during both MESSENGER flybys display distributions peaked at high latitudes (Fig. 1, F and G), a feature commonly seen in ground-based observations (*10*, *18*–*20*). These enhancements are consistent with a scenario in which energetic Na ions are ejected from the surface by ion sputtering at high latitudes (*10*, *19*). The conclusion that there is substantial high-latitude enhancement is robust, although tracings of the lines of sight through a detailed, three-dimensional model are required to rule out the possibility that some fraction results from an observational bias produced by the larger out-of-plane viewing angles that occur near the end of the tail observations. A high-latitude enhancement is further supported by the fantail observations of Na, which also showed a considerable increase toward the north pole (Fig. 2, A and C). If the Na distribution were symmetric about the Sun-Mercury line, the fantail would show uniformly increasing emission as the LOS rolled from dawn to dusk, because the field of view would intersect a monotonically increasing density (and therefore monotonically increasing emission brightness) while the spacecraft approached the planet's nightside. The ratio of observed emission in the dawn and dusk directions is compatible with a distribution that is symmetric about the Sun-Mercury line and increases toward the terminator, as would result from a symmetric source process such as photon-stimulated desorption; however, the northern excess requires an additional, high-latitude source of Na atoms, most probably related to solar-wind sputtering of Na atoms (Fig. 2C).

During the first flyby, Na emission appeared relatively bright in the northern hemisphere [Fig. 1G; see also figure 1 in (*14*)]. In contrast, Na emission strengths were nearly equal to the north and south during the second flyby. This result is consistent with MESSENGER magnetosphere observations, which suggest that the solar wind plasma impingement on Mercury's surface was directed toward higher northern latitudes during the first flyby but more uniformly distributed during the second flyby (*21*–*24*).

In contrast to Na, the UVVS Ca tail-region observations show a definite equatorial peak and no high-latitude enhancements (Fig. 1E). Furthermore, there is a clear concentration of Ca emission in the dawn equatorial region during the fantail observations (Fig. 2, A and C). Calcium's ionization lifetime at Mercury is 1700 s, and the effect of radiation pressure is relatively small; therefore, Ca atoms released from the surface must be extremely energetic (~5 to 7 eV) to travel down the tail to 4 or 5 R_M before being ionized. If the Ca observed here were released to the exosphere by solar-wind sputtering or by meteoroid impact, it must come from the high-energy tails of these source processes. Alternatively, it has been suggested that CaO is released from the surface into the exosphere, where it is photodissociated, producing energetic Ca atoms (e.g., *25*).

The dawn-dusk asymmetry in Ca emission, observed in both flybys, may result in part from enhanced meteoroid impact velocity and flux on the dawn side resulting from Mercury's orbital motion. An additional contribution may come from exospheric atoms that return to the surface on the nightside and are subsequently lofted by photon desorption after sunrise (the energy imparted by thermal desorption is insufficient to produce a population of Ca atoms behind the planet).

Although the Mg tail (Fig. 1D) and fantail emissions (Fig. 2, A and C) are most consistent with an isotropic distribution, there is statistically significant evidence for weak high-latitude components in the tail region. Mg and Ca are chemically similar; however, the atomic mass of Mg is a factor of 1.65 smaller than Ca, its ionization lifetime is 124 times longer, and radiation pressure is negligible for Mg. Thus, an anti-sunward release velocity of 3.7 km s^{-1}, corresponding to ~1.7 eV minimum (>2.4 eV average) energy, is required to propel it to an altitude of ~4 R_M, and a radial velocity of 4.3 km s^{-1} is required for escape. The small radiation pressure and long lifetime suggest that the majority of the Mg atoms will most likely return to the surface rather than be photoionized like Ca or escape down the tail like Na.

In the near-terminator region, the observed emissions from the exosphere increase as the illuminated column between the spacecraft and

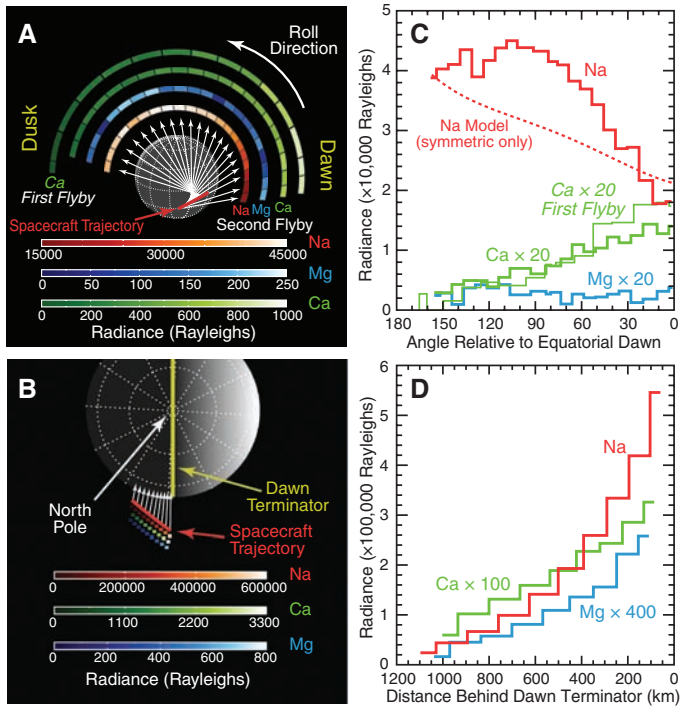

Fig. 2. Emission from Mg, Ca, and Na during (**A**) the "fantail" and (**B**) the near-dawn terminator. The arrows in each panel indicate the direction of the UVVS LOS during the Na observations. During the near-terminator observations, the LOS is pointed at the surface of Mercury, approximately in the equatorial plane. In both images, the lines of sight for Mg and Ca are approximately equally spaced between adjacent Na observations because the three species are measured consecutively before the sequence repeats. (**C**) Line plots of the fantail emissions. A model profile consistent with emission from a Na distribution that increases toward the terminator and is symmetric about the Sun-Mercury line (dashed line; calculated from a model that includes symmetric impact vaporization and photon-stimulated desorption sources only) must be supplemented by an additional component concentrated to the north to reproduce the observations. In contrast, Ca exhibits a nearly linear decline from dawn to dusk, consistent with being most abundant toward dawn, while Mg is approximately uniform with direction. Ca emission observed in similar sequences during the first Mercury flyby (thin green line) showed nearly identical fantail behavior. In the near-terminator region, the observed emissions from the exosphere increase as the illuminated column length between the spacecraft and the surface grows. (**D**) Line plots of emission as functions of LOS distance behind the terminator.

Table 1. Transport and photoionization parameters.

Species	Radiation acceleration/surface gravity*	Ionization lifetime (s)	Column density factor* (atoms cm^{-2} R^{-1})
Mg	4.7×10^{-3}	2.1×10^{5}	3.15×10^{6}
Ca	0.12	1.7×10^{3}	4.42×10^{4}
Na	0.47	2.0×10^{4}	1.63×10^{4}

*Acceleration due to radiation pressure as a fraction of surface gravity and column density factor for an atom at rest with respect to Mercury (–9.5 km s^{-1} with respect to the Sun) at the true anomaly angle corresponding to the time of the second MESSENGER flyby. As Na and Ca atoms accelerate anti-sunward, the presence of deep absorption lines in the solar spectrum first causes a decrease in these values, followed by an increase.

the surface grows. Line plots of emission as functions of LOS distance behind the terminator (Fig. 2D) reveal a more rapid increase for Na than for Ca and Mg. This difference is consistent with the view that there is a substantial concentration of low-energy Na relative to Ca and Mg near the terminator.

In the fantail and near-terminator regions, emission rates were converted to approximate LOS abundances using column density factors (Table 1) calculated from *g* values (the emission probability per atom, expressed as photons s^{-1} $atom^{-1}$) for atoms at rest with respect to Mercury (*26*). These estimates indicate that although the average Na and Mg abundances measured by MASCS in the near-planet exosphere are comparable, those for Ca are smaller than Na by a factor of ~35 to 40. Because flyby observations do not provide complete coverage, it is not possible to determine whether these differences result from the relative amounts of Mg, Ca, and Na released to the exosphere or from differences in photoionization lifetimes and transport.

The detection of Mg in Mercury's exosphere is not a surprising result and supports the identification of Mg^+ in the planet's magnetosphere during MESSENGER's first flyby (*27*). Ground-based spectroscopic observations of the regolith indicate the presence of Mg-bearing minerals as well as those of Ca and Na (*28*). Additionally, analysis of global-scale color images obtained during the MESSENGER flybys argues for a substantial Mg component in Mercury's crust (*29*). Therefore, a considerable portion of the Mg in the exosphere must be derived from Mercury's surface materials (*15*, *19*, *20*). On the other hand, the differences in spatial distributions observed here, particularly those of the chemically similar elements Mg and Ca, were unexpected and remain unexplained.

References and Notes

1. W. H. Smyth, M. L. Marconi, *Astrophys. J.* **441**, 839 (1995).
2. A. E. Potter, R. M. Killen, T. H. Morgan, *Icarus* **186**, 571 (2007).
3. R. M. Killen, M. Sarantos, A. E. Potter, P. Reiff, *Icarus* **171**, 1 (2004).
4. A. L. Broadfoot, S. Kumar, M. J. S. Belton, M. B. McElroy, *Science* **185**, 166 (1974).
5. D. E. Shemansky, A. L. Broadfoot, *Rev. Geophys. Space Phys.* **15**, 491 (1977).
6. A. E. Potter, T. H. Morgan, *Science* **229**, 651 (1985).
7. A. E. Potter, T. H. Morgan, *Icarus* **67**, 336 (1986).
8. T. Bida, R. M. Killen, T. H. Morgan, *Nature* **404**, 159 (2000).
9. A. E. Potter, R. M. Killen, T. H. Morgan, *Meteorit. Planet. Sci.* **37**, 1165 (2002).
10. A. E. Potter, R. M. Killen, *Icarus* **194**, 1 (2008).
11. J. Baumgardner, J. Wilson, M. Mendillo, *Geophys. Res. Lett.* **35**, L03201, 10.1029/2007GL032337 (2008).
12. W. E. McClintock, M. R. Lankton, *Space Sci. Rev.* **131**, 481 (2007).
13. S. C. Solomon *et al.*, *Space Sci. Rev.* **131**, 3 (2007).
14. W. E. McClintock *et al.*, *Science* **321**, 62 (2008).
15. R. M. Killen *et al.*, *Space Sci. Rev.* **132**, 433 (2007).
16. W. F. Huebner, J. J. Keady, S. P. Lyon, *Astrophys. Space Sci.* **195**, 1 (1992).
17. M. Fulle *et al.*, *Astrophys. J.* **661**, L93 (2007).
18. A. L. Sprague *et al.*, *Icarus* **129**, 506 (1997).
19. R. M. Killen *et al.*, *J. Geophys. Res.* **106**, 20509 (2001).
20. F. Leblanc *et al.*, *Geophys. Res. Lett.* **35**, L18204, 10.1029/2008GL035322 (2008).
21. J. A. Slavin *et al.*, *Science* **321**, 85 (2008).
22. B. J. Anderson *et al.*, *Eos Trans. AGU* **89** (fall meeting suppl.), abstr. U12A-04 (2008).
23. J. A. Slavin *et al.*, *Science* **324**, 606 (2009).
24. M. Sarantos *et al.*, *Geophys. Res. Lett.* **36**, 10.1029/2008GL036207 (2009).
25. R. M. Killen, T. A. Bida, T. H. Morgan, *Icarus* **173**, 300 (2005).
26. R. M. Killen, D. E. Shemansky, N. Mouawad, *Astrophys. J.* **181** (suppl.), 351 (2009).
27. T. H. Zurbuchen *et al.*, *Science* **321**, 90 (2008).
28. A. L. Sprague *et al.*, *Planet. Space Sci.* **57**, 364 (2009).
29. B. W. Denevi *et al.*, *Science* **324**, 613 (2009).

30. We thank M. Lankton and M. Kochte for their important contributions to the acquisition and analysis of the data reported here. The MESSENGER project is supported by the NASA Discovery Program under contracts NAS5-97271 to Johns Hopkins University Applied Physics Laboratory and NASW-00002 to Carnegie Institution of Washington. R.J.V., R.M.K., and A.L.S. are supported by the MESSENGER Participating Scientist Program.

19 February 2009; accepted 8 April 2009
10.1126/science.1172525

The Evolution of Mercury's Crust: A Global Perspective from MESSENGER

Brett W. Denevi,[1]* Mark S. Robinson,[1] Sean C. Solomon,[2] Scott L. Murchie,[3] David T. Blewett,[3] Deborah L. Domingue,[3] Timothy J. McCoy,[4] Carolyn M. Ernst,[3] James W. Head,[5] Thomas R. Watters,[6] Nancy L. Chabot[3]

Mapping the distribution and extent of major terrain types on a planet's surface helps to constrain the origin and evolution of its crust. Together, MESSENGER and Mariner 10 observations of Mercury now provide a near-global look at the planet, revealing lateral and vertical heterogeneities in the color and thus composition of Mercury's crust. Smooth plains cover approximately 40% of the surface, and evidence for the volcanic origin of large expanses of plains suggests that a substantial portion of the crust originated volcanically. A low-reflectance, relatively blue component affects at least 15% of the surface and is concentrated in crater and basin ejecta. Its spectral characteristics and likely origin at depth are consistent with its apparent excavation from a lower crust or upper mantle enriched in iron- and titanium-bearing oxides.

Two close-approach flybys of Mercury (on 14 January 2008 and 6 October 2008) by the MESSENGER spacecraft, together with Mariner 10 observations, provide high-resolution images of 90% of this enigmatic planet's surface (*1*). These data permit a planet-wide assessment of the processes that shaped Mercury's crust: volcanism, deformation, and impact cratering. Crustal stresses play an important role in modulating and directing magmatic activity, impacts localize both volcanic and tectonic activity, and craters and ejecta provide our only probe deep into the crust. Here, we present a global catalog of the major geologic terrains and their stratigraphy and distribution across the surface, as well as an assessment of their implications for the formation and evolution of Mercury's crust.

MESSENGER's second flyby has confirmed the prediction (*2*), made on the basis of Mariner 10 images of less than half of Mercury's surface, that tectonic features on Mercury are dominantly contractional (*3*, *4*). Because a lithospheric stress state dominated by compression inhibits the ascent of magma, the timing of deformation recorded by lobate scarps (Fig. 1A) and other contractional landforms is important for understanding the history of volcanism on Mercury (*5*). The second MESSENGER flyby also reinforced the view that volcanism was an important process in Mercury's geologic history (*6*–*8*). Similar to features seen in images from the first flyby (*6*, *7*), spectrally distinct plains deposits (Fig. 2), lobate margins, crater embayment and flooding relationships, and wrinkle-ridge rings (Fig. 1A) provide evidence for widespread effusive volcanism. Rimless depressions surrounded by material of higher albedo and a steeper spectral slope (Fig. 1B) are additional candidates for sites of explosive volcanism (*6*, *7*).

MESSENGER's flybys have emphasized that first-order albedo and color contrasts on the planet are largely dominated by fresh crater materials. The second flyby revealed the rays and interiors of two large rayed craters, termed "A" and "B," that were first discovered with Earth-based radar (*9*). The rays of crater A (85 km in diameter and centered at 34°S, 12°E) extend approximately 1900 km, and those of crater B reach at least 4500 km (Fig. 1C). On the Moon, rays rarely exceed 2000 km in length (*10*). Rays of such great extent are thus unexpected on

[1]School of Earth and Space Exploration, Arizona State University, Tempe, AZ 85251, USA. [2]Department of Terrestrial Magnetism, Carnegie Institution of Washington, Washington, DC 20015, USA. [3]Johns Hopkins University Applied Physics Laboratory, Laurel, MD 20723, USA. [4]National Museum of Natural History, Smithsonian Institution, Washington, DC 20560, USA. [5]Department of Geological Sciences, Brown University, Providence, RI 02912, USA. [6]Center for Earth and Planetary Studies, National Air and Space Museum, Smithsonian Institution, Washington, DC 20560, USA.

*To whom correspondence should be addressed. E-mail: bdenevi@ser.asu.edu

Mercury, given the higher gravitational acceleration and comparatively limited extent of continuous ejecta deposits (*11*). Among the possible explanations for these findings are that the two Mercury craters are substantially younger than the lunar crater Tycho, ray material coalesces more efficiently to make distal rays more distinctive, space weathering on Mercury is less efficient at erasing rays than on the Moon, or ray material travels farther on Mercury than predicted. In addition to exposing fresh material, impact events also excavate material from depths as great as tens of kilometers below the surface, providing a means to assess vertical heterogeneities in the crust (Fig. 2).

The latest MESSENGER data confirm the presence on Mercury of albedo and color variations related to compositional heterogeneities (*8*). These variations are subtle compared with those of the Moon. Mercury shows variations smaller in relative reflectance of mature terrain than does the Moon (factor of 1.7 versus 2.6 at 750 nm) but larger than variations across the lunar highlands (1.1) or among major mare units (1.4). Multispectral images from the Mercury Dual Imaging System (MDIS) (*1*) and ultraviolet (UV)–visible–near-infrared (NIR) spectra from the Mercury Atmospheric and Surface Composition Spectrometer (MASCS) show that Mercury's major color units all share red-sloped reflectance spectra without strong crystal-field absorptions by iron-bearing silicates for both mature and immature materials (*12*, *13*) (Fig. 3A). Color variations among units are thus primarily products of changes in the steepness of the spectral slope (430 to 1020 nm), with steeper slopes termed relatively red and shallower slopes relatively blue.

Spectral slope, relative reflectance, and morphology distinguish three major terrain types (*13*) on Mercury: smooth plains, intermediate terrain (IT), and low-reflectance material (LRM). The second flyby color data demonstrate that these three terrains are broadly sufficient to describe the majority of Mercury's surface and allow further subdivision.

The smooth plains have a lower density of impact craters (*14*) and typically fill low-lying areas such as impact craters and basins. Their reflectance and spectral slope vary from unit to unit, and three subtypes are identified from global color data (Fig. 3A). High-reflectance red plains (HRP) are the most conspicuous of the smooth plains, with reflectances of up to 20% above the global mean and relatively steep spectral slopes. These plains typically display sharp color and morphologic boundaries with surrounding terrain (*6*, *13*). Intermediate plains (IP) have reflectance and color properties similar to the global mean. They also exhibit sharp morphologic boundaries with the surrounding terrain, as well as color boundaries where they overlie LRM. Low-reflectance blue plains (LBP) have reflectances 15% below the global mean and spectral properties intermediate to IP and LRM. A decrease in spectral slope of ~3% is observed from HRP to LBP.

The IT includes areas with a higher crater density than smooth plains and generally corresponds to regions mapped as heavily cratered terrain and intercrater plains from Mariner 10 images (*15*, *16*). The reflectance and color properties of the IT are similar to the global mean, although they show moderate variation.

The LRM exhibits reflectances as low as 30% below the global mean, and its spectral slope is ~5% lower than that of the HRP (Fig. 3A). At wavelengths below ~500 nm, spectra of the LRM exhibit a relative upturn, most clearly observed in ratioed MASCS spectra (*12*). The spectral properties of LRM are remarkably consistent and show little change whether they are freshly exposed in crater ray deposits or have been long exposed to the space-weathering environment on the surface. LRM occurs as broad regions with diffuse margins as well as in concentrated "centers" typically comprised of crater or basin ejecta. The LRM does not exhibit distinctive morphologic characteristics; it includes terrain that would typically be mapped as IT, were it not for its color properties.

We created enhanced color images from 11-band, photometrically corrected wide-angle camera (WAC) (*1*) mosaics (0.5 to 5.0 km per pixel) and combined the second principal component, first principal component, and 430/1000–nm ratio into red-green-blue composite images (Fig. 4A) (*13*). The second principal component largely removes the spectral effects of maturity, so that the red-blue planes encode compositional variations in the surface material, whereas the green plane is dominated by maturity variations and therefore highlights fresh craters. Together with narrow-angle camera (NAC) (*1*) high-resolution (0.3 to 0.5 km per pixel) images, these products allow near-global mapping on the basis of both color and morphology. Areas of MDIS mosaics with high Sun illumination, which is disadvantageous for viewing topography and texture, were supplemented with Mariner 10 images (1 km per pixel) (*17*) where available; otherwise, these high-Sun-illumination areas were excluded.

These data demonstrate that smooth plains are widespread on Mercury: They cover ~40% of the surface and are globally distributed (Fig. 4B). On the basis of Mariner 10 images, estimates for the areal extent of smooth plains varied from 15 to 40% (*2*, *18*). Individual deposits range from hundreds of square kilometers to 1.7 million km^2 (the Caloris basin interior plains), rivaling the sizes of the largest flood basalt units on the Earth or Moon. The majority of smooth plains are probably of volcanic origin (*2*, *6*), although impact melt and basin ejecta are likely explanations for a subset of plains units. Vast expanses of smooth plains deposits with features that are diagnostic of volcanically emplaced materials

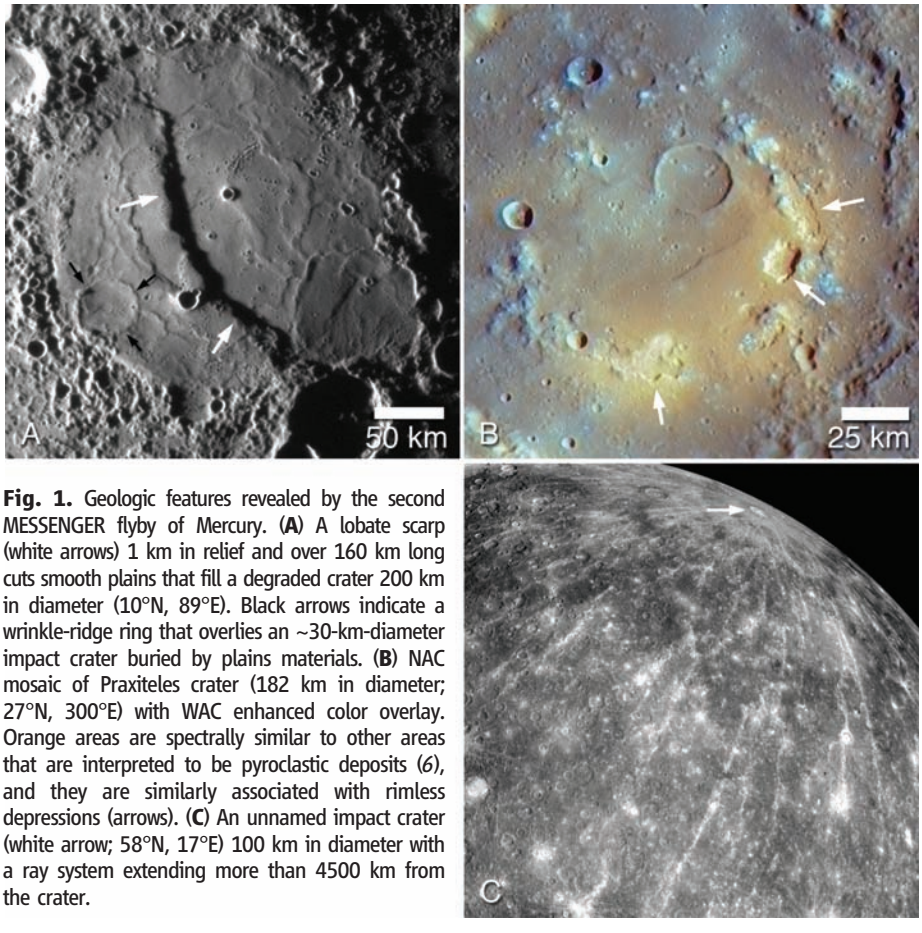

Fig. 1. Geologic features revealed by the second MESSENGER flyby of Mercury. (**A**) A lobate scarp (white arrows) 1 km in relief and over 160 km long cuts smooth plains that fill a degraded crater 200 km in diameter (10°N, 89°E). Black arrows indicate a wrinkle-ridge ring that overlies an ~30-km-diameter impact crater buried by plains materials. (**B**) NAC mosaic of Praxiteles crater (182 km in diameter; 27°N, 300°E) with WAC enhanced color overlay. Orange areas are spectrally similar to other areas that are interpreted to be pyroclastic deposits (*6*), and they are similarly associated with rimless depressions (arrows). (**C**) An unnamed impact crater (white arrow; 58°N, 17°E) 100 km in diameter with a ray system extending more than 4500 km from the crater.

(*2*, *6*, *7*, *18*) demonstrate that volcanism was extensive on Mercury. In many areas, a sequence of several generations of smooth plains can be observed, and crater excavation relationships demonstrate that smooth plains can be as thick as 5 km (*6*, *19*). The globally distributed intercrater plains of the IT may simply be older and more degraded smooth plains that formed through widespread volcanism during or at the end of the late heavy bombardment (*16*); however, emplacement as basin ejecta remains a possibility (*20*).

Observations from the second MESSENGER flyby confirm that the LRM is a key terrain type (*13*): It covers at least 15% of Mercury, and individual regions of LRM can be greater than 4 million km^2 in extent (Fig. 4). Because of the diffuse nature of regional LRM deposits, most LRM boundaries are mapped as approximate. At least 65 craters and basins greater than 20 km in diameter exhibit some form of LRM ejecta, implying depths of origin of the LRM from several kilometers to as much as 25 km. The association with impact crater and basin ejecta and the observation that regional LRM deposits are often without clear morphologic boundaries (aside from distinct margins in crater and basin ejecta, or where embayed by smooth plains) and occur as thin surficial deposits in many locations indicate a subsurface origin through impact excavation and subsequent distribution across the surface as an ejecta veneer (Fig. 2). Thus, LRM source material appears to originate at depth and may represent a component of the lower crust or upper mantle that was redistributed on the surface. However, the absence of LRM in the ejecta of many large impact craters demonstrates heterogeneous distribution of its source material throughout the crust both horizontally and vertically (Fig. 3B). In some cases, diffuse LRM deposits may have originally been magmatically emplaced as intrusive or extrusive deposits, now degraded and mixed through impact processes.

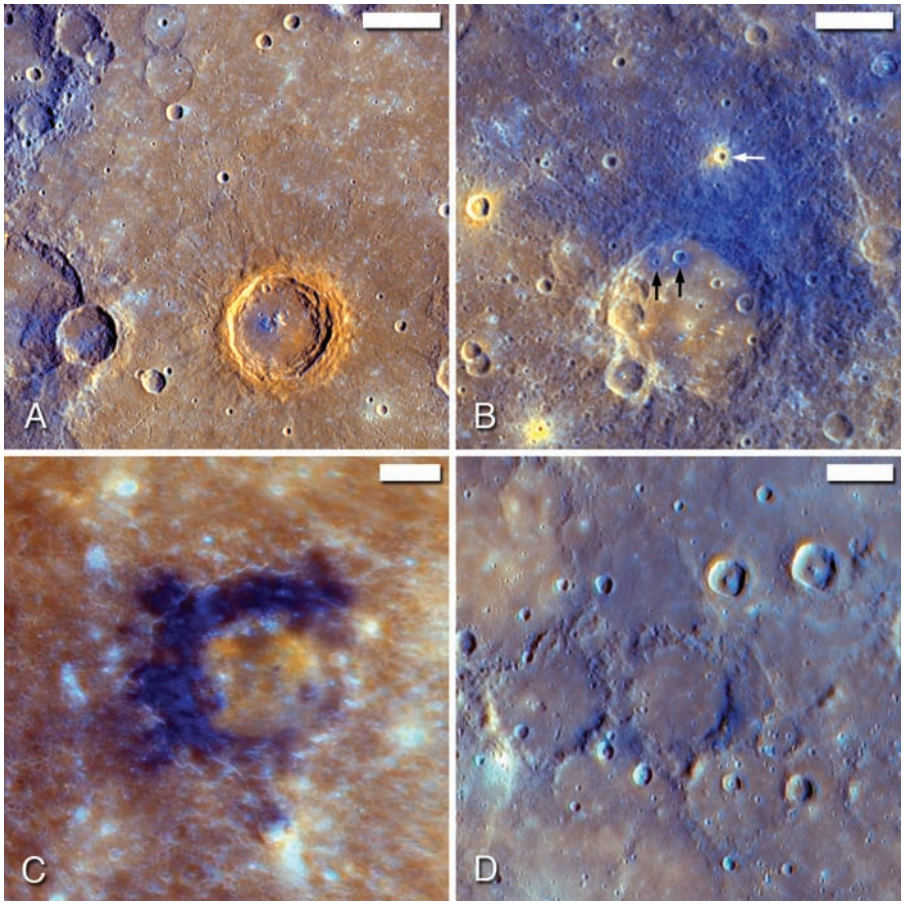

Fig. 2. Key stratigraphic relationships observed by MDIS. (A) and (B) show portions of the highest-resolution color images (462 m per pixel); (C) and (D) are composites of NAC and WAC mosaics. (**A**) Smooth plains fill a degraded basin near the crater Rudaki (image centered at 4°S, 304°E). The ejecta of the 68-km-diameter crater near the center has an elevated albedo and steeper spectral slope than the surrounding plains, suggesting that the surface layer of IP buried an HRP unit exposed by this crater. Portions of the central peak have exhumed LRM from an estimated depth (*38*) of 7 to 10 km. (**B**) Crater Titian (121 km in diameter; 4°S, 317°E) excavated LRM from beneath smooth plains; this LRM ejecta masks the spectral character of older smooth plains, except where small craters re-expose plains material (white arrow). Younger smooth plains fill Titian, and small impacts expose LRM from below these plains (black arrows). (**C**) LRM center in unnamed crater (165 km in diameter; 9°S, 20°E). The asymmetrical distribution of LRM exposed by impact craters is common. (**D**) LBP northwest of Caloris basin (43°N, 121°E). The LBP are spectrally indistinguishable from the older craters they embay and do not have a sharp morphologic boundary with IP/HRP. Within the LBP, large impact craters typically do not have spectrally distinct ejecta [as opposed to those in (A) to (C)]. All scale bars are 50 km.

The relationship between the diffuse LRM deposits and LBP is complex. In some places, LRM ejecta constitute a thin surface coating on HRP or IP, masking the inherent color properties of the plains (Fig. 2B). The circum-Caloris plains, the largest expanse of LBP, are also the most complicated. Several observations imply a relationship with Caloris ejecta: The plains generally have no distinct boundaries with the hummocky plains of the Odin Formation (interpreted to be basin ejecta); radially away from Caloris, they are often interfingered with IP/HRP; in portions of their distal margins, they have no distinct morphologic or color boundaries and grade into HRP; and in some areas with distinct morphologic boundaries, their color properties are indistinguishable from the terrain they embay (Fig. 2D) (*7*, *13*). However, crater counts indicate that they are younger than the Caloris interior plains, which in turn are younger than Caloris rim materials (*14*, *21*), and thus these LBP are interpreted to be the result of later resurfacing that was potentially of volcanic origin (*14*, *21*). These conflicting observations must be reconciled before the nature of the LBP can be confidently understood.

The widespread distribution of smooth plains that are interpreted to be of volcanic origin demonstrates that the global compressive lithospheric stresses indicated by lobate scarps did not preclude extensive volcanism at least until well after the formation of the Caloris basin. Wrinkle ridges and lobate scarps (Fig. 1A) in many smooth plains units suggest that contractional deformation continued after the emplacement of the youngest volcanic plains (*4*). Understanding the ascent and eruption of magma requires knowledge of the mechanical structure and the evolution of stress both globally and locally as well as the density and thickness of the crust and of mantle-derived magmas (*5*, *22*). Observations to date make it difficult to place precise constraints on these parameters, although current compositional interpretations argue against a large density contrast between Mercury's crust and upper mantle.

The interpretation of MDIS color units in terms of lithologic units poses a challenge. Earth-based reflectance spectra (*23*), confirmed by MESSENGER observations of mature and immature material (*12*, *13*), show no 1-μm absorption band, implying a low (<6 weight percent) ferrous iron (FeO) content of silicate minerals (*23, 24*). Thermal emission measurements at microwave wavelengths (0.3 to 20.5 cm) indicate that Mercury's surface is 40% more transparent than the lunar highlands (*25*). These two observations have led to the inference that

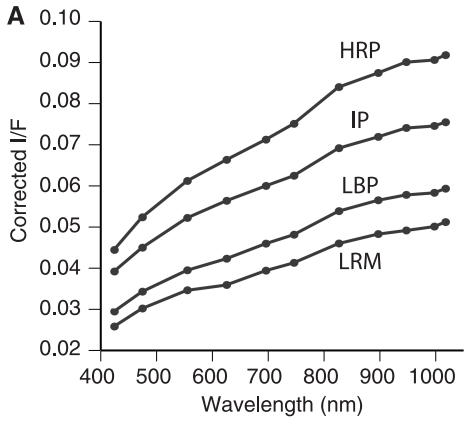

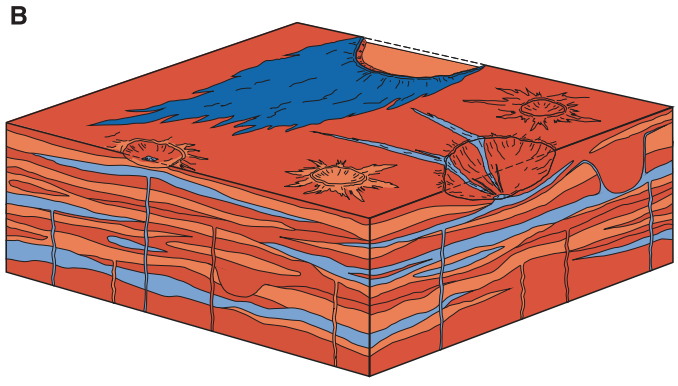

Fig. 3. (**A**) MDIS spectra (photometrically corrected to an incidence angle of 30° and an emission angle of 0°, both measured from the vertical) of the three type examples of smooth plains and the LRM. I/F (radiance factor, known as reflectance) is the observed radiance divided by the expected radiance from a normally solar-illuminated Lambertian surface. Remaining uncertainties in the calibration contribute to the small wiggles seen in these spectra. (**B**) Schematic of the complex vertical and lateral heterogeneities expected as a result of the accumulation of Mercury's crust through extrusive and intrusive volcanism over time. Colors show the compositional variation among HRP (light orange), IP (dark orange), LBP (light blue) deposits, and LRM centers (dark blue). The sectioned crater on the left depicts a possible origin for color variations, such as those of Fig. 2A. Rim materials excavate buried HRP, and the central peak exposes buried LBP. The sectioned crater on the right shows the morphology of LRM streamers, such as those of Mozart crater, which may be due to the excavation of LRM or LBP (see also Fig. 2, B and C). In the background are continuous LRM ejecta (dark blue) and lava fill of the basin as observed at Tolstoj basin, illustrating the proposed origin of LRM centers as excavated components of the lower crust or upper mantle relatively enriched in the proposed low-reflectance mineral. This diagram is simplified, and more vertical mixing is expected through intrusions of rising magma, such as dikes and sills (*6*), and impacts of various sizes throughout the crustal formation process. The illustration is not to scale.

Mercury's crust contains lower abundances of iron (Fe) plus titanium (Ti) than the lunar highlands (*23*–*25*). However, Mercury's average reflectance is similar to, or lower than, the reflectance of the integrated lunar nearside (*26*), 30% of which is covered by high-Fe, high-Ti basalts. Mercury's reflectance cannot be ascribed solely to differential space weathering of a lunarlike anorthositic crust, because immature materials on Mercury are also as much as 30% lower in reflectance than comparable material on the Moon (*13*, *17*). This result indicates that Mercury's crust is not dominantly anorthositic but instead possibly rich in low-Fe pyroxene or olivine (both of which have reflectances lower than that of anorthite) and a spatially variable low-reflectance component. During MESSENGER's second Mercury flyby, MASCS observations detected magnesium (Mg) in the exosphere, a result that requires a substantial source of Mg at Mercury's surface (*27*), such as magnesian pyroxene.

The lack of a 1-μm band, the presence of the spatially variable LRM, and Mercury's overall low albedo imply the presence of an opaque phase (*28*, *29*), and iron, titanium, and carbon are the most cosmochemically abundant elements that contribute to strong absorptions at UV-through-NIR wavelengths. Carbon is unlikely to be responsible because it is effectively sequestered to the core during early planetary differentiation (*30*) and lost through volatilization in volcanic eruptions. Ti alone is not highly absorbing at visible-NIR wavelengths unless it is paired with another transition metal, such as Fe; Fe alone is typically red-sloped or exhibits a 1-μm band if contained in silicates. In oxide minerals, Fe and Ti together have a strong, broad, charge-transfer absorption that results in low reflectance and a neutral spectrum, in some cases with a shallow upturn at short wavelengths. Thus, opaque Fe- and Ti-bearing minerals such as ilmenite ($FeTiO_3$), or possibly any oxide with considerable abundances of Fe and Ti (*31*), match the spectral characteristics of the LRM. To estimate potential abundances of Fe- and Ti-bearing oxides, we used a radiative transfer model based on the equations of Hapke (*32*). Spectra were converted to single-scattering albedo (the probability of a photon being scattered by a particle), and HRP spectra were mixed linearly with ilmenite spectra (used as a proxy for any Fe- and Ti-bearing oxide) so as to match the characteristics of the IP and LRM. Up to 15% ilmenite is required to match MDIS spectra of the IT, and up to 40% ilmenite is needed for spectra of the most extreme LRM center (a portion of the Tolstoj basin annulus). These abundances are maximum values because of the assumption that all of the decrease in reflectance is due to ilmenite.

The maximum ilmenite abundance required to match intermediate terrain is consistent with MESSENGER's Neutron Spectrometer measurements, which observed predominantly intermediate terrain and are interpreted as indicating abundances of neutron-absorbing elements (Fe, Ti, gadolinium, samarium) within the range of lunar soil samples from Luna 16 to Luna 24 (*33*). These soils contain moderate to high abundances of Fe and Ti, which if contained predominantly in oxide minerals would explain their high abundance without a corresponding 1-μm band. Early crystallization of Fe- and Ti-bearing oxides such as ilmenite under reducing conditions (near the iron-wüstite buffer) from a Ti-rich and relatively FeO-poor melt limits FeO incorporation into later-crystallizing pyroxene (*34*). In such an environment, Mg-calcium–bearing pyroxenes would be expected to form after substantial amounts of ilmenite crystallize. High abundances of Fe and/or Ti are contrary to the inferences from Earth-based microwave measurements (*25*). However, the interpretation of the microwave data also predicts that Mercury's albedo is higher than that of the lunar highlands (*25*), which is not observed (*26*). Earth-based photometric observations indicate that Mercury's regolith is more backscattering than the average lunar terrain; its scattering properties (typically related to opaque content) are more similar in character to lunar maria than to lunar highlands (*26*). Radar observations indicate that LRM centers, such as the Tolstoj annulus, show low radar returns similar to the lunar maria and in contrast to HRP, which is consistent with a higher Fe and Ti content in LRM (*9*).

Such high abundances of ilmenite (or any Fe- and Ti-bearing oxide) for the LRM are improbable for extrusive volcanic rocks and are more plausible if the LRM material originates from cumulate deposits. Such cumulates can form as late-stage products of a large-scale magma ocean or from crystal-liquid fractionation within subsurface magma chambers. These modes of occurrence are consistent with the stratigraphy of LRM deposits that are exposed on the surface by impact excavation. The smooth plains materials, containing a smaller fraction of dense Fe- and Ti-bearing oxides, would be more likely to reach the surface in volcanic eruptions (*5*, *22*).

The global view of Mercury indicates that widespread resurfacing probably obscured early events in the planet's geological history. Evidence for large-scale volcanic deposits several kilometers thick (*6*, *7*, *19*) suggests that a substantial volume of the crust was created through repeated volcanic eruptions. Basins such as Caloris, filled nearly to their rims both inside and out, hint at the probable existence of older basins that are not yet recognized because of volcanic burial and impact degradation. Little evidence is found for an ancient feldspar-rich flotation crust such as that of the lunar high-

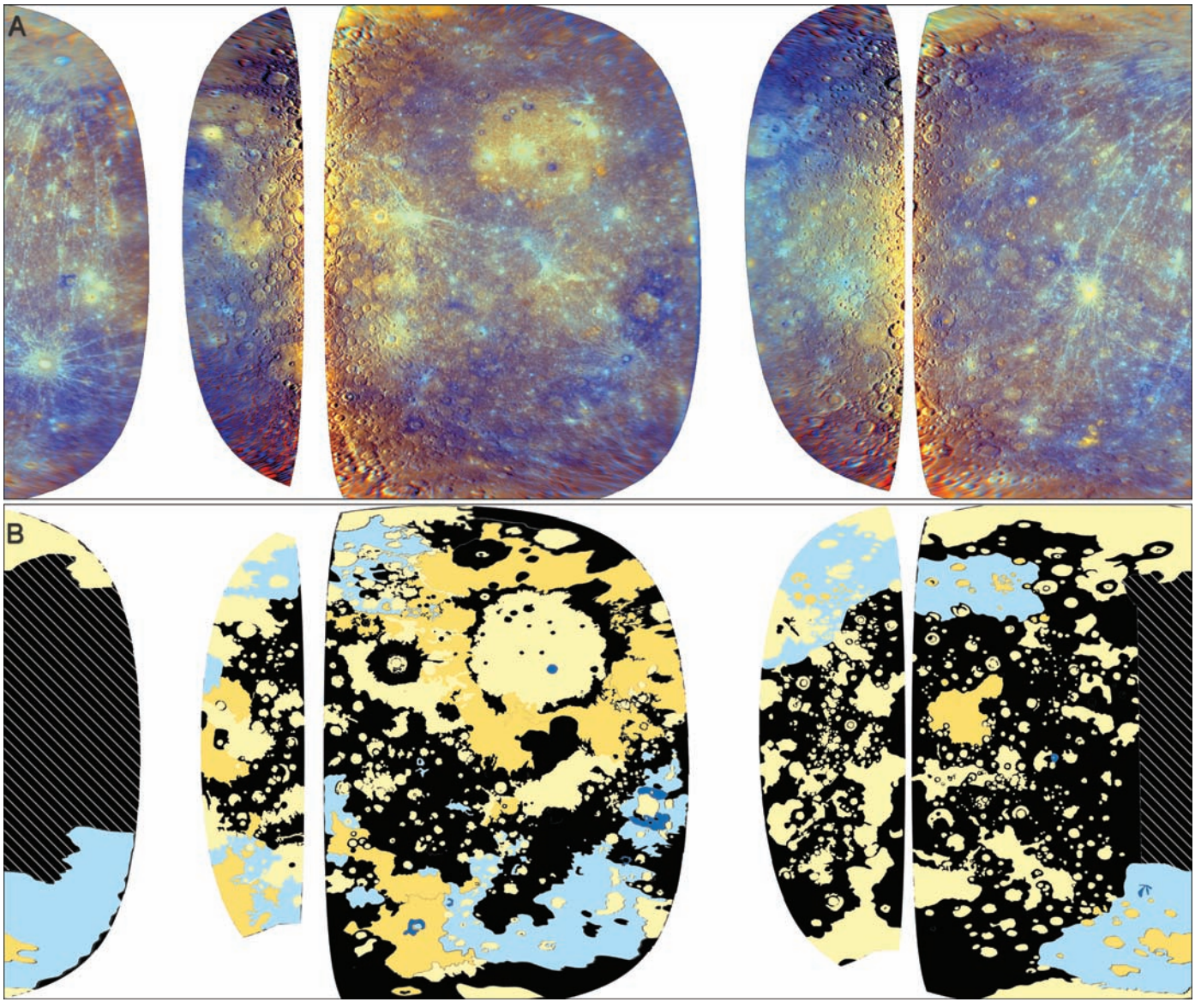

Fig. 4. Two simple cylindrical views of Mercury over ±75° latitude, 0° to 360°E longitude. (**A**) Enhanced color MDIS WAC mosaics. Areas in white are regions not yet imaged by MESSENGER. (**B**) Geologic map of Mercury from MESSENGER WAC and NAC mosaics and Mariner 10 clear-filter mosaics. Light yellow, HRP and IP; dark yellow, LBP; light blue, regional LRM; dark blue, LRM center; black, other (fresh crater ejecta or IT); and white, no data. Crosshatches indicate areas not mapped because of high Sun illumination. Areas near the terminator in (A) appear unnaturally red; until the final WAC calibration is available, color distinctions are subject to revision.

lands, which is thought to be the result of the crystal-liquid fractionation of a global magma ocean. If such an early crust existed, it may now be buried by younger volcanic material, but there is no definitive indication that feldspar-rich material has been excavated from depth. Removal of Mercury's earliest crust by a giant impact or vaporization in a hot solar nebula has been proposed to account for Mercury's high bulk density (*35*, *36*). If such an event occurred, crustal formation continued thereafter, most likely obscuring any record of early crustal stripping. The main inference from the combined MESSENGER data are that much of Mercury's crust formed as a result of the eruptions of magmas of varying composition over an extended duration of geologic time.

References and Notes

1. MESSENGER images were acquired with the MDIS, which includes the 11 filters (430 to 1020 nm) of the WAC and the monochrome (750 nm) NAC described in (*37*).
2. R. G. Strom, N. J. Trask, J. E. Guest, *J. Geophys. Res.* **80**, 4062 (1975).
3. S. C. Solomon *et al.*, *Science* **321**, 59 (2008).
4. T. R. Watters *et al.*, *Earth Planet. Sci. Lett.*, 10.1016/j.epsl.2009.01.015 (2009).
5. S. C. Solomon, *Geophys. Res. Lett.* **5**, 461 (1978).
6. J. W. Head *et al.*, *Science* **321**, 69 (2008).
7. S. L. Murchie *et al.*, *Science* **321**, 73 (2008).
8. M. S. Robinson, P. G. Lucey, *Science* **275**, 197 (1997).
9. J. K. Harmon *et al.*, *Icarus* **187**, 374 (2007).
10. R. B. Baldwin, *The Measure of the Moon* (Univ. of Chicago Press, Chicago, 1963).
11. D. E. Gault, J. E. Guest, J. B. Murray, D. Dzurisin, M. C. Malin, *J. Geophys. Res.* **80**, 2444 (1975).
12. W. E. McClintock *et al.*, *Science* **321**, 62 (2008).
13. M. S. Robinson *et al.*, *Science* **321**, 66 (2008).
14. R. G. Strom, C. R. Chapman, W. J. Merline, S. C. Solomon, J. W. Head III, *Science* **321**, 79 (2008).
15. N. J. Trask, J. E. Guest, *J. Geophys. Res.* **80**, 2461 (1975).
16. M. C. Malin, *Geophys. Res. Lett.* **3**, 581 (1976).
17. B. W. Denevi, M. S. Robinson, *Icarus* **197**, 239 (2008).
18. P. D. Spudis, J. E. Guest, in *Mercury*, F. Vilas, C. R. Chapman, M. S. Mathews, Eds. (Univ. of Arizona Press, Tucson, 1988), pp. 118–164.
19. C. M. Ernst, S. L. Murchie, O. S. Barnouin-Jha, M. S. Robinson, B. W. Denevi, *Lunar Planet. Sci.* **40**, abstr. 1900 (2009).
20. D. E. Wilhelms, *Icarus* **28**, 551 (1976).
21. C. I. Fassett *et al.*, *Lunar Planet. Sci.* **40**, abstr. 1889 (2009).
22. J. W. Delano, *Proc. Lunar Planet. Sci. Conf.* **20**, 3 (1990).
23. F. Vilas, in *Mercury,* F. Vilas, C. R. Chapman, M. S. Matthews, Eds. (Univ. of Arizona Press, Tucson, 1988), pp. 59-76.
24. D. T. Blewett, B. R. Hawke, P. G. Lucey, *Meteorit. Planet. Sci.* **37**, 1245 (2002).
25. D. L. Mitchell, I. de Pater, *Icarus* **110**, 2 (1994).
26. J. Warell, *Icarus* **167**, 271 (2004).

27. W. E. McClintock *et al.*, *Science* **324**, 610 (2009).
28. B. Rava, B. Hapke, *Icarus* **71**, 397 (1987).
29. D. T. Blewett *et al.*, *Earth Planet. Sci. Lett.*, 10.1016/j.epsl.2009.02.021 (2009).
30. V. J. Hillgren, C. K. Gessman, J. Li, in *Origin of the Earth and Moon*, R. M. Canup, K. Righter, Eds. (Univ. Arizona Press, Tucson, 2000), pp. 245–263.
31. M. A. Riner, P. G. Lucey, S. J. Desch, F. M. McCubbin, *Geophys. Res. Lett.* **36**, L02201 (2009).
32. B. Hapke, *Theory of Reflectance and Emittance Spectroscopy: Topics in Remote Sensing 3* (Cambridge Univ. Press, New York, 1993).
33. D. J. Lawrence, W. C. Feldman, J. O. Goldsten, *Lunar Planet. Sci.* **40**, abstr. 1761 (2009).
34. T. M. Usselman, G. E. Lofgren, C. H. Donaldson, R. J. Williams, *Proc. Lunar Sci. Conf.* **6**, 997 (1975).
35. A. G. W. Cameron, *Icarus* **64**, 285 (1985).
36. W. Benz, W. L. Slattery, A. G. W. Cameron, *Icarus* **74**, 516 (1988).
37. S. E. Hawkins III *et al.*, *Space Sci. Rev.* **131**, 247 (2007).
38. M. J. Cintala, R. A. F. Grieve, *Meteorit. Planet. Sci.* **33**, 889 (1998).
39. We gratefully acknowledge the MESSENGER engineers and technical support team. N. Laslo, H. Kang, R. Vaughan, A. Harch, R. Shelton, and A. Berman designed the imaging sequences used here. S. Turner, K. Becker, and C. Hash contributed to data calibration and processing. The MESSENGER project is supported by the NASA Discovery Program under contracts NAS5-97271 to the Johns Hopkins University Applied Physics Laboratory and NASW-00002 to the Carnegie Institution of Washington.

12 February 2009; accepted 8 April 2009
10.1126/science.1172226

Evolution of the Rembrandt Impact Basin on Mercury

Thomas R. Watters,[1]* James W. Head,[2] Sean C. Solomon,[3] Mark S. Robinson,[4] Clark R. Chapman,[5] Brett W. Denevi,[4] Caleb I. Fassett,[2] Scott L. Murchie,[6] Robert G. Strom[7]

MESSENGER's second Mercury flyby revealed a ~715-kilometer-diameter impact basin, the second-largest well-preserved basin-scale impact structure known on the planet. The Rembrandt basin is comparable in age to the Caloris basin, is partially flooded by volcanic plains, and displays a unique wheel-and-spoke–like pattern of basin-radial and basin-concentric wrinkle ridges and graben. Stratigraphic relations indicate a multistaged infilling and deformational history involving successive or overlapping phases of contractional and extensional deformation. The youngest deformation of the basin involved the formation of a ~1000-kilometer-long lobate scarp, a product of the global cooling and contraction of Mercury.

Impact basins, generally in excess of several hundred kilometers in diameter, are among the most important landforms created early in planetary history (*1*). Because of their typically ancient ages, most basins have been modified and filled with volcanic plains, which obscure their initial state and early evolution. A few basins, such as Orientale on the Moon, remain largely unfilled and provide substantial insight into basin formation and early modification (*2*, *3*). During its second flyby of Mercury in October 2008, the MESSENGER spacecraft imaged ~30% of the planet not previously seen by spacecraft. These images revealed a relatively unmodified basin centered near 33°S, 88°E (Fig. 1A). The interior of the basin, recently named Rembrandt, differs considerably from that of the well-preserved and larger Caloris basin, imaged by Mariner 10 (*4*, *5*) and during MESSENGER's first Mercury encounter (*6*–*11*). The Caloris basin contains substantial infill by plains of volcanic origin that cover its entire floor. On the basis of MESSENGER observations, we here assess the characteristics of the Rembrandt basin and their geological implications.

The Rembrandt basin (Fig. 1A) has a topographically distinct main rim crest made up of rugged, high-relief, inward-facing scarps and massifs. At ~715 km, its mean rim crest diameter is larger than the intermediate-scale, partly filled impact basins Beethoven (~625 km) and Tolstoj (~510 km) (*5*) and about half the size of the largest known basin, Caloris (>1500 km) (*7*, *8*). Numerous large impact craters are superposed on the rim of the basin (Fig. 1A). The number of craters ≥20 km in diameter per million square kilometers is not distinguishable from that for the rim of the Caloris basin [see supporting online material (SOM), figs. S1 to S3]. The crater size-frequency distribution (SFD) for the Rembrandt basin rim (Fig. 1B) is also similar to that for the Caloris basin rim (*11*). These results suggest that Rembrandt, like Caloris, is one of the youngest basins on Mercury, younger than Tolstoj and Beethoven, yet sufficiently old to show the pattern of fewer small-diameter craters relative to large-diameter craters that is characteristic of terrains formed before the end of the late heavy bombardment of the inner solar system (~3.9 billion years ago) (*12*).

Exterior to the basin rim crest are blocky and radially lineated ejecta deposits, well preserved to the north and northeast of the basin rim, respectively (Fig. 1, A and C). These deposits are comparable to the annuli of radially textured ejecta outside the rims of the Caloris basin (*5*, *11*) and the lunar Orientale basin (*2*, *3*). Basin interior units include a hummocky unit and a smooth plains unit. The hummocky unit extends inward from the basin rim by up to ~130 km (Fig. 1D) and is distinguished by knobs that rise up to hundreds of meters (from shadow measurements) above patches of rolling hills near the basin margin (Fig. 1C). This unit forms a discontinuous ring in the basin interior, confined to the northern margin. Two large, angular blocks or massifs on the southern edge of the hummocky unit have a maximum relief of >1.5 km (Fig. 1D). The inner edge of the hummocky unit and the massifs may mark the remnants of a ringlike structure with a diameter of ~450 km (Figs. 1 and 2). The hummocky and domical morphology of the unit and its position just inside the basin rim are similar to those of the Montes Rook Formation in Orientale, interpreted to have been formed by collapse and inward translation of the transient cavity rim and modification of radially textured rim deposits into domical blocks (*2*, *3*). This interpretation is supported by remnant radial crater-chain–like structures (Fig. 1D), similar to occurrences in Orientale, and suggests that the inner edge and massifs of this unit delineate the remnant of the transient cavity rim (*2*).

Smooth plains constitute the most areally extensive unit in the Rembrandt basin; occupy much of the basin interior; and extend to the southern, eastern, and parts of the western rim (Fig. 2A). In the lunar Orientale basin, non-mare smooth and rough plains inside the transient cavity are interpreted to be impact melt (*1*–*3*). On the basis of laboratory experiments and theoretical scaling arguments, the volume of impact melt formed in basins is predicted to increase with basin size and perhaps even to fill entirely the basin interior at the largest diameters (*13*). If the regional plains are impact melt, they would have been emplaced in the immediate aftermath of basin formation and collapse, before formation of any subsequent major impact craters, as has been documented for the lunar Orientale basin (*14*). Furthermore, they should have spectral characteristics appropriate for a physical mixture of the target materials.

Broadly distributed spectral units on Mercury identified from global principal component analysis and spectral ratios of MESSENGER's 11-color wide-angle camera (WAC) images include low-reflectance material (LRM), spectrally intermediate terrain, and three types of smooth plains: (i) high-reflectance red plains (HRP), (ii) intermediate plains, and (iii) low-reflectance blue plains (LBP) (*10*, *15*). Comparison of color data between the Rembrandt basin and other regions of the planet is complicated by the area's near-

[1]Center for Earth and Planetary Studies, National Air and Space Museum, Smithsonian Institution, Washington, DC 20560, USA. [2]Department of Geological Sciences, Brown University, Providence, RI 02912, USA. [3]Department of Terrestrial Magnetism, Carnegie Institution of Washington, Washington, DC 20015, USA. [4]School of Earth and Space Exploration, Arizona State University, Tempe, AZ 85251, USA. [5]Southwest Research Institute, 1050 Walnut Street, Boulder, CO 80302, USA. [6]Johns Hopkins University Applied Physics Laboratory, Laurel, MD 20723, USA. [7]Lunar and Planetary Laboratory, University of Arizona, Tucson, AZ 85721, USA.

*To whom correspondence should be addressed. E-mail: watterst@si.edu

terminator lighting and oblique viewing geometry during the flyby. Relative color and reflectance differences across the basin region show that ejecta and interior hummocky units of Rembrandt are lower in reflectance than the interior smooth plains (Fig. 3) and broadly similar spectrally to LRM and LBP. The high relative reflectance of the interior plains is analogous to that of HRP, interpreted to be of volcanic origin (*10*, *15*). Moreover, the exterior ejecta of several major craters in the interior smooth plains have been embayed by plains units (Fig. 2B), and there is evidence of breached rims and interior crater infilling by smooth plains (Fig. 2A), suggesting a prolonged period of plains formation. The distinct spectral

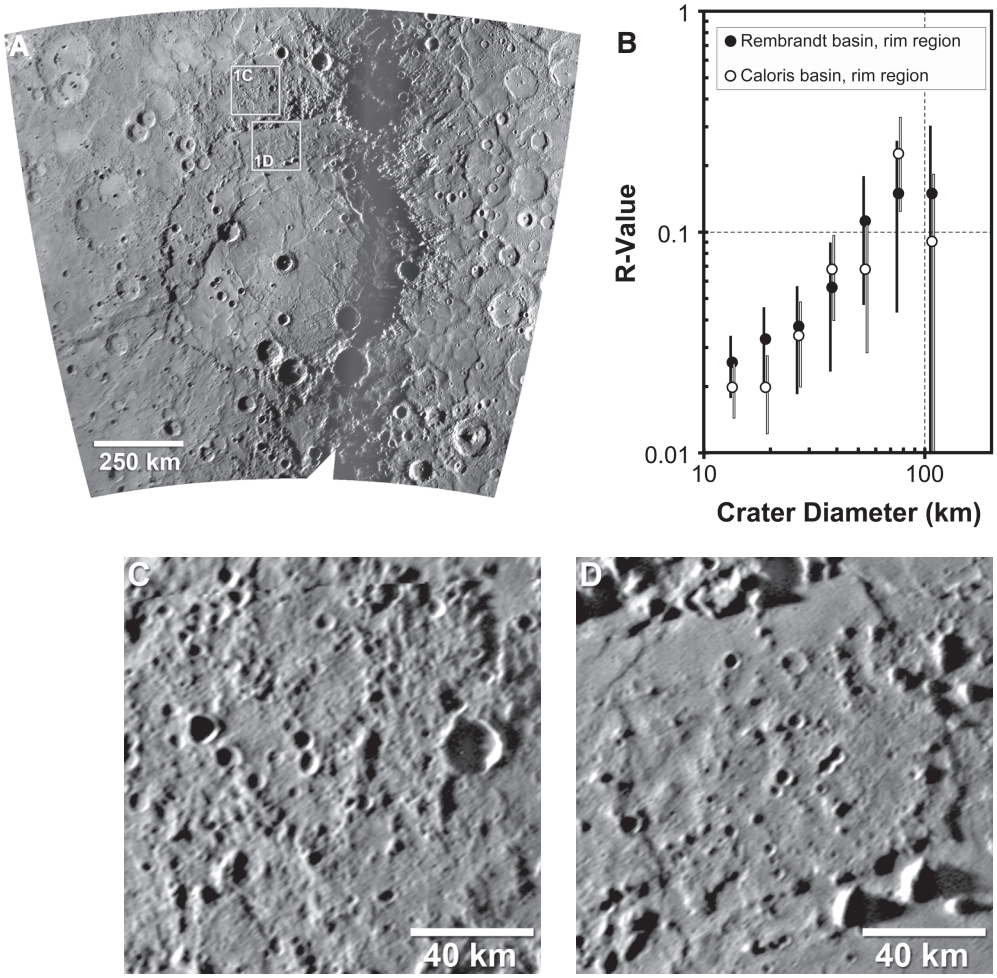

Fig. 1. The Rembrandt basin. (**A**) NAC mosaic (*24*) combining images obtained during MESSENGER's first and second flybys, including frames EN0108828198M, EN0108828203M, EN0108828250M, EN0108828255M, EN0108828302M, EN0108828307M, EN0131766380M, EN0131766396M, EN0131766401M, EN0131766417M, and EN0131766422M. White boxes outline areas shown in (C) and (D). (**B**) Impact crater SFD for the Rembrandt basin rim compared with that for the Caloris rim. This plot is an R plot (see SOM), a version of the differential crater SFD (*12*). Errors shown are inversely proportional to the square root of the number of craters in each crater-diameter interval. (**C**) Blocky terrain on the basin rim interpreted to be ejecta deposits. Image taken from NAC frame EN0131766417M. (**D**) Hummocky terrain in the basin interior made up of isolated knobs, interpreted to be ejecta deposits modified by basin collapse. Image taken from NAC frame EN0131766417M.

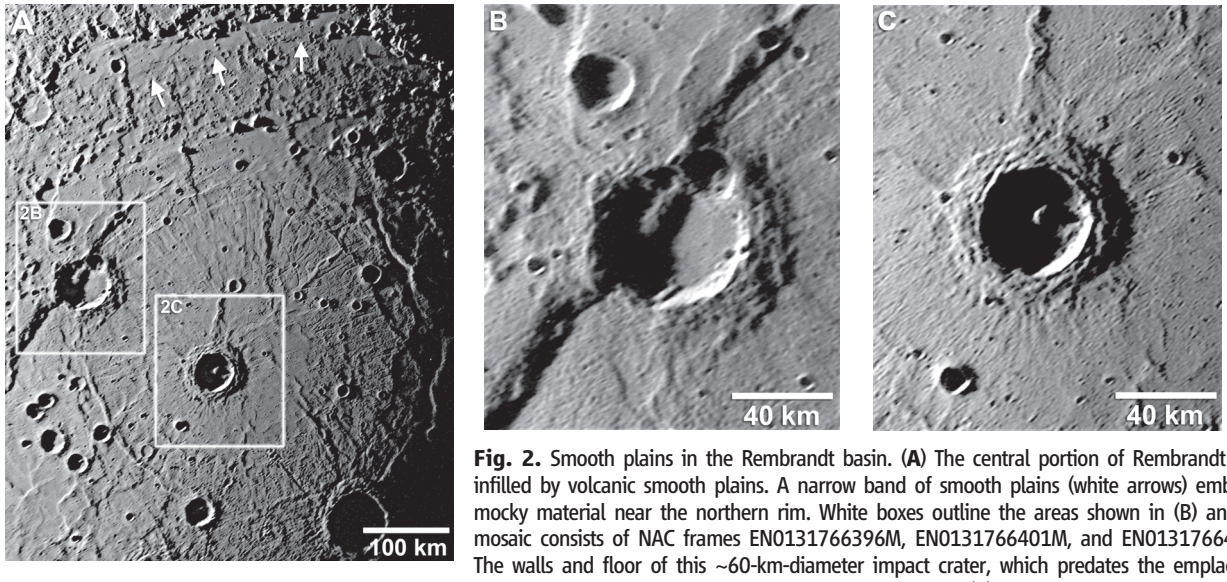

Fig. 2. Smooth plains in the Rembrandt basin. (**A**) The central portion of Rembrandt has been infilled by volcanic smooth plains. A narrow band of smooth plains (white arrows) embays hummocky material near the northern rim. White boxes outline the areas shown in (B) and (C). The mosaic consists of NAC frames EN0131766396M, EN0131766401M, and EN0131766417M. (**B**) The walls and floor of this ~60-km-diameter impact crater, which predates the emplacement of some of the volcanic plains, are cross-cut and offset by a lobate scarp. Image taken from NAC frame EN0131766396M. (**C**) This ~44-km-diameter impact crater postdates the emplacement of the smooth plains. Image taken from NAC frame EN0131766401M.

characteristics of the interior plains, the embayment relations between interior plains material and the interior hummocky deposits, and the embayed and partially flooded impact craters, all similar to relations seen in the Caloris basin interior (*7*–*9*), support a volcanic origin for the smooth plains material in the Rembrandt basin.

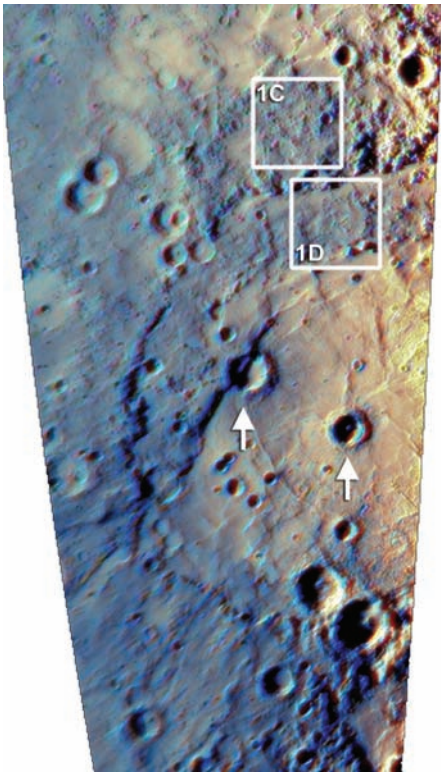

Fig. 3. Color composite of the spectral parameters used to separate units on the basis of principal component analysis of WAC 11-color images (*10*, *15*). The first principal component (PC1) emphasizes variations in reflectance, and the second principal component (PC2) emphasizes spectral variations related to the physical state or chemistry of the material. The dominant variation represented by PC2 is the slope of the spectral continuum. A color composite in which PC2, PC1, and the 430-nm/1000-nm reflectance ratio are shown in the red, green, and blue image planes, respectively, is overlaid on the NAC mosaic. White boxes show the locations of exterior ejecta (Fig. 1C, upper box) and interior ejecta and collapse deposits (Fig. 1D, lower box). White arrows indicate the locations of impact craters shown in Fig. 2B (left arrow) and Fig. 2C (right arrow). The spectral character of the interior plains (relatively high reflectance) differs from that of the ejecta and hummocky deposits (relatively low reflectance). The extreme incidence (>78°) and phase (>130°) angles for WAC images of the Rembrandt area (where the incidence angle is the angle between the direction to the Sun and the surface normal, and the phase angle is the angle between the solar incidence direction and the camera boresight direction at the planet's surface) complicate comparisons with color units elsewhere on the planet. Image taken from MDIS WAC approach color sequence (EW0131764500C to EW0131764550A).

The thickness of volcanic fill in the Rembrandt basin varies greatly. Along the northern interior, the hummocky deposit is embayed but not completely buried (Fig. 1C), suggesting a relatively thin sequence of volcanic plains in this area. Near the basin center, a ~44-km-diameter crater superposed on the smooth plains (Fig. 2, A and C, and Fig. 3) exhibits predominantly plains-like spectral material in its rim and ejecta, indicating that the underlying crust and basin material were not excavated and exposed (Figs. 2C and 3). Given a depth of excavation for complex craters of ~5% of the crater diameter, a lower bound on the thickness of the volcanic plains is ~2 km near the center of the basin, a thickness similar to that interpreted in the center of Caloris (*8*) and some lunar basins (*16*). The Rembrandt basin thus represents a stage of filling by presumably volcanic plains that is intermediate between those of the largely unfilled lunar Orientale basin, where mare basalts are patchy and considerably less than 1 km thick (*2*), and the Caloris and lunar Imbrium basins, where basin-interior ring structures and impact melt deposits are almost completely buried by volcanic infill (*1*, *3*, *7*–*10*).

The tectonic features in the Rembrandt basin show evidence for both basin-localized and global-scale deformation. Extensional troughs and wrinkle ridges are confined to the spectrally distinct, volcanic plains. Wrinkle ridges with orientations that are both basin-radial and basin-concentric are common (Figs. 2A and 4A) and are interpreted to be contractional features resulting from a combination of folding and thrust faulting (*17*–*19*). Basin-concentric wrinkle ridges form an almost complete ~375-km-diameter ring in the interior. This second ringlike structure is ~50 to 60 km inside the hummocky unit and massifs (Fig. 2A). Basin-radial wrinkle ridges occur both interior and exterior to this ring, although most of them are inside (Fig. 4, B and C). Their widths vary greatly (<1 to 10 km), and the longest ridges (one over 180 km) (Fig. 4C) form the interior ring. Basin-concentric and basin-radial wrinkle ridges are also found in Caloris (*7*, *8*) and in lunar maria (e.g., Imbrium, Serenitatis, Crisium) (*16*–*18*). In lunar maria, however, basin-concentric wrinkle ridges generally occur in the basin interior and basin-radial wrinkle ridges near the margins (*16*, *20*). In contrast, in the Rembrandt basin, many basin-radial wrinkle ridges occur interior to the concentric wrinkle ridges. The distinctive ring of ridges in the basin may reflect deformation localized by a buried interior basin ring, as is interpreted to be the case on the Moon (*17*).

The interior plains are cut by a series of linear and curvilinear troughs that also form a basin-radial and basin-concentric pattern (Figs. 2A and 4A). Of these, the basin-radial troughs are the most abundant and are located largely interior to the ring of wrinkle ridges (Fig. 2A and Fig. 4, B and C). Some of the radial troughs are adjacent and parallel to basin-radial ridges (Fig. 4, B and C). Unlike the radial troughs of Pantheon Fossae in Caloris that extend outward from a zone near the center of the basin (*7*, *8*), the radial graben of the Rembrandt basin are confined to a zone that extends inward less than ~100 km from the interior ridge ring. Some radial and concentric troughs in the basin form a polygonal pattern near the outer margin of the interior ridge ring (Fig. 4B), similar to the polygonal pattern formed by troughs near the margin of the Caloris basin (*7*, *8*). From the similarity of individual landforms as well as this similarity in distribution, we interpret the troughs in the Rembrandt basin to be graben, extensional features consisting of opposite-facing normal faults. Trough widths vary (<1 to ~3 km) but by a smaller range than in Caloris. The spatial distribution of these graben differs substantially from that in lunar basins, where graben tend to occur near the outer margins of the mare deposits or in adjacent highlands (*3*, *16*, *20*). The basin-radial graben and wrinkle ridges form a unique wheel-spoke pattern of tectonic landforms.

Episodes of contractional and extensional deformation in the basin are suggested by cross-cutting relations among the tectonic features. Radial and concentric graben cross-cut both basin-concentric and basin-radial wrinkle ridges (Fig. 4, B to D), indicating that much of the contractional deformation of the smooth plains preceded extensional deformation. This sequence of tectonic events is similar to that observed in Caloris (*7*, *8*). However, evidence that some concentric and radial wrinkle ridges cross-cut graben and older ridges indicates that the contraction and extension were not separated temporally into distinct deformational episodes (Fig. 4, B and D). Later contraction, for instance, may have been in response to a later stage of infilling by volcanic material in the center of the basin, as suggested by embayment relations between the more heavily deformed smooth plains inward of the ring of wrinkle ridges and the less deformed smooth plains (those lacking radial graben) near the basin center (Fig. 4B).

In parallel with scenarios invoked for the Caloris basin (*6*–*10*), effusive volcanism at some time after basin formation is inferred to have resulted in a thick sequence of volcanic material in the basin center. Loading by volcanic infill induced subsidence and near-surface compressional stresses that formed wrinkle ridges radial and concentric to the basin center in the interior smooth plains. Models of stresses in lunar mascon basins, however, predict a basin-radial pattern of wrinkle ridges far from the basin center (*21*). The formation of radial and concentric graben in the interior of the Rembrandt basin points to uplift of the basin floor and extension that postdated or perhaps overlapped interior loading. After uplift and extension of the basin floor, a later episode of volcanic infilling suggested by embayment relations in the basin center (Fig. 4B) could have resulted in renewed subsidence and contraction of the interior plains. One possible mechanism for basin floor uplift is inward flow of the lower crust driven by hori-

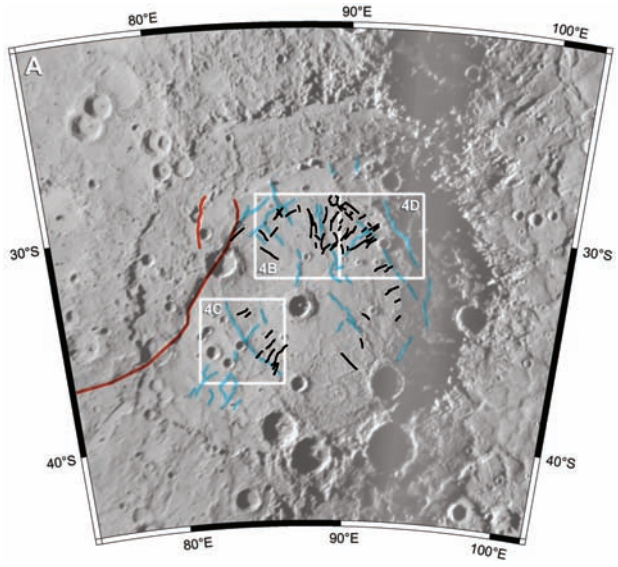

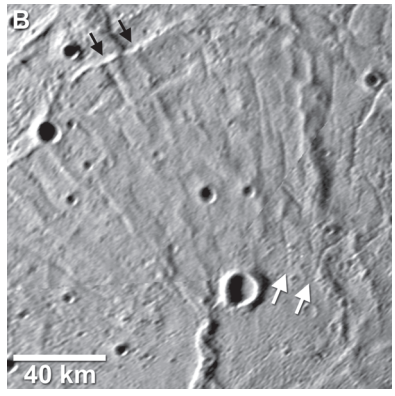

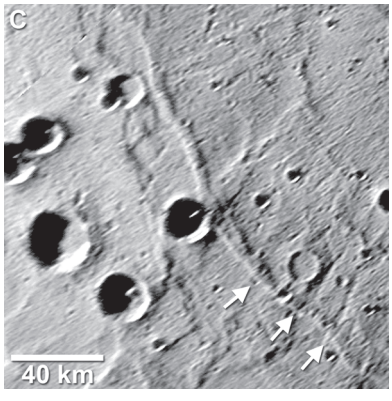

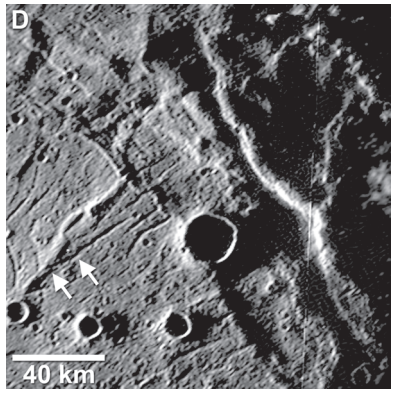

Fig. 4. (**A**) Map of tectonic features in the basin, including wrinkle ridges (blue), troughs or graben (black), and lobate scarps (red) digitized from and overlaid on a NAC mosaic. (**B**) In this complex pattern of wrinkle ridges and extensional troughs, some concentric wrinkle ridges are superposed on radial wrinkle ridges and graben (black arrows). Smooth plains material near the basin center appears to embay and partially bury plains cut by graben (white arrows). NAC mosaic includes frames EN0131766396M and EN0131766401M. (**C**) A basin-concentric wrinkle ridge, part of the interior ring of ridges, appears to be cross-cut by basin-radial graben (white arrows). NAC mosaic includes frames EN0131766401M and EN0131766417M. (**D**) A basin-radial wrinkle ridge appears to cross-cut a basin-radial graben (white arrows). NAC mosaic includes frames EN0131766401M and EN0108828250M.

zontal pressure gradients induced by differences in elevation and crustal thickness (*20*). Alternatively, loading by volcanic plains emplaced exterior to the basin could have led to flexural uplift of the basin interior (*22*, *23*).

Global tectonic evolution also influenced the region. The most recent event in the deformation of the basin appears to have been the formation of a cross-cutting lobate scarp, the longest yet documented on Mercury (Figs. 1A, 2B, and 4A). This lobate scarp, representative of a common tectonic landform interpreted as the surface expression of a major thrust fault (*4*), cuts the rim of the basin and extends nearly 400 km across the basin floor, offsetting the smooth plains material and the rims and floors of two ~60-km-diameter impact craters. The orientation of this northeast-southwest segment of the lobate scarp is approximately tangential to the interior ring of wrinkle ridges, suggesting that the buried interior ring surmised to underlie the ridge ring may also have influenced the thrust fault. The scarp extends for almost 600 km beyond the rim of the basin, cutting intercrater plains and transecting two other large impact craters. A second, shorter lobate scarp lies west of the northernmost segment of the large scarp and deforms interior smooth plains and hummocky material (Fig. 4A). Stresses produced by the global contraction that accompanied cooling of the planetary interior led to the formation of the lobate scarps that cut the rim and interior units of the basin and contributed to a stress regime less favorable to extrusive volcanism (*6*).

References and Notes

1. P. D. Spudis, *The Geology of Multi-Ring Impact Basins: The Moon and Other Planets* (Cambridge Univ. Press, New York, 1993).
2. J. W. Head, *Moon* **11**, 327 (1974).
3. D. E. Wilhelms, *U.S. Geol. Surv. Prof. Pap.* **1348**, 302 (1987).
4. R. G. Strom, N. J. Trask, J. E. Guest, *J. Geophys. Res.* **80**, 2478 (1975).
5. P. D. Spudis, J. E. Guest, in *Mercury*, F. Vilas, C. R. Chapman, M. S. Matthews, Eds. (Univ. of Arizona Press, Tucson, AZ, 1988), pp. 118–164.
6. S. C. Solomon *et al.*, *Science* **321**, 59 (2008).
7. S. L. Murchie *et al.*, *Science* **321**, 73 (2008).
8. T. R. Watters *et al.*, *Earth Planet. Sci. Lett.*; 10.1016/j.epsl.2009.01.025 (2009).
9. J. W. Head *et al.*, *Science* **321**, 69 (2008).
10. M. S. Robinson *et al.*, *Science* **321**, 66 (2008).
11. C. I. Fassett *et al.*, *Lunar Planet. Sci.* **40**, abstr. 1899 (2009)
12. R. G. Strom, C. R. Chapman, W. J. Merline, S. C. Solomon, J. W. Head, *Science* **321**, 79 (2008).
13. M. Cintala, R. A. F. Grieve, *Meteorit. Planet. Sci.* **33**, 889 (1998).
14. J. W. Head *et al.*, *J. Geophys. Res.* **98**, 17149 (1993).
15. B. W. Denevi *et al.*, *Science* **324**, 613 (2009).
16. S. C. Solomon, J. W. Head, *Rev. Geophys. Space Phys.* **18**, 107 (1980).
17. T. R. Watters, *J. Geophys. Res.* **93**, 10236 (1988).
18. M. P. Golombek, J. B. Plescia, B. J. Franklin, *Proc. Lunar Planet. Sci. Conf.* **21**, 679 (1991).
19. R. A. Schultz, *J. Geophys. Res.* **105**, 12035 (2000).
20. T. R. Watters, F. Nimmo, M. S. Robinson, *Geology* **33**, 669 (2005).
21. A. M. Freed, H. J. Melosh, S. C. Solomon, *J. Geophys. Res.* **106**, 20603 (2001).
22. H. J. Melosh, W. B. McKinnon, in *Mercury*, F. Vilas, C. R. Chapman, M. S. Matthews, Eds. (Univ. of Arizona Press, Tucson, AZ, 1988), pp. 374–400.
23. P. J. Kennedy, A. M. Freed, S. C. Solomon, *J. Geophys. Res.* **113**, E08004 (2008); 10.1029/2007JE002992.
24. A Mercury Dual Imaging System (MDIS) narrow-angle camera (NAC) mosaic at ~420 to 500 m per pixel and an 11-color WAC frame at ~5 km per pixel, obtained during the second MESSENGER flyby, revealed ~80% of the Rembrandt basin. The easternmost portion of the basin was imaged by MESSENGER during the first flyby at a comparable resolution.

25. We are grateful to the MESSENGER engineers and technical support personnel. The MESSENGER project is supported by the NASA Discovery Program under contracts NASW-00002 to the Carnegie Institution of Washington and NAS5-97271 to Johns Hopkins University Applied Physics Laboratory. This work is also supported by NASA grant NNX07AR60G.

Supporting Online Material

www.sciencemag.org/cgi/content/full/324/5927/618/DC1
SOM Text
Figs. S1 to S3
References

10 February 2009; accepted 9 April 2009
10.1126/science.1172109

High-Frequency Holocene Glacier Fluctuations in New Zealand Differ from the Northern Signature

Joerg M. Schaefer,[1]* George H. Denton,[2] Michael Kaplan,[1] Aaron Putnam,[2] Robert C. Finkel,[3,4] David J. A. Barrell,[5] Bjorn G. Andersen,[6] Roseanne Schwartz,[1] Andrew Mackintosh,[7] Trevor Chinn,[8] Christian Schlüchter[9]

Understanding the timings of interhemispheric climate changes during the Holocene, along with their causes, remains a major problem of climate science. Here, we present a high-resolution ^{10}Be chronology of glacier fluctuations in New Zealand's Southern Alps over the past 7000 years, including at least five events during the last millennium. The extents of glacier advances decreased from the middle to the late Holocene, in contrast with the Northern Hemisphere pattern. Several glacier advances occurred in New Zealand during classic northern warm periods. These findings point to the importance of regional driving and/or amplifying mechanisms. We suggest that atmospheric circulation changes in the southwest Pacific were one important factor in forcing high-frequency Holocene glacier fluctuations in New Zealand.

Natural climate variability during the interglacial conditions of the Holocene (the past 11,500 years) is a fundamental baseline for evaluating the anthropogenic impact on global climate. Recent studies using marine and terrestrial samples from the North Atlantic region and the tropics (*1*, *2*) challenge the traditional view of a stable Holocene climate. Northern Hemisphere paleoclimate records suggest that temperatures cooled through the Holocene [e.g., (*3*)] and that this long-term trend was overprinted by millennial-scale variations (*4*), culminating in the Medieval Warm Period (MWP)/Little Ice Age (LIA) oscillation (*5*, *6*). Terrestrial paleoclimate data are sparse in the Southern Hemisphere, and it remains unclear whether the northern trend of progressive cooling was followed in the south [e.g., (*7*) versus (*6*)] and whether northern millennial-scale climate changes, including the MWP/LIA oscillation, were globally extensive. We explored this problem via the question: Were Holocene glacier advances in New Zealand generally coeval with those in the Northern Hemisphere? We present a high-resolution surface-exposure chronology of Holocene climate fluctuations derived from moraines deposited at the culmination of glacier advances in New Zealand's Southern Alps and evaluate the pattern of southern versus northern glacier behavior as a means of insight into Holocene climate forcing.

Glaciers are highly sensitive to variations in temperature and precipitation (*8*) [supporting online material (SOM text)], but difficulties in obtaining reliable ages have been an impediment to placing glacier records in a global context. We focused on the large Mueller, Hooker, and Tasman valley glaciers (Fig. 1 and table S1) that drain east and south from the Main Divide of the Southern Alps. Their terminal zones are fringed by well-preserved Holocene moraine complexes (Figs. 1 and 2). Large greywacke boulders protruding from the moraines were the targets of our surface-exposure dating program (*9*).

Previous chronological studies of these moraines {including tree rings, radiocarbon bracketing ages [e.g., (*10*–*12*)], lichenometry [e.g., (*13*, *14*)], rock-weathering rinds (*15*, *16*), and Schmidt hammer investigations [e.g., (*6*, *17*)]} suggested that the most recent cool interval in New Zealand was equivalent to the termination of the northern LIA (mid-19th century). However, recent tree ring studies argued for a glacier maximum in the south that is somewhat older than the northern LIA termination (*18*, *19*).

Our geomorphologic maps (Fig. 1) document the detail and complexity of the preserved Holocene moraine sequences. We sampled a total of 74 boulders, with one duplicate (Figs. 1 and 2 and table S2), for ^{10}Be surface-exposure dating. We focused on the Mueller Glacier Holocene moraines comprising the most complete succession of preserved ridges, with complementary samples from the moraine sequences of Hooker and Tasman glaciers. We interpret the moraine exposure ages as dating the completion of moraine formation and thus the termination of a glacier event (SOM text). Individual boulder exposure ages within 2σ analytical uncertainties are plotted in fig. S1. Moraine ages are defined by arithmetic means of all boulder ages from the respective moraine within analytical standard deviation. The ages are calculated by using the recent production rates given in (*20*); given errors include a 5% production rate estimate. The variances between different published production rates do not affect any of the conclusions drawn below (table S3) (*9*).

The ^{10}Be chronology (Figs. 1 and 2, fig. S1, and table S3) includes some of the youngest exposure ages reported so far. The ^{10}Be measurements show low uncertainties, and the ^{10}Be boulder ages from individual moraines are remarkably consistent (*9*). All ages are compatible with position in the moraine sequence except for two boulders from the outermost margin of the right lateral Hooker moraines [–930 and –931 (Fig. 1)], which are incompatibly young. Lying at the downslope margin of an alluvial fan, it is plausible that they fell from the nearby mountainside onto the moraine subsequent to its formation. Ages of Kiwi-904 and -X60 plot outside the 95% confidence level (fig. S1). Otherwise, the data set is free of outliers. Hence, we include 70 out of 74 boulders (and 71 of the 75 ^{10}Be measurements) in the discussion (*9*).

The innermost moraine of the Mueller sequence (Figs. 1 and 2) represents a historically documented glacier position from the mid- to late 1800s (*9*, *12*). Three boulders from this ridge yielded ^{10}Be ages of 132 ± 17 years, 164 ± 22 years, and 185 ± 22 years (mean: 160 ± 30 years). The general correspondence between the ^{10}Be dating and the historic age of the moraine provides confidence in the ^{10}Be method and implies a maximum preexposure signal, the concentration of ^{10}Be atoms produced in the sampled boulder surface before boulder deposition on the moraine, of less than 100 years [difference between older bound of the oldest age, 210 years, and the historic age (SOM text)]. An outboard set of at least three moraines, the innermost of which is thought to be historic (*10*–*12*), yielded ages of 220 ± 10 years (n = 2), 270 ± 50 years (n = 10), and 400 ± 70 years (n = 9). A little outside lies a complex of ridges dominating the last-millennium moraine sequence of Mueller Glacier, 570 ± 70 years (n = 12) in age. The outermost left lateral Holocene ridge gave an age of 2000 ± 150 years (n = 2), consistent with the 2100 ± 100 year age of Kiwi-X66 from the right lateral sequence. Seven boulders from at least two distinct moraines slightly inboard yielded ages ranging from 1720 years to 1990 years, with a mean of 1840 ± 130 years. The outermost well-preserved right lateral moraine yielded a mean age of 3230 ± 220 years (n = 4), and, lastly, an isolated mound of moraine (Foliage Hill; Fig. 1) represents the outermost preserved remnant dated to 6370 ± 760 years (n = 1).

At Hooker Glacier (Fig. 1), two prominent left lateral ridges yielded ages of 1020 ± 70 years (n = 5) for the inner and 1370 ± 180 years (n = 6) for the outer ridge. One boulder from an

[1]Geochemistry, Lamont-Doherty Earth Observatory (LDEO), Palisades, NY 10964, USA. [2]Department of Earth Sciences and Climate Change Institute, University of Maine, Orono, ME 04469, USA. [3]Department of Earth and Planetary Sciences, University of California, Berkeley, Berkeley, CA 95064, USA. [4]CEREGE (Centre Européen de Recherche et d'Enseignement des Géosciences de l'Environnement), 13545 Aix-en-Provence, Cedex 4, France. [5]GNS Science, Dunedin 9054, New Zealand. [6]Department of Geology, University of Oslo, 0316 Oslo, Norway. [7]Victoria University of Wellington, Wellington 6140, New Zealand. [8]Alpine and Polar Processes Consultancy, Lake Hawea, Otago 9382, New Zealand. [9]Institut für Geologie, Universität Bern, CH-3012 Bern, Switzerland.

*To whom correspondence should be addressed. E-mail: schaefer@ldeo.columbia.edu

isolated ridge inside gave an age of 810 ± 70 years (–927).

At Tasman Glacier, an inner moraine ridge yielded an age of 1040 ± 100 years (n = 1), coinciding with the 1020-year moraine of Hooker Glacier, whereas an outer ridge gave 1650 ± 110 years (n = 3). An isolated remnant of moraine projecting a few meters from the outwash plain (Little Hump) has an age of 6550 ± 370 years (n = 5). Its overlap with the oldest Mueller Glacier moraine (6370 years) suggests that both represent coeval glacier positions, distal to the late Holocene moraines.

This precise, high-frequency ^{10}Be chronology of Holocene fluctuations of the Mueller, Hooker, and Tasman glaciers compares well with a radiocarbon (^{14}C) chronology from wood within soils buried by tills in the lateral moraines (*11*). The ^{14}C ages date glacier expansion events after periods of reduced ice and distal soil formation (table S4). Together, the ^{10}Be and ^{14}C data define a minimum number of 15 pulses of glacier advance and retreat since the mid-Holocene, with the timing of the advance (^{14}C) and/or termination (^{10}Be) of events at about 6500 years ago (termination, ^{10}Be), 3650 to 3200 years [advance commencing 3650

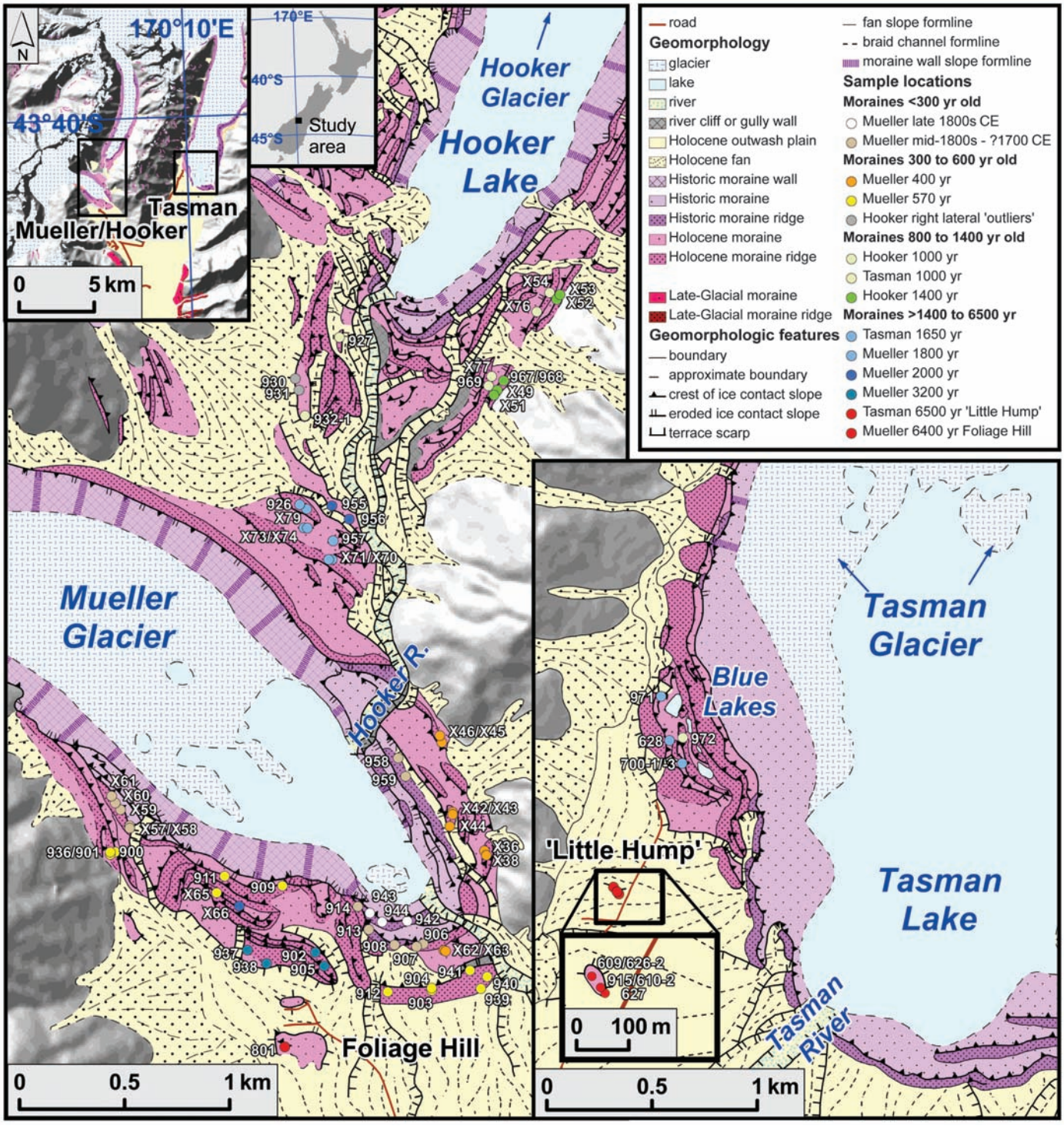

Fig. 1. Glacial geomorphology map, compiled at 1:5000 scale, of the Holocene moraine sequences of Mueller, Hooker, and Tasman glaciers, showing locations of sample sites. The map differentiates between discrete moraine ridges and areas of more diffuse moraine morphology.

years ago (^{14}C), progressive ice buildup for 400 years (^{14}C), terminating around 3200 years ago (^{10}Be)], 2300 years (^{14}C), 2000 to 1650 years (at least three events; ^{10}Be and ^{14}C), 1400 years (^{10}Be), 1000 years (^{10}Be and ^{14}C), 850 (^{14}C) to 800 years (^{10}Be, sample –927), 650 (^{14}C) to 570 years (^{10}Be), 400 years (at least two events; ^{10}Be and ^{14}C), and 270 years to ~110 years (historic and ^{10}Be).

Episodic fluctuations of the large valley glaciers at Mount Cook since mid-Holocene time have resulted in ice front advances to, and returning from, positions only short distances outside the mid- to late 19th century glacier termini, with a decrease in amplitude during the last millennium. The summer temperature time series based on tree-ring data from the nearby Oroko Swamp (*21*) (Fig. 3) shows similarly the coldest period during the past 1100 years around 1000 common era (C.E.), followed by abrupt climate fluctuations superimposed on a trend to slightly warmer temperatures. Collectively, these data point to a coherent record of summer temperature changes and concomitant glacier fluctuations in the Southern Alps during the late Holocene.

To evaluate the wider implications of our results, we compared the Holocene moraine record from Mount Cook over the past 4000 years with Northern Hemisphere records (Fig. 3). Three main conclusions can be drawn. First, there is a notable interhemispheric disparity in the timing of the maximum ice extent. The Mount Cook glaciers were further advanced about 6500 years ago than at any subsequent time. In contrast, most Northern Hemisphere glaciers reached their greatest Holocene extents during the LIA (1300 to 1860 C.E.).

Second, several glacier advances beyond the extent of the 19th century termini occurred in New Zealand during northern warm periods characterized by diminished or even smaller-than-today northern glaciers, such as between 7500 and 5500 years ago in the Swiss Alps (*22*) and Scandinavia (*23*), during the Bronze Age Optimum [about 1500 to 900 before the common era (B.C.E.)], during the Roman Age Optimum (200 B.C.E. to 300 C.E.), and during the MWP (800 C.E. to 1300 C.E.).

Third, the greatest coherency between the Mount Cook and Northern Hemisphere records was during the Dark Ages (300 C.E. to 700 C.E.), and broad similarities were apparent during the past 700 years (the northern LIA), with multiple glacier advances followed by a general termination commencing in the mid- to late 19th century. However, northern Holocene moraine sequences are dominated by the LIA-maximum terminal moraine less than 400 years old (typically mid-19th century in the Swiss Alps and mid-18th century in Scandinavia), whereas the most prominent moraine of the past millennium at Mueller Glacier is about 570 years old and is followed inboard by several smaller moraines. This pattern of broad consistency but differing detail of glacier behavior has continued over the past 150 years (SOM text).

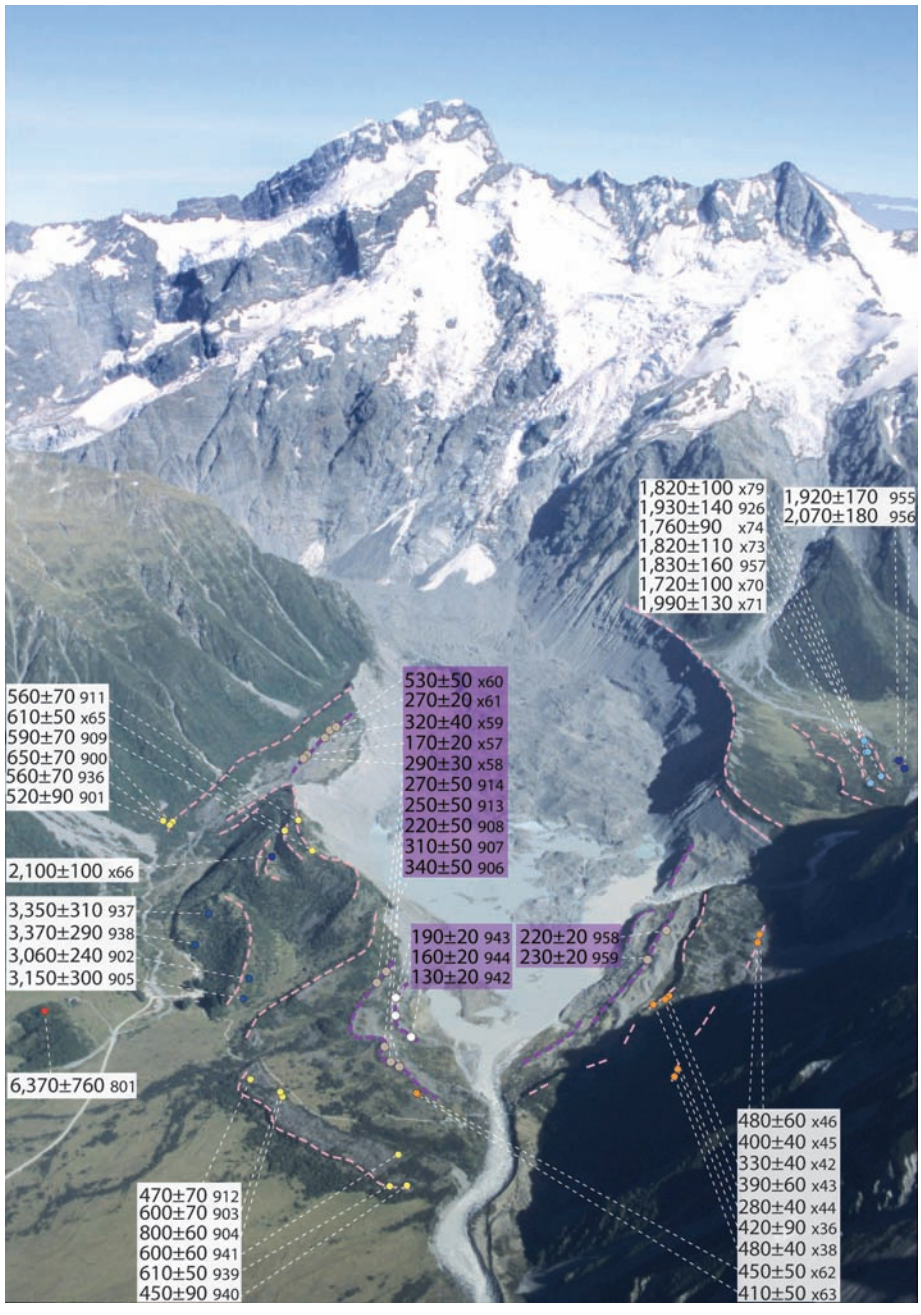

Fig. 2. Oblique view of the Holocene moraines of Mueller Glacier together with the ^{10}Be chronology. The ^{10}Be ages are given in years together with analytical uncertainties (2σ) and sample number (fig. S1 and tables S2 and S3). The innermost moraine ridge (dark purple) was deposited during the mid- to late 19th century (*12*).

Decreasing extent of New Zealand Holocene glaciers conflicts with nearby mean-annual sea surface temperature proxies [e.g., (*24*)] that show progressive cooling. However, melt-layer records in West Antarctic ice (*25*) that indicate increasing Holocene summer maximum temperatures are more commensurate with New Zealand glacier behavior.

Our results are in accord neither with the hypothesis of interhemispheric synchrony of mid- to late Holocene climate change nor with a rhythmic asynchrony, downplaying the importance of global driving mechanisms. This includes solar irradiation changes translating quasi-linearly into near-surface climate. However, recent studies show that climate models driven by solar changes can induce regionally distinct temperature changes (*26*), and indeed the Mount Cook moraine chronology shows some similarities to the solar record [e.g., (*26*)]. Alternatively, variations in the strength of deep-water production between the north and the south have been proposed (*27*) to explain interhemispheric incoherencies in Holocene climate. But this mechanism predicts strictly antiphased glacier behavior in north and south and it is not

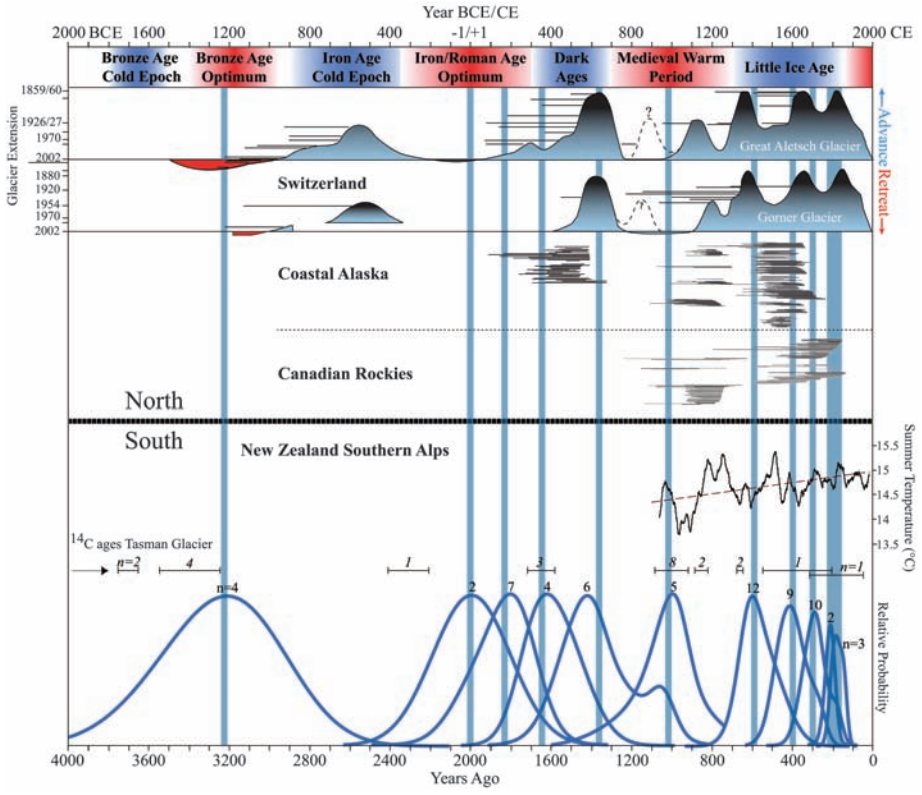

Fig. 3. The timing of Holocene glacier fluctuations near Mount Cook in New Zealand's Southern Alps (**bottom**), together with published ^{14}C ages on soils buried by Mount Cook glacier expansion events (*11*) over the past 4000 years, and a tree ring reconstruction of austral summer temperature in New Zealand over the past 1100 years (*21*), compared with glacier fluctuations in the Northern Hemisphere (**top**). The probability plots at the bottom are summary curves of all individual ^{10}Be boulder ages from each moraine dated in New Zealand. The blue bars show the arithmetic means of the moraine age (fig. S1 and table S3). The ^{10}Be ages are from Mueller Glacier moraines, except for the 1650-year moraine (Tasman Glacier) and 1370- and 1020-year moraines (Hooker Glacier). Note that we have identified a moraine corresponding to each ^{14}C soil age except for the 2300-year soil. The top graph shows fluctuations of two index glaciers in the Swiss Alps, the Great Aletsch Glacier and the Gorner Glacier, reconstructed from historical accounts and tree ring and radiocarbon data from fossil wood by (*30*). The middle graph shows the glacier advances in coastal Alaska (*31*) and the Canadian Rockies (*32*). These northern records feature high-precision glacier chronologies derived primarily from dendrochronology. Each bar shows the length of a tree ring record. The right end of each bar represents a glacier kill date.

obvious how such large-scale ocean variations may account for contemporary regional contrasts, as exhibited by the general advance of glaciers in New Zealand and southernmost South America in unison with the retreat of glaciers on the Antarctic Peninsula and northern Patagonia (*28*). Alternatively, we suggest that regional ocean-atmosphere oscillations may account for the observed glacier fluctuation pattern. Analogous to the correlation between the Atlantic Multidecadal Oscillation and glaciers in the Swiss Alps (*27*), the Interdecadal Pacific Oscillation (IPO) (SOM text) has been an important influence on glacier behavior in New Zealand over the past few decades (*29*): The IPO switched to a negative mode about 1940 C.E., bringing warmer and drier conditions to New Zealand's Southern Alps before reverting to a positive, colder, and wetter mode in 1978 C.E. These changes are well reflected in New Zealand's glacier length fluctuations. Whether or not this mechanism is generally applicable to the Holocene period, our study shows that mid- to late Holocene glacier fluctuations were neither in phase nor strictly antiphased between the hemispheres, and therefore it is likely that regional driving or amplifying mechanisms have been an important influence on climate. The ability to obtain high-precision ages for Holocene moraines, including historic times, opens the way for defining much-improved chronologies of glacier fluctuations at key sites in north and south and may help finally to solve the puzzle of what drove Holocene climate variations.

References and Notes

1. G. H. Haug *et al.*, *Science* **299**, 1731 (2003).
2. M. Stuiver, P. M. Grootes, *Quat. Res.* **53**, 277 (2000).
3. K. M. Cuffey, G. D. Clow, *J. Geophys. Res.* **102**, 26383 (1997).
4. G. Bond *et al.*, *Science* **294**, 2130 (2001); published online 15 November 2001 (10.1126/science.1065680).
5. W. S. Broecker, *Science* **291**, 1497 (2001).
6. J. M. Grove, *The Little Ice Ages* (Routledge, New York, 2004).
7. M. E. Mann, R. S. Bradley, M. K. Hughes, *Nature* **392**, 779 (1998).
8. J. Oerlemans, *Science* **308**, 675 (2005); published online 3 March 2005 (10.1126/science.1107046).
9. Materials and methods are available as supporting material on *Science* Online.
10. C. J. Burrows, *N. Z. J. Geol. Geophys.* **16**, 831 (1973).
11. C. J. Burrows, *N. Z. J. Geol. Geophys.* **39**, 205 (1989).
12. C. J. Burrows, *Julius Haast in the Southern Alps* (Canterbury Univ. Press, Christchurch, New Zealand, 2005).
13. D. B. Lawrence, E. G. Lawrence, *Mazama* **47**, 17 (1965).
14. P. Wardle, *N. Z. J. Bot.* **11**, 349 (1973).
15. T. J. Chinn, *Arct. Alp. Res.* **13**, 33 (1981).
16. A. F. Gellatly, *Arct. Alp. Res.* **16**, 225 (1984).
17. S. Winkler, *Holocene* **14**, 911 (2004).
18. C. J. Burrows, *Processes of Vegetation Changes* (Unwin, Hyman, London, 1990).
19. K. M. McKinzey, W. Lawson, D. Kelly, A. Hubbard, *J. R. Soc. N. Z.* **34**, 381 (2004).
20. G. Balco, J. P. Briner, J. Rayburn, J. C. Ridge, J. M. Schaefer, *Quat. Geochronology* **4**, 93 (2009).
21. E. R. Cook, J. G. Palmer, R. D. D'Arrigo, *Geophys. Res. Lett.* **29**, 1667 (2002).
22. U. E. Joerin, K. Nicolussi, A. Fischer, T. F. Stocker, C. Schlüchter, *Quat. Sci. Rev.* **27**, 337 (2008).
23. S. O. Dahl, A. Nesje, *Holocene* **6**, 381 (1996).
24. T. T. Barrows, S. J. Lehman, L. K. Fifield, P. De Dekker, *Science* **318**, 86 (2007).
25. S. B. Das, R. B. Alley, *J. Geophys. Res.* **113**, D02112 (2008).
26. E. Bard, G. M. Raisbeck, F. Yiou, J. Jouzel, *Tellus* **52B**, 985 (2000).
27. G. H. Denton, W. S. Broecker, *Quat. Sci. Rev.* **27**, 1939 (2008).
28. World Glacier Monitoring Services, *Global Glacier Changes: Facts and Figures* (United Nations Environmental Programme, Geneva, 2007), www.grid.unep.ch/glaciers/.
29. B. B. Fitzharris, T. J. Chinn, G. N. Lamont, *Int. J. Climatol.* **17**, 745 (1997).
30. H. Holzhauser, M. Magny, H. J. Zumbuhl, *Holocene* **15**, 789 (2005).
31. G. C. Wiles, D. J. Barclay, P. E. Calkin, T. V. Lowell, *Global Planet. Change* **60**, 115 (2008).
32. B. H. Luckman, *Geomorphology* **32**, 357 (2000).

33. J.M.S. acknowledges NSF support of this study (grants EAR-0823521 and EAR-0345835). The Comer Science and Educational Foundation supported J.M.S., M.K., and A.P. The New Zealand Foundation for Research, Science, and Technology (contract C05X0701) provided support for the glacial geomorphic mapping and the participation of D.J.A.B. We thank the Department of Conservation (DOC), R. Bellringer of the Mount Cook DOC, and Te Rünanga o Ngäi Tahu for permission to work in Mount Cook National Park. National Oceanic and Atmospheric Administration (NOAA) supported the participation of G.H.D., D.J.A.B., T.C., A.P., and B.G.A. A.M. acknowledges support by Mardsen Fund contract VUW0611. C.S. was supported by the Swiss National Fond, proposal no. 200020-105220/1. We thank the staff of the Center for Accelerator Mass Spectrometry (AMS) at Lawrence Livermore National Laboratory for their tireless support throughout the AMS measurements and S. Travis and A. Doughty for help during field work. This is LDEO contribution number 7243.

Supporting Online Material

www.sciencemag.org/cgi/content/full/324/5927/622/DC1
Materials and Methods
SOM Text
Figs. S1 to S4
Tables S1 to S4
References

3 December 2008; accepted 11 March 2009
10.1126/science.1169312

Biomolecular Characterization and Protein Sequences of the Campanian Hadrosaur *B. canadensis*

Mary H. Schweitzer,[1,2]* Wenxia Zheng,[1] Chris L. Organ,[3] Recep Avci,[4] Zhiyong Suo,[4] Lisa M. Freimark,[5] Valerie S. Lebleu,[6,7] Michael B. Duncan,[6,7] Matthew G. Vander Heiden,[8] John M. Neveu,[9] William S. Lane,[9] John S. Cottrell,[10] John R. Horner,[11] Lewis C. Cantley,[5,12] Raghu Kalluri,[6,7,13] John M. Asara[5,14]*

Molecular preservation in non-avian dinosaurs is controversial. We present multiple lines of evidence that endogenous proteinaceous material is preserved in bone fragments and soft tissues from an 80-million-year-old Campanian hadrosaur, *Brachylophosaurus canadensis* [Museum of the Rockies (MOR) 2598]. Microstructural and immunological data are consistent with preservation of multiple bone matrix and vessel proteins, and phylogenetic analyses of *Brachylophosaurus* collagen sequenced by mass spectrometry robustly support the bird-dinosaur clade, consistent with an endogenous source for these collagen peptides. These data complement earlier results from *Tyrannosaurus rex* (MOR 1125) and confirm that molecular preservation in Cretaceous dinosaurs is not a unique event.

Soft tissues and cell-like structures observed in a variety of vertebrate fossils (*1*, *2*) raise the question of whether, and to what extent, original molecular components remain associated with these structures and the bones containing them. A suite of experiments supported the presence of original collagen molecules in the bony matrix of *Tyrannosaurus rex* [Museum of the Rockies (MOR) 1125] (*3*), and phylogenetic analysis of tryptic fragments sequenced by mass spectrometry (*4*, *5*) placed *T. rex* within Archosauria, closer to birds than other vertebrate taxa in the sampled database (*6*, but see also *7*–*10*).

Deep burial in sandstone seems to favor exceptional preservation (*2*). We recovered a single femur from an articulated hind limb of *Brachylophosaurus canadensis* (MOR 2598). The pes elements, tibia, and fibula were collected in 2006; the femur was untouched and protected under ~7 m of Judith River Fomation sandstones, Eastern Montana, USA, until recovery in 2007. The femur was not exposed in the field but jacketed with ~10 to 12 cm of sediments to maintain equilibrium. Immediately after opening the jacket, bone and sediment samples were collected with sterile instruments, wrapped in layers of foil, and placed in sealed jars with desiccation crystals until laboratory analyses were performed. Bone and/or processed samples were dispersed to multiple institutions for independent analyses. Some bone fragments were subjected to chemical extraction (*3*, *10*), and others were demineralized, showing marked preservation of microstructures resembling soft, transparent vessels, cells, and fibrous matrix in this pristine bone (Fig. 1 and fig. S1) (*10*).

Under field-emission scanning electron microscopy (FESEM) (*10*), demineralized bone matrix was fibrous, with fibers arranged either in distinct layers at ~30° (Fig. 1A) that retain the original plywoodlike orientation of collagen fibers in bone (*11*, *12*) or arranged in parallel (Fig. 1B). Microstructures with filipodial extensions and internal contents, consistent in size and morphology to vertebrate osteocytes (*13*, *14*), were visible at matrix layer boundaries (Fig. 1A, arrows). The matrix was virtually indistinguishable from recent demineralized ostrich bone (Fig. 1C) imaged under the same parameters. In transmitted light, demineralized matrix appeared white and fibrous (Fig. 1D) and autofluoresced when illuminated with a mercury lamp, similar to extant bone collagen (*15*).

Transparent, flexible vessels were observed; some contained spherical microstructures (Fig. 1E), whereas others contained an amorphous red substance (Fig. 1F) that is superficially similar to degraded blood products in vessels recovered from extant bone (Fig. 1G) (*2*). *B. canadensis* vessels were hollow (Fig. 1H), with walls of uniform thickness, and possessed a surface texture that differed from exterior to luminal surfaces, features not consistent with the relatively amorphous texture of biofilm (*7*). Vessel surface texture differed substantially from the fibrous matrix but was similar to that seen in extant ostrich vessels (Fig. 1I) (*1*) after demineralization and collagenase digestion. Osteocytes were closely associated with vessels in both extant and *B. canadensis* samples (Fig. 1, H and I, arrows). The variation in texture, microstructure, and color of dinosaur material is consistent with extant tissues and not plausibly explained by biofilm (*7*).

Ovoid red "cells" with long filipodia, similar in morphology to extant osteocytes, were embedded in or associated with white matrix (Fig. 1J and fig. S1) or vessels (Fig. 1H). In some cases, these were attached by their filipodia to adjacent cells (Fig. 1J, inset), forming an interconnecting network as in extant bone. The cells contain internal microstructures suggestive of nuclei. Red filipodia extend from cell bodies into the white fibrous matrix (Fig. 1J and fig. S1), reflecting original chemical differences at submicron levels between cells and matrix and inconsistent with recent microbial invasion (*7*). Under FESEM (*10*), *B. canadensis* osteocytes and filipodia (Fig. 1K) are similar in morphology, surface texture, and size to extant ostrich osteocytes isolated from bone digests (Fig. 1L) (*1*, *2*, *13*, *14*).

MOR 2598 bone fragments were chemically extracted (*2*, *10*) for use in multiple analyses. Electrophoretic separation revealed a smear of silver-stainable material, not present in either buffer controls or surrounding sediment extracted in tandem with the bone. A dark-staining high–molecular weight band was consistently seen in guanidine extracts, whereas a low–molecular weight smear was visible in trichloroacetic acid extractions (fig. S2) (*10*).

Both chemical extracts and demineralized dinosaur tissues showed binding of antibodies raised against collagen and other extant proteins. Enzyme-linked immunosorbent assays (fig. S3A) and immunoblots (figs. S3B and S9) of bone extracts showed positive reactivity to antibodies raised against avian collagen I and/or osteocalcin; controls of extraction buffers alone or coextracted sediments were nonreactive (figs. S3A and S9). Results were repeated in two separate laboratories (labs of R.K. and L.C.C.) on separate extractions of MOR 2598 bone fragments.

In situ immunohistochemical analyses conducted on demineralized dinosaur extracellular matrix showed positive reactivity to polyclonal antibodies raised against avian collagen I (Fig. 2A), osteocalcin (Fig. 2D), and ostrich whole bone extracts (fig. S4) (*10*), but monoclonal antibodies raised against a specific osteocalcin epitope (fig. S5) showed no binding. This may indicate that the single epitope targeted by the monoclonal antibody was either not preserved or not present originally in *B. canadensis* protein. Negative controls of secondary antibody only (no primary added) showed no binding (fig. S5), and specificity controls of inhibition (blocking antibody binding sites by first incubating with excess collagen, see Fig. 2B) and tissue digestion with collagenase before antibody exposure (Fig. 2C) resulted in the reduction of binding. Antibodies to ostrich whole bone extracts (fig. S4) bound dinosaur tissues slightly stronger than commercial

[1]North Carolina State University, Raleigh, NC 27695, USA. [2]North Carolina Museum of Natural Sciences, Raleigh, NC 27601, USA. [3]Department of Organismic and Evolutionary Biology, Harvard University, Cambridge, MA 02138, USA. [4]Imaging and Chemical Analysis Laboratory, Montana State University, Bozeman, MT 59717, USA. [5]Division of Signal Transduction, Beth Israel Deaconess Medical Center, Boston, MA 02115, USA. [6]Division of Matrix Biology, Beth Israel Deaconess Medical Center, Boston, MA 02115, USA. [7]Department of Medicine, Harvard Medical School, Boston, MA 02115, USA. [8]Dana Farber Cancer Institute, Boston, MA 02115, USA. [9]Faculty of Arts and Sciences Center for Systems Biology, Harvard Univeristy, Cambridge, MA 02138, USA. [10]Matrix Science Ltd., 64 Baker Street, London, W1U 7GB, UK. [11]Museum of the Rockies, Bozeman, MT 59717, USA. [12]Department of Systems Biology, Harvard Medical School, Boston, MA 02115, USA. [13]Department of Biological Chemistry and Molecular Pharmacology and Harvard-MIT Division of Health Sciences and Technology, Harvard University, Cambridge, MA 02139, USA. [14]Department of Pathology, Harvard Medical School, Boston, MA 02115, USA.

*To whom correspondence should be addressed. E-mail: schweitzer@ncsu.edu (M.H.S.); jasara@bidmc.harvard.edu (J.M.A.)

chicken collagen antibodies (Fig. 2A), possibly indicating more shared epitopes between *B. canadensis* and ostrich bone proteins than this dinosaur and chicken. These results support the hypothesis that original epitopes of bone proteins are preserved in these 80-million-year-old dinosaur skeletal elements.

Because elastin, laminin, and hemoglobin are commonly associated with blood vessels in tetrapods, we used antibodies raised against these proteins to test for epitopes preserved in *B. canadensis* vessels. Elastin is a highly conserved, vertebrate-specific molecule generally resistant to degradation (*16*), and antibodies to this protein bound dinosaur vessels above background levels in all cases, both

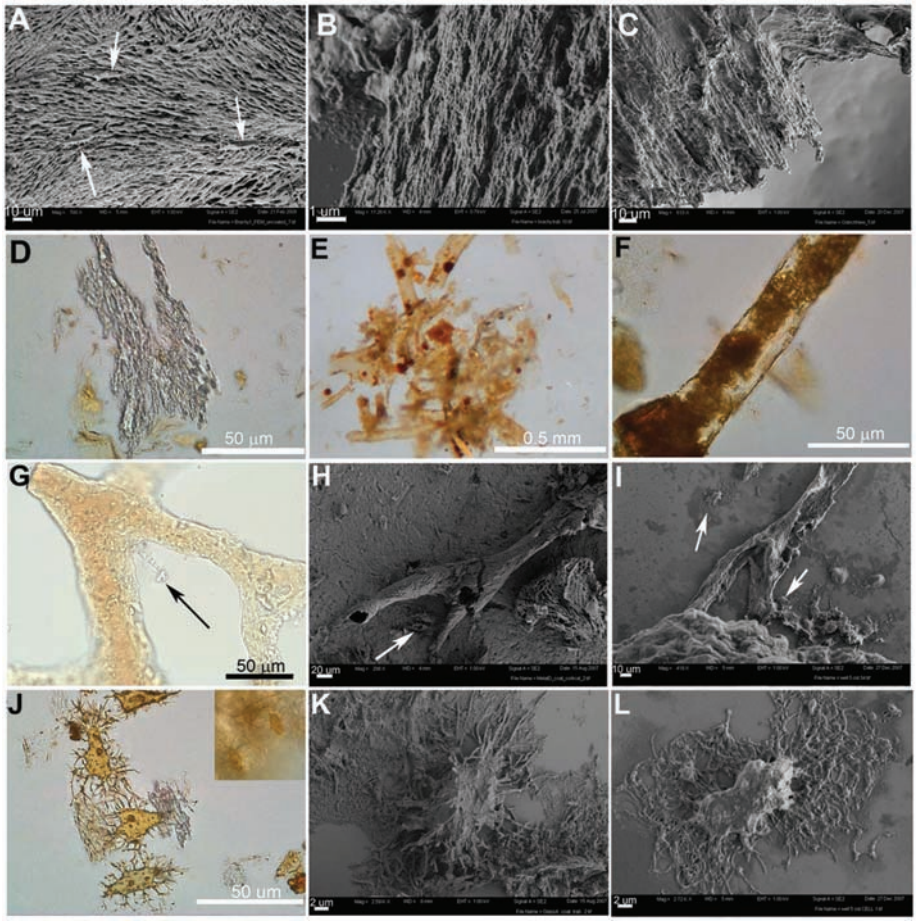

Fig. 1. FESEM and transmitted light micrographs of demineralized *B. canadensis* (MOR 2598) bone matrix, vessels, and cells, compared with extant ostrich components imaged under similar conditions. (**A**) Low-magnification of FESEM demineralized MOR 2598 shows fibers in a plywood-like array characteristic of bone. Arrows indicate osteocytes in lacunae within fibers. (**B**) Demineralized matrix showing detail of fibers. (**C**) Demineralized ostrich bone matrix imaged under the same parameter as in (B). (**D**) Demineralized bone matrix from MOR 5928 is white under transmitted light. (**E**) MOR 2598 vessels and matrix after EDTA demineralization show rounded red inclusions (*10*). (**F**) Higher magnification of isolated MOR 5923 vessel, showing amorphous red intravascular contents. (**G**) Ostrich vessel with amorphous contents and associated osteocyte (arrow). (**H**) FESEM shows hollow *B. canadensis* vessels, often associated with osteocytes (arrow). (**I**) FESEM image of collapsed ostrich vessel and associated matrix with osteocytes (arrows). (**J**) Osteocytes attached by interconnected filipodia, with filipodia embedded in fibrous matrix. (**K**) FESEM of single *B. canadensis* osteocyte with long filipodia. (**L**) Single ostrich osteocyte isolated from demineralized, digested bone.

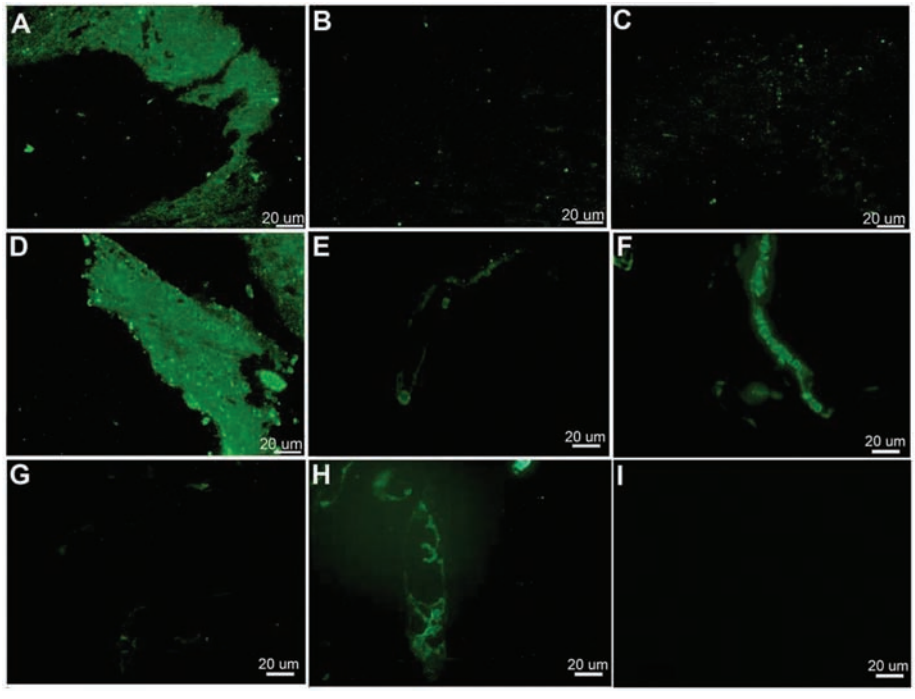

Fig. 2. In situ immunohistochemistry of demineralized *B. canadensis* bone matrix and vessels. (**A**) Incubated with antibodies against avian collagen I . (**B**) Anti-collagen antibodies inhibited with avian collagen, then incubated with tissues as in (A). (**C**) Demineralized bone matrix digested with collagenase, then incubated with anti-collagen antibodies as in (A). (**D**) *B. canadensis* demineralized bone matrix incubated with anti-osteocalcin polyclonal antibodies (*10*). (**E**) *B. canadensis* vessels incubated with polyclonal antibodies against laminin (*10*) show weak binding above background levels. (**F**) Vessels incubated with antibodies against elastin proteins. (**G**) Vessels digested with elastase, then incubated with elastin antibodies as in (F). (**H**) *B. canadensis* vessels incubated with polyclonal antibodies against ostrich hemoglobin. (**I**) Ostrich hemoglobin antibodies incubated with excess hemoglobin to inhibit binding, then incubated with dinosaur vessels as in (H). Panels (A) to (D) were taken at 79-ms integration, 63× objective; (E) to (I) were taken at 120-ms integration, 63× objective, magnification as shown.

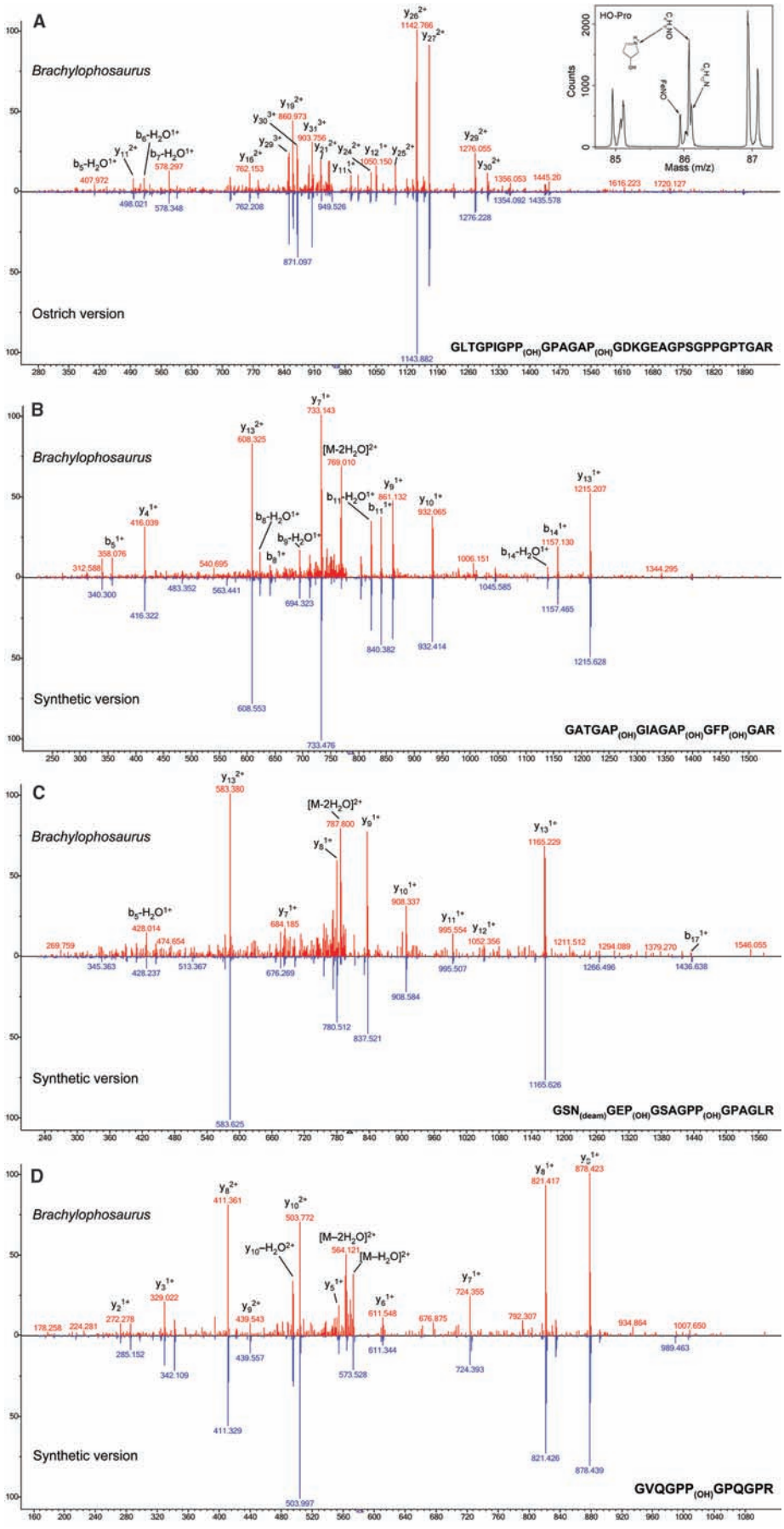

Fig. 3. Mass spectrometry analyses of *B. canadensis* tissues and extracts. (Inset to A) Collagen-specific Pro-OH functional group positively identified by TOF-SIMS in situ analysis of demineralized *B. canadensis* tissues by a preparation method distinct from tandem mass spectrometry analyses [see text and (*10*)]. (**A** to **D**) Product ion spectra recorded during tandem mass spectrometry (LC/MS/MS) analyses with CID of chemical extracts of bone. The four collagen peptides scoring lowest on Mascot search engine scores (but top-ranked versus the Swiss-Prot database) acquired from the LTQ-Orbitrap XL mass spectrometry were validated with high-confidence versions of the same sequences with a computational spectral comparison tool. (A) *B. canadensis* collagen a1(I) [M+3H]3+ peptide ion GLTGPIGPP(OH)GPAGAP (OH)GDKGEAGPSGPPGPTGAR using the MS Search 2.0 spectral comparison algorithm shows excellent alignment of fragment ion *m/z* values and relative intensities and was ranked first to a previously acquired high-confidence ostrich version of the same sequence [reverse match factor (RMF = 779)] in a database of >200,000 spectra. (B) Collagen a1(I) [M+2H]2+ peptide ion GATGAP(OH)GIAGAP(OH)GFP(OH)GAR was a top match to the synthetic peptide version of the same sequence (RMF = 494). (C) The collagen a2(I) [M+2H]2+ peptide ion GSN(deam)GEP(OH)GSAGPP(OH)GPAGLR versus a synthetically derived version (RMF = 482), and (D) the collagen a1(I) [M+2H]2+ peptide ion GVQGPP(OH)GPQGPR validated with a synthetic peptide (RMF = 562). (B, C, and D) Significant fragment ions attributed to water losses from the precursor ion are present in the spectra from *Brachylophosaurus* but are less apparent in synthetic or ostrich comparisons. The four other highest-scoring statistically significant MS/MS spectra are shown in fig. S9 in the SOM.

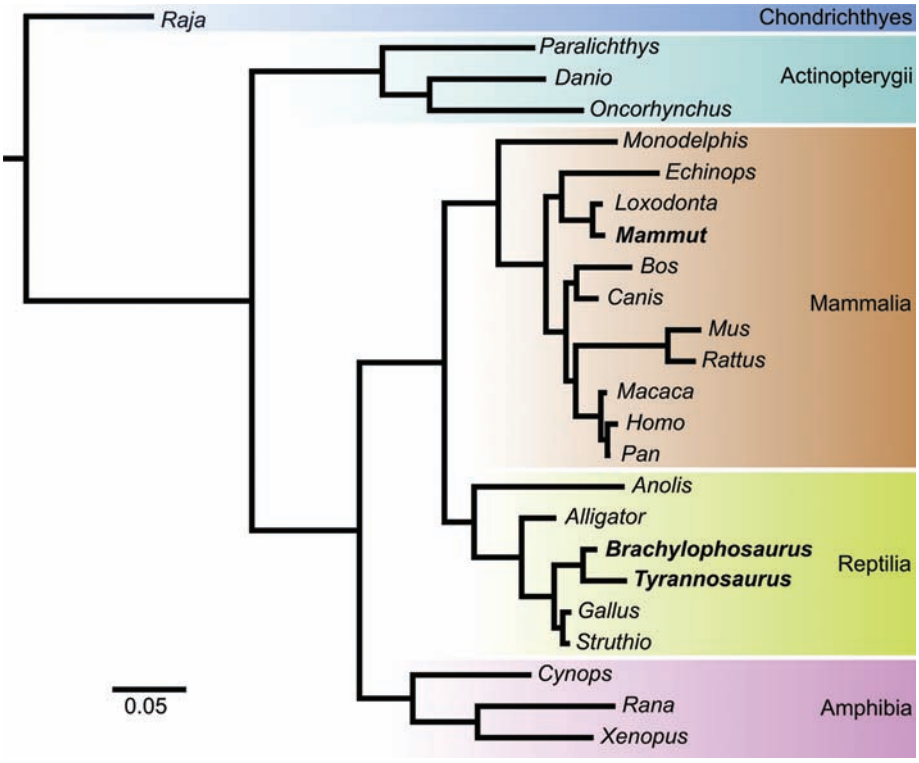

Fig. 4. Consensus of the posterior distribution of phylogenetic trees including *M. americanum* (Mastodon, MOR 605) and the extinct dinosaurs *B. canadensis* (MOR 2598) and *T. rex* (MOR 1125, in bold). Colored backgrounds designate monophyletic groups. All nodes have 100% posterior probability (PP) support except the *Gallus/Struthio* group, which has 36% PP support. Branch lengths are reported as the mean of the expected number of changes per site.

in immunohistochemistry (Fig. 2F) and immunoblot (fig. S6A). Antibodies to both laminin and elastin proteins showed specific binding, though they differed in binding strength in both assays. Three relatively high–molecular weight bands can be seen within a smear of stained material in immunoblot (fig. S6A, thin arrows), whereas two faint bands indicating laminin antibody binding were observed at different molecular weights when compared with elastin-reactive bands (fig. S6A, short arrows). Vessel extracts did not show binding to antibodies raised against ostrich hemoglobin, but hemoglobin antibodies bound specifically in in situ tests (Fig. 2H). A second set of experiments, conducted in a separate lab (by R.K.), confirm these results (fig. S6B). Laminin antibodies known to react to avian and reptilian proteins (*10*) demonstrate specific binding to *B. canadensis* extracts. Controls for spurious antibody binding were negative.

Attenuated total reflection infrared spectroscopy demonstrated clear amide I and amide II bands (fig. S7) in lyophilized vessels and surrounding demineralized matrix. This method cannot be used to identify which proteins are present or the source/endogeneity of these proteins, only characteristic bond vibration patterns. However, the data are consistent with other in situ data supporting the presence of proteinaceous material in *B. canadensis* tissues.

Posttranslational hydroxylation of proline is an identifying feature of collagen, and microbes cannot produce this modification (*17*, *18*). Whole vessels and matrix from demineralized *B. canadensis* bone

Table 1. Collagen α1(I) and α2(I) sequences acquired by ion trap and Orbitrap mass spectrometry for *B. canadensis*. *m/z* values of the peptide ion, molecular weight, mass spectrometer used, database search engine scores, expectation values, sequence validation method, and sequence identity based on BLAST searches versus the all-species NCBInr protein database and internally acquired ostrich and alligator sequences are shown. The interpretation of the sequence GLPGESGAVGPAGPP$_{(OH)}$GSR was aided by the high mass accuracy of the Orbitrap, because hydroxyproline is more accurate than isoleucine/leucine at position 15 by 0.0364 daltons.

m/z (obsd)	Mr (calc)	Mass error	Instrument	rank	Mascot score	Mascot expectation value	Sequest Xcorr	Validation	Peptide sequence	Protein	BLAST sequence identity
960.487	2878.421	0.0047*	Orbitrap	1	40.0	0.59	4.53	Search stats; ostrich peptide	GLTGPIGPP(OH)GPAGAP(OH) GDKGEAGPSGPPGPTGAR	Collagen α1(1)	Ostrich and mammals
730.740	1458.685	0.7793	Ion trap	1	73.7	0.00027	3.99	Search stats	GSAGPP(OH)GATGFP(OH) GAAGR	Collagen α1(1)	*T. rex*, chicken, and mammals
786.901	1571.769	0.0180*	Orbitrap	1	37.2	0.84	3.13	Search stats; synthetic peptide	GATGAP(OH)GIAGAP(OH) GFP(OH)GAR	Collagen α1(1)	*T. rex*, chicken, alligator, and amphibia
766.877	1531.738	0.0005	Orbitrap	1	52.7	0.023	2.70	Search stats	GETGPAGPAGPP(OH)GPAGAR	Collagen α1(1)	Chicken
582.160	1161.589	0.7164	Ion trap	1	65.8	0.0015	2.48	Search stats; synthetic peptide	GVQGPP(OH)GPQGPR	Collagen α1(1)	*T. rex*, chicken, alligator, and opossum
653.824	1305.631	0.0013	Orbitrap	1	56.9	0.012	2.63	Search stats	GPSGPQGPSGAP(OH)GPK	Collagen α1(1)	Chicken, alligator, rat, and opossum
805.875	1609.734	0.0012	Orbitrap	1	40.5	0.54	2.32	Search stats; synthetic peptide	GSN(deam)GEP(OH)GSAGPP (OH)GPAGLR	Collagen α2(1)	Chicken and alligator
789.898	1577.782	0.0005	Orbitrap	1	54.3	0.023	3.97	Search stats	GLPGESGAVGPAGPP(OH)GSR	Collagen α2(1)	*T. rex*

*For two sequences [GLTGPIGPP$_{(OH)}$ GPAGAP$_{(OH)}$ GDKGEAGPSGPPGPTGAR and GATGAP$_{(OH)}$GIAGAP$_{(OH)}$GFP$_{(OH)}$GAR] acquired with the Orbitrap, MS/MS was triggered on the *m/z* ratio representing the ^{13}C stable isotope containing ion rather than the monoisotopic version.

were subjected to in situ time-of-flight–secondary ion mass spectrometry (ToF-SIMS) with imaging capability (*10*) in a separate laboratory (the lab of R.A.). Focused Ga^+ and Au^+ ions generated molecular fragments from tissues that were detected with sufficient high mass resolution ($m/\Delta m \sim 4000$) to uniquely identify hydroxylated proline (Pro-OH), as well as Lys, Pro, Lys-OH, Ala, Gly, and Leu from demineralized dinosaur tissues (fig. S8). A number of organic fragments containing nitrogen were also detected, including unusual complexes between C, N, and Fe (Fig. 3A, inset, and fig. S8), suggesting alteration and modification to preserved organics, more consistent with an ancient source than recent contamination.

We used mass spectrometry (performed by J.M.A.) to analyze whole bone extracts of *B. canadensis* (MOR 2598) that were fibrous and lighter in color than those from *T. rex* (MOR 1125) (*4*, *5*). Bone extracts (*10*) were proteolyzed with trypsin, purified, and concentrated by microreversed phase chromatography, then analyzed by reversed-phase microcapillary liquid chromatography tandem mass spectrometry (LC/MS/MS) using both linear ion trap and hybrid linear ion trap–orbitrap mass spectrometers (*19*). We searched fragmentation spectra from data-dependent acquisitions against the reversed Swiss-Prot protein database using Sequest (*20*) and Mascot (*21*) algorithms. We identified eight total collagen peptide sequences, six from collagen α1 type I and two from collagen α2 type I. The eight peptides totaled 149 amino acids from four different samples (six LC/MS/MS data sets), nearly double the number of amino acids (89) recovered from *T. rex* (MOR 1125) (*4*, *5*). The eight peptides identified as collagen (Table 1) were top-ranked matches versus the Swiss-Prot target protein database. Four of the eight peptides, derived from three separate bone extracts, were sequenced from multiple scan events across multiple data files. We validated the sequences using scoring statistics, decoy databases, manual inspection, and spectral comparisons to high-confidence spectra obtained from synthetic peptides and peptides of identical sequence from extant organisms. One peptide sequence showed evidence of deamidation of asparagine, and all reported sequences contained at least one Pro-OH residue.

The eight peptide sequences for collagen α1 type I and collagen α2 type I represent 7.8 and 2.5% of the full-length sequence for related organisms, respectively. In addition, three peptide sequences were confirmed in a separate laboratory (in the lab of W.S.L.) from two samples from a single bone extraction. Coextracted sediment and buffer controls were consistently negative for collagen peptidic material by all methods of analyses including mass spectrometry sequencing, although common contaminants including human keratins, ubiquitous in all labs, and some microbial peptides were sequenced from these bone extracts.

All eight sequences derived from *B. canadensis* extracts are high-confidence, and their spectra produced expectation values of <1 from Mascot searches. Four dinosaur spectra were high-confidence matches to existing protein databases, and statistical validation is sufficient for identification. The four lowest-scoring MS/MS spectra from *Brachylophosaurus* bone extracts, acquired with the use of collision-induced dissociation (CID) in the linear ion trap of an LTQ-Orbitrap XL mass spectrometer, are shown in Fig. 3, A to D. These MS/MS spectra were subjected to an extra level of validation with the MS Search 2.0 spectral comparison algorithm from the National Institute of Standards and Technology (NIST) against a database of >200,000 random peptide fragmentation spectra from various taxa (*22*, *23*), including high-confidence versions of MS/MS spectra from four collagen sequences by adding previously acquired ostrich or synthetic peptides to the NIST spectral database. These four sequences derived from *B. canadensis* were top matches to high-confidence versions of the same sequences by fragment ion mass/charge ratio (m/z) values and relative intensities of fragment ions, providing additional validation of the data. All sequence data from *Brachylophosaurus* and validating sources are available in the supporting online material (SOM). The complete raw data from all 27,791 spectra, as well as previously reported sequences from *T. rex*, are available from the PRIDE database (www.ebi.ac.uk/pride/). In addition, we have shown *B. canadensis* collagen sequences to be statistically significant, and false discovery rates for MOR 2598 sequence data have been calculated (*10*).

In a separate lab (that of L.C.C.), *B. canadensis* bone extracts showed positive reactivity by immunoblot to a mixture of collagen type I polyclonal antibodies at high molecular weights (~250 to 300 kD), whereas surrounding sediments showed negative reactivity (fig. S9). This supports the identification of collagen fragments in bone extracts and suggests modifications (for example, cross-linking) of collagen molecules (*2*). Although silver-stained material in gels (fig. S2) suggest concentrations within the low end of current mass spectrometry sensitivity thresholds (low nanogram), it is likely that most of the protein is present in unsequenceable form(s); that is, cross-linked and/or modified so as to make them incapable of resolution by current mass spectrometry technology and software. We hypothesize that processes contributing to preservation of these otherwise labile components make analyses difficult, but conversely, the low recovery and diagenetic alteration support an endogenous source, as these chemical modifications are not observed in modern proteins.

B. canadensis collagen sequences were aligned with collagen sequences from 21 extant taxa and two extinct organisms: *Mammut americanum* (MOR 605) and *T. rex* (MOR 1125) (see table S1 and SOM appendix) (*6*). The *Anolis carolinensis* amino acid sequence was inferred with the use of FGENESH+ (gene prediction on the basis of protein homology; www.softberry.com). Additional collagen α2(I) sequence data for five species were obtained from online public databases (table S1).

We used BayesPhylogenies (*24*) to infer phylogenetic relationships from collagen sequences with the Dayhoff amino acid substitution model (*6*). The resulting consensus tree of the posterior distribution (Fig. 4) was well resolved, as was a phylogeny inferred by maximum likelihood (fig. S11). Whereas the first molecular phylogeny containing a non-avian dinosaurian [*T. rex*, MOR 1125, (*6*)] resulted in a tree that misplaced *A. carolinensis* (*6*), additional sequence data from several extant species (fig. S11 and table S1) corrected this misplacement and improved clade support to 100% (number of times a clade was inferred in the posterior distribution of trees) for all groups except the *Gallus*/*Struthio* group (Aves), which had 36% support. Under a majority-rule criterion to building a consensus tree, Dinosauria (the group containing the two extinct dinosaurs and the two birds) collapsed into a three-way polytomy.

Removing *T. rex* from the phylogeny resulted in a three-way polytomy as well. The amount of missing data in *B. canadensis* and *T. rex* sequences relative to extant samples resulted in relatively low resolution within Dinosauria, but even so, the phylogenetic relationship of recovered *B. canadensis* sequences supports the species' placement within Archosauria, closer to birds than *Alligator*. However, on the basis of well-established morphological analyses (*25*), we predict that *T. rex* is more closely related to birds than it is to the ornithischian hadrosaur *B. canadensis*. Despite ambiguity within Dinosauria, obvious phylogenetic signal resides within recovered collagen sequences, supporting endogeneity (fig. S11) (*10*).

The hypothesis that endogenous proteins can persist across geological time, as first reported for *T. rex* (MOR 1125), was met with appropriate skepticism (*7*–*9*). However, the inclusion of additional sequence data from extant reptiles (*6*) and *B. canadensis* strengthens the hypothesis that the molecular signal is preserved at least to the Late Cretaceous.

The submicron differences in texture (Fig. 1 and fig. S1), elemental differentiation, sub-"cellular" inclusions in osteocytes and vessels, identification of the posttranslational Pro-OH modification not produced by microbes (*18*), differential binding of antibodies by both in situ and immunoblot studies, collagen protein sequences, and phylogenetic analyses do not support a microbial origin for either these microstructures or peptide fragments (*7*). Coupled with evidence for cross-linking and unusual chemical modifications, the congruence of evidence strongly supports an endogenous origin for this material. The most parsimonious explanation, thus far unfalsified, is that original molecules persist in some Cretaceous dinosaur fossils. Still unknown is the chemistry behind such preservation.

References and Notes

1. M. H. Schweitzer, J. L. Wittmeyer, J. R. Horner, J. K. Toporski, *Science* **307**, 1952 (2005).
2. M. H. Schweitzer, J. L. Wittmeyer, J. R. Horner, *Proc. R. Soc. London Ser. B Biol. Sci.* **274**, 183 (2007).

3. M. H. Schweitzer *et al.*, *Science* **316**, 277 (2007).
4. J. M. Asara, M. H. Schweitzer, L. M. Freimark, M. Phillips, L. C. Cantley, *Science* **316**, 280 (2007).
5. J. M. Asara *et al.*, *Science* **317**, 1324 (2007).
6. C. L. Organ *et al.*, *Science* **320**, 499 (2008).
7. T. G. Kaye, G. Gaugler, Z. Sawlowicz, *PLoS One* **3**, e2808 (2008).
8. M. Buckley *et al.*, *Science* **319**, 33c (2008).
9. P. A. Pevzner, S. Kim, J. Ng, *Science* **321**, 1040b (2008).
10. Materials and methods are available as supporting material on *Science* Online.
11. S. Weiner, H. D. Wagner, *Annu. Rev. Mater. Sci.* **28**, 271 (1998).
12. S. Weiner, W. Traub, H. D. Wagner, *J. Struct. Biol.* **126**, 241 (1999).
13. D. N. Menton, D. J. Simmons, S. L. Chang, B. Y. Orr, *Anat. Rec.* **209**, 29 (1984).
14. M. L. Knothe Tate, J. R. Adamson, A. E. Tami, T. W. Bauer, *Int. J. Biochem. Cell Biol.* **36**, 1 (2004).
15. G. A. Wagnieres, M. Willem, W. M. Star, B. C. Wilson, *Photochem. Photobiol.* **68**, 603 (1998).
16. R. P. Mecham, J. E. Heuser, in *Cell Biology of the Extracellular Matrix*, E. D. Hay, Ed. (Plenum, New York, 1991), pp. 79–109.
17. P. S. Ebert, D. J. Prockop, *Biochem. Biophys. Res. Commun.* **8**, 305 (1962).
18. M. Rasmussen, M. Jacobsson, L. Björck, *J. Biol. Chem.* **278**, 32313 (2003).
19. Q. Hu *et al.*, *J. Mass Spectrom.* **40**, 430 (2005).
20. J. K. Eng, A. L. McCormack, J. R. Yates III, *J. Am. Soc. Mass Spectrom.* **5**, 976 (1994).
21. D. N. Perkins, D. J. Pappin, D. M. Creasy, J. S. Cottrell, *Electrophoresis* **20**, 3551 (1999).
22. H. Lam *et al.*, *Proteomics* **7**, 655 (2007).
23. J. M. Asara, M. H. Schweitzer, L. C. Cantley, J. S. Cottrell, *Science* **321**, 1040c (2008).
24. M. Pagel, A. Meade, *Syst. Biol.* **53**, 571 (2004).
25. D. Pisani *et al.*, *Proc. R. Soc. London Ser. B Biol. Sci.* **269**, 915 (2002).

26. We thank B. Harmon, N. Peterson, and the MOR crew responsible for recovery of MOR 2598; N. Equall and S. Brumfield for microscopy assistance; G. Fisher (Physical Electronics) for PHI nanoTOF assistance; T. Cleland for assistance with gel analyses; X. Yang for help with mass spectrometry sample preparation; S. Stein and Y. Mirokhin for MS Search 2.0 software enhancements; J. Starkey and R. Mecham for antibodies; B. Anderson for Fourier transform infrared spectroscopy access; T. Collier for sample preparation; E. Leithold for access to equipment; J. C. Fountain for support; and the Montana Department of Natural Resources and Conservation for land access. C.L.O. thanks S. V. Edwards for postdoctoral support. We acknowledge funding from NSF [awards EAR 0722702 and EAR 0634136 (J.M.A.) and EAR 0548847 and EAR-0541744 (M.H.S.)]; the David and Lucile Packard Foundation (M.H.S.); United Negro College Fund–Merck Postdoctoral Science Research Fellowship (M.B.D.); the Taplin Funds for Discovery (Harvard Medical School); partial support by NASA–Expermental Project to Simulate Competitive Research under grant NCC5-579 (R.A. and Z.S.); Damon Runyon Cancer Research Foundation (M.G.V.H.); NIH grants DK 55001, DK 62987, AA 13913, DK 61866, and CA 125550; and the Department of Medicine for the Division of Matrix Biology at the Beth Israel Deaconess Medical Center. Correspondence and requests for materials should be addressed to M.H.S. for biochemical and morphological analyses and to J.M.A. for mass spectrometry and molecular phylogenetics analyses.

Supporting Online Material

www.sciencemag.org/cgi/content/full/324/5927/626/DC1
Materials and Methods
SOM Text
Figs. S1 to S12
Table S1
References
Appendix S1
Database S1

25 August 2008; accepted 12 March 2009
10.1126/science.1165069

A Gross-Pitaevskii Treatment for Supersolid Helium

Philip W. Anderson

Understanding the observations of nonlinear rotational susceptibility in samples of solid helium below temperatures of 1 to 200 millikelvin (mK) has been a subject of some controversy. Here, the observations are conjectured to be describable in terms of a rarified Gross-Pitaevskii superfluid of vacancies, with a transition temperature of about 50 mK, whose density is locally enhanced by crystal imperfections. The observations can be greatly affected by this density enhancement. I argue that every pure Bose solid's ground state is a supersolid.

At least half a dozen groups by now have confirmed the original observation (*1*) made with a torsional oscillator that solid helium-4 (^{4}He) loses a fraction of its classical moment of inertia when it is below an onset temperature of around 200 mK. The first observations showed a strong dependence on velocity of motion; however, at lower temperatures, such as in the <50 mK range, the observations show thermal hysteresis, and in some circumstances the signal is quite robust. The observations can only indicate superfluid flow, though as yet no direct experiment has demonstrated that. However, an observed considerable sensitivity to crystal quality leaves open the question of whether the flow is intrinsic to the pure solid; a vocal faction argues that it cannot be. I here address these issues from a different point of view.

The Gross-Pitaevskii equation for the order parameter (*2*, *3*), and the corresponding free energy, has become standard for treating Bose condensation in cold atomic gases. The assumption on which this theory was based, essentially that the bosons are dilute relative to the range of their interaction, are well satisfied in these systems but not for superfluid helium (He II) (correspondingly, there are complications in He II, specifically the roton spectrum and the large depletion of the condensate). One might think that the Gross-Pitaevskii equation would be even less applicable to solid He, but the opposite may be the case.

The solid is of course dense, but the experiments indicating supersolidity show that the amount of matter that actually flows is a few percent of the atoms, and in good crystals much less matter flows than that. The earliest theoretical paper on supersolidity (*4*) proposed that supersolidity might consist of Bose condensation of a small density of vacancies in the solid substrate. The wave function that I have proposed as a heuristic description of the phenomena (*5*) can be interpreted in those terms. Vacancy flow within a rigid lattice and substrate atom flow are essentially equivalent, so as a shorthand I will discuss "vacancies" and a quantum (boson) field representing them. The term vacancies is used henceforth as a shorthand for the fluctuations in particle number that make it possible to define a phase of the particle field. In the pure crystal, they may be equally matched between particles and holes, and the superfluidity can be caused by an overlap of local boson wave functions [see the supporting online material (SOM) text].

Vacancies certainly interact repulsively as hard-core bosons, because no two vacancies can be on the same site. There may also be a long-range interaction due to elasticity, which is thought to be attractive but probably does not play any dynamical role; elasticity simply changes the chemical potential. The vacancy density is, especially in a good crystal, very low and experimentally on the order of 3×10^{-4} per site.

The Gross-Pitaevskii energy is

$$E = |(\hbar\nabla\Psi)|^2/2m^* + V(r)|\Psi|^2 + \frac{1}{2}g|\Psi|^4 \quad (1)$$

and the Gross-Pitaevskii equation is

$$\mu\Psi = -\hbar^2\nabla^2\Psi/2m^* + V(r)\Psi + g|\Psi|^2\Psi \quad (2)$$

Here, $\hbar$ is the reduced Planck constant, Ψ is the "order parameter" (the mean of the vacancy boson field), m^* is an effective mass, g is the coupling constant ($\hbar^2 a/\pi m^*$, where a is the scattering length and presumed repulsive), and μ is the chemical potential for vacancies. $V(r)$ is in the gas state simply the trap potential, but in here $V(r)$ is included to take into account the fact that dislocations, surfaces, grain boundaries, and possibly ^{3}He impurities are all attractive sites for vacancies. All of these parameters and their values need further discussion because my physical conclusions depend on them. Equation 1 essentially is just a coarse-graining of the mean-field Schrödinger equation. The time-dependent equation that controls collective modes and vortex behavior is obtained by replacing μ with $\frac{\hbar\partial}{i\partial t}$.

The chemical potential tells us how many vacancies there are. The strong arguments presented in (*6*, *7*), which are based on a Bijl-Jastrow wave

Department of Physics, Princeton University, Princeton, NJ 08525, USA.

function for the ground state, as well as recent estimates (*8*, *9*) are in favor of there being vacancies at the 10^{-4} per site level, even in the pure crystal (SOM text). Repeated efforts by Clark *et al.* to grow perfect, pure, single crystals have always observed nonclassical rotational inertia (NCRI) on the 10^{-4} level relative to the classically expected value (*10*), and this level or higher has been confirmed by others (*11*–*13*). Simulations (*14*, *15*) performed using the path-integral Monte Carlo method have been claimed to prove the nonexistence of vacancies; however, among other difficulties the equivalent temperature in these simulations is well above the relevant temperature at which Bose condensation takes place. In any case, simulating 10^4 atoms well enough to find a single defect is beyond the capabilities of those methods. I used a background density ($|\Psi|^2$) relative to the solid for pure ^{4}He) of 2×10^{-4} to 3×10^{-4}, which fixes μ in terms of g.

I assumed m^* to be fairly light relative to that of a helium atom (m_{He}) and used an estimate that is often quoted,$1/3m_{\mathrm{He}}$ (other estimates are even smaller). This effective mass is such that the uncertainty energy that is necessary to localize the mass on a single site is on the order of 10 K. This is the same magnitude as estimates in (*10*) of the energy cost of a vacancy and suggests that those estimates may not have taken into account the kinetic energy that could be gained by delocalization. Regarding vacancies classically as strictly local configurations of the lattice is not reasonable.

m^* and the density of the boson field allow an estimate of the superfluid transition temperature from the Bose-Einstein equation

$$k_{\mathrm{B}} T_{\mathrm{c}} = \frac{2\pi\hbar^2}{m^*}\left(\frac{N}{2.61V}\right)^{2/3} \qquad (3)$$

where N/V is the vacancy density, k_{B} is Boltzmann's constant, and T_{c} is the transition temperature.

By entering into Eq. 3 a typical solid density, a vacancy concentration of 2×10^{-4} to 3×10^{-4} per site, and a mass of $1/3m_{\mathrm{He}}$, the resulting transition temperature is ~50 to 70 mK. This is very close to the transition temperature at which thermal hysteresis in the NCRI has been reported (*12*, *16*). I have discussed elsewhere (*17*) why reversible NCRI appears so far above T_{c}. One expects true superflow to be observable only below this T_{c}, if at all.

The parameter g, or equivalently the scattering length a, is not something one can accurately estimate. I next discuss here the consequences of assuming that g is reasonably small. This perhaps can be justified, again, from the fact that a light mass implies a somewhat extended lattice distortion. Here, I define a correlation length as

$$\xi = 1/\sqrt{8\pi n_0 a} \qquad (4)$$

where $n_0 = |\Psi^2|$, which is the exponential decay length of a small perturbation in the vacancy field, according to Eq. 1. Given that $n_0 = 3 \times 10^{-4}$, even if a is a whole lattice constant, ξ is 10 lattice constants or 3 nm; it would be reasonable for ξ to be an order of magnitude larger. This is still not quite the scale at which the variation of surface-to-volume ratio in NCRI occurs (*18*), but almost.

What is of most interest is the effect of defects being attractive sites for vacancies. A dislocation core, for instance, is said to attract on the order of one vacancy per atomic length, calculated on the basis of localized high-energy vacancies (*19*). This amounts to a potential well in V that could be estimated as $VR^2 \approx 10$ to 15 K, where R is the well's radius. Balancing this against the repulsive interaction $g\Psi^4$, a dislocation core might be capable of attracting a cloud of $\propto 1/g$ vacancies with a radius on the order of ξ. Thus, the effect of dislocations can be somewhat magnified. Correspondingly, one would expect there to be similar diffuse densities of delocalized vacancies around grain boundaries and near surfaces. I would consider this to be one of the few possibile explanations for the degree to which crystal imperfection appears to enhance NCRI.

Why small concentrations of ^{3}He produce large effects remains an open question.

It seems possible to provide an accounting of most of the puzzling properties of low-temperature solid He by describing it as a Gross-Pitaevskii fluid of delocalized quantum vacancies. The idea that the superfluid is an intrinsic property of the pure crystal, which is locally enhanced by imperfections, seems to account for the low and reasonably invariant genuine superfluid transition and the large variations in the quantity of superflow, which otherwise appear to be irreconcilable.

References and Notes

1. E. Kim, M. H. W. Chan, *Phys. Rev. Lett.* **97**, 115302 (2006).
2. E. P. Gross, *Phys. Rev.* **106**, 161 (1957).
3. L. P. Pitaevskii, *Sov. Phys. JETP* **4**, 439 (1957).
4. A. F. Andreev, I. M. Lifshitz, *Sov. Phys. JETP* **29**, 1107 (1969).
5. P. Anderson, http://arXiv.org/abs/cond-mat/0504731 (2005).
6. L. Reatto, *Phys. Rev.* **183**, 334 (1969).
7. L. Reatto, G. V. Chester, *Phys. Rev.* **155**, 88 (1967).
8. M. Rossi, E. Vitali, D. E. Galli, L. Reatto, *J. Low Temp. Phys.* **153**, 250 (2008).
9. C. Cazorla, G. E. Astrakarchik, J. Casulleras, J. Boronat, http://arXiv.org/abs/0804.1851 (2008).
10. A. C. Clark, J. T. West, M. H. W. Chan, http://arXiv.org/abs/0706.0906v2 (2007).
11. A. Penzev, Y. Yasuta, M. Kubota, *J. Low Temp. Phys.* **148**, 677 (2007).
12. A. S. C. Rittner, J. Reppy, *Phys. Rev. Lett.* **97**, 165301 (2006).
13. Y. Aoki, J. C. Graves, H. Kojima, *Phys. Rev. Lett.* **99**, 015301 (2007).
14. N. Prokof'ev, B. Svistunov, *Phys. Rev. Lett.* **94**, 155302 (2005).
15. D. M. Ceperley, B. Bernu, *Phys. Rev. Lett.* **93**, 155303 (2004).
16. A. C. Clark, J. D. Maynard, M. H. W. Chan, http://arXiv.org/abs/0711.3619 (2007).
17. P. W. Anderson, *Phys. Rev. Lett.* **100**, 215301 (2008).
18. A. C. S. Rittner, J. Reppy, *Phys. Rev. Lett.* **98**, 175302 (2007).
19. L. Pollet *et al.*, *Phys. Rev. Lett.* **101**, 097202 (2008).

20. I acknowledge the hospitality of the Fondation des Treilles for the workshop in which this work was conceived and the lectures and valuable discussions of M. H. W. Chan, J. Beamish, L. Reatto, J. Dalibard, J. Boronat, S. Balibar, and J. Reppy at that workshop.

Supporting Online Material

www.sciencemag.org/cgi/content/full/324/5927/631/DC1
SOM Text
References

8 December 2008; accepted 2 March 2009
10.1126/science.1169456

Evidence for a Superglass State in Solid ^{4}He

B. Hunt,[1*] E. Pratt,[1*] V. Gadagkar,[1] M. Yamashita,[1,2] A. V. Balatsky,[3] J. C. Davis[1,4]†

Although solid helium-4 (^{4}He) may be a supersolid, it also exhibits many phenomena unexpected in that context. We studied relaxation dynamics in the resonance frequency $f(T)$ and dissipation $D(T)$ of a torsional oscillator containing solid ^{4}He. With the appearance of the "supersolid" state, the relaxation times within $f(T)$ and $D(T)$ began to increase rapidly together. More importantly, the relaxation processes in both $D(T)$ and a component of $f(T)$ exhibited a complex synchronized ultraslow evolution toward equilibrium. Analysis using a generalized rotational susceptibility revealed that, while exhibiting these apparently glassy dynamics, the phenomena were quantitatively inconsistent with a simple excitation freeze-out transition because the variation in f was far too large. One possibility is that amorphous solid ^{4}He represents a new form of supersolid in which dynamical excitations within the solid control the superfluid phase stiffness.

A "classic" supersolid (*1*–*5*) is a bosonic crystal with an interpenetrating superfluid component. Solid ^{4}He has long been the focus of searches for this state (*6*). To demonstrate its existence unambiguously, macroscopic quantum phenomena (*7*) such as persistent mass currents, circulation quantization, quantized vortices, or the superfluid Josephson effect must be observed. None of these effects have been detected in solid ^{4}He.

There are, however, indications that this material could be a supersolid. This is because high-Q torsional oscillators (TOs) containing solid ^{4}He exhibit an increase in resonance frequency

$f(T)$ at low temperatures. This is detectable below a temperature $T_C \sim 65$ mK in the purest, most crystalline samples; below $T_C \sim 300$ mK in more amorphous samples; and below at least $T_C \sim 500$ mK when dilute concentrations of ^{3}He exist (*8*–*11*). A strong dissipation peak in $D(T) \equiv Q^{-1}(T)$ occurs in association with the rapid rise of $f(T)$ (*9*, *10*, *12*), but their relation has not been explained. These results [now widely reproduced (*12*–*15*)] can be interpreted as a ^{4}He supersolid whose rotational inertia is reduced due to its superfluid component. Support for this interpretation comes from the reductions in the net frequency increase when the TO annuli containing solid ^{4}He are blocked (*9*, *16*).

But many phenomena inexplicable in the context of a classic superfluid are also observed in equivalent samples of solid ^{4}He. These include, for example, maximum dc mass flow rates inconsistent with the TO dynamics (*17*–*19*), large increases in T_C with the introduction of dilute ^{3}He concentrations (*8*, *11*), strong effects of annealing on the magnitude of TO frequency shifts (*12*, *20*), velocity hysteresis in the frequency shift (*13*), and shear stiffening of the solid coincident with the TO frequency increase (*21*). These phenomena indicate some unanticipated interplay between dynamical degrees of freedom of the solid and any superfluid component.

In response, new theories have been proposed that solid ^{4}He is (i) a nonsuperfluid glass (*22*, *23*), (ii) a fluid of fluctuating quantum vortices (*24*), (iii) a superfluid network at linked grain boundaries (*25*), (iv) a viscoelastic solid (*26*), or a superglass—a type of granular superfluid within an amorphous solid (*27*–*30*). To help discriminate between such ideas, we focus on the relaxation dynamics of solid ^{4}He, which should distinguish a simple superfluid state from a purely glassy state.

Using a TO containing solid ^{4}He (Fig. 1A), we measure $f(T)$ and $D(T)$ effects that are in good agreement with those of other research groups (*8*–*16*). Figure 1 shows the evolution of $f(T)$ (blue circles) and $D(T)$ (red triangles) for our typical sample; the change in $f(T)$ between 300 and 10 mK would represent a "supersolid fraction" of 4.8% if the frequency shift were entirely attributable to a superfluid decoupling. Our samples, while formed by the "blocked capillary" procedure and therefore amorphous, are of the type most widely studied in the field (*8*, *9*, *11*–*15*). Thus, they are representative of the full spectrum of solid ^{4}He effects to be explained. Equivalent effects were detected in four different samples studied in two different cells of this type (*31*). All our experiments were performed at a maximum wall velocity of less than 4.5 μm/s.

To examine the relaxational characteristics of solid ^{4}He, we perform the experiments outlined in fig. S1 (*31*). The temperature is decreased stepwise from an initial temperature T_i to a final equilibrium temperature T_{eq}, and the rapid coevolution of f and D is observed as the ther-

[1]Laboratory of Atomic and Solid State Physics, Department of Physics, Cornell University, Ithaca, NY 14853, USA. [2]Department of Physics, Kyoto University, Kyoto 606-8502, Japan. [3]T-Division, Center for Integrated Nanotechnologies, MS B 262, Los Alamos National Laboratory, Los Alamos, NM 87545, USA. [4]Scottish Universities Physics Alliance, School of Physics and Astronomy, University of St. Andrews, St. Andrews, Fife KY16 9SS, Scotland, UK.

*These authors contributed equally to this work.
†To whom correspondence should be addressed. E-mail: jcdavis@ccmr.cornell.edu

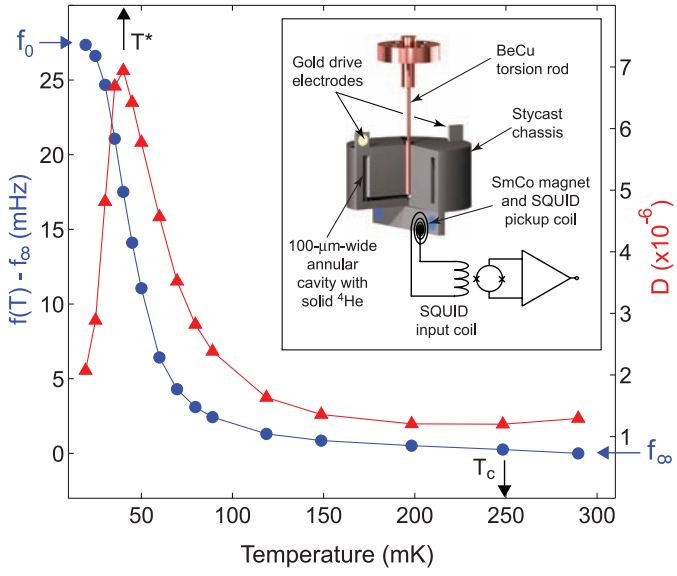

Fig. 1. The resonant frequency shift $f(T) - f_\infty$ (blue circles) and dissipation $D(T) \equiv Q^{-1}(T)$ (red triangles) for our TO-solid ^{4}He system. Indicated with black arrows are T^*, the temperature at which $D(T)$ peaks and the slope of $f(T) - f_\infty$ is maximal, and T_c, the temperature at which a change in $f(T) - f_\infty$ becomes detectable above the noise. (**Inset**) A schematic of the superconducting quantum interference device (SQUID)–based torsional oscillator (TO). Applying an ac voltage to the drive electrodes rotates the Stycast chassis (containing the solid ^{4}He in a 100-μm-wide annular cavity of radius 4.5 mm) about the axis of the BeCu torsion rod. The angular displacement of a SmCo magnet mounted on the TO generates a change in the magnetic flux through the stationary pickup and input coils of a dc-SQUID circuit and thereby a voltage proportional to displacement.

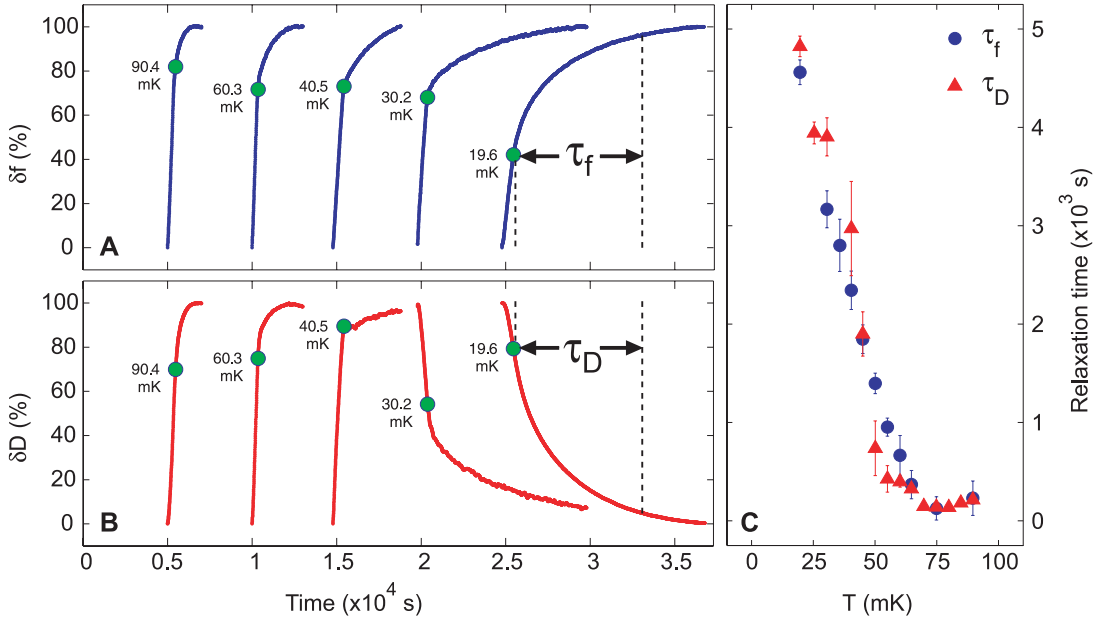

Fig. 2. Measured traces of (**A**) $f(t,T)$ and of (**B**) $D(t,T)$ for the stepwise-cooling experiment described in the text and fig. S1. These traces are recorded for times $t < t_{eq}$ while the mixing-chamber temperature cools from T_i to T_{eq} (before the green dot) and then slow relaxation of $f(t,T_{eq})$ and $D(t,T_{eq})$ for longer times $t > t_{eq}$. The traces are normalized according to $\delta f \equiv [f(t,T) - f(0,T_i)]/[f(\infty,T_{eq}) - f(0,T_i)]$ and $\delta D \equiv [D(t,T) - D(0,T_i)]/[D(\infty,T_{eq}) - D(0,T_i)]$ for comparison at different temperatures T_{eq}. (**C**) Measured temperature dependence of $\tau_f(T)$ and $\tau_D(T)$, the relaxation time constants for frequency and for dissipation as defined in the text.

mometers approach T_{eq}. More importantly, the subsequent changes after the thermometers equilibrate, $f(t,T_{eq})$ and $D(t,T_{eq})$, are measured. Data from five representative experiments are shown in Fig. 2, A and B, with each trace offset by 5000 s for clarity. In Fig. 2A, the vertical axis represents the percentage of the total frequency change during each experiment. In Fig. 2B, it represents the percentage of the equivalent total dissipation change. The green circles denote the time t_{eq} at which the mixing-chamber temperature equilibrates. Though for the initial $t < t_{eq}$ part of each trace both $f(t)$ and $D(t)$ change rapidly with temperature, their slopes change sharply at t_{eq}, indicating that the solid inside the TO maintains thermal equilibrium with the mixing chamber.

Before the "supersolid" signature appears, Fig. 2, A and B, reveal that these relaxation rates are independent of temperature and less than 100 s. But below this temperature, they begin to increase rapidly. The time constants for relaxation processes in f and D, $\tau_f(T)$ and $\tau_D(T)$, are indicated schematically in Fig. 2, A and B. They are measured by fitting the exponential $f(t) = C_1 - C_2 \exp(-t/\tau_f(T))$ and $D(t) = C_3 - C_4 \exp(-t/\tau_D(T))$ to each trace for times $t > t_{eq} = 0$. Both $\tau_f(T)$ and $\tau_D(T)$ increase rapidly on indistinguishable trajectories (Fig. 2C), indicating that the ultraslow relaxation processes in f and D are intimately linked. Such ultraslow dynamics in the "supersolid" state have also been observed elsewhere (*20*, *32*, *33*). It is difficult to reconcile any of these effects with thermal relaxation in a superfluid. Therefore, a better understanding of the relaxation dynamics of amorphous solid ^{4}He is required.

We first examine the relation between the relaxation dynamics of dissipation and the frequency shift as both approach their long-time equilibrium states. In the relevant experiment [fig. S2 (*31*)], the ^{4}He sample is cooled to 17 mK and then equilibrated for a time $t > 20{,}000$ s to achieve an unchanging state. It is then heated abruptly to a temperature T, and the subsequent relaxation dynamics in both $f(t,T)$ and $D(t,T)$ are monitored. The resulting time dependence of dissipation $D(t,T)$ is shown in Fig. 3A. At short times after temperature stabilization, the dissipation increases slightly (dark blue in Fig. 3A). However, these dissipative processes are actually very far out of equilibrium. As time passes, the dissipation slowly increases on a trajectory indicated by the transition from the blue line representing $D(t,T)$ at $t \sim 50$ s to the dark red line representing $D(t,T)$ at ~5000 s. In the same experiment, the time dependence of $f(t,T)$ is also measured (Fig. 3B). It differs from that of $D(t,T)$; at shortest times after stabilization at T the frequency has already changed greatly from its lowest-temperature value (Fig. 3B). This means that much of the frequency change responds immediately to the mixing-chamber temperature change (and therefore also that rapid thermal equilibrium always exists between the sample and the mixing-chamber thermometer). The subsequent evolution of the remaining component of the frequency shift exhibits an ultraslow reduction in f, as indicated by the transition from the blue line at $t \sim 50$ s to the dark red line representing $t \sim 5000$ s in Fig. 3B. These data illustrate how the slowing relaxation dynamics within $D(t,T)$ and $f(t,T)$ are synchronized in such samples of solid ^{4}He.

They also imply that thermal hysteresis should occur when temperatures are swept faster than the relevant time constants in Fig. 3, A and B. In Fig. 3C, swept-temperature measurements on the same sample show that thermal hysteresis occurs in both $f(t,T)$ and $D(t,T)$, with their long-time equilibrium values (solid circles) falling within the hysteresis loops as expected.

These extraordinary relaxation dynamics in $D(t,T)$ and $f(t,T)$ are unexpected in the context of a familiar superfluid. But effects analogous to these are seen during the freeze-out of excitations at a dielectric glass transition (*34*).Thus, the phenomenology of solid ^{4}He might also be due to a freeze-out of an ensemble of excitations within the solid (*22*). Indeed, there have been numerous proposals (*27*–*30*) that solid ^{4}He is a "superglass"—some form of granular superfluid within an amorphous solid.

To examine such hypotheses, we consider the total rotational susceptibility $\chi(\omega,T)$ of the TO plus solid ^{4}He sample (*22*). A classic Debye susceptibility describing the freeze-out of an ensemble of identical excitations with decay time $\tau(T)$ is $\chi_D^{-1}(\omega, T) = g_0/(1 - i\omega\tau(T))$. For solid ^{4}He, g_0/ω_0^2 would represent the rotational inertia associated with the relevant excitations. Their "back action" on the TO would appear in the total susceptibility as

$$\chi^{-1}(\omega, T) = K - I\omega^2 - i\gamma\omega - g_0/(1 - i\omega\tau(T)) \quad (1)$$

where γ is the intrinsic damping constant of the TO ($\omega_0 = \sqrt{K/I} = 2\pi f_0$; Fig. 1). The effect of changing the temperature can be captured entirely by the Debye term χ_D^{-1}, whose real and imaginary parts are

$$\Re[\chi_D^{-1}(T)] = \frac{g_0}{1 + \omega_0^2\tau^2}$$

$$\Im[\chi_D^{-1}(T)] = \frac{g_0\omega_0\tau}{1 + \omega_0^2\tau^2} \quad (2A, 2B)$$

at $\omega = \omega_0$. Thus, when one susceptibility component changes due to the $\tau(T)$ term, the other

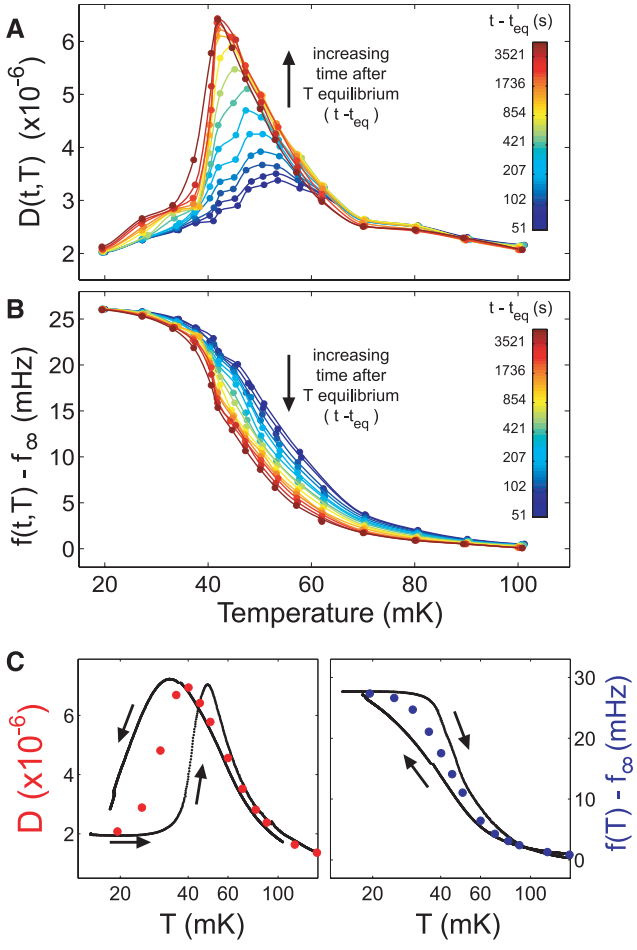

Fig. 3. Measured time evolution of (**A**) $D(t,T)$ and (**B**) $f(t,T)$ for the abrupt warming experiment described in the text and fig. S2. The data are colored circles and the lines are smooth interpolations, intended as a guide to the eye. The dark blue lines represent $D(t,T)$ and $f(t,T)$ at $t \sim 50$ s, while the dark red lines represent $D(t,T)$ and $f(t,T)$ at ~5000 s. (**C**) Thermal hysteresis in the dynamical response as shown by the black curves in $D(T)$ (left) and in $f(T)$ (right), with the direction of the temperature change indicated by a black arrow. The data indicated by red and blue circles were acquired after waiting $t >> 5 \times 10^3$ s at each temperature as the dynamical response [of (A) and (B)] asymptotically approached the infinite-time limit.

must always change in a quantitatively related manner. Such changes are measurable because

$$\frac{2(f_0 - f(T))}{f_0} = \frac{1}{I\omega_0^2}\Re[\chi_D^{-1}(T)]$$

$$D(T) - D_\infty = \frac{1}{I\omega_0^2}\Im[\chi_D^{-1}(T)] \qquad (3A, 3B)$$

within the Debye model with suitable approximations (*31*); $D_\infty \equiv \gamma/I\omega_0$. Moreover a well-defined characteristic temperature T^* for such a susceptibility occurs when $\omega_0\tau(T^*) = 1$; both the $f(T)$ slope and the dissipation $D(T)$ achieve their maxima at T^* (Fig. 1).

In Fig. 4A (left), we show a fit of Eq. 3B to the measured $D(T)$ as a red line, while Fig. 4A (right) shows the resulting prediction from Eq. 3A for $f(T)$ as the blue line. Comparison to the measured $f(T)$ (solid blue circles) shows that this Debye susceptibility is inconsistent with the relation between $D(T)$ and $f(T)$. Nevertheless, as the relaxation processes of $D(t,T)$ and $f(t,T)$ are synchronized (Fig. 3), there must be an intimate relation between $\Re[\chi^{-1}(t,T)]$ and $\Im[\chi^{-1}(t,T)]$. To study this relation, one should replot the data from Fig. 3, A and B, in the complex plane with axes defined by $\Im[\chi_D^{-1}]$ and $\Re[\chi_D^{-1}]$ [a Davidson-Cole (D-C) plot (*31*)]. This is a classic technique in which departures of the data from the Debye model appear as geometric features that can reveal characteristics of the underlying physical mechanism linking $\Re[\chi^{-1}(t,T)]$ and $\Im[\chi^{-1}(t,T)]$.

We therefore plot $\Delta D(T) = D(T) - D_\infty$ versus $\frac{2(f_0 - f(T))}{f_0}$ in Fig. 4B. It reveals that, instantaneously upon warming, the D-C plot is a symmetric elliptical curve, whereas after several thousand seconds, the response has evolved into the skewed D-C curve more familiar from studies of the dielectric glass transition (*34*). But the maximum frequency shift expected from the maximum observed dissipation within the Debye susceptibility (vertical dashed lines) is again far too small. Moreover, no temperature equilibration lag between the solid ^{4}He sample and the mixing chamber could generate the complex dynamics reported in Fig. 4 because, for any given frequency shift, a wide variety of different dissipations are observed [see supporting online material (SOM) text].

A simple superfluid transition is inconsistent with all these observations because there should be no synchronized dissipation peak associated with $f(T)$ (Figs. 1 and 4) and no ultraslow dynamics in $f(t,T)$ and $D(t,T)$ (Figs. 2 and 3). Indeed, these phenomena are more reminiscent of the characteristics of a glass transition (*34*). Nevertheless, a simple freeze-out of excitations described by a Debye susceptibility is also quantitatively inconsistent because the dissipation peak is far too small to explain the observed frequency shift (Fig. 4A). Thus, when considered in combination with implications of the blocked annulus experiments (*9*, *16*), our observations motivate a new hypothesis in which amorphous solid ^{4}He is a supersolid, but one whose superfluid phase-stiffness can be controlled by the freeze-out of an ensemble of excitations within the solid.

Within such a model, generation of excitations at higher temperatures would suppress superfluid phase stiffness. The complex relaxation dynamics (Figs. 3 and 4) would reveal the excitation freeze-out processes. Further, the anomalously large frequency shifts (Fig. 4) would occur predominantly because of superfluid phase stiffness appearing after excitation freezing. Such a model might also explain the diverse phenomenology of solid ^{4}He. For example, the ω dependence of T^* (*13*) would occur because T^* is the temperature for which $\tau(T^*)\omega = 1$. The shear modulus stiffening (*21*) would occur because of the freeze-out of motion of these excitations, and T^* would increase with ^{3}He concentration (*8*, *11*) because, with pinning, higher temperatures would be required to achieve the excitation rate $\tau(T^*)\omega_0 = 1$. Finally, sample-preparation effects (*10*, *12*) and different responses from different TO types would occur because the amorphousness allowing these excitations would depend on annealing and TO design.

Independent of these hypotheses, important new features of solid ^{4}He are revealed here. We find synchronized ultraslow relaxation dynamics of dissipation $D(T)$ and a component of frequency shift of $f(T)$ in TOs containing amorphous solid ^{4}He (Fig. 3). Such phenomena are reminiscent of the glassy freeze-out of an ensemble of excitations and inconsistent with a simple superfluid transition. Nevertheless, although the evolutions of $f(T)$ and $D(T)$ are linked dynamically, the situation is also inconsistent with the simple excitation freezing transition because there is an anomalously large frequency shift (Fig. 4). One possible explanation is that solid ^{4}He is not a supersolid and that the appropriate rotational susceptibility model for its transition will be identified eventually. But if superfluidity is the correct interpretation of blocked annulus experiments (*9*, *16*), then our results indicate that solid ^{4}He supports an exotic supersolid in which the glassy freeze-out at T^* of an unknown excitation within the amorphous solid controls the superfluid phase stiffness. Such a state could be designated a "superglass."

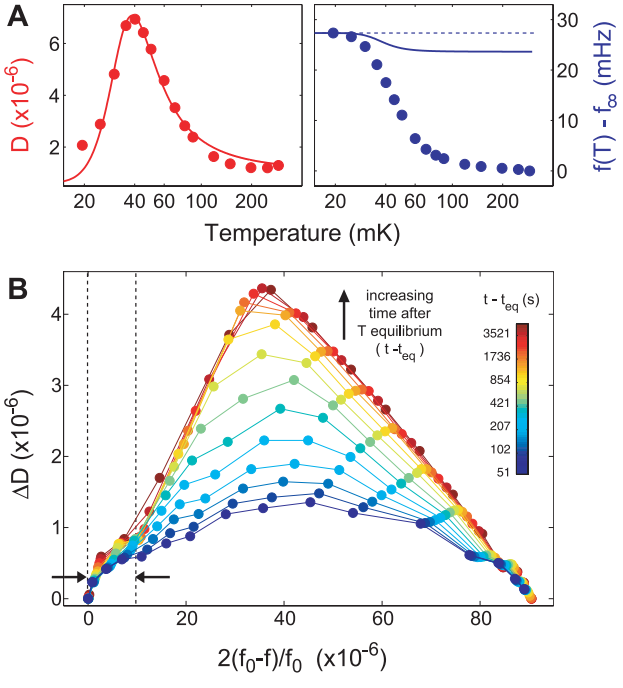

Fig. 4. (**A**) Comparison of equilibrated $D(T)$ and $f(T)$ data with simple Debye model of susceptibility in Eq. 1. The long-time equilibrated data $D(T)$ (left) and $f(T)$ (right) are plotted as filled circles. The dashed line indicates f_0. The solid curves represent the predicted relation between the susceptibilities for a simple glassy freeze-out transition. Although the dissipation $D(T)$ can be fit reasonably well by this model (*22*), the magnitude of the frequency shift that is then predicted is markedly smaller than observed. (**B**) Time-dependent D-C plot. This is a parametric plot of the data shown in Fig. 3, A and B, made by removing the explicit dependence on temperature, with axes defined by $\Im[\chi_D^{-1}]$ and $\Re[\chi_D^{-1}]$ (Eq. 3). The vertical dashed lines indicate the maximum value of $2(f_0 - f)/f_0$ that would be predicted by the Debye susceptibility (Eq. 1), given the peak height of $\Delta D = D - D_\infty$ (*31*).

References and Notes

1. D. Thouless, *Ann. Phys.* **52**, 403 (1969).
2. A. F. Andreev, I. M. Lifshitz, *Sov. Phys. JETP* **29**, 1107 (1969).
3. L. Reatto, *Phys. Rev.* **183**, 334 (1969).
4. G. V. Chester, *Phys. Rev. A* **2**, 256 (1970).
5. A. J. Leggett, *Phys. Rev. Lett.* **25**, 1543 (1970).
6. M. W. Meisel, *Physica B* **178**, 121 (1992).
7. D. R. Tilley, J. Tilley, *Superfluidity and Superconductivity* (IOP, Bristol, UK, ed. 3, 1990).
8. E. Kim, M. H. W. Chan, *Nature* **427**, 225 (2004).
9. E. Kim, M. H. W. Chan, *Science* **305**, 1941 (2004).
10. A. C. Clark, J. T. West, M. H. W. Chan, *Phys. Rev. Lett.* **99**, 135302 (2007).
11. E. Kim *et al.*, *Phys. Rev. Lett.* **100**, 065301 (2008).
12. A. S. C. Rittner, J. D. Reppy, *Phys. Rev. Lett.* **97**, 165301 (2006).
13. Y. Aoki, J. C. Graves, H. Kojima, *Phys. Rev. Lett.* **99**, 015301 (2007).
14. A. Penzev, Y. Yasuta, M. Kubota, *J. Low Temp. Phys.* **148**, 677 (2007).
15. M. Kondo, S. Takada, Y. Shibayama, K. Shirahama, *J. Low Temp. Phys.* **148**, 695 (2007).
16. A. S. C. Rittner, J. D. Reppy, *Phys. Rev. Lett.* **101**, 155301 (2008).
17. S. Sasaki, R. Ishiguro, F. Caupin, H. J. Maris, S. Balibar, *Science* **313**, 1098 (2006).
18. J. Day, J. Beamish, *Phys. Rev. Lett.* **96**, 105304 (2006).
19. M. W. Ray, R. B. Hallock, *Phys. Rev. Lett.* **100**, 235301 (2008).

20. A. C. Clark, J. D. Maynard, M. H. W. Chan, *Phys. Rev. B* **77**, 184513 (2008).
21. J. Day, J. Beamish, *Nature* **450**, 853 (2007).
22. Z. Nussinov, A. V. Balatsky, M. J. Graf, S. A. Trugman, *Phys. Rev. B* **76**, 014530 (2007).
23. A. F. Andreev, *JETP Lett.* **85**, 585 (2007).
24. P. W. Anderson, *Nat. Phys.* **3**, 160 (2007).
25. L. Pollet *et al.*, *Phys. Rev. Lett.* **98**, 135301 (2007).
26. C.-D. Yoo, A. Dorsey, *Phys. Rev. B* **79**, 100504 (2009).
27. M. Boninsegni *et al.*, *Phys. Rev. Lett.* **96**, 105301 (2006).
28. J. Wu, P. Phillips, *Phys. Rev. B* **78**, 014515 (2008).
29. J. Bossy, J. V. Pearce, H. Schober, H. R. Glyde, *Phys. Rev. B* **78**, 224507 (2008).
30. G. Biroli, C. Chamon, F. Zamponi, *Phys. Rev. B* **78**, 224306 (2008).
31. Materials and methods are available as supporting material on *Science* Online.
32. Y. Aoki, M. C. Keiderling, H. Kojima, *Phys. Rev. Lett.* **100**, 215303 (2008).
33. V. N. Grigor'ev *et al.*, *Phys. Rev. B* **76**, 224524 (2007).
34. B. K. P. Scaife, *Principles of Dielectrics* (Clarendon, Oxford, UK, 1989).
35. We acknowledge and thank J. Beamish, M. W. H. Chan, A. Clark, A. Dorsey, M. Graf, E. Mueller, S. Nagel, M. Paalanen, R. E. Packard, J. Parpia, J. D. Reppy, A. S. Rittner, J. Saunders, J. P. Sethna, and Wm. Vinen for helpful discussions and communications. These studies were initiated under NSF grant DM-0434801 and are now partially supported under grant DMR-0806629 and by Cornell University; B.H. acknowledges support by the Natural Sciences and Engineering Research Council of Canada. M.Y. acknowledges support from the Japan Society for the Promotion of Science. Work at Los Alamos was supported by the U.S. Department of Energy.

Supporting Online Material

www.sciencemag.org/cgi/content/full/324/5927/632/DC1
Materials and Methods
SOM Text
Figs. S1 to S6
References

9 December 2008; accepted 18 March 2009
10.1126/science.1169512

Competition for Light Causes Plant Biodiversity Loss After Eutrophication

Yann Hautier,[1]* Pascal A. Niklaus,[1,2] Andy Hector[1]

Human activities have increased the availability of nutrients in terrestrial and aquatic ecosystems. In grasslands, this eutrophication causes loss of plant species diversity, but the mechanism of this loss has been difficult to determine. Using experimental grassland plant communities, we found that addition of light to the grassland understory prevented the loss of biodiversity caused by eutrophication. There was no detectable role for competition for soil resources in diversity loss. Thus, competition for light is a major mechanism of plant diversity loss after eutrophication and explains the particular threat of eutrophication to plant diversity. Our conclusions have implications for grassland management and conservation policy and underscore the need to control nutrient enrichment if plant diversity is to be preserved.

Fertilization experiments (*1*–*4*) and studies of nutrient deposition in terrestrial ecosystems (*5*) show that increases in the availability of nitrogen (*5*, *6*), phosphorus (*7*), and other nutrients—both alone and in combination (*1*, *4*)—usually increase primary productivity and decrease plant diversity. Given that anthropogenic activity has doubled global phosphorus liberation and plant-available nitrogen during the past 50 years (*8*, *9*), and that nutrient inputs are predicted to be one of the three major drivers of biodiversity loss this century (*10*), understanding the mechanisms responsible for diversity loss after eutrophication will be important for the development of effective conservation policies (*11*).

Most of the hypotheses proposed to explain the reduction in plant diversity after eutrophication focus on changes in competition (*12*–*15*). Fertilization may increase the strength of competition generally—that is, both above and below ground (*15*)—or it could increase the strength of aboveground competition for light only: an asymmetric process due to the directional supply of this resource (*13*, *14*). The hypothesis of increased competition for light (*14*) predicts that as productivity increases, availability of light to plants in the understory is reduced, leading to their exclusion by faster-growing or taller species that preempt this directionally supplied resource (*16*, *17*). Surprisingly, 35 years after these alternative hypotheses were suggested, there is no consensus on the role of competition as a mechanism of plant diversity loss after eutrophication (*18*, *19*).

To test whether diversity loss after eutrophication is due to increased competition for light, we added light to the understory of fertilized grassland communities—a manipulation inspired by competition experiments with algae (*20*, *21*). A key advance of our approach relative to earlier work (*22*) is that it restores light to the species in the lower canopy that are thought to decrease in diversity as a result of deeper shading after the increase in aboveground productivity caused by eutrophication. We conducted a glasshouse experiment that combined addition of fertilizer and supplementary light in a fully factorial design. The 32 experimental plant communities were pregrown in the field for 4 years (*23*) before they were extracted with intact soil blocks and moved to the glasshouse. For generality, the communities comprised four different sets of six species (*23*) that had similar levels of diversity and, as we show, responded similarly to the experimental treatments.

Light was added to the understory of each treated community using a system of three fluorescent tubes that were raised as the canopy grew (Fig. 1). Reflectors were placed above the fluorescent tubes to direct light into the understory and to prevent it from shining up onto the underside of the leaves of the taller species. To keep conditions other than light and fertilization as similar as possible, we installed the same system of fluorescent tubes in communities without supplementary light, but in this case reflectors were placed above and below the tubes to form a closed chamber from which the light could not escape. With this system, we were able to experimentally manipulate light in the understory while holding other conditions (such as temperature) constant. Aboveground biomass was harvested twice a year during 2006 and 2007 to coincide with the cutting regimes typical of European meadows, and other key variables (including belowground biomass production, canopy height, availability of light in the understory, soil pH, and plant diversity) were regularly monitored (*24*).

After 2 years of treatment, fertilization had increased net aboveground biomass production and decreased diversity (*24*). During the second year, fertilization significantly increased production from an average of 356 ± 39 g m^{-2} (mean ± SEM) per harvest in the control communities to 450 ± 39 g m^{-2} in the fertilized treatment (Fig. 2A and table S1). The percentage of photosynthetically active radiation in the understory of the fertilized plots (5 ± 4%) was significantly lower than for the controls (13 ± 4%) (Fig. 2B). Notably, when increased production was accompanied by decreased light in the understory, fertilization significantly reduced species richness (Fig. 2C): On average, 2.6 species were lost in the fertilization treatment relative to the control, around one-third of the original species richness. This loss of diversity after eutrophication is consistent with longer-term field studies (*1*, *5*).

When applied together with fertilization, the additional understory light compensated for the increased shading caused by the greater aboveground biomass production and generated levels of understory light (12 ± 4%) that were indistinguishable from those in the control plots (13 ± 4%) (Fig. 2B and table S1). Supplementing understory light in the fertilization treatment to levels similar to the control plots prevented the loss of

[1]Institute of Environmental Sciences, University of Zürich, Winterthurerstrasse 190, CH-8057 Zürich, Switzerland. [2]Institute of Plant Sciences, ETH Zürich, Universitätstrasse 2, CH-8092 Zürich, Switzerland.

*To whom correspondence should be addressed. E-mail: yhautier@uwinst.uzh.ch

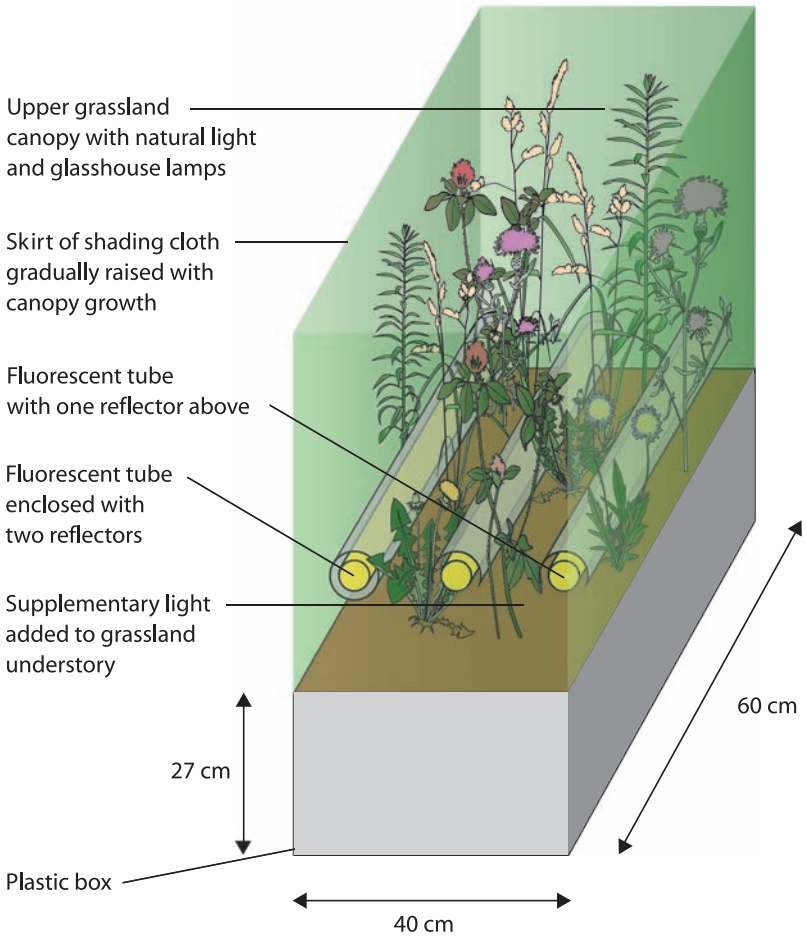

Fig. 1. Schematic representation of the experimental understory light addition. To save space, two open lights and one closed light are shown in the same experimental unit. The four treatment combinations were "control" (unfertilized, closed lights), "fertilization" (fertilized, closed lights), "light" (unfertilized, open lights), and "fertilization + light" (fertilized, open lights). For generality these four treatments were applied to four different plant communities, with each combination replicated twice ($n = 4 \times 4 \times 2 = 32$).

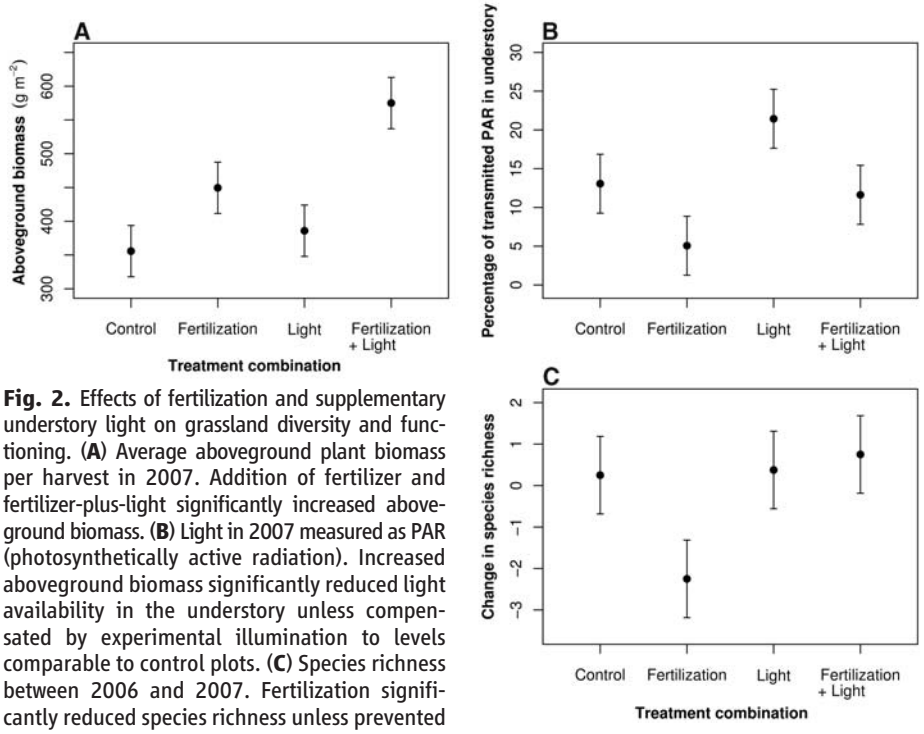

Fig. 2. Effects of fertilization and supplementary understory light on grassland diversity and functioning. (**A**) Average aboveground plant biomass per harvest in 2007. Addition of fertilizer and fertilizer-plus-light significantly increased aboveground biomass. (**B**) Light in 2007 measured as PAR (photosynthetically active radiation). Increased aboveground biomass significantly reduced light availability in the understory unless compensated by experimental illumination to levels comparable to control plots. (**C**) Species richness between 2006 and 2007. Fertilization significantly reduced species richness unless prevented by the addition of supplementary light to the understory. Points denote treatment means, and the intervals show least significant differences (treatments with nonoverlapping intervals are significantly different at $P = 0.05$).

species and maintained comparable levels of diversity (Fig. 2C). This result was general across the four different plant communities used in the experiment; the variance component for the different species mixtures accounted for only 10% of the total of the summed variance components and was nonsignificant (likelihood ratio test: log likelihood = 1.05; $\chi^2 = 2.10$; $P = 0.15$). By mitigating the loss of diversity caused by fertilization, this result supports the hypothesis that increased competition for light was the mechanism responsible for the decline in species richness after eutrophication.

Our communities experienced species turnover that resulted from the loss of resident species and the gain of new species from the seed bank. As in several previous studies (*25*–*27*), the decrease in diversity caused by fertilization was due mainly to a decline in the numbers of species gained (Fig. 3), from 3.2 in the controls to 1.6 in the fertilized plots (table S2). This result was also consistent across the four nonoverlapping communities used in our experiment: The variance component for the different species mixtures only accounted for 2.5% of the total of the summed variance components and was nonsignificant (likelihood ratio test: log likelihood = 0.81; $\chi^2 = 1.61$; $P = 0.20$). There was a marginally significant bias against the establishment of short-statured

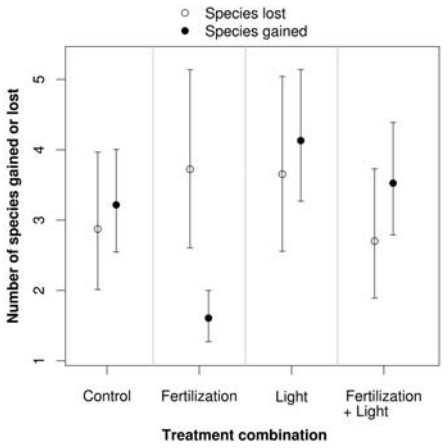

Fig. 3. Species turnover. Decreased diversity in fertilized plots was mainly caused by reduced numbers of species gained. Results are shown as in Fig. 2.

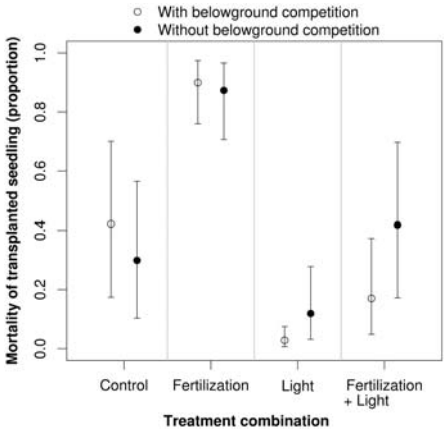

Fig. 4. Seedling mortality. Fertilization significantly increased seedling mortality. Removing belowground competition had little impact on seedling mortality, which suggests that competition for soil resources plays no detectable role in diversity loss. Results are shown as in Fig. 2.

perennial grasses and forbs, but the overall response was not driven by particular species (*24*).

Our understory light addition treatment also had consequences for ecosystem functioning. Net aboveground biomass production in the controls was limited by nutrients (although we cannot exclude light limitation of the taller species as well) because it was increased by fertilization (Fig. 2A and table S1). Without fertilization, the productivity of plants in the understory was not light-limited, because supplementary light had no effect when applied to unfertilized communities (Fig. 2A). However, the productivity of plants in the understory of the fertilization treatment was light-limited, because in fertilized communities the additional light increased average net aboveground production per harvest to 575 ± 39 g m^{-2} (Fig. 2A). These responses suggest colimitation of productivity by light and nutrients, where the taller species are nutrient-limited while understory species in the fertilization treatment are light-limited. More generally, our results suggest that productivity of the upper canopy and understory can be limited by different factors as a result of the directional supply of light.

Species loss could be due to increased competition both above and below ground (*15*). To address this possibility, in the second year of the glasshouse experiment we added seedlings of two species not originally present to the 32 experimental communities to measure the strength of belowground competition. Transplanted seedlings planted in plastic tubes to reduce belowground competition were compared with seedlings exposed to full root competition. The results were consistent with competition for light as the main mechanism of diversity loss: When grown without root exclusion tubes (that is, with belowground competition), seedling mortality (as a proportion) strongly increased with nutrient addition from 0.29 to 0.87, but was comparable to control plots when fertilization occurred together with understory lighting (Fig. 4 and table S3A). The results provided no support for a role of belowground competition in the loss of biodiversity (table S4): Removing belowground competition from fertilized plots had no detectable impact on seedling mortality (table S3B) or seedling biomass (change in biomass = 0.3 g, 95% confidence interval = –1.0 to 1.4).

Although other processes can also contribute to diversity loss, there was no evidence that they were important in our study. Fertilization can reduce grassland diversity through acidification (*2*) or through the accumulation of plant litter (*25*, *26*, *28*, *29*). However, we found no detectable differences in pH after fertilization (fig. S1 and table S5). There was also little buildup of litter during our experiment, which suggests that the negative effects of increased aboveground productivity might have strengthened in the longer term if litter accumulation had occurred.

Together, our results are consistent with increased competition for light as a major mechanism of diversity loss after eutrophication of grassland communities. Fertilization increased productivity and canopy height, and led to reduced light in the understory. In turn, this led to a reduction in diversity, particularly of low-statured perennial grasses and forbs, mainly through reduced recruitment. Other mechanisms also cause loss of plant diversity, but they played no detectable role in our case. Supplementing levels of understory light in fertilized communities reduced competition for light, sustained seedling establishment, and maintained plant diversity despite the additional nutrient inputs.

Some earlier studies (*30*) have demonstrated the importance of competition for light indirectly by tying back the vegetation. Our results advance a long-running debate in community ecology by providing a direct experimental demonstration of the importance of asymmetric competition for light as a mechanism of plant diversity loss. More generally, our work explains and emphasizes the need to develop conservation policies and management procedures that prevent eutrophication if biodiversity is to be conserved.

References and Notes

1. W. S. Harpole, D. Tilman, *Nature* **446**, 791 (2007).
2. J. Silvertown *et al.*, *J. Ecol.* **94**, 801 (2006).
3. L. Gough, C. W. Osenberg, K. L. Gross, S. L. Collins, *Oikos* **89**, 428 (2000).
4. M. J. Crawley *et al.*, *Am. Nat.* **165**, 179 (2005).
5. C. J. Stevens, N. B. Dise, J. O. Mountford, D. J. Gowing, *Science* **303**, 1876 (2004).
6. C. M. Clark, D. Tilman, *Nature* **451**, 712 (2008).
7. M. J. Wassen, H. O. Venterink, E. D. Lapshina, F. Tanneberger, *Nature* **437**, 547 (2005).
8. P. M. Vitousek, H. A. Mooney, J. Lubchenco, J. M. Melillo, *Science* **277**, 494 (1997).
9. D. Tilman *et al.*, *Science* **292**, 281 (2001).
10. O. E. Sala *et al.*, *Science* **287**, 1770 (2000).
11. D. Tilman, K. G. Cassman, P. A. Matson, R. Naylor, S. Polasky, *Nature* **418**, 671 (2002).
12. J. P. Grime, *Plant Strategies, Vegetation Processes, and Ecosystem Properties* (Wiley, Chichester, UK, ed. 2, 2002).
13. D. Tilman, *Resource Competition and Community Structure* (Princeton Univ. Press, Princeton, NJ, 1982).
14. E. I. Newman, *Nature* **244**, 310 (1973).
15. J. P. Grime, *Nature* **242**, 344 (1973).
16. K. N. Suding *et al.*, *Proc. Natl. Acad. Sci. U.S.A.* **102**, 4387 (2005).
17. E. Vojtech, L. A. Turnbull, A. Hector, *PLoS One* **2**, e499 (2007).
18. C. M. Clark *et al.*, *Ecol. Lett.* **10**, 596 (2007).
19. T. K. Rajaniemi, *Oikos* **101**, 449 (2003).
20. J. Huisman, R. R. Jonker, C. Zonneveld, F. J. Weissing, *Ecology* **80**, 211 (1999).
21. J. Passarge, S. Hol, M. Escher, J. Huisman, *Ecol. Monogr.* **76**, 57 (2006).
22. L. Eek, K. Zobel, *Ecography* **24**, 157 (2001).
23. L. Wacker, O. Baudois, S. Eichenberger-Glinz, B. Schmid, *Basic Appl. Ecol.* **9**, 467 (2008).
24. See supporting material on *Science* Online.
25. B. L. Foster, K. L. Gross, *Ecology* **79**, 2593 (1998).
26. D. Tilman, *Ecology* **74**, 2179 (1993).
27. M. H. H. Stevens, D. E. Bunker, S. A. Schnitzer, W. P. Carson, *J. Ecol.* **92**, 339 (2004).
28. F. Berendse, *Trends Ecol. Evol.* **14**, 4 (1999).
29. E. G. Lamb, *Ecology* **89**, 216 (2008).
30. N. C. Emery, P. J. Ewanchuk, M. D. Bertness, *Ecology* **82**, 2471 (2001).

31. We thank E.-D. Schulze and C. Körner for discussion of light manipulation, B. Schmid and L. Turnbull for comments on the manuscript, and L. Wacker, E. Vojtech, G. Feichtinger, and T. Zwimpfer for helpful suggestions and field work assistance. Y.H. is funded by Swiss National Foundation grant 3100A0-107572 to A.H. The project was conceived by A.H., designed by A.H., P.A.N., and Y.H., conducted by Y.H., analyzed by Y.H. and A.H., and written up by Y.H. and A.H. with input from P.A.N.

Supporting Online Material

www.sciencemag.org/cgi/content/full/324/5927/636/DC1
Materials and Methods
SOM Text
Figs. S1 to S3
Tables S1 to S7
References

11 December 2008; accepted 19 February 2009
10.1126/science.1169640

γ-Secretase Heterogeneity in the Aph1 Subunit: Relevance for Alzheimer's Disease

Lutgarde Serneels,[1,2*] Jérôme Van Biervliet,[1,2*] Katleen Craessaerts,[1,2] Tim Dejaegere,[1,2] Katrien Horré,[1,2] Tine Van Houtvin,[1,2] Hermann Esselmann,[3,4] Sabine Paul,[3,4] Martin K. Schäfer,[5] Oksana Berezovska,[6] Bradley T. Hyman,[6] Ben Sprangers,[7] Raf Sciot,[8] Lieve Moons,[9] Mathias Jucker,[10] Zhixiang Yang,[11] Patrick C. May,[11] Eric Karran,[12]† Jens Wiltfang,[3,4] Rudi D'Hooge,[13] Bart De Strooper[1,2]‡

The γ-secretase complex plays a role in Alzheimer's disease and cancer progression. The development of clinically useful inhibitors, however, is complicated by the role of the γ-secretase complex in regulated intramembrane proteolysis of Notch and other essential proteins. Different γ-secretase complexes containing different Presenilin or Aph1 protein subunits are present in various tissues. Here we show that these complexes have heterogeneous biochemical and physiological properties. Specific inactivation of the Aph1B γ-secretase in a mouse Alzheimer's disease model led to improvements of Alzheimer's disease–relevant phenotypic features without any Notch-related side effects. The Aph1B complex contributes to total γ-secretase activity in the human brain, and thus specific targeting of Aph1B-containing γ-secretase complexes may help generate less toxic therapies for Alzheimer's disease.

γ-Secretase activity is responsible for the final cleavage of the amyloid precursor protein (APP), causing release of the Aβ peptide that accumulates in the amyloid plaques characteristic for Alzheimer's disease (AD) (*1*). The same activity cleaves Notch, N-Cadherin, and other important signaling molecules. γ-Secretase activity is mediated by a multiprotein complex consisting of Presenilin (PS), Aph1, Pen2, and Nicastrin (NCT) (*2*). Two *presenilin* (*PS1* and *PS2*) genes and two *APH1* (*APH1A* and *APH1B*) genes, which are alternatively spliced, contribute to the heterogeneity of the complexes (*3*, *4*). The Aph1A complexes are crucial for Notch signaling during embryogenesis (*5*, *6*), although functional analysis of APH1B (~58% homologous to APH1A) is complicated because of the rodent-specific duplication of the gene (*Aph1C*). The combined inactivation of *Aph1B* and *Aph1C* (*Aph1BC*$^{-/-}$) does not result in any overt phenotype, although disruption of Nrg1 cleavage in the brain of *Aph1BC*$^{-/-}$ mice (*7*) results in behavioral changes that are very similar to the ones observed in β-secretase–deficient (Bace1$^{-/-}$) mice (*8*).

To evaluate the specific biochemical properties of the different Aph1 subunits, we rescued

[1]Department for Molecular and Developmental Genetics, VIB, KULeuven, Herestraat 49, 3000 Leuven, Belgium. [2]Center for Human Genetics, KULeuven, Herestraat 49, 3000 Leuven, Belgium. [3]Department of Psychiatry and Psychotherapy, University of Erlangen-Nuremberg, 91054 Erlangen, Germany. [4]Department of Psychiatry and Psychotherapy, Rhine State Hospital Essen, University of Duisburg-Essen, D-45147 Essen, Germany. [5]Department of Molecular Neurosciences, Institute of Anatomy and Cell Biology, Philipps University, D-35032 Marburg, Germany. [6]Harvard Medical School, Massachusetts General Hospital, MassGeneral Institute for Neurodegenerative Disorders, Charlestown, MA 02129, USA. [7]Laboratory of Experimental Transplantation, KULeuven, 3000 Leuven, Belgium. [8]Laboratory of Morphology and Molecular Pathology, KULeuven, 3000 Leuven, Belgium. [9]Laboratory of Neural Circuit Development and Regeneration, Department of Biology, KULeuven, 3000 Leuven, Belgium. [10]Department of Cellular Neurology, Hertie-Institute for Clinical Brain Research, University of Tübingen, D-72076 Tübingen, Germany. [11]Neuroscience Discovery Research, Lilly Research Labs, Eli Lilly and Co., Indianapolis, IN 46285, USA. [12]Lilly Research Centre, Erl Wood Manor, Windlesham, Surrey GU20 6PH, UK. [13]Laboratory of Biological Psychology, Department of Psychology, KULeuven, 3000 Leuven, Belgium.

*These authors contributed equally to this work.
†Present address: Johnson and Johnson, Pharmaceutical Research and Development, 2340 Beerse, Belgium.
‡To whom correspondence should be addressed. E-mail: bart.destrooper@med.kuleuven.be

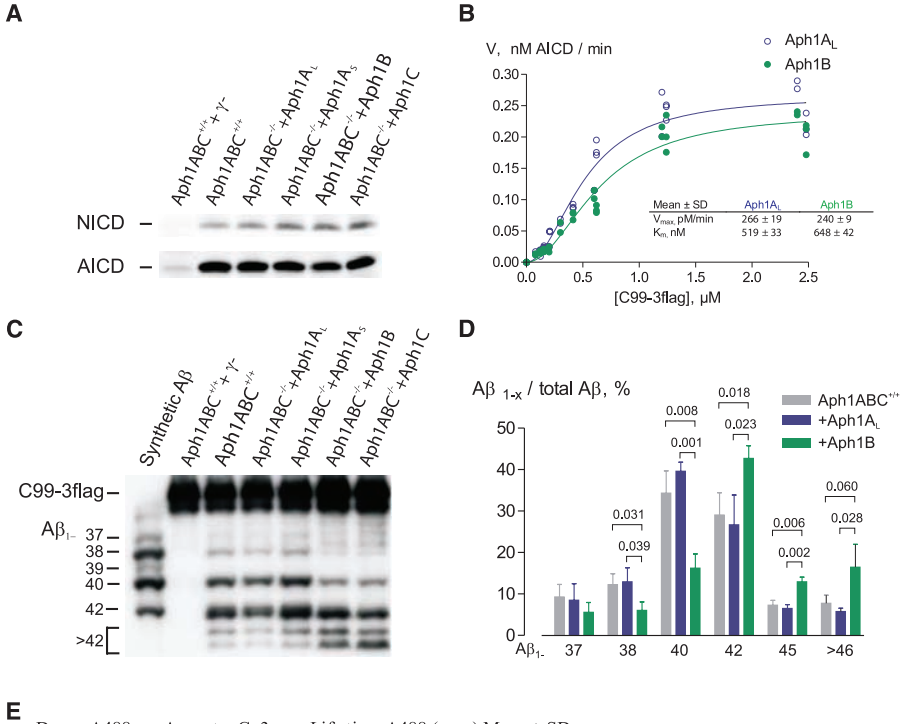

Fig. 1. Aph1B γ-secretase complexes are functional and structurally distinct relative to the Aph1A γ-secretase complexes. (**A** and **B**) Immunoblot analysis of microsomal fractions of Aph1ABC$^{+/+}$ and Aph1ABC$^{-/-}$ MEFs rescued with the indicated Aph1 isoforms demonstrates that both complexes perform ε cleavage of APP and Notch substrate. Specificity of the reaction was validated with a γ-secretase inhibitor (γ^{-}: 10 μM L-685,458). (B) The velocity, or amount of AICD generated after 3 hours, was plotted against C99-3flag concentrations. The kinetics of AICD fit a Michaelis-Menten plot with positive cooperation (Hill factor of cooperativity $h = 2$) equation. Apparent V_{max} and K_M values for AICD were statistically indistinguishable (mean ± SD, $n = 5$ independent experiments). (**C** and **D**) Urea–SDS-PAGE (polyacrylamide gel electrophoresis) of solubilized Aph1B γ-secretase complexes from MEFs results in more long ($Aβ_{1≥42}$) and fewer short ($Aβ_{1-≤40}$) Aβ species (mean ± SD, $n = 3$, $P < 0.05$ to 0.01). (**E**) Aph1ABC$^{-/-}$ MEFs reconstituted with Aph1A$_L$ or Aph1B were cotransfected with wild-type human PS1 cDNA, and Alexa488 lifetimes were measured in the absence or presence of fluorescence resonance energy transfer; Aph1B γ-secretase displays a significantly shorter life time (mean ± SD; the number of cells counted in three to four independent transfections is indicated in parentheses, $P <$ 0.01), implying a closer proximity between the donor and acceptor as schematically represented.

E

Donor A488	Acceptor Cy3	Life time A488 (psec) Mean ± SD Aph1A	Aph1B
PS1-NTF	None	2137 ± 149 (31)	
PS1-NTF	PS1-CTF	1561 ± 174 (20)	1303 ± 200** (28)
PS1-NTF	PS1-loop	1754 ± 143 (77)	1659 ± 135** (91)

triple-deficient *Aph1A*$^{-/-}$*B*$^{-/-}$*C*$^{-/-}$ (*Aph1ABC*$^{-/-}$) mouse embryonic fibroblasts (MEFs) with a single Aph1 homolog (*Aph1A*$_L$, *Aph1A*$_S$, *Aph1B*, *Aph1C*). All Aph1 homologs restored complex formation as evaluated by Blue Native polyacrylamide gel electrophoresis (fig. S1). Their activity was measured in vitro with the recombinant substrates APPC99-3flag and NotchΔE. All complexes supported AICD (APP intracellular domain) and NICD (Notch intracellular domain) production [ε cleavage (*9*)] in vitro (Fig. 1A), and the kinetic parameters K_m (the Michaelis constant) and V_{max} (the maximum rate of reaction) for AICD production were similar for the Aph1A$_L$ and Aph1B γ-secretase complexes (Fig. 1B). Thus, the "physiological" ε-cleavage was maintained. However, the Aph1B or Aph1C γ-secretase complexes produced a greater proportion of longer Aβ peptide species (Aβ$_{1-42}$, Aβ$_{1-45}$, Aβ$_{1-46}$, and Aβ$_{1-49}$,) relative to shorter Aβ peptides (Aβ$_{1-37}$, Aβ$_{1-38}$, and Aβ$_{1-40}$) (Fig. 1, C and D, and fig. S1). In an additional independent assay, specific γ-secretase pools were prepared from wild-type mouse brain by immunoprecipitation with Aph1A$_L$-, Aph1B-, or PS1-specific antibodies or preimmune serum. The immunoprecipitates were assessed for γ-secretase activity in both the depleted (unbound) and enriched (bound) fractions (fig. S2). Comparison of the Aβ spectra generated confirmed that production of longer Aβ species was proportionately higher in Aph1B- versus Aph1A$_L$-containing immunoprecipitates. The opposite trend was observed in the depleted fractions (unbound). Given that changes in the relative ratio of secreted Aβ$_{1-42}$ to Aβ$_{1-40}$ are believed to be important for AD progression (*10*), we determined the Aβ$_{1-42}$/$_{1-40}$ ratio in culture supernatants of fibroblasts and primary neurons in vitro and in hippocampal and cortical extracts from *Aph1BC*$^{-/-}$ mice in vivo. The Aβ$_{1-42}$/$_{1-40}$ ratio was maintained between the genotypes (table S1), confirming that Aph1B does not influence this pathological parameter directly (*11*). However, we observed a significant reduction in total Aβ peptide production in brain extracts from *Aph1BC*$^{-/-}$ mice, demonstrating the important contribution of the Aph1B complex to total γ-secretase activity in the mouse brain.

We then investigated whether the structural heterogeneity deduced from the in vitro assays was preserved in intact cells. Fluorescent lifetime imaging microscopy (*12*) measures the proximity between fluorophores attached to different domains of a molecule and can detect conformational alterations in the γ-secretase complex (*12*).

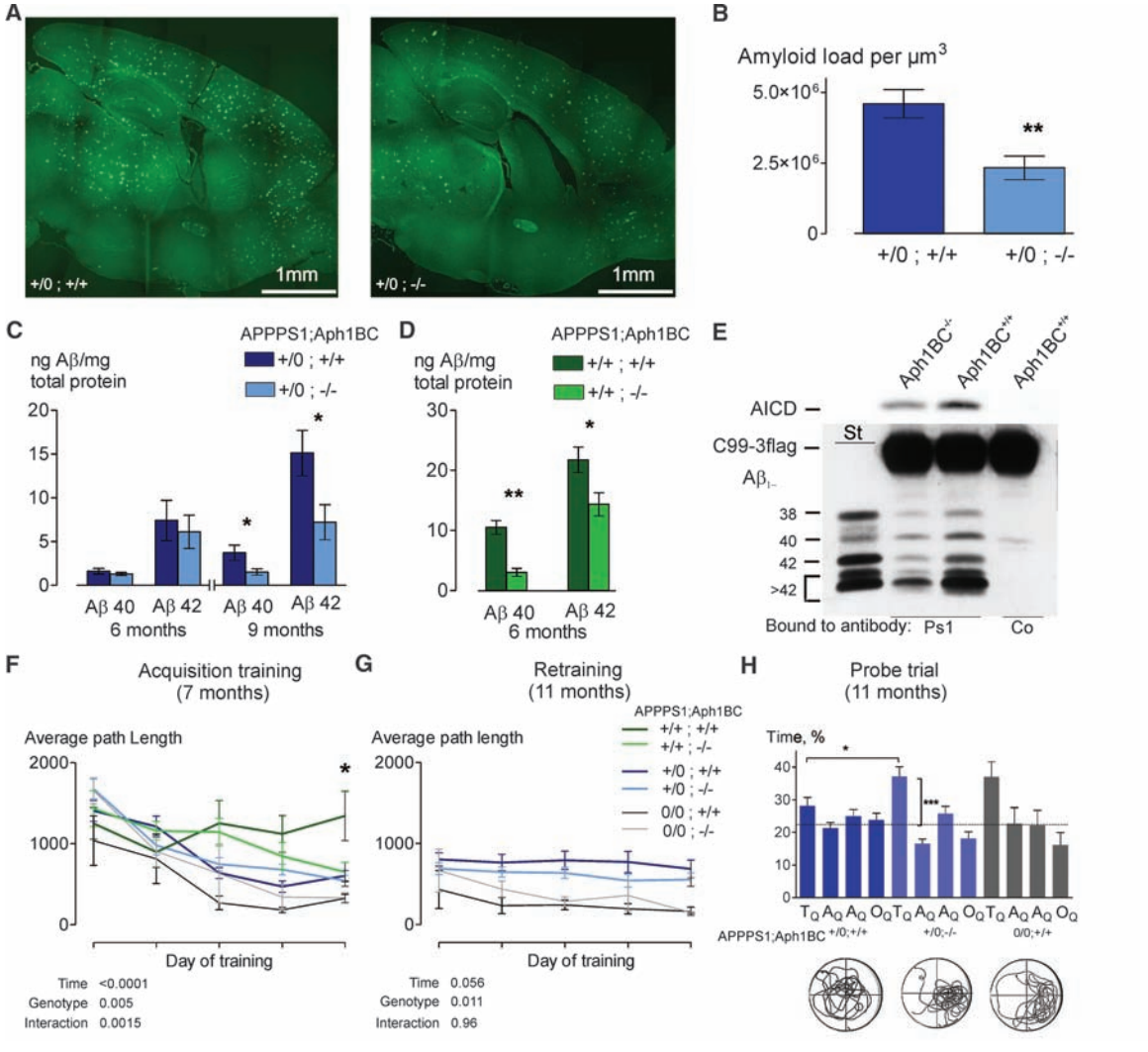

Fig. 2. Deletion of *Aph1BC* abolishes age-dependent increase in Aβ abundance in the brain and rescues learning and memory deficits. (**A** and **B**) Decreased amyloid burden was evident in *APPPS1*$^{+/0}$;*Aph1BC*$^{-/-}$ mice at 9 months of age (representative sections shown, measured by quantitative stereology (n = 5, P < 0.01, absolute amyloid load per unit volume, P < 0.01). (**C** and **D**) Though the use of Aβ$_{x-40}$- and Aβ$_{x-42}$-specific enzyme-linked immunosorbent assay, Aβ abundance in the hippocampus was measured and normalized to total protein content. Accumulation of Aβ$_{x-40}$ and Aβ$_{x-42}$ was rescued in *APPPS1*$^{+/0}$ and *APPPS1*$^{+/+}$ mice (n = 5, P < 0.05). (**E**) Purification of the γ-secretase complexes from *APPPS1*$^{+/0}$;*Aph1BC*$^{+/+}$ and *APPPS1*$^{+/0}$;*Aph1BC*$^{-/-}$ brains with the same PS1-specific antibody, followed by an in vitro activity assay for AICD and Aβ production, resulted in a quantitative decrease in *APPPS1*$^{+/0}$;*Aph1BC*$^{-/-}$ mouse brain γ-secretase activity (56 ± 1%) and a statistically significant qualitative shift in the pattern of Aβ produced (n = 4, P < 0.01). (**F**) At a young age (median 6.5 months; range 4.8 to 7.6), learning, as measured by decreasing path length, occurred in all genotypes, except *APPPS1*$^{+/+}$;*Aph1BC*$^{+/+}$ (mean ± SEM: genotype effect P < 0.01; genotype × time interaction P < 0.01). This deficit was significantly improved in the *APPPS1*$^{+/+}$;*Aph1BC*$^{-/-}$ mice (P < 0.05). (**G**) Retraining of the same mice at 11 months of age (median 10.7 months; range 9.2 to 12.2 months) showed that APPPS1$^{+/0}$;Aph1BC$^{+/+}$ mice were significantly worse than APPPS1$^{+/0}$;Aph1BC$^{-/-}$ mice in finding the hidden platform during all retraining days (two-way repeated measures analysis of variance between *APPPS1*$^{+/0}$ genotypes: genotype effect P < 0.01). (**H**) Probe trial results confirm that *Aph1BC* deletion prevents spatial memory deficits in hemizygous *APPPS1*$^{+/0}$;*Aph1BC*$^{+/+}$ mice (percent time spent in target quadrant T$_Q$, adjacent quadrants A$_{Q1}$-A$_{Q2}$, and opposite quadrant O$_Q$, P < 0.05; vertical comparison bars: t test with hypothetical mean 25% or chance level, P < 0.001).

The lifetime of the donor fluorophore at the PS1 N terminus was shortened by the presence of an acceptor fluorophore at an internal loop or at the C terminus, demonstrating that the fluorophores are in close vicinity. Complexes containing only Aph1B consistently demonstrated a significantly shorter lifetime than Aph1A-containing complexes (Fig. 1E). The shorter lifetime indicates a more "closed" conformation of PS1 and is similar (but milder) in effect to that of long-form Aβ-enhancing familial Alzheimer's disease (FAD)–associated presenilin mutations (*12*). Thus, the Aph1 component of the γ-secretase complex has a notable effect on the conformation of the PS1 subunit in situ.

To determine whether specifically targeting Aph1B/C complexes alters the phenotype of a mouse AD model overexpressing both mutated *APP* (*APP*^{Swe}-KM670/671NL) and *PS1* (*PS1*-L166P) from a single locus ("*APPPS1*") (*13*), we crossed *APPPS1* mice with *Aph1BC*$^{-/-}$ mice. We analyzed mice that were either homozygous or hemizygous for the *APPPS1* locus and homozygous for the *Aph1BC* locus. At 9 months of age, *APPPS1*$^{+/0}$;*Aph1BC*$^{+/+}$ mice displayed a massive amyloid burden, which was significantly lowered in *APPPS1*$^{+/0}$;*Aph1BC*$^{-/-}$ mice (Fig. 2, A and B). In hippocampal extracts, we observed a signifi-

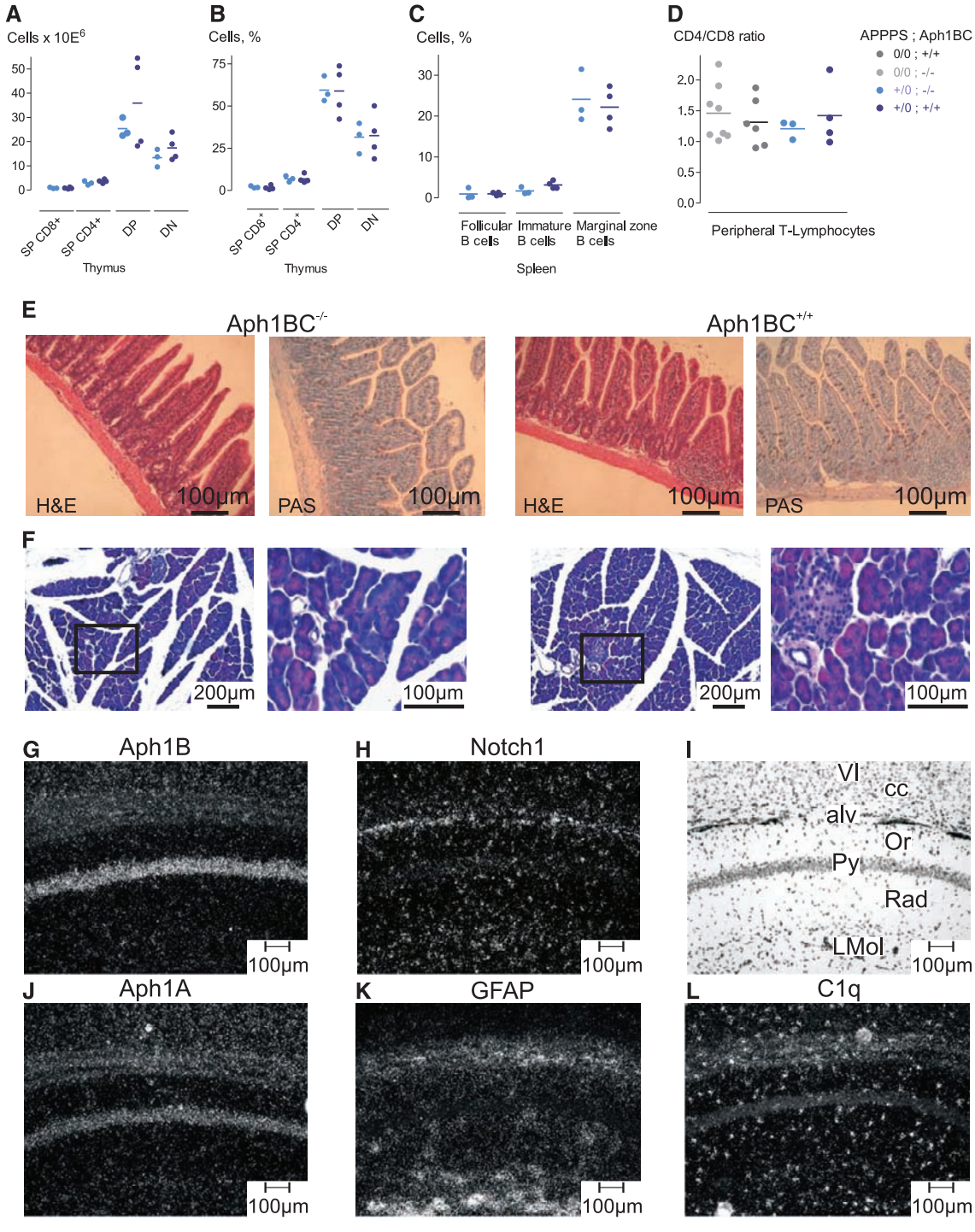

Fig. 3. Absence of Notch-signaling defects in *Aph1BC*$^{-/-}$ mice and expression of Aph1B/C in neurons of the adult mouse brain. (**A** to **C**) Sensitive T and B cell populations in the thymus (A and B) or in the spleen (C) were not distinguishable by fluorescence-activated cell sorting (FACS) in age-matched *Aph1BC*$^{+/+}$ ($n = 4$) and *Aph1BC*$^{-/-}$ mice ($n = 3$). (**D**) CD4$^+$/CD8$^+$ ratios of peripheral T lymphocytes were identical in both *APPPS1*$^{0/0}$ (*Aph1BC*$^{-/-}$: $n = 3$; *Aph1BC*$^{+/+}$: $n = 4$) and *APPPS1*$^{+/0}$ mice (*Aph1BC*$^{-/-}$: N=8; *Aph1BC*$^{+/+}$: $n = 7$). (**E**) Intestinal mucosal and (**F**) pancreas morphology, evaluated in a blind study, was identical in both genotypes ($n = 3$; hematoxylin and eosin and periodic acid–Schiff; representative sections). (**G** and **H**, **J** to **L**) High-power dark-field micrographs of hippocampal region (CA1) hybridized with the indicated antisense probes demonstrate that Aph1B/C expression is restricted to the pyramidal cell layer of the CA1 region and neuronal cell layers of cerebral cortex (layer VI) (G). Notch1 is predominantly expressed in non-neuronal layers containing mainly glial cells (H). Aph1A is widely expressed in both neuronal- and glia-enriched regions (J). Notch1 expression is generally low and partially overlaps with the nonneuronal markers GFAP (glial fibrillary acidic protein) (astrocytes) (K) and C1q (microglia, perivascular macrophages) (L). Hippocampal and cortical layers are identified by bright-field photography of section depicted in (**I**). VI: lamina six of parietal cortex; cc: corpus callosum; alv: alveus of the hippocampus (astrocytes); Or: stratum oriens of the CA1 region; Py: contains typical pyramidal neurons; Rad: stratum radiatum (glia); LMol: stratum lacunosum molecolare (glia).

cant decrease in $A\beta_{x\text{-}40}$ and $A\beta_{x\text{-}42}$ accumulation in *Aph1BC*$^{-/-}$ mice (Fig. 2, C and D).

We also evaluated the functional consequence of *Aph1BC* deletion. Homozygous *APPPS1*$^{+/+}$; *Aph1BC*$^{+/+}$ mice were underrepresented in the breeding program, probably owing to a perinatal mortality associated with *APPPS1* homozygosity (*14*–*16*). Mendelian ratios were restored in the *Aph1BC*$^{-/-}$ background (fig. S3). The animals also displayed abnormal cage activity (*17*), which improved with *Aph1BC* deficiency (fig. S4). Seven-month-old *APPPS1* homozygous mice displayed a profound acquisition deficit in the Morris water maze test for spatial learning and memory and were unable to improve any performance measure by training (Fig. 2F). No overt genotypic effect on swimming velocity was observed, and visual-evoked potentials, motor coordination, and exploratory and locomotor abilities were normal in all genotypes. Deletion of *Aph1BC* prevented the learning deficit in *APPPS1*$^{+/+}$ mice. Seven-month-old hemizygous *APPPS1*$^{+/0}$ mice that were either *Aph1BC*$^{+/+}$ or *Aph1BC*$^{-/-}$ displayed acquisition (Fig. 2F) and probe trial performance similar to those of control mice. Retraining at 11 months of age showed that *APPPS1*$^{+/0}$;*Aph1BC*$^{+/+}$ mice had largely retained their (procedural) ability to find the hidden platform but performed worse than controls during all retraining days. *APPPS1*$^{+/0}$;*Aph1BC*$^{-/-}$ mice performed slightly better than *APPPS1*$^{+/0}$;*Aph1BC*$^{+/+}$ mice, throughout the retraining (Fig. 2G). *APPPS1*$^{+/0}$;*Aph1BC*$^{-/-}$ mice still displayed normal spatial memory, whereas their *Aph1BC*$^{+/+}$ counterparts failed to show any preference for the target quadrant (Fig. 2H). Thus, *Aph1BC* deletion considerably improves the AD-like phenotype of an AD mouse model.

Aph1BC deficiency had little effect on the health of mice. Extensive behavioral and neurochemical testing revealed only a mild disturbance in prepulse inhibition, which is extremely mild in comparison to the effect of γ-secretase inhibition on Notch-dependent processes (*7*) (Fig. 3). *Aph1BC* deficiency did not affect B or T cell maturation in thymus or spleen, nor did it alter steady-state $CD4^+/CD8^+$ ratios (*18*, *19*). The intestinal and pancreatic morphology was also unaffected in Aph1BC$^{-/-}$ mice (*18*, *20*). Finally, expression of *Notch1* and its target genes (*HES1*, *HES5*, and *ACSL1*) (*21*, *22*), which are directly or indirectly dependent on γ-secretase activity, were similar in hippocampi of *APPPS1*$^{+/0}$;*Aph1BC*$^{-/-}$ and *APPPS1*$^{+/0}$;*Aph1BC*$^{+/+}$ mice (fig. S5). We further investigated expression of the *Aph1* genes in hippocampi, pancreas, spleen, gut, and thymus (fig. S6). Expression of *Aph1B* mRNA is relatively high in the hippocampus and pancreas. In situ hybridization experiments with brain tissue sections confirmed the neuronal *Aph1B* expression in regions relevant for AD (*7*) (Fig. 3 and fig. S6), whereas *Notch1* mRNA signal is predominantly expressed in nonneuronal and neuronal precursor cells and overlapped appreciably with Aph1A, but not Aph1B, expression (Fig. 3). Therefore, the complete ablation of a γ-secretase subunit can be generated in an adult mouse without any Notch-related phenotypes (*23*).

The extent to which the APH1B γ-secretase complex contributes to Aβ production in the human brain is unknown. Specific γ-secretase pools were prepared from the human brain as described above with $Aph1A_L$-, Aph1B-, and PS1-specific antibodies or preimmune serum, and then both the depleted (unbound) as well as the enriched (bound) fractions were used for in vitro cleavage assays (Fig. 4 and fig. S7). Depletion of APH1B γ-secretase from the endogenous pool of human brain complexes decreased AICD and Aβ production considerably. Conversely, the isolated APH1B γ-secretase complex was active (Fig. 4). APH1B γ-secretase complexes (APH1B-bound) are a major contributor to total γ-secretase activity (PS1-bound) in the human brain. Furthermore, similar changes were observed in the Aβ peptide spectrum generated in vitro as seen in the mouse system.

Here we provide evidence that the Aph1 protein contributes directly to the proteolytic activity of the γ-secretase complex by influencing the conformation of the catalytic PS1 subunit in situ. Targeting specifically the Aph1B-containing complexes results in notable improvements of multiple severe AD-related phenotypes in a mouse model. The lack of Notch-related side effects should be compared with what was observed in other full and partial knockouts of γ-secretase subunits [summarized in (*23*)]. A 50% reduction in γ-secretase activity in *Nct*$^{+/-}$ heterozygous mice is associated with severe Notch side effects (*24*). By contrast, we have observed here the complete removal of a γ-secretase complex component without Notch-related problems and with efficient reduction of the amyloid pathology in the mouse brain. Because the APH1B γ-secretase complex is present and active in the human brain, the selective inhibition of this complex has the potential to translate into an approach to reduce Aβ peptide production in human AD with relatively few side effects. Our work has also implications for other fields, as γ-secretase is, for instance, involved in hematopoietic and other cancers. It might be important to analyze the role of the different complexes in these different diseases as well (*25*).

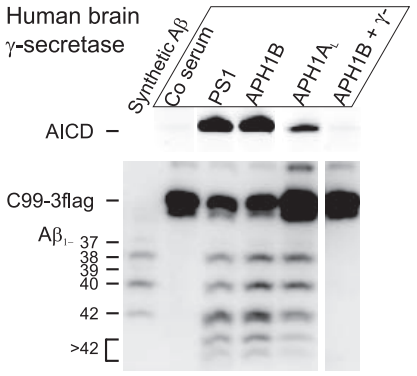

Fig. 4. Aph1B γ-secretase contributes to Aβ production in human brain. Different pools of γ-secretase were prepared from microsomal membranes of human brain tissue by immunoprecipitation with preimmune serum (Co serum), or with PS1-, Aph1B-, or $Aph1A_L$-specific antibody. γ-Secretase activity was then measured in vitro. Production of AICD and Aβ species was measured by SDS-PAGE or urea–SDS-PAGE and specific antibodies. Comparison of the $Aph1A_L$ and Aph1B precipitated pools reveals a statistically significant shift in the pattern of Aβ production (mean ± SD, $n = 3$, $P < 0.05$ to 0.01). $Aph1A_L$ immunoprecipitate is less active, and four times as much sample was loaded. γ$^-$: 10 μM γ-secretase inhibitor L-685,458.

References and Notes

1. B. De Strooper *et al.*, *Nature* **391**, 387 (1998).
2. B. De Strooper, *Neuron* **38**, 9 (2003).
3. S. S. Hebert *et al.*, *Neurobiol. Dis.* **17**, 260 (2004).
4. K. Shirotani, D. Edbauer, S. Prokop, C. Haass, H. Steiner, *J. Biol. Chem.* **279**, 41340 (2004).
5. L. Serneels *et al.*, *Proc. Natl. Acad. Sci. U.S.A.* **102**, 1719 (2005).
6. G. Ma, T. Li, D. L. Price, P. C. Wong, *J. Neurosci.* **25**, 192 (2005).
7. T. Dejaegere *et al.*, *Proc. Natl. Acad. Sci. U.S.A.* **105**, 9775 (2008).
8. A. V. Savonenko *et al.*, *Proc. Natl. Acad. Sci. U.S.A.* **105**, 5585 (2008).
9. C. Haass, D. J. Selkoe, *Nat. Rev. Mol. Cell Biol.* **8**, 101 (2007).
10. D. Scheuner *et al.*, *Nat. Med.* **2**, 864 (1996).
11. K. Shirotani, M. Tomioka, E. Kremmer, C. Haass, H. Steiner, *Neurobiol. Dis.* **27**, 102 (2007).
12. O. Berezovska *et al.*, *J. Neurosci.* **25**, 3009 (2005).
13. R. Radde *et al.*, *EMBO Rep.* **7**, 940 (2006).
14. K. K. Hsiao *et al.*, *Neuron* **15**, 1203 (1995).
15. D. L. King, G. W. Arendash, *Physiol. Behav.* **75**, 627 (2002).
16. P. L. Pugh, J. C. Richardson, S. T. Bate, N. Upton, D. Sunter, *Behav. Brain Res.* **178**, 18 (2007).
17. P. Hollingworth *et al.*, *J. Am. Geriatr. Soc.* **54**, 1348 (2006).
18. G. T. Wong *et al.*, *J. Biol. Chem.* **279**, 12876 (2004).
19. J. Tournoy *et al.*, *Hum. Mol. Genet.* **13**, 1321 (2004).
20. J. T. Siveke *et al.*, *Gastroenterology* **134**, 544 (2008).
21. A. Louvi, S. Artavanis-Tsakonas, *Nat. Rev. Neurosci.* **7**, 93 (2006).
22. T. Kawai, N. Takagi, M. Nakahara, S. Takeo, *Neurosci. Lett.* **380**, 17 (2005).
23. S. H. Choi, E. Norstrom, *J. Neurosci.* **27**, 13579 (2007).
24. T. Li *et al.*, *J. Neurosci.* **27**, 10849 (2007).

25. We thank C. Peeters for assistance in pathological evaluations, C. Mathieu for FACS analysis, L. Van Aerschot for assistance with behavioral testing, S. Terclavers and H. Schieb for technical assistance, and A. Thathiah for proofreading the manuscript. This work was supported by a Pioneer award from the Alzheimer's Association; the Fund for Scientific Research Flanders (to R.D. and B.D.S.); KULeuven (Geconcerteerde onderzoeksacties); Federal Office for Scientific Affairs, Belgium; a Methusalem grant of the Flemish Government; MEMOSAD (F2-2007-200611) of the European Union; and NIH grants P01AG015379, R01AG026593, and AG026593 (to B.T.H.) and NIH AG 13579 (to B.T.H. and O.B.). B.D.S. is a paid consultant for Eli Lilly and Envivo Pharmaceuticals; B.T.H. is a paid consultant for Elan, Genentech, Pfizer, Takeda, Link, and Neurophage.

Supporting Online Material

www.sciencemag.org/cgi/content/full/1171176/DC1
Materials and Methods
SOM Text
Figs. S1 to S7
Table S1
References

21 January 2009; accepted 6 March 2009
Published online 19 March 2009;
10.1126/science.1171176
Include this information when citing this paper.

Burst Spiking of a Single Cortical Neuron Modifies Global Brain State

Cheng-yu T. Li,[1,2] Mu-ming Poo,[1] Yang Dan[1,2]*

Different global patterns of brain activity are associated with distinct arousal and behavioral states of an animal, but how the brain rapidly switches between different states remains unclear. We here report that repetitive high-frequency burst spiking of a single rat cortical neuron could trigger a switch between the cortical states resembling slow-wave and rapid–eye-movement sleep. This is reflected in the switching of the membrane potential of the stimulated neuron from slow UP/DOWN oscillations to a persistent-UP state or vice versa, with concurrent changes in the temporal pattern of cortical local field potential (LFP) recorded several millimeters away. These results point to the power of single cortical neurons in modulating the behavioral state of an animal.

Different behavioral states of the animal are characterized by distinct patterns of global brain activity. For example, slow-wave sleep is associated with slow oscillations, with UP-DOWN membrane potential transitions in cortical neurons and high-amplitude, low-frequency local field potential (LFP) and electroencephalogram (EEG) signals (*1*–*6*). In contrast, low-amplitude high-frequency cortical activity prevails during rapid–eye-movement (REM) sleep and wakefulness, with neuronal membrane potentials fluctuating around a depolarized level (*3*). In recent years, significant progress has been made in identifying the neuromodulatory circuits in the hypothalamus, brain stem, and basal forebrain that are involved in regulating the global brain state (*7*–*12*). However, the role of cortical neurons in this regulation remains unclear. Inspired by recent findings that activation of a single cortical neuron can significantly modulate sensory perception and motor output (*13*, *14*), we set out to test whether single neuron stimulation can modify the global brain state.

Whole-cell patch recordings were made from the superficial layers of visual or somatosensory cortex of urethane-anesthetized adult rats (*15*) (Fig. 1A and fig. S1A). We routinely observed two types of spontaneous activity: The membrane potential (E_m) exhibited either a bimodal distribution with UP/DOWN transitions at ~1 Hz (Fig. 1, B and D, left, hereafter referred to as "*UP/DOWN*" state) or a unimodal distribution with high-frequency fluctuations around a depolarized level (right, "*persistent-UP*" state). Each of these states observed in a single cell corresponded to a distinct pattern of LFP, recorded simultaneously in a cortical region 0.3 to 6 mm from the patch electrode (Fig. 1A). *UP/DOWN* E_m transitions were highly correlated with high-amplitude slow LFP deflections (*1*–*3*, *16*) (Fig. 1C, left), whereas the *persistent-UP* state of the single neuron was accompanied by low-amplitude, fast-LFP fluctuations (*3*, *16*) (right). The power spectra of these LFP signals (Fig. 1E) showed a prominent difference at low frequencies (0.5 to 4 Hz). Thus, the *UP/DOWN* and *persistent-UP* states of single neurons reflect distinct global cortical states, which resemble slow-wave and REM sleep, respectively (*4*, *16*, *17*).

High-frequency burst spiking of the patched neuron induced by depolarizing current injections (350 to 600 ms per step, 30 to 40 steps with 4- to 4.5-s intervals, or 8 ms per pulse, 5 to 15 pulses per burst, 40 to 80 bursts with 2- to 2.5-s intervals) could trigger a switch between these cortical states. In the example in Fig. 2A, the recorded visual cortical neuron was in stable *UP/DOWN* state (exhibiting bimodal E_m distribution) for >20 min. Repeated burst spiking at 50 Hz (for ~3 min) (*15*) caused a switch from the *UP/DOWN* to *persistent-UP* state (exhibiting unimodal E_m distribution), which lasted through the duration of recording (~30 min). Concurrent with the change in E_m distribution of the patched neuron, there was a marked reduction of low-frequency signals in the LFP recorded ~1 mm away (Fig. 2B), indicating a switch from the cortical state characteristic of slow-wave sleep to that of REM sleep (*17*). In another example (Fig. 2, D and E), LFP was recorded ~5 mm from the patch electrode. In this case, both the single neuron E_m and the LFP reverted to their original patterns after ~5 min. A third example is shown in fig. S1, where burst

[1]Division of Neurobiology, Department of Molecular and Cell Biology, Helen Wills Institute of Neuroscience, University of California, Berkeley, CA 94720, USA. [2]Howard Hughes Medical Institute, University of California, Berkeley, CA 94720, USA.

*To whom the correspondence should be addressed. E-mail: ydan@berkeley.edu

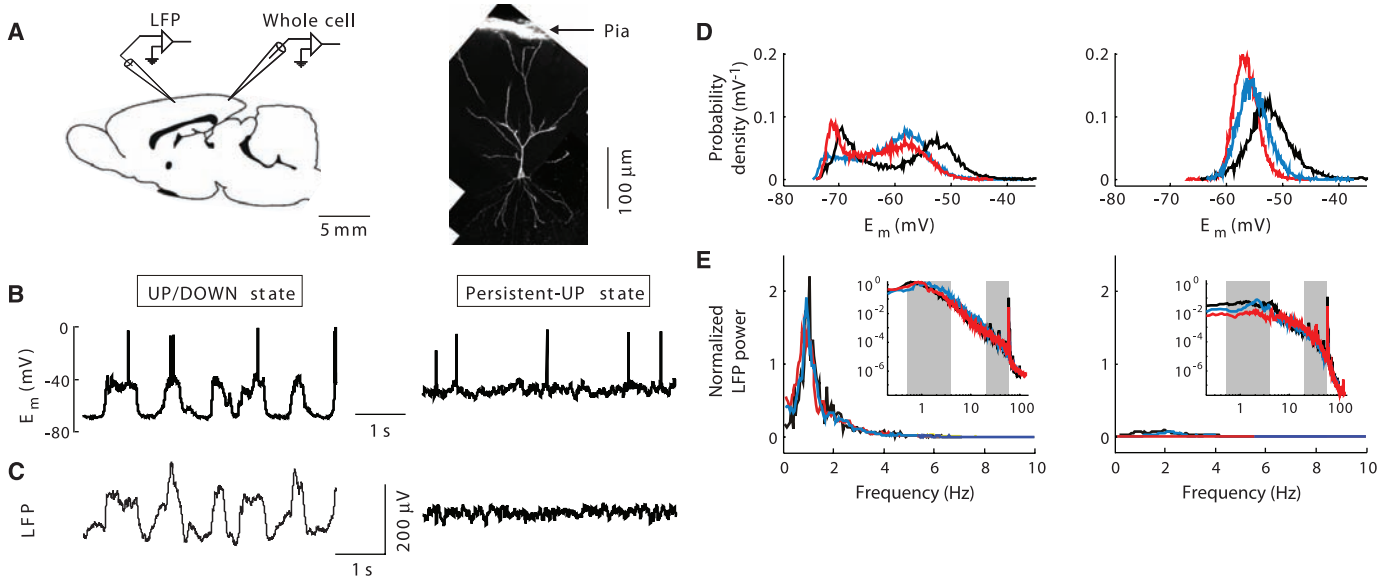

Fig. 1. *UP/DOWN* and *persistent-UP* states observed in simultaneous whole-cell and LFP recordings in rat cortex. (**A**) (left) Schematic illustration of recording configuration. Whole-cell and LFP electrodes were separated by 0.3 to 6 mm. (Right) A whole-cell recorded pyramidal neuron in somatosensory cortex. (**B**) *UP/DOWN* (left) and *persistent-UP* (right) states observed in a visual cortical neuron. (**C**) LFP recorded 2 mm from the patch recording in (B). (**D**) Distributions of membrane potentials (E_m) during *UP/DOWN* (left) and *persistent-UP* (right) states. Data are from three cells (marked by different colors). (**E**) LFP power spectra from the same experiments as in (D), each normalized by the mean power at 0.5 to 1.5 Hz during *UP/DOWN* state. (Insets) Power spectra on log-log scales. Gray shadings, low and high frequency ranges for computing L/H power ratio.

spiking of a somatosensory cortical neuron changed the global cortical state, as revealed by both LFP and EEG recordings. Single-neuron burst spiking also induced a similar switch of cortical state under isoflurane anesthesia (fig. S2), which indicated that the effect is not specific to urethane anesthesia.

The high-frequency bursts of a single neuron could also cause a switch in the opposite direction, from the *persistent-UP* to *UP/DOWN* state. In the example shown in Fig. 3, A and B, the cortex was in the *persistent-UP* state for >10 min, as indicated by both the unimodal E_m distribution (Fig. 3A) and low-amplitude, fast LFP fluctuations (Fig. 3B). Repetitive burst spiking of the patched neuron caused a switch into the *UP/DOWN* state, with bimodal E_m distribution (Fig. 3A) and high-amplitude, slow LFP deflections (Fig. 3B) that lasted for >20 min. But in another example of burst-induced switch from the *persistent-UP* to *UP/DOWN* state (Fig. 3, D and E), the cortex spontaneously reverted to the *persistent-UP* state after ~3 min.

To quantify the burst-induced changes in cortical state, we computed the ratio between LFP power in the ranges of 0.5 to 4 Hz and 20 to 60 Hz (referred to as "L/H power ratio") (*15*). As shown in Figs. 2, C and F, and 3, C and F, marked increase or decrease of L/H power ratio was found after single-neuron burst spiking. To determine

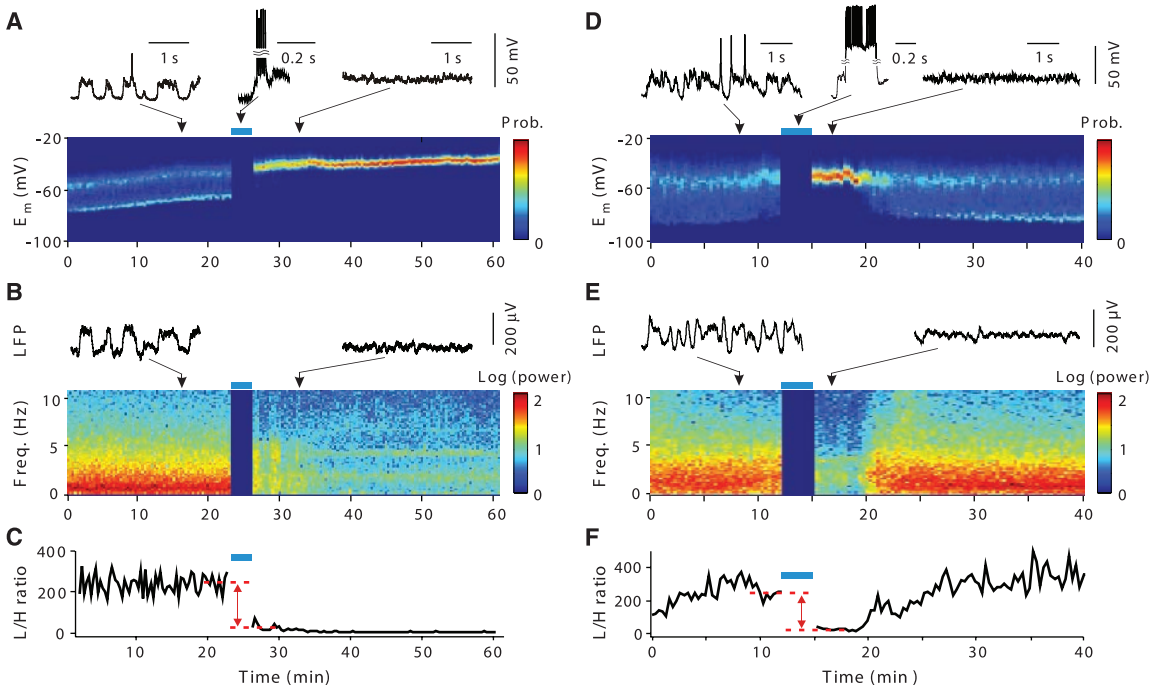

Fig. 2. Switch from *UP/DOWN* to *persistent-UP* state induced by single-neuron burst spiking. (**A**) State switch indicated by change from bimodal to unimodal E_m distribution (color coded, computed in 20-s windows). Blue bar, burst spiking period. Insets above, sample whole-cell recording traces during periods marked by arrows. (**B**) State switch indicated by change in LFP power spectrum (color coded, log scale, computed in 20-s windows) recorded ~1 mm from whole-cell electrode. (Tops) Sample LFP traces. (**C**) L/H power ratio (between 0.5 to 4 Hz and 20 to 60 Hz) for LFP in (B). Dashed red lines are averaged values 3 min before and 3 min after burst spiking; the distance between these lines was used to measure burst-induced L/H ratio change. (**D** to **F**) Similar to (A to C), from another experiment; LFP was recorded ~5 mm from the patch electrode.

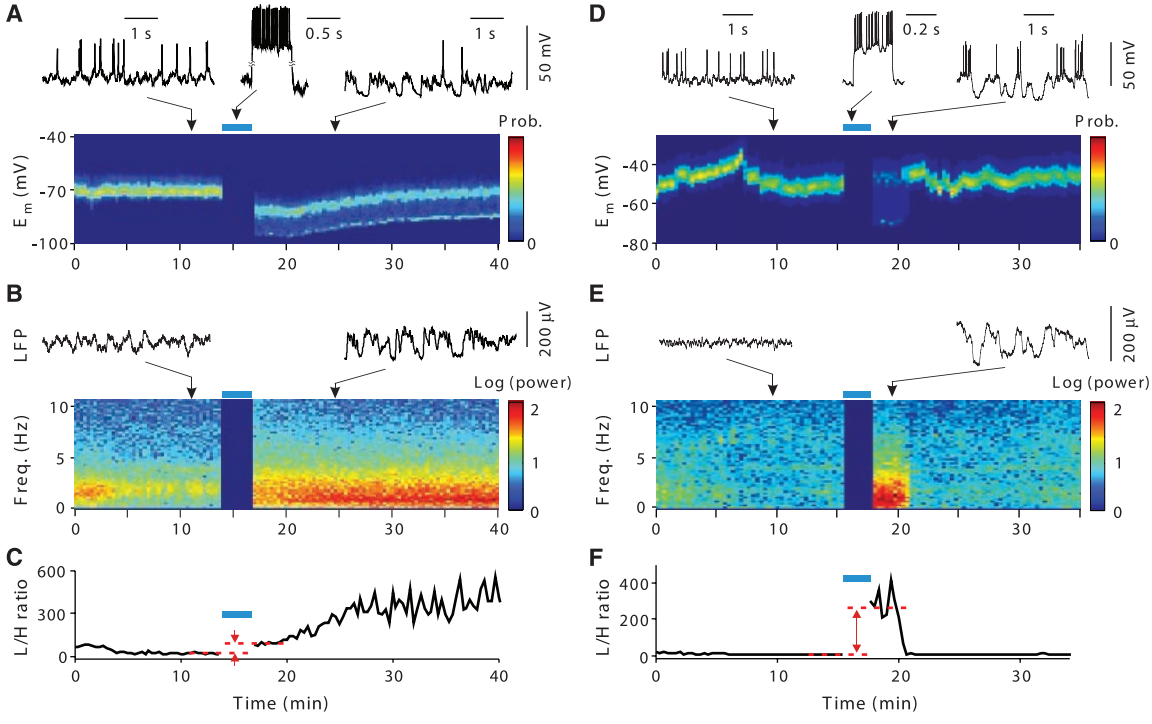

Fig. 3. Switch from *persistent-UP* to *UP/DOWN* state induced by single-neuron spiking. (**A**) State switch indicated by change from unimodal to bimodal E_m distribution. (**B**) State switch indicated by change in LFP power spectrum (recorded ~5 mm from whole-cell electrode). (**C**) L/H power ratio, for LFP in (B). (**D** to **F**) Similar to (A to C), from another experiment; LFP was recorded ~1 mm from patch electrode.

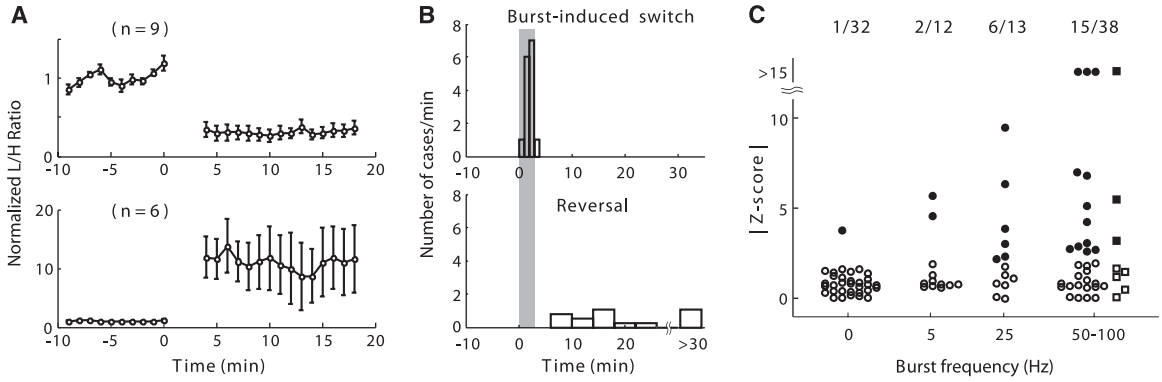

Fig. 4. Time course and frequency dependence of the switch of cortical state. (**A**) Average LFP L/H power ratio for 15 out of 38 experiments with significant ratio changes induced by spiking at 50 to 100 Hz [solid symbols in (C)]. (Top) Average of nine experiments showing significant *UP/DOWN* to *persistent-UP* transitions; (bottom), average of six experiments showing *persistent-UP* to *UP/DOWN* transitions. L/H ratio of each experiment was normalized by its mean before spiking. Error bar, ±SEM. (**B**) Distributions of time for spiking-induced switch (top) and spontaneous reversal (bottom) for the same 15 experiments as in (A). Gray stripe, burst spiking period. (**C**) |*Z* score| for burst-induced LFP L/H ratio change versus burst frequency. Each point represents one experiment performed on one whole-cell recorded neuron in visual (circle) or somatosensory (square) cortex. Solid symbols, experiments with significant ratio changes ($P < 0.05$); "0 Hz," control experiments with no spiking during the 3-min sham period. Compared with "0 Hz," *Z*-score distribution was significantly different for 25 Hz ($P = 0.010$, two-sample Kolmogorov-Smirnov test) and 50 to 100 Hz ($P = 0.0014$) but not for 5 Hz ($P = 0.20$). Probability of burst-induced transition (percentage of solid symbols) is significantly higher for 25 Hz [46%, $P < 0.001$, bootstrap (*15*)] and 50 to 100 Hz (39%, $P < 0.001$), but not for 5 Hz (16%, $P = 0.11$).

whether in each experiment the observed change in L/H ratio over the ~3-min spiking period could be explained by a spontaneous change of the cortical state, we used the control period of 10 to 30 min before burst spiking to estimate the spontaneous variation of L/H ratio over each 3-min interval. The burst-induced change was compared with the distribution of this spontaneous variation to determine its statistical significance. We found significant changes in LFP L/H ratio ($P < 0.05$) after evoking high-frequency bursts (50 to 100 Hz, 200 to 1000 spikes total) in single neurons in 15 out of 38 experiments (Fig. 4A, nine from *UP/DOWN* to *persistent-UP* state and six in the opposite direction, with each experiment performed on a different neuron). In these 15 experiments, the abrupt change indicative of cortical state switch often occurred during the period of burst spiking [(Fig. 4B, top), 2.0 ± 0.8 min after burst onset, mean ± SD]. On the other hand, the time for spontaneous reversal to the original state showed large variations [(Fig. 4B, bottom), data from the same 15 experiments], with 4 out of 15 cases showing no reversal within the 30-min recording after burst spiking.

We next examined the dependence of the cortical state switch on burst frequency by varying the spike frequency within each burst from 0 to 100 Hz. In 32 control experiments, in which no spiking was evoked during a 3-min "sham period" (0 Hz, 20 to 23 min after establishing whole-cell recording), we found only one case with significant L/H ratio change ($P < 0.05$). At a burst frequency of 5 Hz, only 2 out of 12 cases showed significant ratio change. However, between 25 and 100 Hz, ~40% (6 out of 13 at 25 Hz and 15 out of 38 at 50 to 100 Hz) of the cases showed significant changes (Fig. 4C). Thus, the switch of cortical states by single neurons requires high-frequency bursting.

Slow oscillations have been shown to be initiated in deep layers of the cortex (*18*–*20*). In this study, most of the stimulated neurons appeared to be excitatory neurons in superficial layers, as judged by their spiking patterns when current was injected (Figs. 2, A and D, and 3, A and D), depths of the recording electrodes (in most cases <500 μm from pia), and histological reconstruction of a subset of recorded neurons (Fig. 1A and fig. S1A). Each of these neurons is likely to project to several thousand cortical neurons (*21*), and a small percentage of these connections may be strong enough to trigger postsynaptic spiking (*22*, *23*) and to activate a local network (*24*). The high-frequency bursts required for triggering the state switch (Fig. 4C) could further enhance the effect of single neuron spiking through temporal summation of postsynaptic potentials and short-term synaptic facilitation (*25*), e.g., those found at excitatory synapses onto Martinotti cells (*26*). Given the extensive connections from layer 2/3 to layer 5 (*21*), the spiking activity in layer 2/3 may strongly modulate the dynamics in deep cortical layers, which results in either initiation or termination of slow oscillations. Such local activity modulation may spread globally through either cortico-cortical connections or the thalamo-cortico-reticular loop (*4*, *27*). In addition, the transitions between slow-wave sleep, REM sleep, and awake cortical states are known to be regulated by neuromodulatory systems in the hypothalamus, brainstem, and basal forebrain (*4*, *8*–*12*, *28*, *29*), which project diffusely to the thalamus and cortex and are capable of triggering synchronous state changes across multiple brain areas. Thus, the switch of global brain states induced by cortical neuronal burst spiking could be mediated by descending projections from the cortex to these modulatory circuits (*10*, *28*). In particular, the naturally occurring bidirectional switches between slow-wave and REM sleep are thought to be controlled by a flip-flop circuit consisting of mutually inhibitory REM-ON and REM-OFF areas (*10*). Spiking activity in the cortex may tip the balance between REM-ON and REM-OFF neurons, thus causing the observed state change. Future studies on both the flip-flop circuit and their cortical inputs will help elucidate the mechanisms underlying the switches among different brain states.

Previous studies have shown that stimulation of a single motor cortical neuron can evoke whisker movement (*13*) and that spiking of a single somatosensory cortical neuron can induce behaviorally reportable effect (*14*). Our study showed that burst spiking of a single neuron can trigger a switch in the global brain state, which further underscores the functional importance of individual neuronal activity.

References and Notes

1. M. Steriade, A. Nunez, F. Amzica, *J. Neurosci.* **13**, 3252 (1993).
2. D. Contreras, M. Steriade, *J. Neurosci.* **15**, 604 (1995).
3. M. Steriade, I. Timofeev, F. Grenier, *J. Neurophysiol.* **85**, 1969 (2001).
4. M. Steriade, D. McCormick, T. Sejnowski, *Science* **262**, 679 (1993).
5. J. Anderson, I. Lampl, I. Reichova, M. Carandini, D. Ferster, *Nat. Neurosci.* **3**, 617 (2000).
6. C. J. Wilson, P. M. Groves, *Brain Res.* **220**, 67 (1981).
7. M. Steriade, R. W. McCarley, *Brainstem Control of Wakefulness and Sleep* (Plenum, New York, 1990).
8. C. M. Sinton, R. W. McCarley, *Semin. Neurol.* **24**, 211 (2004).
9. C. B. Saper, T. E. Scammell, J. Lu, *Nature* **437**, 1257 (2005).
10. J. Lu, D. Sherman, M. Devor, C. B. Saper, *Nature* **441**, 589 (2006).
11. C. G. Behn, E. N. Brown, T. E. Scammell, N. J. Kopell, *J. Neurophysiol.* **97**, 3828 (2007).
12. G. Moruzzi, *Ergeb. Physiol.* **64**, 1 (1972).
13. M. Brecht, M. Schneider, B. Sakmann, T. W. Margrie, *Nature* **427**, 704 (2004).
14. A. R. Houweling, M. Brecht, *Nature* **451**, 65 (2008).
15. Materials and methods are available as supporting material on *Science* Online.
16. A. Destexhe, D. Contreras, M. Steriade, *J. Neurosci.* **19**, 4595 (1999).
17. D. Gervasoni *et al.*, *J. Neurosci.* **24**, 11137 (2004).
18. M. Steriade, A. Nunez, F. Amzica, *J. Neurosci.* **13**, 3266 (1993).
19. I. Timofeev, F. Grenier, M. Bazhenov, T. J. Sejnowski, M. Steriade, *Cereb. Cortex* **10**, 1185 (2000).
20. M. V. Sanchez-Vives, D. A. McCormick, *Nat. Neurosci.* **3**, 1027 (2000).
21. R. J. Douglas, K. A. Martin, *Annu. Rev. Neurosci.* **27**, 419 (2004).
22. S. Song, P. J. Sjostrom, M. Reigl, S. Nelson, D. B. Chklovskii, *PLoS Biol.* **3**, e68 (2005).

23. Z. A. Peterlin, J. Kozloski, B. Q. Mao, A. Tsiola, R. Yuste, *Proc. Natl. Acad. Sci. U.S.A.* **97**, 3619 (2000).
24. M. Bazhenov, I. Timofeev, M. Steriade, T. J. Sejnowski, *J. Neurosci.* **22**, 8691 (2002).
25. R. S. Zucker, W. Regehr, *Annu. Rev. Physiol.* **64**, 355 (2002).
26. G. Silberberg, H. Markram, *Neuron* **53**, 735 (2007).
27. D. A. McCormick, T. Bal, *Annu. Rev. Neurosci.* **20**, 185 (1997).
28. E. F. Pace-Schott, J. A. Hobson, *Nat. Rev. Neurosci.* **3**, 591 (2002).
29. B. E. Jones, *Prog. Brain Res.* **145**, 157 (2004).
30. This work was supported by grants from NIH and NSF (SBE-0542013 to Temporal Dynamics of Learning Center, TDLC). We thank W. Sun for technical help.

Supporting Online Material
www.sciencemag.org/cgi/content/full/324/5927/643/DC1
Materials and Methods
Figs. S1 and S2

18 December 2008; accepted 13 March 2009
10.1126/science.1169957

Self-Control in Decision-Making Involves Modulation of the vmPFC Valuation System

Todd A. Hare,[1]* Colin F. Camerer,[1,2] Antonio Rangel[1,2]

Every day, individuals make dozens of choices between an alternative with higher overall value and a more tempting but ultimately inferior option. Optimal decision-making requires self-control. We propose two hypotheses about the neurobiology of self-control: (i) Goal-directed decisions have their basis in a common value signal encoded in ventromedial prefrontal cortex (vmPFC), and (ii) exercising self-control involves the modulation of this value signal by dorsolateral prefrontal cortex (DLPFC). We used functional magnetic resonance imaging to monitor brain activity while dieters engaged in real decisions about food consumption. Activity in vmPFC was correlated with goal values regardless of the amount of self-control. It incorporated both taste and health in self-controllers but only taste in non–self-controllers. Activity in DLPFC increased when subjects exercised self-control and correlated with activity in vmPFC.

The concept of self-control in decision-making has occupied philosophers and scientists throughout recorded history because the ability to exercise it is central to human success and well-being. Behavioral studies have examined the problem of self-control and provided valuable insights that suggest it is exhaustible in the short term (*1*–*3*), can be enhanced by cognitive strategies (*4*–*7*), and is correlated with measures of intelligence (*8*–*10*). However, little is known about the neurobiological underpinnings of self-control and how these neural mechanisms might differ between successful and unsuccessful self-controllers.

We investigated which neural processes are responsible for the deployment of self-control and how these processes interact with the brain's valuation and decision-making circuitry. We hypothesized that goal-directed decisions have their basis in a value signal encoded in the ventromedial prefrontal cortex (vmPFC). This hypothesis has its basis in neuroimaging studies that have found a correlation between activity in this area and behavioral measures of value (*11*–*16*), as well as findings from electrophysiology studies (*17*, *18*). We also hypothesized that self-control involves modulation by the dorsolateral prefrontal cortex (DLPFC) of the value signals computed in vmPFC. This hypothesis has its basis in the role of DLPFC in cognitive control (*19*, *20*), working memory (*21*, *22*), and emotion regulation (*23*).

To test these hypotheses, we recruited self-reported dieters and used functional magnetic resonance imaging (fMRI) to study the neural activity in vmPFC and DLPFC while the participants made real decisions about which foods to eat. Participants performed three tasks in the scanner (Fig. 1A) (*24*). In the first two parts, they rated 50 different food items for taste and health separately. On the basis of these ratings, we selected a reference item for each subject that was rated neutral in both taste and health. In the final part, subjects were asked to choose between each of the foods and the reference item. One decision was randomly selected and implemented at the end of the study. Participants indicated the strength of their decision by using a five-point scale (strong no, no, neutral, yes, and strong yes), which provided a measure of their relative value for eating that food instead of the reference item. Following the previous literature (*11*), we refer to this measure as a goal value, which refers to the amount of expected reward associated with consuming the food. Note that dieters should be concerned with the healthiness of the foods, and not only with their taste, and that optimal decision-making requires integrating these two separate concerns.

Participants were classified as self-controllers (SCs; $n = 19$) or non–self-controllers (NSCs; $n = 18$) on the basis of their decisions (*24*). There was a stark difference between the SC and NSC groups (Fig. 1B): Whereas SCs made decisions on the basis of both health and taste, rejecting most liked-but-unhealthy items, the NSC group made decisions on the basis of taste alone.

We made four predictions about the patterns of neural activity, which we tested by using the fMRI data. First, activity in vmPFC should be correlated with participants' goal values regardless of whether or not they exercise self-control. Second, activity in the vmPFC should reflect the health ratings in the SC group but not in the NSC group. Third, the DLPFC should be more active during successful than failed self-control trials. Fourth, DLPFC and vmPFC should exhibit functional connectivity during self-control trials.

We tested the first prediction by estimating a general linear model (GLM) of blood oxygen

[1]Division of Humanities and Social Sciences, California Institute of Technology, Pasadena, CA 91125, USA. [2]Computational and Neural Systems, California Institute of Technology, Pasadena, CA 91125, USA.

*To whom correspondence should be addressed. E-mail: thare@hss.caltech.edu

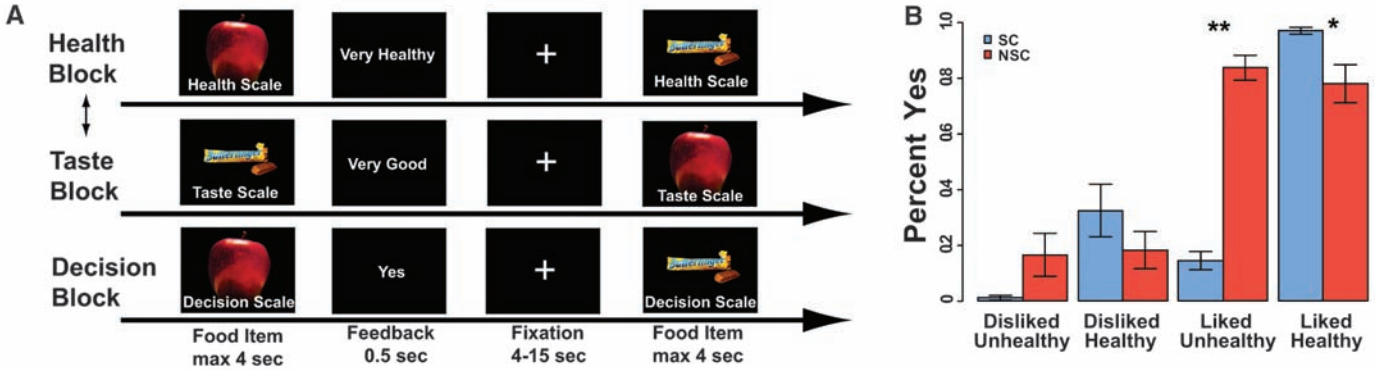

Fig. 1. (**A**) The task proceeded in three parts: taste ratings, health ratings, and decisions. (**B**) Percentage of the time participants chose the food over the reference item. The SC group chose not to eat liked-unhealthy food items more often than the NSC group did (**$t_{31} = 12.5$; $P < 0.0000$). The SC group also ate liked-healthy food items more often than the NSC group did (*$t_{18} = 2.74$; $P < 0.05$). Error bars denote standard errors.

level–dependent activity that included a parametric regressor for goal values at the time of evaluation. Activity in vmPFC was correlated with goal values for all participants regardless of the amount of self-control exercised (Fig. 2, A and B; fig. S1; and table S2). The areas of vmPFC identified largely overlap with regions that have been associated with valuation in other tasks that require no self-control (*11*–*15*) (Fig. 2C).

To test the second prediction, we estimated a new GLM that included parametric regressors for health and taste ratings. The beta values for both parametric regressors were extracted from the voxels in vmPFC that exhibited the strongest correlation with goal values for each participant. In the SC group, vmPFC activity was modulated by both health ($t_{18} = 4.20$, $P < 0.001$) and taste ($t_{18} = 3.31$, $P < 0.005$) (Fig. 2D), whereas in the NSC group it was only modulated by taste ($t_{17} = 7.28$, $P < 0.001$). We tested this relationship further by estimating a linear regression of the impact of health ratings on each participant's behavior against a measure of the impact of health ratings on the participant's vmPFC activity (regression coefficient = 0.847, $t_{35} = 5.57$, $P < 0.001$) (Fig. 2E).

We tested the third prediction by comparing the neural responses during the decision period in three different types of trials: those in which self-control was not needed, those in which self-control was successfully deployed, and those in which participants failed to use self-control. We found greater left DLPFC activity [inferior frontal gyrus (IFG) and Brodmann's area (BA) 9 (IGF/BA9)] in the SC group than in the NSC group during successful self-control trials (Fig. 3A and table S3). However, both groups had greater activity in this region for successful self-control trials compared with that of failed self-control trials (SC group $t_{14} = 2.29$, NSC group $t_{13} = 2.62$, $P < 0.05$) (Fig. 3B).

We tested the fourth prediction by performing a linear regression of left DLPFC activity during self-control trials on the response of vmPFC to the presentation of liked-but-unhealthy food items (regression coefficient = –0.688, $t_{17} = –2.26$; $P < 0.05$) (Fig. 3C). Self-control in this type of trial requires ramping down the weight given to taste in computing the goal value. A similar decrease in vmPFC activity was seen in gamblers who chose not to gamble in losing conditions (*25*).

We also investigated whether left DLPFC and vmPFC exhibited task-related functional connectivity. An initial analysis of the psychophysiological interactions (PPI) using left DLPFC as the seed showed connectivity with several regions (fig. S4 and table S4), including the left IFG/BA46 but not the vmPFC, which ruled out direct modulation from DLPFC. However, DLPFC might modulate the vmPFC through its effect in a third region, such as IFG/BA46. This area was of particular interest because it is involved in working memory and goal maintenance (*21*, *22*), it has anatomical connections to vmPFC (*26*), and previous studies have shown that IFG/BA46 activity is correlated with goal values (*11*, *13*). Thus, we used this area as the seed for a second PPI analysis and found positive task-related functional connectivity with the vmPFC (fig. S3 and table S5). A conjunction analysis confirmed that this was the same area of vmPFC that was correlated with goal values. Thus, the vmPFC was functionally connected to the left DLPFC through a two-node network (Fig. 4, B and C).

The results provide insight into two open questions in behavioral neuroscience. First, they suggest that self-control problems arise in situations where various factors (e.g., health and taste) must be integrated in vmPFC to compute goal values and that DLPFC activity is required for higher-order factors, such as health, to be incorporated into the vmPFC value signal. We speculate that the vmPFC originally evolved to forecast the short-term value of stimuli and that humans developed the ability to incorporate long-term considerations into values by giving structures such as the DLPFC the ability to modulate the basic value signal.

Second, a fundamental difference between successful and failed self-control might be the extent to which the DLPFC can modulate the vmPFC. Individual differences in the ability of DLPFC to modulate vmPFC might be due to differences within the DLPFC or to differences in connectivity between the DLPFC and other areas. The areas of DLPFC that we have found to play a role in self-control are similar to areas that are at work in cognitive control (*27*, *28*) and in emotional regulation (*23*, *29*). Our results are consistent with previous theories of the role of DLPFC in cognitive control, which posit that it sends signals to other brain regions to promote task-relevant processing and suppress irrelevant activity (*20*). Thus, our findings could be the start of an explanation for why general intelligence, cognitive control, and emotional regulation are all correlated with various behavioral measures of self-control (*5*, *8*–*10*).

Our findings also have implications for an ongoing debate in decision neuroscience and psychology. McClure *et al*. (*30*, *31*) have proposed that intertemporal choice involves the interaction of multiple independent valuation systems (some characterized by very large discount rates and a hypersensitivity to immediate rewards and others that are more patient and thus more sensitive to long-term considerations) that compete with each other for behavioral control. They have also proposed that the shortsighted valuation network includes the vmPFC and that the foresighted one includes the DLPFC. In contrast, Kable and Glimcher (*12*) have argued that there is a common valuation system and that the values that guide behavior are computed in the vmPFC-striatal network. However, they do not provide any theory or evidence about which neural mechanisms

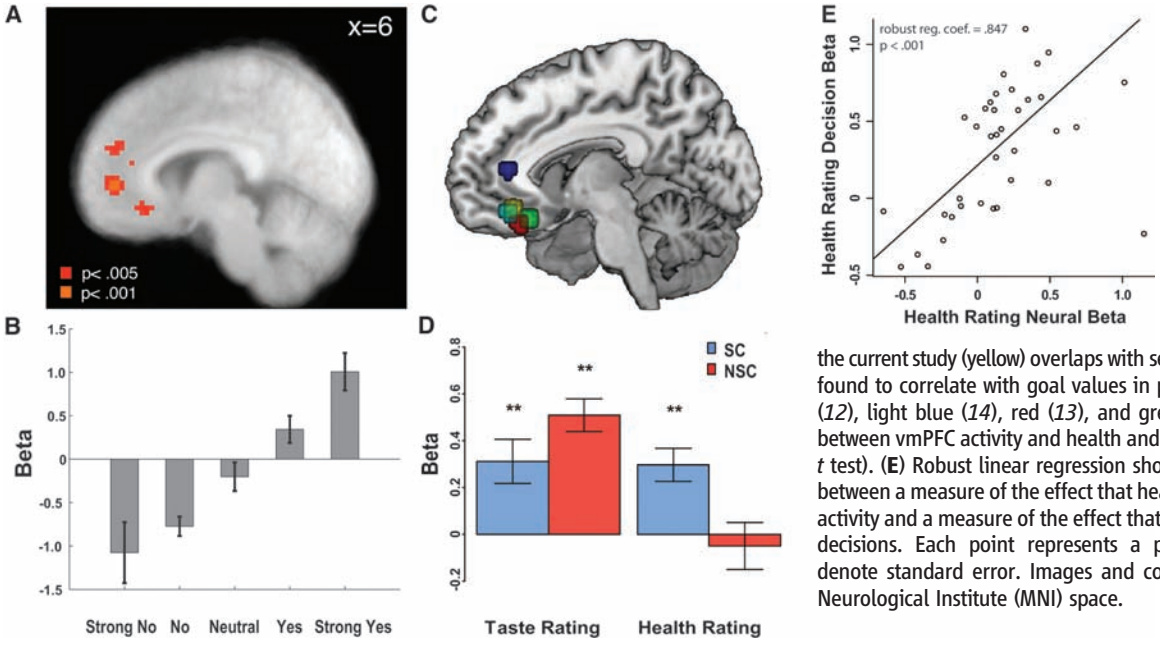

Fig. 2. (**A**) Regions of vmPFC in which activity correlated with goal values across all participants and regardless of their degree of self-control. See tables S1 to S5 for the statistics corrected for multiple comparisons. (**B**) Beta values in vmPFC increased with goal values. (**C**) The vmPFC area reflecting goal values in the current study (yellow) overlaps with several areas that have been found to correlate with goal values in previous studies [dark blue (*12*), light blue (*14*), red (*13*), and green (*11*)]. (**D**) Correlations between vmPFC activity and health and taste ratings (**$P < 0.005$, *t* test). (**E**) Robust linear regression showing a strong relationship between a measure of the effect that health ratings have on vmPFC activity and a measure of the effect that the health ratings have on decisions. Each point represents a participant. All error bars denote standard error. Images and coordinates are in Montreal Neurological Institute (MNI) space.

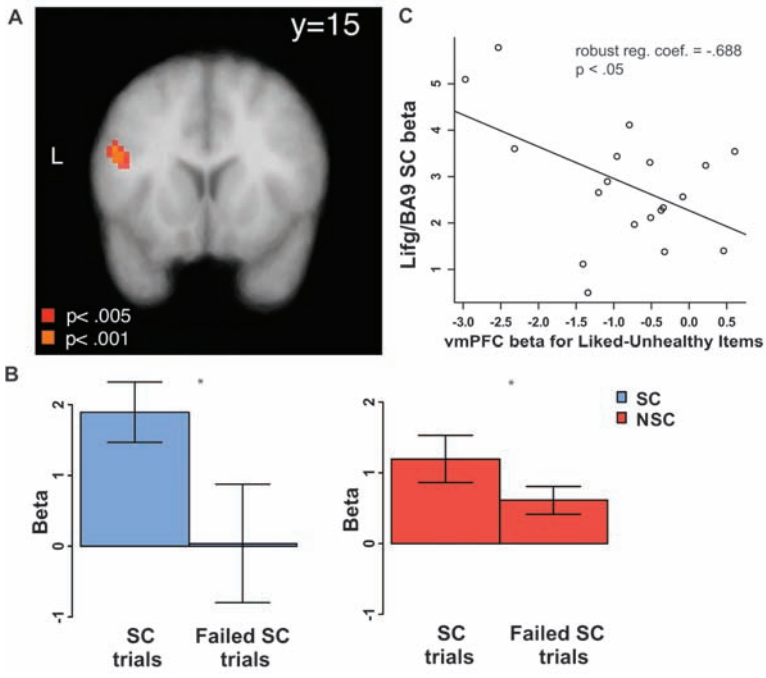

Fig. 3. (**A**) Region of left DLPFC showing greater activity in successful self-control trials in the SC than the NSC group. Images and coordinates are in MNI space. (**B**) Both groups showed greater activity in DLPFC for successful versus failed self-control trials (*$P < 0.05$, paired t test). (**C**) Activity in left DLPFC (IFG/BA9) was negatively correlated with vmPFC activity in the SC group during trials in which liked-but-unhealthy foods were avoided. Each point represents a participant in the SC group.

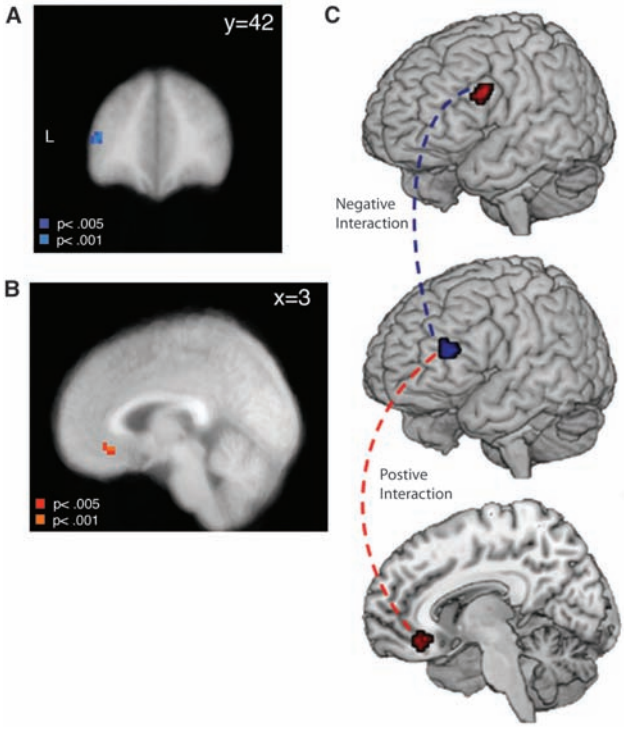

Fig. 4. (**A**) Left IFG/BA46 showed negative task-related functional connectivity with the left DLPFC during decisions about unhealthy items by the SC group. (**B**) Conjunction analysis showing voxels that were correlated with goal values and exhibiting significant positive task-related functional connectivity with IFG/BA46 (reported P values based on the PPI analysis). (**C**) Diagram summarizing the results of the PPI analyses and illustrating the path through which the left DLPFC might modulate activity in the vmPFC. Blue lines represent negative interactions, and red lines represent positive ones. Images and coordinates are in MNI space.

modulate the value signal in order to exercise self-control. Our results bring a substantial amount of resolution to this debate. Like Kable and Glimcher, we find strong evidence for the existence of a common valuation signal in the vmPFC that drives choices regardless of the degree of self-control deployed by the participants. Like McClure *et al*., our results suggest that the DLPFC plays a critical role in the deployment of self-control. Contrary to their theory, however, we show that this is not because an alternative value signal is encoded in DLPFC, which in our experiment would require a nonexistent correlation between activity in this area and the health ratings (fig. S5). Instead, the DLPFC influences self-control by modulating the value signal encoded in vmPFC.

Lastly, an improved understanding of the neurobiology of self-control in decision-making will have applications to clinical practice in domains such as obesity and addiction, to economic and public policy analysis in problems such as suboptimal savings and health behaviors, and to legal thinking about which criteria should be used in determining if an individual is in full command of his decision-making faculties and thus accountable to the law.

References and Notes

1. M. Muraven, D. M. Tice, R. F. Baumeister, *J. Pers. Soc. Psychol.* **74**, 774 (1998).
2. B. Shiv, A. Fedorikhin, *J. Consum. Res.* **26**, 278 (1999).
3. K. D. Vohs *et al*., *J. Pers. Soc. Psychol.* **94**, 883 (2008).
4. G. Ainslie, J. R. Monterosso, *J. Exp. Anal. Behav.* **79**, 37 (2003).
5. W. Mischel, Y. Shoda, M. I. Rodriguez, *Science* **244**, 933 (1989).
6. J. Monterosso, G. Ainslie, *Drug Alcohol Depend.* **90** (suppl. 1), S100 (2007).
7. E. Siegel, H. Rachlin, *J. Exp. Anal. Behav.* **64**, 117 (1995).
8. A. L. Duckworth, M. E. Seligman, *Psychol. Sci.* **16**, 939 (2005).
9. N. A. Shamosh *et al*., *Psychol. Sci.* **19**, 904 (2008).
10. J. P. Tangney, R. F. Baumeister, A. L. Boone, *J. Pers.* **72**, 271 (2004).
11. T. A. Hare, J. O'Doherty, C. F. Camerer, W. Schultz, A. Rangel, *J. Neurosci.* **28**, 5623 (2008).
12. J. W. Kable, P. W. Glimcher, *Nat. Neurosci.* **10**, 1625 (2007).
13. H. Plassmann, J. O'Doherty, A. Rangel, *J. Neurosci.* **27**, 9984 (2007).
14. E. T. Rolls, C. McCabe, J. Redoute, *Cereb. Cortex* **18**, 652 (2008).
15. S. M. Tom, C. R. Fox, C. Trepel, R. A. Poldrack, *Science* **315**, 515 (2007).
16. V. V. Valentin, A. Dickinson, J. P. O'Doherty, *J. Neurosci.* **27**, 4019 (2007).
17. C. Padoa-Schioppa, J. A. Assad, *Nature* **441**, 223 (2006).
18. J. D. Wallis, E. K. Miller, *Eur. J. Neurosci.* **18**, 2069 (2003).
19. C. S. Carter, V. van Veen, *Cogn. Affect. Behav. Neurosci.* **7**, 367 (2007).
20. E. K. Miller, J. D. Cohen, *Annu. Rev. Neurosci.* **24**, 167 (2001).
21. M. Watanabe, K. Hikosaka, M. Sakagami, S. Shirakawa, *Exp. Brain Res.* **166**, 263 (2005).
22. J. Duncan, A. M. Owen, *Trends Neurosci.* **23**, 475 (2000).
23. K. N. Ochsner, J. J. Gross, *Trends Cogn. Sci.* **9**, 242 (2005).
24. Materials and methods are available as supporting material on *Science* Online.
25. D. K. Campbell-Meiklejohn, M. W. Woolrich, R. E. Passingham, R. D. Rogers, *Biol. Psychiatry* **63**, 293 (2008).
26. H. Barbas, D. N. Pandya, *J. Comp. Neurol.* **286**, 353 (1989).
27. D. Badre, A. D. Wagner, *Neuron* **41**, 473 (2004).
28. A. W. MacDonald 3rd, J. D. Cohen, V. A. Stenger, C. S. Carter, *Science* **288**, 1835 (2000).
29. M. R. Delgado, M. M. Gillis, E. A. Phelps, *Nat. Neurosci.* **11**, 880 (2008).
30. S. M. McClure, K. M. Ericson, D. I. Laibson, G. Loewenstein, J. D. Cohen, *J. Neurosci.* **27**, 5796 (2007).
31. S. M. McClure, D. I. Laibson, G. Loewenstein, J. D. Cohen, *Science* **306**, 503 (2004).

32. This work was funded by the Moore Foundation and the Economic Research Service of the U.S. Department of Agriculture on Behavioral Health Economics Research on Dietary Choice and Obesity.

Supporting Online Material

www.sciencemag.org/cgi/content/full/324/5927/646/DC1
Materials and Methods
Figs. S1 to S5
Tables S1 to S5
References

12 November 2008; accepted 12 March 2009
10.1126/science.1168450

Exchange of Genetic Material Between Cells in Plant Tissue Grafts

Sandra Stegemann and Ralph Bock*

Tissue grafting includes applications ranging from plant breeding to animal organ transplantation. Donor and recipient are generally believed to maintain their genetic integrity, in that the grafted tissues are joined but their genetic materials do not mix. We grafted tobacco plants from two transgenic lines carrying different marker and reporter genes in different cellular compartments, the nucleus and the plastid. Analysis of the graft sites revealed the frequent occurrence of cells harboring both antibiotic resistances and both fluorescent reporters. Our data demonstrate that plant grafting can result in the exchange of genetic information via either large DNA pieces or entire plastid genomes. This observation of novel combinations of genetic material has implications for grafting techniques and also provides a possible path for horizontal gene transfer.

Grafting is widely used in plant breeding programs in order to modify plant architecture, improve vigor, or increase disease resistance. Grafting also occurs naturally; for example, when the stems or roots of trees contact each other (*1*). Although the grafted tissues fuse and establish vascular connections, the stock (the lower part of the graft) and scion (the upper part, usually supplying solely aerial parts to the graft) are thought not to exchange their genetic materials (*2*).

To test this assumption, we generated two transgenic tobacco lines carrying different selection markers and reporters. One line, Nuc-kan:yfp, harbors a kanamycin resistance gene (*nptII*) and the yellow fluorescent protein gene (*yfp*) in its nuclear genome, whereas the other, Pt-spec:gfp, possesses a spectinomycin resistance gene (*aadA*) and the green fluorescent protein gene (*gfp*) in its plastid (chloroplast) genome (Fig. 1A and fig. S1).

We performed grafting experiments in which Pt-spec:gfp scions were grafted onto Nuc-kan:yfp

Max-Planck-Institut für Molekulare Pflanzenphysiologie, Am Mühlenberg 1, D-14476 Potsdam-Golm, Germany.

*To whom correspondence should be addressed. E-mail: rbock@mpimp-golm.mpg.de

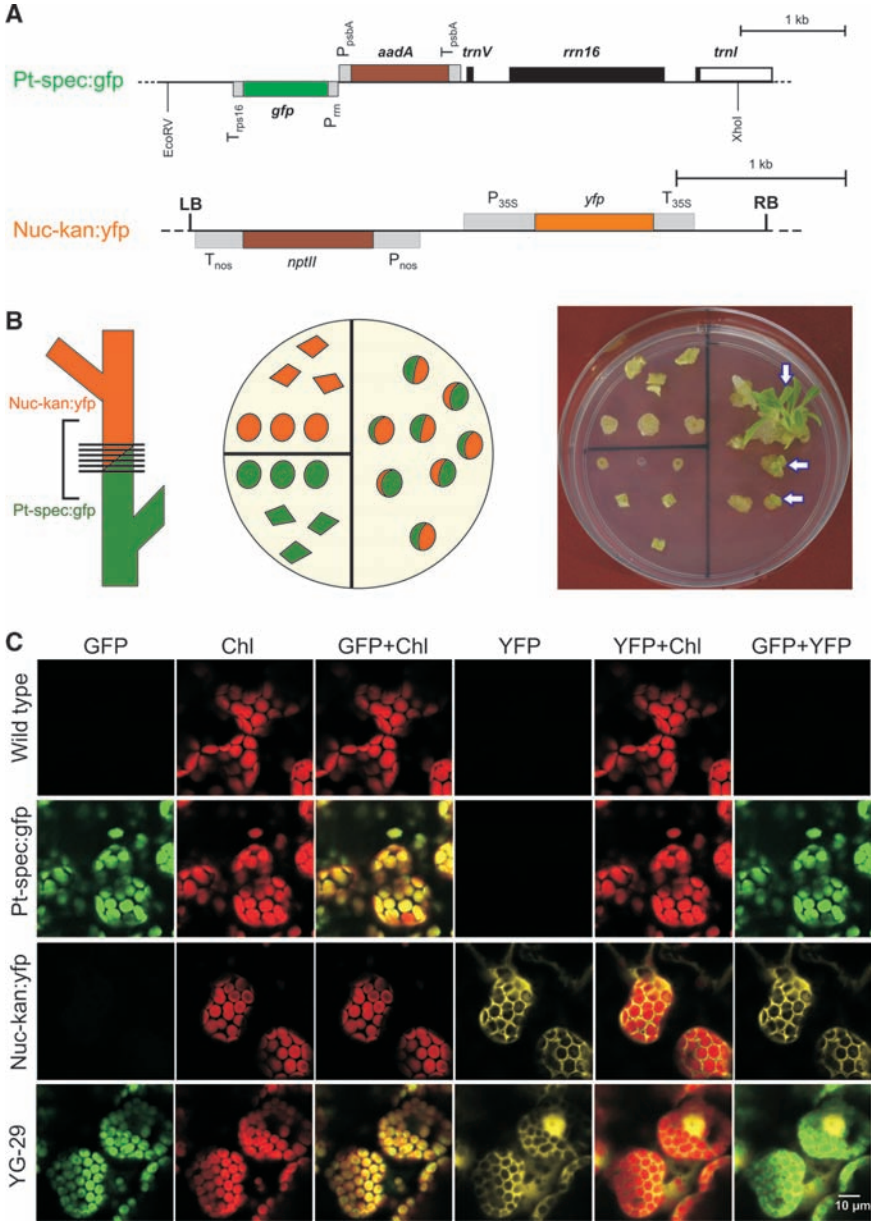

Fig. 1. Genetic screen for intercellular gene transfer. (**A**) Maps of the plastid genome in Pt-spec:gfp plants and the transgenic locus in Nuc-kan:yfp plants. P_{psbA} and T_{psbA}, promoter and terminator from the plastid *psbA* gene; P_{rrn}, promoter from the plastid rRNA operon; T_{rps16}, terminator from the plastid *rps16* gene; P_{nos} and T_{nos}, promoter and terminator from the nopaline synthase gene from *Agrobacterium tumefaciens*; P_{35S} and T_{35S}, promoter and terminator from the cauliflower mosaic virus 35*S* transcript; LB and RB, left and right borders of the T-DNA region; Eco RV and Xho I, restriction sites used for restriction fragment length polymorphism analysis (fig. S3). (**B**) Selection experiments. The grafted stem region was either sectioned (horizontal lines) or directly exposed to selection (bracket). The middle panel shows the arrangement of tissue explants, the right panel a selection plate (right half, stem sections from the graft site; upper left quarter, three stem sections and three leaf explants from Nuc-kan:yfp; lower left quarter, the corresponding explants from Pt-spec:gfp). After 4 weeks on medium with spectinomycin and kanamycin, some explants from the graft site developed growing callus tissue or regenerating shoots (arrows). (**C**) Expression and subcellular localization of the fluorescent reporters. The wild type, the two grafting partners, and a YG line were assayed for GFP, chlorophyll (Chl), and YFP fluorescence.

stocks and vice versa. After the establishment of a physical connection, the graft site was excised and analyzed for gene flow between scion and stock by testing for the presence of cells that harbor both the kanamycin resistance gene (from Nuc-kan:yfp) and the spectinomycin resistance gene (from Pt-spec:gfp). Exposure of stem sections to double selection for kanamycin and spectinomycin resistance frequently yielded resistant calli (that is, mounds of undifferentiated cells) and regenerating shoots (Fig. 1B). Cell lines isolated from grafts with Pt-spec:gfp as scion and Nuc-kan:yfp as stock are referred to as GY; lines from the reciprocal grafting are referred to as YG.

We next assayed GY and YG lines for expression of the fluorescent reporters. All cells in the regenerated plants showed GFP fluorescence in chloroplasts and YFP fluorescence in the cytosol, indicating that the two reporter proteins were present in the same cell (Fig. 1C and fig. S2). It is known that some proteins and RNAs can travel between cells and across graft junctions (*3*). We therefore performed Northern blot analyses to confirm transcription of all four transgenes in GY and YG lines (Fig. 2A) and also demonstrated the presence of all transgenes at the DNA level (Fig. 2B and fig. S3).

We recovered doubly resistant lines at high frequency (94 events from 74 grafted plantlets, table S1). The frequency of intercellular gene transfer was independent of the orientation of the graft (table S1). When we subjected leaf explants and distant stem sections to selection, no resistant lines were obtained (table S2), suggesting that gene transfer is confined to the graft site and no long-distance transfer may occur. Whether the gene transfer is strictly dependent on direct cell-to-cell contact remains to be investigated.

Experiments in which whole graft sites were subjected to selection (Fig. 1B) also produced resistant cell lines, suggesting that tissue injury (by cross-sectioning) was not involved in the gene transfer process. In contrast, when stock and scion were separated before fusion, no resistant lines were obtained (table S1). Karyotype analyses excluded the possibility that YG and GY plants arose through fusion of Nuc-kan:yfp cells with Pt-spec:gfp cells (fig. S4). Finally, genetic crosses demonstrated stable inheritance of the transferred genes and additionally confirmed the absence of polyploidy (fig. S5).

Two directions of gene transfer are possible: movement of plastid genes from Pt-spec:gfp cells into Nuc-kan:yfp cells or transfer of nuclear genes from Nuc-kan:yfp to Pt-spec:gfp cells. To distinguish between these possibilities by tracking molecular markers in the plastid and nuclear genomes, we grafted two different tobacco varieties, Petit Havana (PH; Pt-spec:gfp) and Samsun NN (SNN; Nuc-kan:yfp). Analysis of a polymorphism in the plastid genomes of the two cultivars [>15 kb away from the transgene insertion site (*4*)] revealed that all GY and YG plants analyzed carried the PH marker (Fig. 2C), indicating that large DNA pieces or even entire plastid genomes are transferred. Polymorphisms in pathogen resistance genes were used as nuclear markers (*5*). All GY and YG plants tested positive for the SNN-specific marker and negative for the PH-specific marker (Fig. 2C), suggesting that the plastid transgenes moved from PH cells into SNN cells. Plant cells are connected via plasmatic bridges called plasmodesmata, but the passage of large macromolecules requires the action of specific plasmodesmata-widening proteins (*3*). Whether large DNA pieces or even

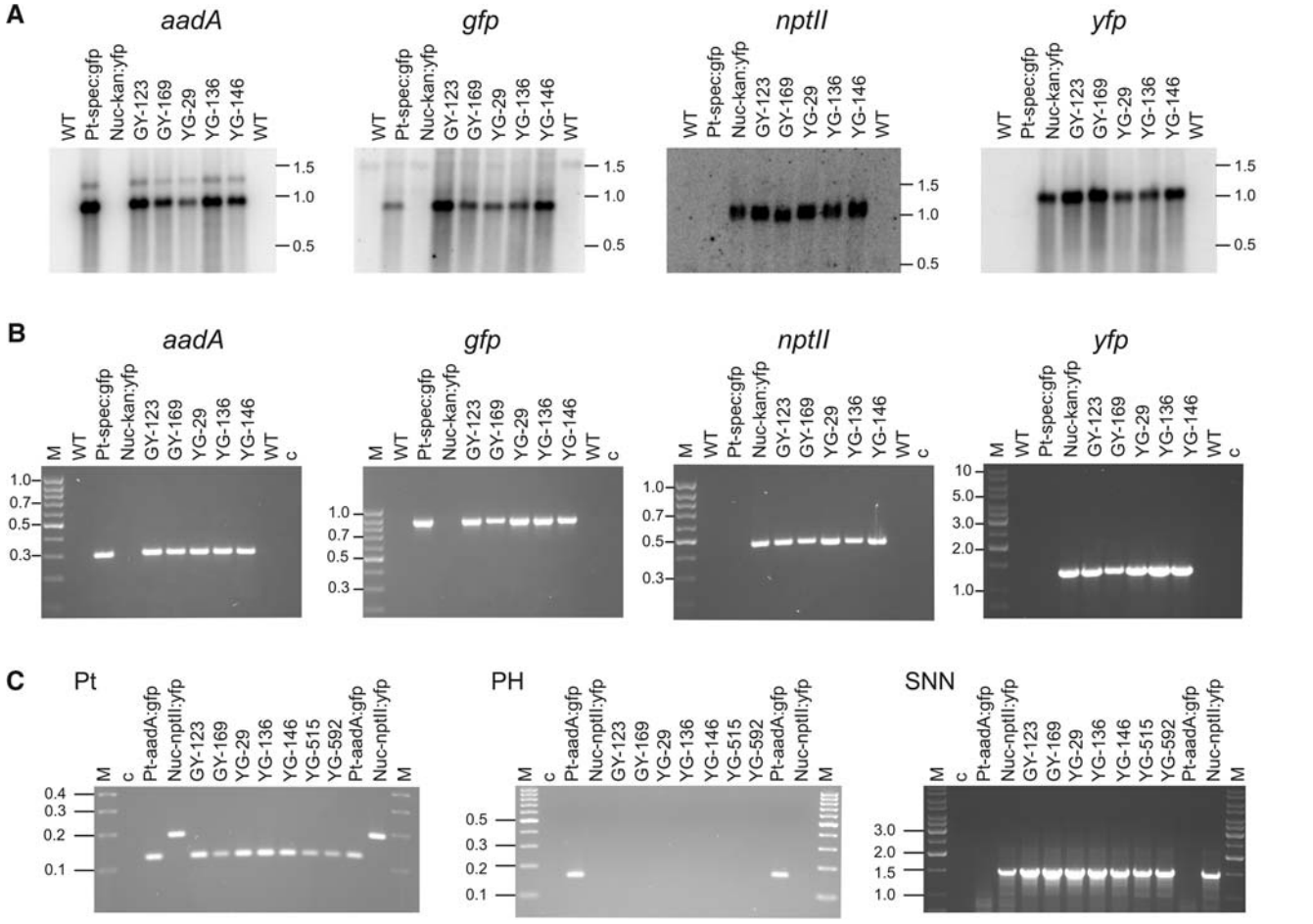

Fig. 2. Analysis of transgenes and molecular markers in gene transfer lines. (**A**) Northern blot analyses of transgene expression. (**B**) Transgene detection at the DNA level by polymerase chain reaction (PCR). (**C**) PCR analysis of plastid and nuclear markers to determine the direction of intercellular gene transfer. Pt, assay of a length polymorphism in the plastid genomes of the two grafted varieties PH [Pt-spec:gfp, 125–base pair (bp) product] and SNN (Nuc-kan:yfp, 191-bp product); PH, a PH-specific nuclear marker (189-bp product); SNN, an SNN-specific nuclear marker (1569-bp product). WT, wild type; M, marker (sizes in kilobase pairs); c, buffer control.

entire organelles can travel through plasmodesmata requires further investigation.

Our discovery of grafting-mediated gene transfer further blurs the boundary between natural gene transfer and genetic engineering and suggests that grafting provides an avenue for genes to cross species barriers. Phylogenetic evidence suggests that DNA can be transferred horizontally between reproductively isolated species (*6*). We propose that grafting (whether natural or assisted) provides a path for horizontal gene transfer.

Finally, although our data demonstrate the exchange of genetic material between grafted plants, they do not lend support to the tenet of Lysenkoism that "graft hybridization" would be analogous to sexual hybridization. Instead, our finding that gene transfer is restricted to the contact zone between scion and stock indicates that the changes can become heritable only via lateral shoot formation from the graft site. However, there is some reported evidence for heritable alterations induced by grafting (*7*) and, in light of our findings, these cases certainly warrant detailed molecular investigation.

References and Notes

1. A. D. Beddie, *Trans. Proc. R. Soc. N. Z.* **71**, 199 (1942).
2. F. Brabec, *Planta* **44**, 562 (1954).
3. W. J. Lucas, J. Y. Lee, *Nat. Rev. Mol. Cell Biol.* **5**, 712 (2004).
4. S. E. Goulding, R. G. Olmstead, C. W. Morden, K. H. Wolfe, *Mol. Gen. Genet.* **252**, 195 (1996).
5. C. Stange, J. T. Matus, A. Elorza, P. Arce-Johnson, *Funct. Plant Biol.* **31**, 149 (2004).
6. P. J. Keeling, J. D. Palmer, *Nat. Rev. Genet.* **9**, 605 (2008).
7. Y. Ohta, P. V. Chuong, *Euphytica* **24**, 355 (1975).

8. We thank M. Lohse and D. Karcher for providing transgenic lines, Y. Weber for technical assistance, and D. Karcher for help with identifying markers. This research was financed by the Bundesministerium für Bildung und Forschung.

Supporting Online Material

www.sciencemag.org/cgi/content/full/324/5927/649/DC1
Materials and Methods
Figs. S1 to S5
Tables S1 and S2
References

30 December 2008; accepted 11 March 2009
10.1126/science.1170397

Circadian Clock Feedback Cycle Through NAMPT-Mediated NAD^+ Biosynthesis

Kathryn Moynihan Ramsey,[1,2,3]* Jun Yoshino,[6]* Cynthia S. Brace,[6]* Dana Abrassart,[1,2] Yumiko Kobayashi,[1,2,3] Biliana Marcheva,[1,2] Hee-Kyung Hong,[2] Jason L. Chong,[2] Ethan D. Buhr,[2] Choogon Lee,[4] Joseph S. Takahashi,[2,5] Shin-ichiro Imai,[6]† Joseph Bass[1,2,3]†

The circadian clock is encoded by a transcription-translation feedback loop that synchronizes behavior and metabolism with the light-dark cycle. Here we report that both the rate-limiting enzyme in mammalian nicotinamide adenine dinucleotide (NAD^+) biosynthesis, nicotinamide phosphoribosyltransferase (NAMPT), and levels of NAD^+ display circadian oscillations that are regulated by the core clock machinery in mice. Inhibition of NAMPT promotes oscillation of the clock gene *Per2* by releasing CLOCK:BMAL1 from suppression by SIRT1. In turn, the circadian transcription factor CLOCK binds to and up-regulates *Nampt*, thus completing a feedback loop involving NAMPT/NAD^+ and SIRT1/CLOCK:BMAL1.

Many aspects of mammalian behavior and physiology are coordinated through interconnected networks of 24-hour central and peripheral oscillators that synchronize cycles of fuel storage and utilization to maintain organismal homeostasis. In mice, circadian disruption has been tied to metabolic disturbance (*1*, *2*), whereas a high-fat diet alters both behavioral and molecular rhythms (*3*, *4*). The underlying mechanism of the mammalian clock consists of a transcription-translation feedback loop in which CLOCK and BMAL1 activate transcription of *Cryptochrome* (*Cry1* and *2*) and *Period* (*Per1*, *2*, and *3*), leading to subsequent repression of CLOCK:BMAL1 by CRY and PER proteins (*5*). An additional feedback loop involves the transcriptional regulation of *Bmal1* by RORα and REV-ERBα (*6*, *7*). Previous studies have also implicated a role for cellular nicotinamide adenine dinucleotide (NAD^+) in the regulation of CLOCK and NPAS2 activity (*8*), an observation consistent with the recent finding that the NAD^+-dependent protein deacetylase SIRT1 modulates activity of the clock complex (*9*, *10*).

NAD^+ is a classic coenzyme that is synthesized from three major precursors: tryptophan, nicotinic acid, and nicotinamide (fig. S1). In yeast, it has been reported that enzymes involved in the NAD^+ salvage pathway play an important role in the regulation of Sir2 activity (*11*, *12*). On the other hand, in mammals, the predominant NAD^+ biosynthetic pathway involves the conversion of nicotinamide and 5′-phosphoribosylpyrophosphate to nicotinamide mononucleotide (NMN) by the rate-limiting enzyme nicotinamide phosphoribosyltransferase (NAMPT) (fig. S1) (*13*–*15*). NAMPT-mediated NAD^+ biosynthesis has been demonstrated to play a critical role in a number of biological processes through the NAD^+-dependent deacetylase SIRT1 (fig. S1) (*13*, *16*–*18*).

These findings led us to hypothesize that circadian regulation of NAD^+ may provide a mechanism for regulation of the core clock. Expression levels of *Nampt* RNA displayed a robust diurnal pattern in both wild-type (WT) mouse liver and white adipose tissue (WAT), peaking at the beginning of the dark period [*zeitgeber* time (ZT) 14] (Fig. 1A) (*19*). Expression levels of NAMPT protein also showed a diurnal pattern of oscillation across the 24-hour light-dark cycle in liver (Fig. 1B), with a reduction in NAMPT protein levels before the onset of the dark period [Fig. 1B and supporting description 1 in the supporting online material (SOM)]. *Nampt* RNA oscillation is circadian in nature, as we found a robust oscillation of *Nampt* RNA for 48 hours in liver isolated from WT mice that had been maintained in constant darkness [$P < 0.01$, one-way analysis of variance (ANOVA)] (Fig. 1C). Furthermore, the levels of *Nampt* RNA and protein were lower across the entire light-dark cycle in liver and WAT of $Clock^{\Delta 19}$ mutant mice, and the diurnal oscillation of *Nampt* RNA and protein was abolished in $Clock^{\Delta 19}$ mutant mice (Fig. 1, A and B). The robust *Nampt* RNA oscillation during constant darkness was also abolished completely in the $Clock^{\Delta 19}$ mutant mouse liver (Fig. 1C), indicating that the core clock machinery is required for the circadian control of NAMPT expression.

Because NAMPT is the rate-limiting enzyme in the predominant NAD^+ biosynthetic pathway in mammals, we tested whether tissue NAD^+ levels also display a circadian oscillation pattern in WT liver across 48 hours from mice maintained in constant darkness. Liver NAD^+ levels showed a very similar bimodal circadian oscillation pattern to that of NAMPT protein, and the lowest levels of NAD^+ occurred with a rhythmicity of 24 hours (Fig. 1D). We also observed a decrease in NAD^+ levels around CT10-14 and again 24 hours later (CT34), generating the observed bimodal oscillation pattern (Fig. 1D and supporting description 1). The degree to which NAD^+ levels increased from baseline (40 to 53%) during these daily cycles, as well as the concentrations of NAD^+ that we measured, fall within the physiological range of reported alterations in NAD^+ levels (supporting description 2) (*20*, *21*).

[1]Department of Medicine, Northwestern University Feinberg School of Medicine, 2200 Campus Drive, Evanston, IL 60208–3500, USA. [2]Department of Neurobiology and Physiology, Northwestern University Feinberg School of Medicine, 2200 Campus Drive, Evanston, IL 60208–3500, USA. [3]NorthShore University Health System Research Institute and Department of Medicine, Evanston, IL 60201, USA. [4]Department of Biomedical Sciences, College of Medicine, Florida State University, Tallahassee, FL 32306, USA. [5]Howard Hughes Medical Institute, Northwestern University, Evanston, IL 60208, USA. [6]Department of Developmental Biology, Washington University School of Medicine, St. Louis, MO 63110, USA.

*These authors contributed equally to this work.
†To whom correspondence should be addressed. E-mail: imaishin@wustl.edu (S.I.); j-bass@northwestern.edu (J.B.)

NAD^+ levels were significantly reduced in $Clock^{\Delta 19}$ mutant liver during both the light (ZT2) and dark (ZT14) periods (Fig. 1E). Furthermore, we observed that mice deficient in *Bmal1* (*Bmal1*$^{-/-}$) (*22*), the heterodimeric binding partner of CLOCK, also exhibited a significant reduction in both *Nampt* RNA and NAD^+ levels in liver (Fig. 1E). Finally, mice deficient for both CRY1 and CRY2 (*23*) displayed a significant increase in *Nampt* RNA levels and a corresponding increase in NAD^+ levels in liver, which is consistent with *Nampt* being a target gene of CLOCK:BMAL1 (Fig. 1E). Thus, the rhythmic oscillation in RNA and protein levels of NAMPT lead to a circadian oscillation of NAD^+ levels in the living animal.

The peak in NAMPT and NAD^+ in the liver of WT mice (Fig. 1, B, D, and E) is consistent with a previous report that endogenous SIRT1, an NAD^+-dependent and nutrient-responsive deacetylase, displays a diurnal oscillation in activity with a peak around ZT15 (*9*). We therefore examined whether SIRT1 activity is affected by altering NAMPT-mediated NAD^+ biosynthesis in primary hepatocytes with the specific chemical inhibitor of NAMPT, FK866 (*24*). FK866 significantly inhibited NAD^+ biosynthesis (Fig. 2A), resulting in ~30% reduction in mRNA expression levels of two major SIRT1 target genes in the liver, *Pepck* (*phosphoenolpyruvate carboxykinase*) and *G6Pase* (*glucose-6-phosphatase*) (*20*), but not an unrelated gene, *Igf-1* (*insulin-like growth factor-1*) (Fig. 2B). Using *Per2:luciferase* transcriptional reporter assays in HEK293 cells (Fig. 2, C to E, and fig. S2), we show that inhibition of NAMPT by FK866 led to a significant increase in the CLOCK:BMAL1-driven transcription of the *Per2:luciferase* reporter (Fig. 2C), indicating that reduced NAMPT-mediated NAD^+ biosynthesis released CLOCK:BMAL1 from the SIRT1-dependent suppression. Consistent with this notion, SIRT1 suppressed transcription of *Per2:luciferase* in a dose-dependent manner (Fig. 2D). Additionally, resveratrol, a putative SIRT1 activator, also inhibited *Per2:luciferase* transcription (figs. S2 and S3A). In contrast, inhibition of SIRT1 by high doses of nicotinamide activated *Per2:luciferase* transcription, and the selective SIRT1 inhibitor EX-527 showed a similar trend (figs. S2 and S3, B and C). Furthermore, FK866 abrogated the SIRT1-dependent suppression of CLOCK:BMAL1-mediated transcription (Fig. 2E).

To investigate the effect of this regulatory pathway on clock gene expression, we first confirmed that SIRT1 binds to BMAL1 (fig. S4) (*9*, *10*) and then determined that SIRT1 localizes to the E-box of the *Per2* promoter (Fig. 3A), suggesting that *Per2* is a target of the NAMPT/NAD^+-driven pathway. We next examined the effect of FK866 on *Per2* rhythms in primary hepatocytes. Serum shock induced a *Per2* oscillation in vehicle-treated hepatocytes that damped rapidly after one cycle (2.2-day damping rate), whereas FK866 treatment prolonged the oscillation of *Per2* (5.3-day damping rate) (Fig. 3B). Reduction in NAMPT-mediated NAD^+ biosynthesis may promote a more robust oscillation of clock target gene expression by releasing CLOCK:BMAL1 from SIRT1-mediated suppression. Consistent with this notion, adenoviral *Sirt1* transduction of primary hepatocytes suppressed the expression and oscillation of *Per2*, although adenoviral infection itself altered the *Per2* oscillation pattern (Fig. 3C). Therefore, the NAMPT/NAD^+-driven pathway modulates circadian transcription patterns in mammals.

To determine if this pathway comprises a feedback loop involving regulation of the *Nampt* gene by CLOCK:BMAL1, we performed chromatin immunoprecipitation (ChIP) to test whether the CLOCK:BMAL1 complex binds to canonical or noncanonical E-box motifs in the promoter and first intron of the *Nampt* gene (fig. S5). ChIP detected CLOCK in these regions (Fig. 3D, first, second, and third panels), but not in a nonspecific upstream region (Fig. 3D, fourth panel). We observed a stronger signal for CLOCK at CT6 as compared with the signal at CT15 (Fig. 3D),

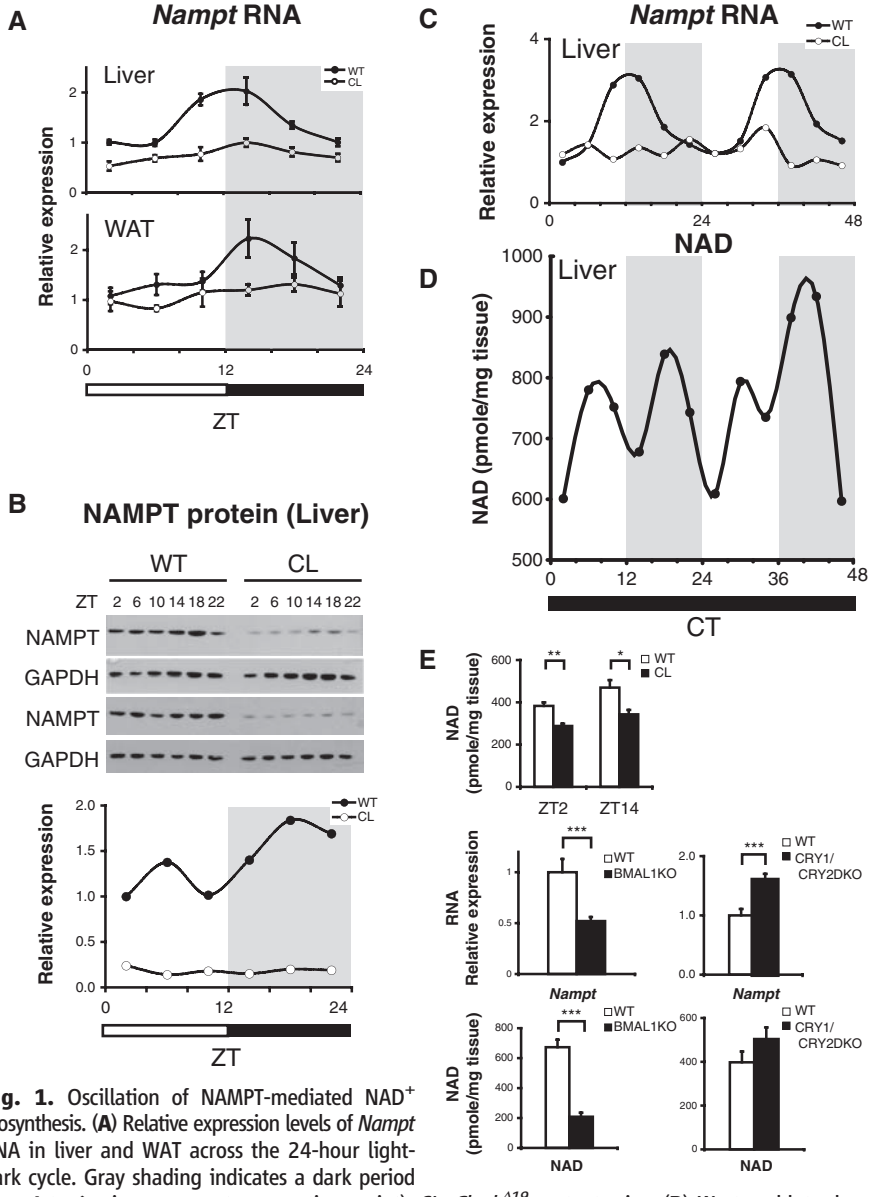

Fig. 1. Oscillation of NAMPT-mediated NAD^+ biosynthesis. (**A**) Relative expression levels of *Nampt* RNA in liver and WAT across the 24-hour light-dark cycle. Gray shading indicates a dark period (n = 4 to 6 mice per genotype per time point). CL, $Clock^{\Delta 19}$ mutant mice. (**B**) Western blots showing NAMPT and glyceraldehyde-3-phosphate dehydrogenase (GAPDH) at indicated ZTs. Quantitation of NAMPT normalized to GAPDH. (**C**) Relative expression levels of *Nampt* RNA across 48 hours in liver of WT and $Clock^{\Delta 19}$ mice in constant darkness. The shading indicates where light and dark periods would normally occur under 12:12 light-dark conditions (n = 2 WT, n = 1 $Clock^{\Delta 19}$ per time point, $P < 0.01$, one-way ANOVA for WT oscillation). (**D**) NAD^+ levels across 48 hours in liver of WT mice in constant darkness (n = 2 WT per time point). (**E**) NAD^+ levels in WT and $Clock^{\Delta 19}$ mutant liver at ZT2 and 14 (n = 3 per genotype per time point) (upper panel). Relative expression levels of *Nampt* RNA (middle panels) and NAD^+ (lower panels) in *Bmal1*$^{-/-}$, *Cry1*$^{-/-}$/*Cry2*$^{-/-}$, and WT liver at ZT7 (n = 4 to 13). *$P < 0.05$; **$P < 0.01$; ***$P < 0.001$. All data are presented as mean ± SEM.

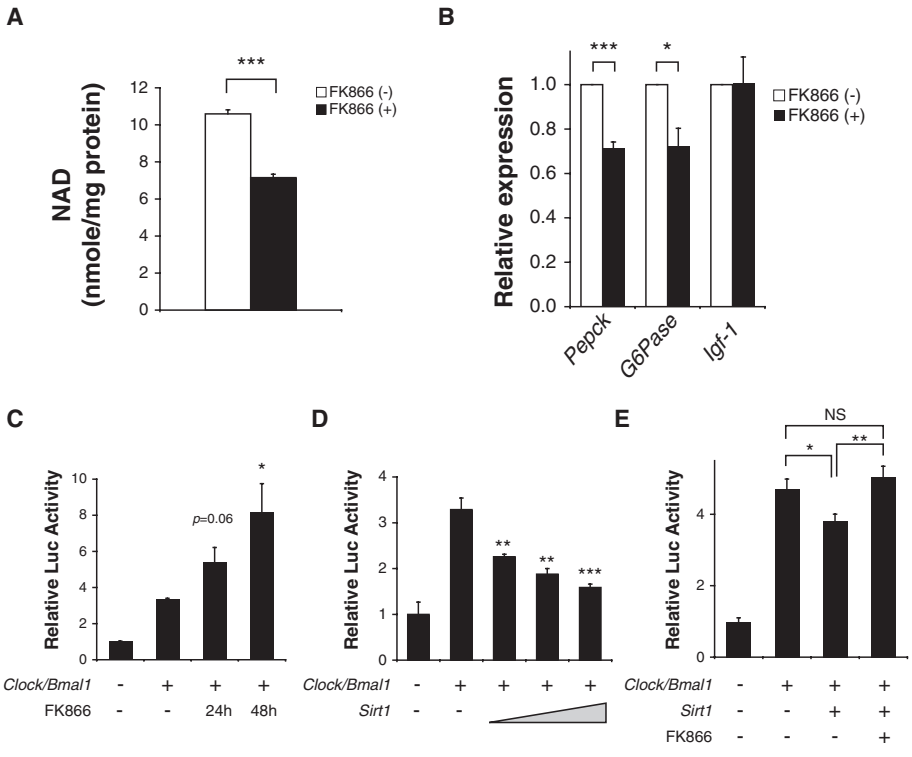

Fig. 2. NAMPT, NAD^+, and SIRT1 regulate CLOCK: BMAL1 activity. (**A** and **B**) NAD^+ levels (A) and relative expression levels of *Pepck*, *G6Pase*, and *Igf-1* RNA (B) in primary hepatocytes incubated with 200 nM FK866 for 24 hours ($n = 3$ per group) (*Pepck*, *G6Pase*, *Igf-1*). (**C** to **E**) Relative luciferase activity of *Per2-luciferase* in the presence of (C) 10 nM FK866 for 24 or 48 hours, (D) increasing doses of *Sirt1* (200, 400, 800 ng), and (E) *Sirt1* (800 ng) alone or *Sirt1* (800 ng) and 10 nM FK866 for 48 hours. $*P < 0.05$; $**P < 0.01$; $***P < 0.001$; NS, not significant. All data are presented as mean ± SEM.

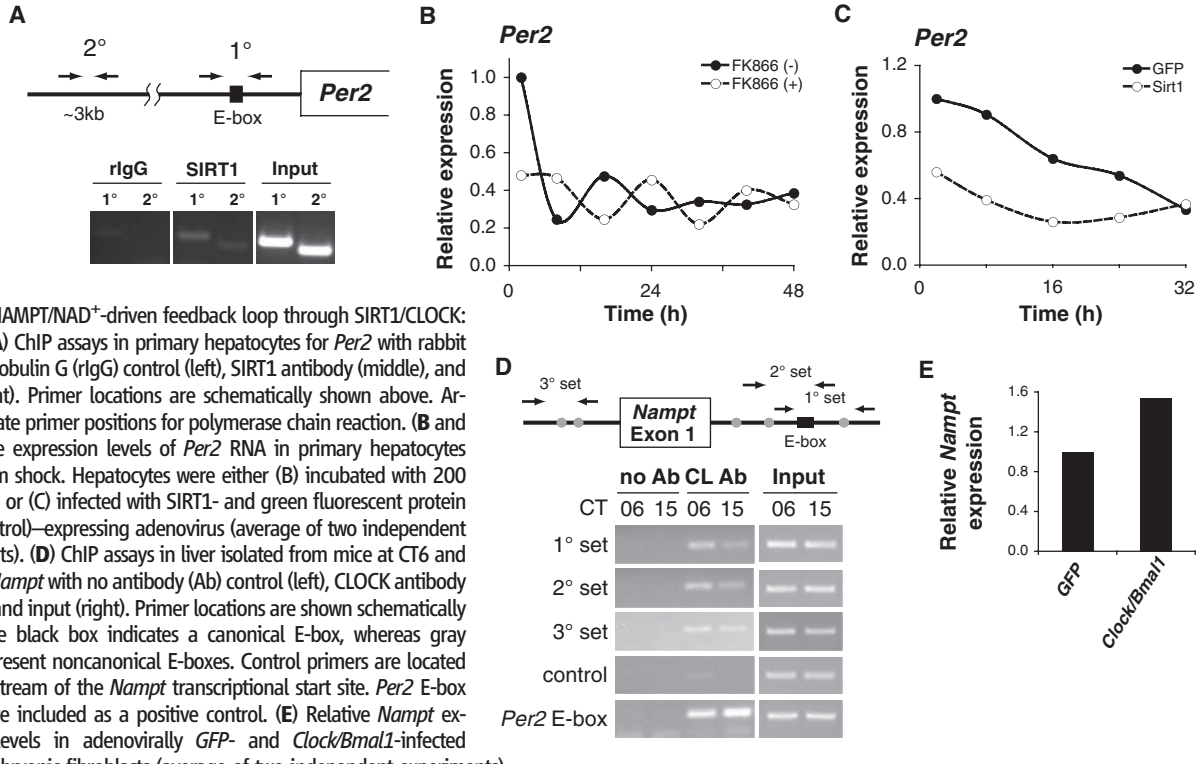

Fig. 3. NAMPT/NAD^+-driven feedback loop through SIRT1/CLOCK: BMAL1. (**A**) ChIP assays in primary hepatocytes for *Per2* with rabbit immunoglobulin G (rIgG) control (left), SIRT1 antibody (middle), and input (right). Primer locations are schematically shown above. Arrows indicate primer positions for polymerase chain reaction. (**B** and **C**) Relative expression levels of *Per2* RNA in primary hepatocytes after serum shock. Hepatocytes were either (B) incubated with 200 nM FK866 or (C) infected with SIRT1- and green fluorescent protein (GFP) (control)–expressing adenovirus (average of two independent experiments). (**D**) ChIP assays in liver isolated from mice at CT6 and CT15 for *Nampt* with no antibody (Ab) control (left), CLOCK antibody (middle), and input (right). Primer locations are shown schematically above. The black box indicates a canonical E-box, whereas gray circles represent noncanonical E-boxes. Control primers are located ~5 kb upstream of the *Nampt* transcriptional start site. *Per2* E-box primers are included as a positive control. (**E**) Relative *Nampt* expression levels in adenovirally *GFP*- and *Clock/Bmal1*-infected mouse embryonic fibroblasts (average of two independent experiments).

which suggests rhythmic binding of CLOCK: BMAL1 in a promoter context-dependent manner (*25*, *26*). Transduction of *Clock/Bmal1* into mouse embryonic fibroblasts appeared to up-regulate *Nampt* expression ~1.6-fold (Fig. 3E). Together, these data demonstrate that NAMPT-mediated NAD^+ biosynthesis comprises a feedback loop in which NAD^+ functions as a metabolic oscillator and regulates the core clock machinery through SIRT1 (fig. S6 and supporting description 3). Given the central role of NAD^+ as a biological cofactor, the rhythmic production of NAD^+ may have a cascade of effects on downstream pathways, including chromatin regulation, metabolism, and aging. We thus propose that the circadian feedback loop through NAMPT-mediated NAD^+ biosynthesis may function to fine-tune the daily cycles of energy storage and utilization and also to coordinate these processes with the rest-activity cycle.

References and Notes

1. F. W. Turek *et al.*, *Science* **308**, 1043 (2005); published online 21 April 2005 (10.1126/science.1108750).
2. R. D. Rudic *et al.*, *PLoS Biol.* **2**, e377 (2004).
3. A. Kohsaka *et al.*, *Cell Metab.* **6**, 414 (2007).

4. M. Barnea, Z. Madar, O. Froy, *Endocrinology* **150**, 161 (2009).
5. J. S. Takahashi, H. K. Hong, C. H. Ko, E. L. McDearmon, *Nat. Rev. Genet.* **9**, 764 (2008).
6. N. Preitner *et al.*, *Cell* **110**, 251 (2002).
7. T. K. Sato *et al.*, *Neuron* **43**, 527 (2004).
8. J. Rutter, M. Reick, L. C. Wu, S. L. McKnight, *Science* **293**, 510 (2001); published online 5 July 2001 (10.1126/science.1060698).
9. Y. Nakahata *et al.*, *Cell* **134**, 329 (2008).
10. G. Asher *et al.*, *Cell* **134**, 317 (2008).
11. R. M. Anderson *et al.*, *J. Biol. Chem.* **277**, 18881 (2002).
12. R. M. Anderson, K. J. Bitterman, J. G. Wood, O. Medvedik, D. A. Sinclair, *Nature* **423**, 181 (2003).
13. J. R. Revollo, A. A. Grimm, S. Imai, *J. Biol. Chem.* **279**, 50754 (2004).
14. J. R. Revollo *et al.*, *Cell Metab.* **6**, 363 (2007).
15. S. Imai, *Curr. Pharm. Des.* **15**, 20 (2009).
16. E. van der Veer *et al.*, *J. Biol. Chem.* **282**, 10841 (2007).
17. M. Fulco *et al.*, *Dev. Cell* **14**, 661 (2008).
18. H. Yang *et al.*, *Cell* **130**, 1095 (2007).
19. Materials and methods are available as supporting material on *Science* Online.
20. J. T. Rodgers *et al.*, *Nature* **434**, 113 (2005).
21. D. Chen *et al.*, *Genes Dev.* **22**, 1753 (2008).
22. M. K. Bunger *et al.*, *Cell* **103**, 1009 (2000).
23. M. H. Vitaterna *et al.*, *Proc. Natl. Acad. Sci. U.S.A.* **96**, 12114 (1999).
24. M. Hasmann, I. Schemainda, *Cancer Res.* **63**, 7436 (2003).
25. C. Lee, J. P. Etchegaray, F. R. Cagampang, A. S. Loudon, S. M. Reppert, *Cell* **107**, 855 (2001).
26. J. A. Ripperger, U. Schibler, *Nat. Genet.* **38**, 369 (2006).
27. We thank S.-H. Yoo and members of the Bass, Imai, and Takahashi laboratories for discussions. Work was supported by grants from the National Institute of Diabetes and Digestive and Kidney Diseases (T32 DK007169) to K.M.R.; the National Institute on Aging (AG02150), the Ellison Medical Foundation, and the Longer Life Foundation to S.I.; NIH (PO1 AG011412), the Chicago Biomedical Consortium Searle Funds, and the *Juvenile Diabetes Research Foundation* to J.B.; and a grant from the National Institute of Mental Health (P50 MH074924) to J.S.T. J.Y. is supported by the Japan Research Foundation for Clinical Pharmacology and Keio University Medical Science Fund, J.S.T. is an Investigator in the Howard Hughes Medical Institute and a cofounder of ReSet Therapeutics, and J.S.T. and J.B. are members of its scientific advisory board. J.B. is also an adviser and receives support from Amylin Pharmaceuticals. S.I. holds a patent related to the work reported in this paper, specifically NAMPT and NMN.

Supporting Online Material

www.sciencemag.org/cgi/content/full/1171641/DC1
Materials and Methods
SOM Text
Figs. S1 to S6
References

30 January 2009; accepted 9 March 2009
Published online 19 March 2009;
10.1126/science.1171641
Include this information when citing this paper.

Circadian Control of the NAD$^+$ Salvage Pathway by CLOCK-SIRT1

Yasukazu Nakahata, Saurabh Sahar, Giuseppe Astarita, Milota Kaluzova, Paolo Sassone-Corsi*

Many metabolic and physiological processes display circadian oscillations. We have shown that the core circadian regulator, CLOCK, is a histone acetyltransferase whose activity is counterbalanced by the nicotinamide adenine dinucleotide (NAD$^+$)–dependent histone deacetylase SIRT1. Here we show that intracellular NAD$^+$ levels cycle with a 24-hour rhythm, an oscillation driven by the circadian clock. CLOCK:BMAL1 regulates the circadian expression of NAMPT (nicotinamide phosphoribosyltransferase), an enzyme that provides a rate-limiting step in the NAD$^+$ salvage pathway. SIRT1 is recruited to the *Nampt* promoter and contributes to the circadian synthesis of its own coenzyme. Using the specific inhibitor FK866, we demonstrated that NAMPT is required to modulate circadian gene expression. Our findings in mouse embryo fibroblasts reveal an interlocked transcriptional-enzymatic feedback loop that governs the molecular interplay between cellular metabolism and circadian rhythms.

Accumulating evidence reveals intriguing links between the circadian clock and cellular metabolism (*1*–*3*), which, at least in part, rely on epigenetic control and chromatin remodeling (*4*). The circadian regulator CLOCK has an intrinsic acetyltransferase activity, which enables circadian chromatin remodeling by acetylating histones (*5*) and nonhistone proteins, including its own partner BMAL1 (*6*). The histone deacetylase (HDAC) that counterbalances the histone acetyltransferase function of CLOCK is SIRT1 (*7*, *8*), an enzyme whose activity is dependent on intracellular NAD$^+$ levels (*9*). Although NAD$^+$ is SIRT1's natural cosubstrate, the reduced form of NAD$^+$ (NADH) and the by-product of NAD$^+$ consumption, nicotinamide (NAM), repress the activity of SIRT1 (*9*) and generate an enzymatic feedback loop on the HDAC function of this enzyme. Two main systems determine NAD$^+$ levels in the cell, the de novo biosynthesis from tryptophan and the NAD$^+$ salvage pathway (*10*). A critical step of the latter pathway is controlled by the enzyme nicotinamide phosphoribosyltransferase (NAMPT) (*11*), also known as visfatin or pre–B cell colony-enhancing factor (PBEF), which catalyzes the first step in the biosynthesis of NAD$^+$ from NAM. NAMPT is implicated in cellular metabolism, senescence, and survival in response to genotoxic stress (*12*–*14*).

Because of the role of SIRT1 in modulating clock function (*7*), we reasoned that circadian tuning may be achieved by NAD$^+$ oscillating levels. Wild-type (WT) mouse embryo fibroblasts (MEFs) were serum-entrained, and cellular NAD$^+$ levels were measured by liquid chromatography coupled to tandem mass spectrometry (LC/MS^n) from total extracts prepared at various time intervals after serum shock (*15*). Cellular NAD$^+$ showed a reproducible circadian oscillation of about 2.5-fold (Fig. 1A). The average NAD$^+$ concentration of 25 pmol/μg protein (~60 μM) found in MEFs is in keeping with recent reports for rat axons using LC coupled to an ultraviolet detector (9 pmol/μg protein) (*16*), mouse erythrocyte using LC/MS/MS (368 μM) (*17*), and HEK293 cells using LC with matrix-assisted laser desorption/ionization (MALDI) MS (365 μM) (*14*). Note that cellular NAD$^+$ oscillation is in phase with SIRT1 deacetylase activity and its phase is opposite to that of acetylation of histone H3 and BMAL1 (*7*).

NAD$^+$ levels did not oscillate in entrained MEFs originated from the *clock/clock* mutant mice (*c/c*) and from the arrhythmic *Cry1/Cry2* double-knockout (KO) mice (*cry*) (Fig. 1B and fig. S1), which demonstrated that NAD$^+$ oscillation is driven by the circadian clock. Total cellular NAM levels measured by LC/MS^n also showed oscillation, albeit more moderate, with a phase opposite to that of NAD$^+$. Also NAM oscillation was abolished in the MEFs from *c/c* and *cry* mice (Fig. 1D). Thus, the circadian clock controls the levels of these metabolites. This analysis also provided a clue: NAD$^+$ and NAM levels are significantly lower in mutant MEFs than in WT cells (for NAD$^+$ only 1.1 pmol/μg protein in *c/c* MEFs, about 5% of that in WT MEFs) (Fig. 1, C and E). This notion points to an involvement of the NAD$^+$ salvage pathway and, because of its dynamic regulation, specifically to NAMPT, whose prominent function in NAD$^+$ production has been demonstrated (*18*–*20*). Furthermore, increased flux through the NAD$^+$ salvage pathway is responsible for sirtuin-dependent responses even under conditions of unaltered steady-state NAD$^+$ levels (*12*).

Next, we analyzed the expression of NAD$^+$ salvage pathway metabolic enzymes. The nicotinamide mononucleotide adenylyltransferases, NMNAT1, NMNAT2, and NMNAT3, are central in NAD biosynthesis; they catalyze the adenylation of nicotinamide mononucleotide (NMN) or nicotinic acid mononucleotide (NaMN) by using the adenosine monophosphate (AMP) moiety of adenosine triphosphate to form NAD$^+$ or nicotinic acid dinucleotide, respectively (Fig. 2A). The expression of these three enzymes is mildly oscillatory (fig. S2). Thus, our attention focused on NAMPT, which operates as rate-limiting enzyme in NAD$^+$ production within the NAD$^+$ salvage pathway (*10*, *14*, *21*). Expression of *Nampt* is robustly circadian in livers from WT mice, whereas oscillation is virtually absent in *c/c* mice (Fig. 2B). Rhythmic expression is observed also in serum-entrained WT MEFs, paralleling *Dbp* oscillation. Again, *Nampt* oscillation is abolished in *c/c* MEFs (Fig. 2C).

The *Nampt* promoter contains three putative, highly conserved, E-box sequences (CACGTG)

Department of Pharmacology, School of Medicine, University of California, Irvine, Irvine, CA 92697, USA.
*Corresponding author: Paolo Sassone-Corsi, psc@uci.edu

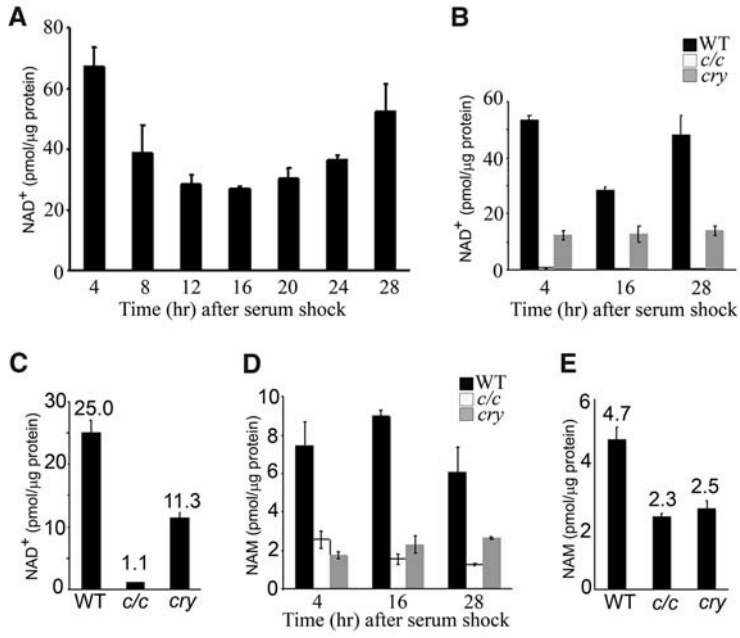

Fig. 1. Circadian oscillation of NAD^+ is controlled by the clock. (**A** and **B**) Cellular NAD^+ was extracted from serum-entrained MEFs derived from WT (A), *clock/clock* mutant mice (*c/c*), and *Cry1/Cry2* double-KO mice (*cry*) (B) at indicated time points and analyzed by LC/MS^n. Three independent experiments were performed, and representative results are shown. All data are means ± SEM of three independent samples. (**C**) Average NAD^+ levels. (means ± SEM of >50 independent samples). (**D**) Cellular NAM was extracted from serum-entrained MEFs derived from WT, *c/c*, and *cry* mice at indicated time points and analyzed by LC/MS^n. (**E**) Average NAM levels (means ± SEM of >50 independent samples).

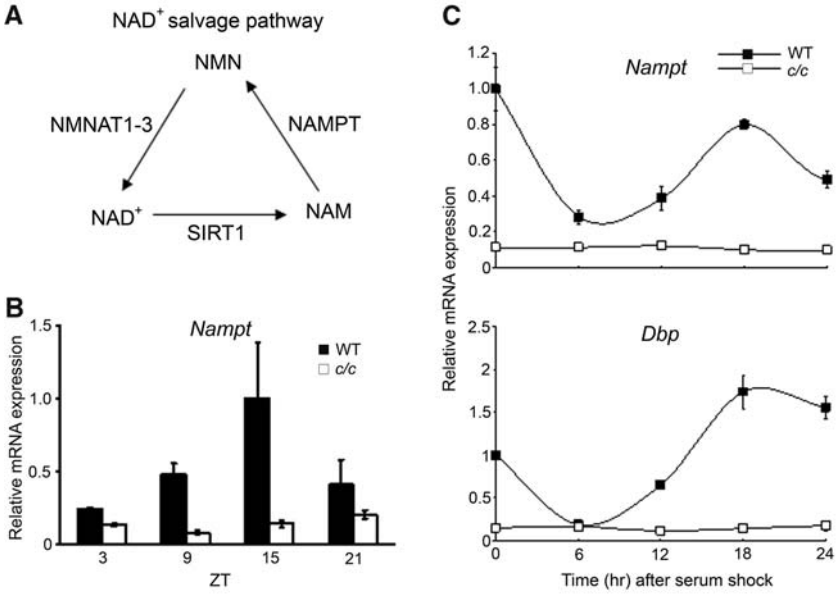

Fig. 2. The circadian clock controls *Nampt* gene expression. (**A**) Scheme of the NAD^+ salvage pathway in mammals. (**B**) *Nampt* gene expression in livers from light-entrained WT and *c/c* mutant mice as measured by quantitative polymerase chain reaction (Q-PCR). *Nampt* gene expression at Zeitgeber time (ZT) 15 in liver from WT mice was set to 1. (**C**) *Nampt* and *Dbp* gene expressions in serum-entrained MEFs from WT and *c/c* mutant mice were quantified by Q-PCR. Expression at time 0 in WT MEFs was set to 1. All data are means ± SEM of three independent samples.

(Fig. 3, A and B). Using promoter mutagenesis and transient expression in cultured cells, we demonstrate that the *Nampt* promoter is readily activated by CLOCK:BMAL1 through the E-boxes (Fig. 3C). Next, using chromatin immunoprecipitation (ChIP), we showed that CLOCK:BMAL1 physically and specifically associates to the E-boxes on the *Nampt* promoter in a time-dependent manner (Fig. 3, D and E), consistent with *Nampt* circadian expression. We have recently demonstrated that SIRT1 is in a complex with CLOCK:BMAL1 (*7*). Dual cross-linking ChIP assays showed that SIRT1 binds to the E-boxes in a time-dependent manner, following the circadian timing of CLOCK:BMAL1 recruitment (Fig. 3, D and E). Thus, as previously shown for *Dbp* and *Per2* (*7*), CLOCK and SIRT1 contribute to circadian chromatin remodeling at the *Nampt* promoter. As NAD^+ intracellular levels directly influence the HDAC activity of SIRT1 (*22*–*24*), an enzymatic-transcription feedback loop seems to operate, in which NAD^+ levels determine the oscillatory synthesis of NAMPT, the key enzyme in the NAD^+ salvage pathway.

To address whether NAMPT is critical in modulating clock function, we took advantage of FK866, a low-molecular-weight specific NAMPT inhibitor. FK866 lowers cellular NAD^+ and NAM levels over a prolonged length of time (*18*) (figs. S3 and S4). Pharmacological inhibition of NAMPT significantly modifies the circadian expression of *Per2* and *Dbp* in serum-stimulated MEFs (Fig. 4A) and causes an earlier onset of the circadian peak for both genes by 3 to 4 hours and increases the amplitude of oscillation by 30 to 40%. This effect of FK866 is highly similar to the one caused by inhibition of SIRT1 (*7*). Thus, we predicted that blocking NAMPT would modify BMAL1 acetylation, a regulatory event critical to clock function (*6*). Using the antibody against acetyl-BMAL1 recently developed in our laboratory (*7*), we showed that inhibition of NAMPT induces a considerable increase and a broader peak of Lys^{537} acetylation (Fig. 4B). This BMAL1 acetylation profile is basically equivalent to the one observed in MEFs and livers from *Sirt1*$^{-/-}$ mice (*7*).

How intimate is the link between cellular metabolism and the circadian clock? Specifically, are metabolic pathways regulating the circadian machinery (*3*, *25*, *26*), or are molecular elements of the clock controlling metabolism (*3*, *27*, *28*)? The findings reported here demonstrate that both pathways exist in the cell, and each utilizes a discrete molecular mechanism of control in which the enzyme NAMPT occupies a pivotal position. Our results reveal the interlocking of two autoregulatory systems, in which a classical transcription circadian loop is coupled to an enzymatic feedback loop (Fig. 4C). These findings point to the oscillation of NAD^+ as a key regulatory step in the modulation of rhythms in metabolic tissues and peripheral clocks. Note that FK866 may be used for treatment of diseases that may be implicated in deregulated apoptosis or act as a sensitizer for genotoxic agents (*18*). Thus, our findings could have multiple implications including avenues to pharmacological intervention.

References and Notes

1. H. Wijnen, M. W. Young, *Annu. Rev. Genet.* **40**, 409 (2006).
2. C. B. Green, J. S. Takahashi, J. Bass, *Cell* **134**, 728 (2008).
3. K. Eckel-Mahan, P. Sassone-Corsi, *Nat. Struct. Mol. Biol.*, in press.
4. W. J. Belden, J. C. Dunlap, *Cell* **134**, 212 (2008).

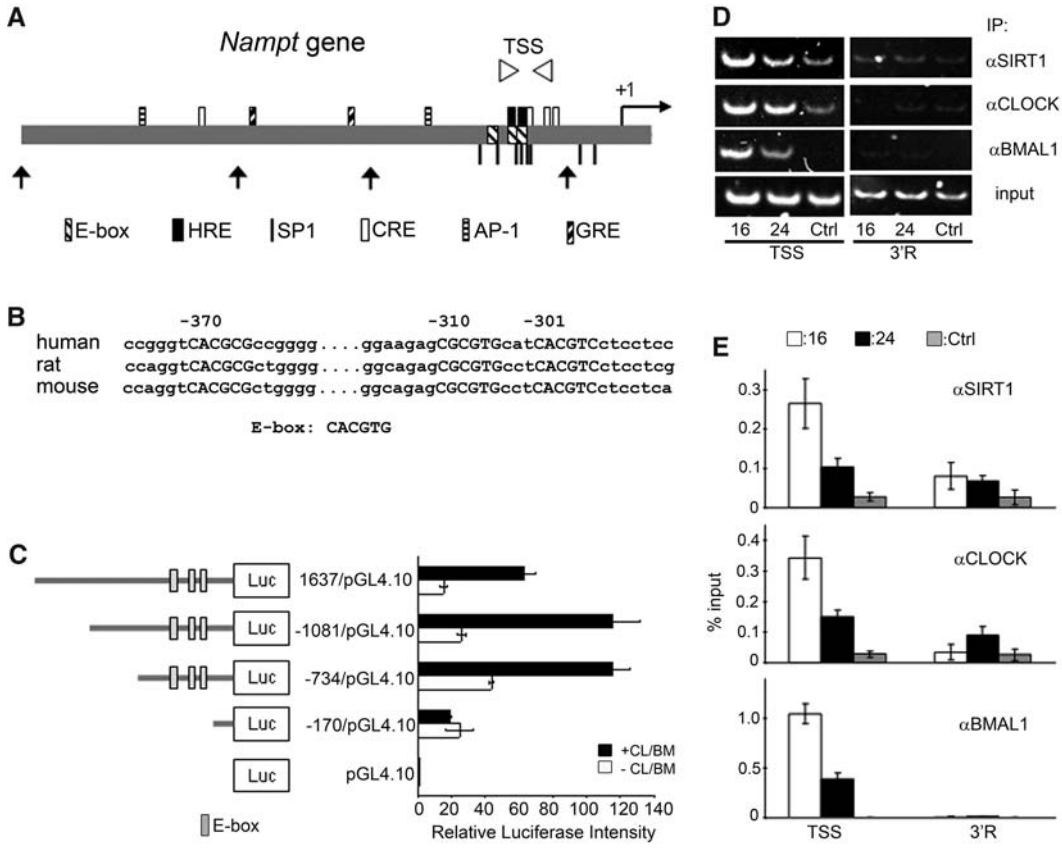

Fig. 3. Regulation of the *Nampt* promoter by CLOCK:BMAL1 and SIRT1. (**A**) Schematic diagram of regulatory elements in human *Nampt* promoter. TSS (transcription start site) primer region for Q-PCR, arrowheads; truncated forms of *Nampt* promoter used in (C), arrows. Putative transcription factor-binding sites are indicated: HRE, hypoxia response element; SP1, specificity protein 1; CRE, cyclic AMP–response element; AP-1, activator protein 1; GRE, glucocorticoid receptor response element. (**B**) Conserved E-boxes (capitalized) are shown. Numbers indicate positions from human TSS. (**C**) Schematic diagram of *Nampt* promoter constructs. Effect of CLOCK:BMAL1 (+CL/BM; black bars) on luciferase activity is shown. Luciferase activity of CLOCK:BMAL1 on the pGL4.10 was set as 1. All data are means ± SEM of three independent samples. (**D**) Representative results of ChIP assays analyzed by semiquantitative PCR. Dual cross-linked nuclear extracts isolated from MEFs after 16 or 24 hours serum shock and subjected to ChIP assay with antibodies against SIRT1, CLOCK, or BMAL1 or no antibody (ctrl). No antibody and 3′R primers were used as controls for immunoprecipitation and PCR, respectively. (**E**) Quantification of ChIP by Q-PCR. Q-PCR was performed on the samples described in (D). All data are means ± SEM of three independent samples.

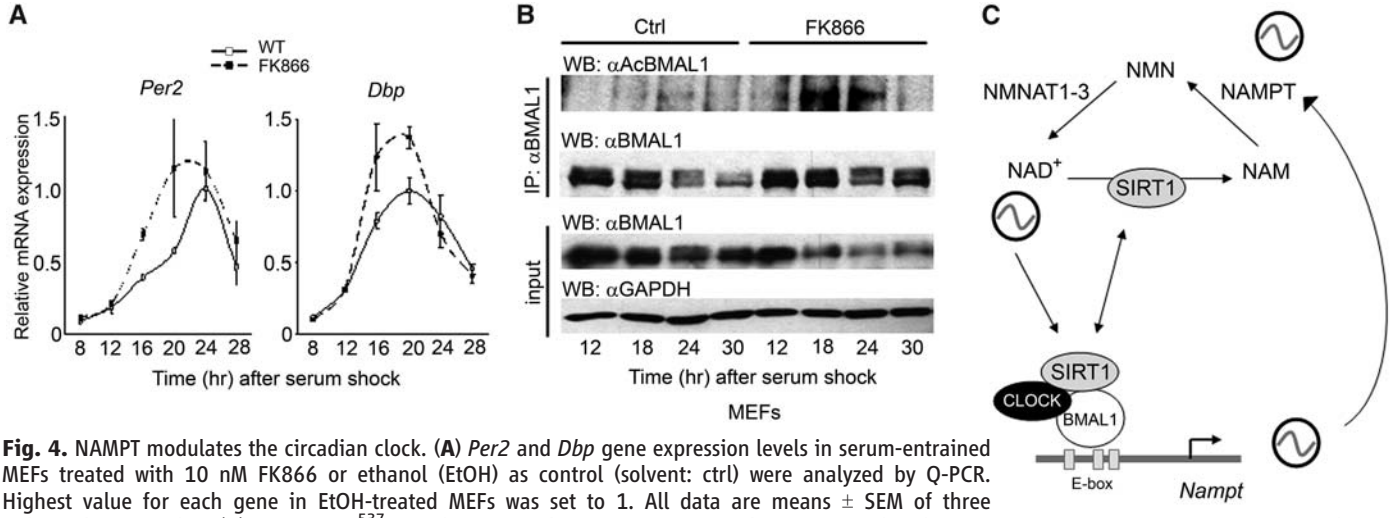

Fig. 4. NAMPT modulates the circadian clock. (**A**) *Per2* and *Dbp* gene expression levels in serum-entrained MEFs treated with 10 nM FK866 or ethanol (EtOH) as control (solvent: ctrl) were analyzed by Q-PCR. Highest value for each gene in EtOH-treated MEFs was set to 1. All data are means ± SEM of three independent samples. (**B**) BMAL1 Lys^{537} acetylation profile in serum-entrained MEFs treated with 10 nM FK866 or EtOH. Extracts prepared from indicated time points and BMAL1 acetylation were monitored (*7*). Input samples were probed with BMAL1- and GAPDH-specific antibodies. (**C**) Scheme of the transcription-enzymatic interplay by which the circadian machinery governs the intracellular levels of NAD$^+$. The NAD$^+$-dependent deacetylase SIRT1 is thereby controlling the oscillatory synthesis of its own coenzyme.

5. M. Doi, J. Hirayama, P. Sassone-Corsi, *Cell* **125**, 497 (2006).
6. J. Hirayama *et al.*, *Nature* **450**, 1086 (2007).
7. Y. Nakahata *et al.*, *Cell* **134**, 329 (2008).
8. G. Asher *et al.*, *Cell* **134**, 317 (2008).
9. L. Bordone, L. Guarente, *Nat. Rev. Mol. Cell Biol.* **6**, 298 (2005).
10. A. Rongvaux, F. Andris, F. Van Gool, O. Leo, *Bioessays* **25**, 683 (2003).
11. J. R. Revollo, A. A. Grimm, S. Imai, *J. Biol. Chem.* **279**, 50754 (2004).
12. R. M. Anderson *et al.*, *J. Biol. Chem.* **277**, 18881 (2002).
13. E. van der Veer *et al.*, *J. Biol. Chem.* **282**, 10841 (2007).
14. H. Yang *et al.*, *Cell* **130**, 1095 (2007).
15. Materials and methods are available as supporting material on *Science* Online.
16. J. Wang *et al.*, *J. Cell Biol.* **170**, 349 (2005).
17. K. Yamada, N. Hara, T. Shibata, H. Osago, M. Tsuchiya, *Anal. Biochem.* **352**, 282 (2006).
18. M. Hasmann, I. Schemainda, *Cancer Res.* **63**, 7436 (2003).
19. U. H. Olesen *et al.*, *Biochem. Biophys. Res. Commun.* **367**, 799 (2008).
20. A. Rongvaux *et al.*, *J. Immunol.* **181**, 4685 (2008).
21. J. R. Revollo *et al.*, *Cell Metab.* **6**, 363 (2007).

22. S. Imai, C. M. Armstrong, M. Kaeberlein, L. Guarente, *Nature* **403**, 795 (2000).
23. J. Landry *et al.*, *Proc. Natl. Acad. Sci. U.S.A.* **97**, 5807 (2000).
24. J. S. Smith *et al.*, *Proc. Natl. Acad. Sci. U.S.A.* **97**, 6658 (2000).
25. F. Damiola *et al.*, *Genes Dev.* **14**, 2950 (2000).
26. K. Kaasik, C. C. Lee, *Nature* **430**, 467 (2004).
27. K. A. Lamia, K. F. Storch, C. J. Weitz, *Proc. Natl. Acad. Sci. U.S.A.* **105**, 15172 (2008).
28. F. W. Turek *et al.*, *Science* **308**, 1043 (2005).

29. Thanks to D. Piomelli for insightful discussions and help. Thanks also to L. Guarente, K. Yamagata, and members of the Sassone-Corsi laboratory for help, reagents, and support. Y.N. was supported by the Japan Society for the Promotion of Science Postdoctoral Fellowships for Research Abroad. S.S. was supported by a postdoctoral fellowship from the American Heart Association, Western States Affiliate. Work supported by the Cancer Research Coordinating Committee of the University of California and NIH (R01-GM081634-01).

Supporting Online Material
www.sciencemag.org/cgi/content/full/1170803/DC1
Materials and Methods
Figs. S1 to S4
References

12 January 2009; accepted 2 March 2009
Published online 12 March 2009;
10.1126/science.1170803
Include this information when citing this paper.

A Cytidine Deaminase Edits C to U in Transfer RNAs in Archaea

Lennart Randau,[1]*† Bradford J. Stanley,[1]* Andrew Kohlway,[1] Sarah Mechta,[1] Yong Xiong,[1]† Dieter Söll[1,2]†

All canonical transfer RNAs (tRNAs) have a uridine at position 8, involved in maintaining tRNA tertiary structure. However, the hyperthermophilic archaeon *Methanopyrus kandleri* harbors 30 (out of 34) tRNA genes with cytidine at position 8. Here, we demonstrate C-to-U editing at this location in the tRNA's tertiary core, and present the crystal structure of a tRNA-specific cytidine deaminase, CDAT8, which has the cytidine deaminase domain linked to a tRNA-binding THUMP domain. CDAT8 is specific for C deamination at position 8, requires only the acceptor stem hairpin for activity, and belongs to a unique family within the "cytidine deaminase–like" superfamily. The presence of this C-to-U editing enzyme guarantees the proper folding and functionality of all *M. kandleri* tRNAs.

The gene sequence of RNA molecules can be altered by editing enzymes that catalyze the deamination of adenosine or cytidine (*1*). In transfer RNA (tRNA), adenosine deaminases acting on tRNA engage in adenosine-to-inosine (A-to-I) editing (*2*–*4*) and are involved in the formation of 1-methylinosine found in some archaeal tRNAs (*5*). Cytidine-to-uridine (C-to-U) editing in tRNA is seen in plant mitochondrial (*6*), eukaryotic, organellar (*7*), and cytoplasmic *Trypanosoma brucei* tRNA (*8*), but the enzyme(s) involved in these conversions are unknown. In *Methanopyrus kandleri*, only four tRNAs ($tRNA^{Gln}_{UUG}$, $tRNA^{Pro}_{GGG}$, $tRNA^{Pro}_{UGG}$, and $tRNA^{Thr}_{GGU}$) possess a U8 (T8 in the tRNA gene), whereas the other 30 tRNA genes encode C8 (*9*, *10*). The highly conserved U8 in tRNAs forms a reverse Hoogsteen tertiary base pair with A14 that stabilizes the sharp kink between the acceptor stem and base A9 (fig. S1) (*11*). A U8C mutation is associated with mitochondrial myopathy in humans (*12*) and destabilizes the tRNA structure, resulting in a molecule unfit in translational initiation and elongation (*13*). The C8 must be modified to U in order to support the tertiary interaction with A14, which is present in all 34 tRNAs.

Sequencing of total small RNA from *M. kandleri* revealed that mature $tRNA^{Asp}$, $tRNA^{Cys}$, and $tRNA^{His}$ species contain U8, whereas their respective genes have C8 (Fig. 1, A and B). Furthermore, precursor $tRNA^{Asp}$ molecules containing 5′ leader and 3′ trailer sequences still have C8, indicating that C-to-U editing occurs at the RNA level (Fig. 1, A and B). Primer extension of an oligonucleotide annealed to the tRNA directly downstream of base 8 with either 2′-deoxyguanosine 5′-triphosphate (dGTP; complementary to the unedited C8) or 2′-deoxyadenosine 5′-triphosphate (dATP; complementary to the edited U8) revealed that most of base C8 in $tRNA^{Asp}$ and $tRNA^{His}$ is edited to U (Fig. 1C).

A computational search for C-to-U editing enzyme candidates in *M. kandleri* used the conserved cytidine deaminase signature zinc-binding motif His-(Ala-Val)-Glu-X_{24-36}-Pro-Cys-X-X-Cys (where X is any amino acid) (*14*), and yielded one candidate, the orphan protein MK0935, which also contained a THUMP domain, shown to mediate activity on the tertiary core of tRNA in thiouridine and pseudouridine synthases (*15*, *16*), and RNA methylases (*15*, *16*). The *MK0935* gene (renamed *CDAT8*, "cytidine deaminase acting on tRNA base C8") was cloned, expressed in *Escherichia coli*, and the recombinant enzyme purified.

The C-to-U editing activity of CDAT8 was verified in vitro by measuring the deamination of cytidine residues including C8 in *M. kandleri* $tRNA^{His}$ transcribed in the presence of [α-^{32}P]cytidine 5′-triphosphate (CTP) (Fig. 2, A and B) (*17*). To analyze the substrate recognition mechanism of CDAT8, we constructed three minimal tRNA substrates based on *M. kandleri* $tRNA^{Asp}$ (Fig. 2C). The smallest substrate (sAsp1 in Fig. 2C) consists only of the acceptor stem microhelix with a bulged-out C8G9GGAC sequence, where GGAC represents the variable loop of $tRNA^{Asp}$. The slightly larger substrates, sAsp2 and sAsp3, additionally contained the tRNA T-stem/loop with bulged-out C8G9 and C8G9GGAC sequences, respectively. All three minimal constructs were substrates for CDAT8, indicating the dispensability of the tRNA anticodon and D-arm for activity (Fig. 2D). Although all three constructs were edited by CDAT8 at 70°C, only sAsp3 was a substrate at 37°C. These results suggest that

[1]Department of Molecular Biophysics and Biochemistry, Yale University, New Haven, CT 06520, USA. [2]Department of Chemistry, Yale University, New Haven, CT 06520, USA.
*These authors contributed equally to this work.
†To whom correspondence should be addressed. E-mail: lennart.randau@yale.edu (L.R.); dieter.soll@yale.edu (D.S.); yong.xiong@yale.edu (Y.X.)

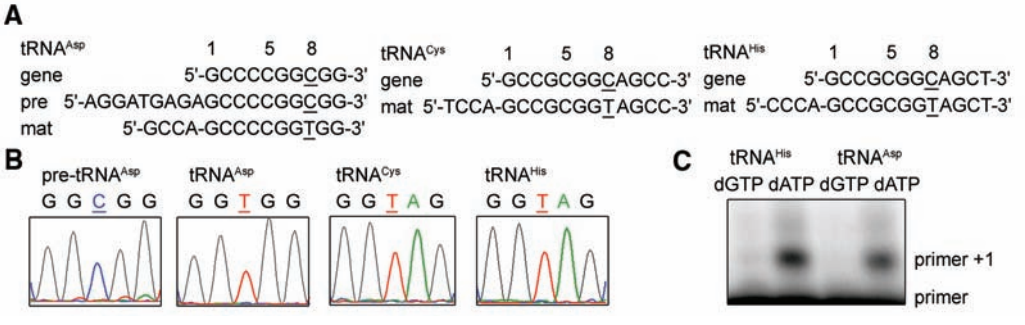

Fig. 1. C8-to-U8 editing in vivo. (**A**) Sequencing results for the indicated tRNA gene and reverse transcription polymerase chain reaction (RT-PCR) products of circularized precursor tRNA (pre, with 5′ and 3′ extensions) and mature tRNA (mat). Only the mature tRNA displays the edited U8 (T8 in DNA, underlined). (**B**) Sequencing traces of RT-PCR products with base 8 underlined. (**C**) The majority of tRNAs are edited to U8 as minisequencing detects extension of a primer to base 8 in the presence of dATP but not dGTP.

CDAT8 is able to recognize 30 different tRNAs mainly by interacting with the tRNA acceptor stem, including the universal 3′-CCA end, and a flexible base C8. A modified sAsp3 substrate containing A8 instead of C8 abolished editing activity (Fig. 2E). An A-to-I tRNA deaminase was reported to also perform C-to-U editing on DNA (*8*). As a test of the possibility of A-to-I editing, the same construct was transcribed with [α-^{32}P]ATP to generate a radioactively labeled A8, which was not edited by CDAT8 (Fig. 2E); this result indicated that CDAT8 performs only C-to-U deamination.

The structure of CDAT8 was solved in two different crystal forms. CDAT8 is composed of three domains: an N-terminal cytidine deaminase domain (CDD), a central ferredoxin-like domain (FLD), and a C-terminal THUMP domain (Fig. 3A). The cytidine deaminase active site has the signature motif His-Ala-Glu-X$_n$-Pro-Cys-X-X-Cys in which the histidine, two cysteine residues, and a water molecule (Fig. 3B) are involved in the tetrahedral coordination of zinc. The CDD of CDAT8 has the same core structure as those of known cytidine deaminases such as APOBEC2 (*18*) and APOBEC3G (*19*, *20*) (Fig. 3C). However, the CDAT8 CDD is much more compact, perhaps because its substrate (tRNA) recognition is provided by additional domains. The FLD and THUMP domains are highly homologous to those of ThiI (*16*) with backbone root mean square deviations of 2.8 and 2.2 Å, respectively (Fig. 3D). These two domains are believed to be responsible for tRNA recognition by ThiI, which is responsible for the 4-thiouridine (S^4) modification at the same position 8 in prokaryotic tRNAs.

CDAT8 forms a dimer with an extensive interaction interface of >1800 Å^2 per monomer. The relative orientation between CDD and the FLD and THUMP domains is different in the two monomers (fig. S2). This asymmetric dimer appears to have a rigid, defined structure, as all four independent dimers in two different crystal forms are identical. The CDAT8 dimer interface is provided by both the CDD and FLD.

Dimerization of CDAT8 appears to facilitate the binding of tRNA and to orient it for deamination at position 8. We propose a model of tRNA interaction in which the tRNA acceptor stem binds to the dimer interface, with the 3′-CCA end at the THUMP domain of one monomer and U8 near the CDD active site of the other monomer (fig. S3). Because of the asymmetric dimer conformation, it appears that only one catalytic site is oriented appropriately for catalysis. Substantial evidence exists for this model of tRNA binding. First, the THUMP domain is known to bind tRNA (*15*, *16*, *21*) and the CDAT8 THUMP domain is structurally homologous to that of ThiI. Second, we determined that a tRNA substrate containing only the acceptor stem microhelix is sufficient for editing. Third, it has been shown that a shortened or blunt CCA end is deleterious to the activity of ThiI (*22*). Because 30 *M. kandleri* tRNAs are edited by a single deaminase, CDAT8 must recognize the conserved, sequence-independent features of tRNAs, such as the 3′-CCA overhang

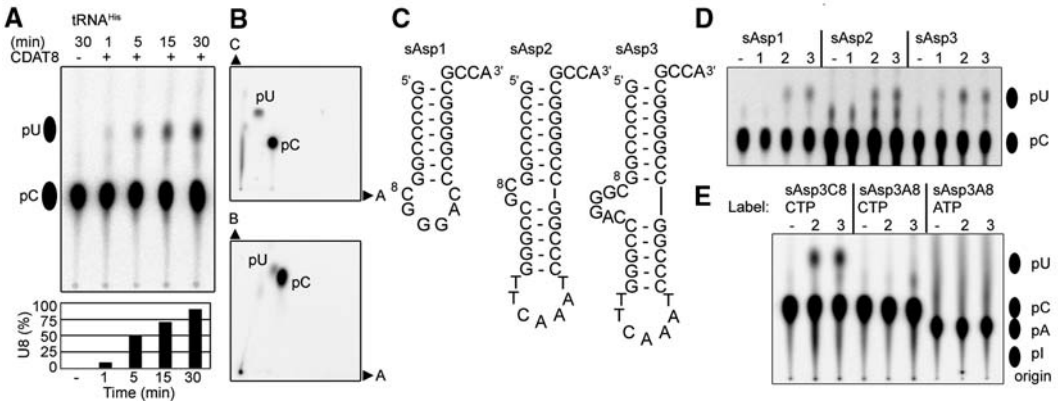

Fig. 2. C8-to-U8 editing in vitro. (**A**) Thin-layer chromatography (TLC) analysis of nuclease P1–digested *M. kandleri* tRNA^{His} transcripts after reaction with BSA (–) and 10 μM CDAT8 for the indicated times (+) at 70°C. The formation of U8 (C8 is one of 30 labeled cytidine residues in tRNA^{His}) is quantified in the lower panel. (**B**) Two-dimensional TLC analysis of the reaction product confirms the identity of the cytidine 5′-monophosphate (pC) and uridine 5′-monophosphate (pU) spots in three different solvents (denoted A, B, and C). The pC and pU markers were visualized by ultraviolet shadowing. (**C**) Sequence and predicted secondary structures of the three *M. kandleri* tRNA^{Asp}–derived minimal substrates sAsp1, sAsp2, and sAsp3. (**D**) TLC analysis of the indicated nuclease P1–digested transcripts after reaction with BSA (–) for 30 min of incubation at 70° and 10 μM CDAT8 after 30 min of incubation at 37°C (1), 50°C (2), or 70°C (3). The additional spots for sAsp2 are generated by nuclease P1 independent of CDAT8 activity. (**E**) TLC analysis of nuclease P1–digested sAsp3 or its C8A mutant (sAsp3A8) after incubation. The internal label ([α-^{32}P]CTP or [α-^{32}P]ATP) of the transcript is indicated.

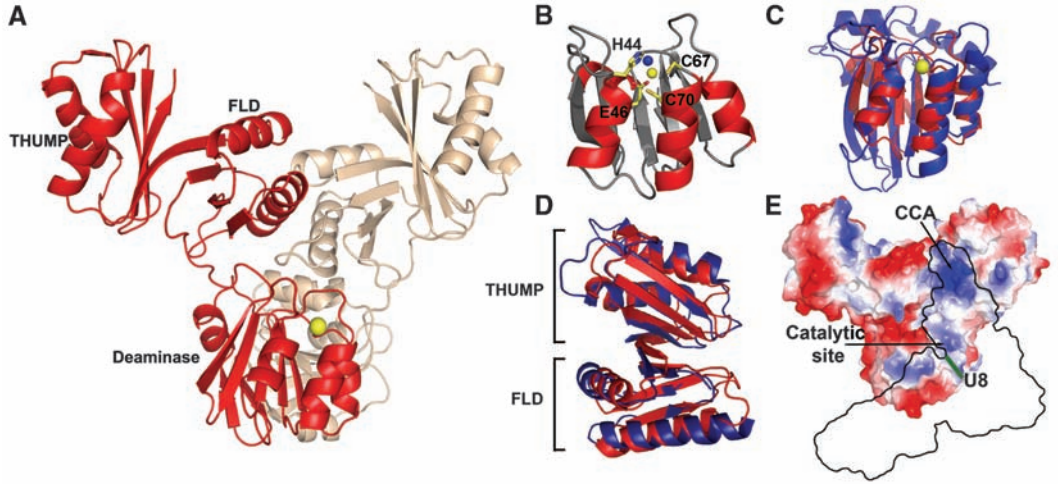

Fig. 3. Crystal structure of CDAT8. (**A**) The overall structure of the CDAT8 dimer (2.4 Å, R_{work}/R_{free} = 21.6%/26.2%) shows the head-to-head arrangement of the cytidine deaminase domains. Individual monomers are displayed in red and brown for clarity, and the active-site zinc is shown as yellow and brown spheres. (**B**) The active-site zinc is coordinated by His^{44}, Cys^{67}, Cys^{70}, and a water molecule (blue). The catalytic glutamic acid (E46) is in close proximity to the active site. (**C**) Superimposition of APOBEC3G (PDB ID 3E1U, blue) onto the deaminase domain of CDAT8 (red). (**D**) Superimposition of the *Bacillus anthracis* ThiI (PDB ID 2C5S) ferredoxin-like and THUMP domains (blue) with the corresponding domains in CDAT8 (red) shows a high degree of structural homology. (**E**) The surface electrostatics of the CDAT8 monomer show a positively charged groove on the enzyme surface. A model of tRNA binding (black outline) shows position 8 of the tRNA adjacent to the enzyme active site.

and the size and shape of the tRNA stems. Finally, a positively charged groove extends from the THUMP domain to the active site of the enzyme. The width of the groove formed between the two monomers could provide a snug fit for the acceptor stem; the length of the groove ensures that binding of the 3′-CCA at the THUMP domains places U8 adjacent to the active site of the CDD.

It is possible that C8 is the result of genetic drift. Alternatively, C8 may be beneficial for *M. kandleri* at the level of the tRNA gene, the primary tRNA transcripts, or the maturation steps that involve folding and modification of the tRNA. Because *M. kandleri* grows at extreme temperatures (up to 110°C), C8 may stabilize the genome at the tRNA gene or aid in tertiary folding and modification events of RNA molecules at such extreme conditions. Perhaps the 4-thiolation of U8 to S^4U8 mediated by ThiI might be regulated by CDAT8, as C8 would not be a ThiI substrate. A C8 may also be beneficial at the level of DNA, as a T8C mutation might prevent the interaction of tRNA genes with mobile genetic elements [e.g., (*23*, *24*)] at this otherwise fixed and convenient target.

References and Notes

1. B. Teng, C. F. Burant, N. O. Davidson, *Science* **260**, 1816 (1993).
2. A. P. Gerber, W. Keller, *Science* **286**, 1146 (1999).
3. S. Maas, A. P. Gerber, A. Rich, *Proc. Natl. Acad. Sci. U.S.A.* **96**, 8895 (1999).
4. J. Wolf, A. P. Gerber, W. Keller, *EMBO J.* **21**, 3841 (2002).
5. H. Grosjean, F. Constantinesco, D. Foiret, N. Benachenhou, *Nucleic Acids Res.* **23**, 4312 (1995).
6. S. Steinhauser, S. Beckert, I. Capesius, O. Malek, V. Knoop, *J. Mol. Evol.* **48**, 303 (1999).
7. G. V. Börner, M. Mörl, A. Janke, S. Pääbo, *EMBO J.* **15**, 5949 (1996).
8. M. A. Rubio *et al.*, *Proc. Natl. Acad. Sci. U.S.A.* **104**, 7821 (2007).
9. J. R. Palmer, T. Baltrus, J. N. Reeve, C. J. Daniels, *Biochim. Biophys. Acta* **1132**, 315 (1992).
10. A. I. Slesarev *et al.*, *Proc. Natl. Acad. Sci. U.S.A.* **99**, 4644 (2002).
11. E. Westhof, P. Dumas, D. Moras, *J. Mol. Biol.* **184**, 119 (1985).
12. C. N. Jones, C. I. Jones, W. D. Graham, P. F. Agris, L. L. Spremulli, *J. Biol. Chem.* **283**, 34445 (2008).
13. T. Sterner, M. Jansen, Y. M. Hou, *RNA* **1**, 841 (1995).
14. A. A. Smith, D. C. Carlow, R. Wolfenden, S. A. Short, *Biochemistry* **33**, 6468 (1994).
15. L. Aravind, E. V. Koonin, *Trends Biochem. Sci.* **26**, 215 (2001).
16. D. G. Waterman, M. Ortiz-Lombardia, M. J. Fogg, E. V. Koonin, A. A. Antson, *J. Mol. Biol.* **356**, 97 (2006).
17. See supporting material on *Science* Online.
18. C. Prochnow, R. Bransteitter, M. G. Klein, M. F. Goodman, X. S. Chen, *Nature* **445**, 447 (2007).
19. K. M. Chen *et al.*, *Nature* **452**, 116 (2008).
20. L. G. Holden *et al.*, *Nature* **456**, 121 (2008).
21. C. J. McCleverty, M. Hornsby, G. Spraggon, A. Kreusch, *J. Mol. Biol.* **373**, 1243 (2007).
22. C. T. Lauhon, W. M. Erwin, G. N. Ton, *J. Biol. Chem.* **279**, 23022 (2004).
23. R. Marschalek, T. Brechner, E. Amon-Bohm, T. Dingermann, *Science* **244**, 1493 (1989).
24. Q. She, K. Brugger, L. Chen, *Res. Microbiol.* **153**, 325 (2002).

25. We thank J. Yuan, P. O'Donoghue, and R. L. Sherrer for help and encouragement; K. O. Stetter for a gift of *M. kandleri* cells; and the staff at the Advanced Photon Source (beamline 24-ID), the National Synchrotron Light Source (beamlines X25 and X6A), and the Center for Structural Biology at Yale University. Atomic coordinates and structure factors have been deposited in the Protein Data Bank (code 3G8Q). Supported by NIH grants GM22854 (D.S.) and AI078831 (Y.X.).

Supporting Online Material

www.sciencemag.org/cgi/content/full/324/5927/657/DC1
Materials and Methods
SOM Text
Figs. S1 to S4
Table S1
References

22 December 2008; accepted 23 February 2009
10.1126/science.1170123

A Yeast Hybrid Provides Insight into the Evolution of Gene Expression Regulation

Itay Tirosh,[1] Sharon Reikhav,[1,2] Avraham A. Levy,[2]* Naama Barkai[1]*

During evolution, novel phenotypes emerge through changes in gene expression, but the genetic basis is poorly understood. We compared the allele-specific expression of two yeast species and their hybrid, which allowed us to distinguish changes in regulatory sequences of the gene itself (cis) from changes in upstream regulatory factors (trans). Expression divergence between species was generally due to changes in cis. Divergence in trans reflected a differential response to the environment and explained the tendency of certain genes to diverge rapidly. Hybrid-specific expression, deviating from the parental range, occurred through novel cis-trans interactions or, more often, through modified trans regulation associated with environmental sensing. These results provide insights on the regulatory changes in cis and trans during the divergence of species and upon hybridization.

Over the past years, extensive variations in gene expression were identified between closely related species (*1*, *2*). The genetic basis of most differences, however, remains unknown. Expression divergence of a specific gene can result from mutations in its regulatory sequences, such as promoter elements (cis effects), or from mutations elsewhere in the genome that alter the abundance or activity of upstream regulators (trans effects). Distinguishing the relative contribution of cis and trans effects to the divergence of gene expression is an essential step in elucidating its genetic basis.

When comparing different strains of the same species, cis and trans effects can be approximated by using linkage analysis (*3*–*5*). Alternatively, for comparison of different species that produce viable hybrids, cis versus trans effects can be distinguished by using the interspecific hybrid (*6*). Within the hybrid, both alleles of each gene are exposed to the same nuclear environment. Thus, differences in the expression of the two hybrid alleles reflect cis effects, whereas expression differences between the parental genes that disappear in the hybrid reflect trans effects. This approach was previously used to analyze several dozen *Drosophila* (*6*, *7*), yeast (*8*), and maize (*9*) genes and recently also a single mammalian chromosome (*10*), but has not yet been applied to a whole genome.

We designed a microarray that enables the measuring of allele-specific expression in a hybrid of *Saccharomyces cerevisiae* and *S. paradoxus*, two yeast species that diverged ~5 million years ago (fig. S1). Hybridization of genomic DNA from the two parental species verified the specificity of the microarray (Fig. 1A) and confirmed the lack of major variations in copy number. Biological repeats were highly correlated [Pearson correlation (r) ~ 0.98], significantly more so than the correlation in expression between species (r ~ 0.85) or between the corresponding alleles within the hybrid (r ~ 0.9) (Fig. 1B).

Using the array, we measured the expression profiles of the two parental species and their hybrid under four different growth conditions and quantified the relative contribution of cis and trans effects to the interspecies divergence (Fig. 1C). As expected, cis (but not trans) effects were correlated with sequence divergence at promoters and regulatory elements (fig. S3), whereas trans (but not cis) effects were enriched with genes whose expression was altered upon deletion of transcription or chromatin regulators (fig. S4 and S5). A small portion of the trans effects (<1%) were enriched within contiguous chromosomal regions that display correlated expression divergence, possibly indicating epigenetic effects (fig. S6).

The relative contribution of cis and trans effects to the divergence of gene expression varied under the different environmental conditions (Fig. 1D). In three of the conditions [rich media, heat shock, and the addition of an Rpd3p inhibitor, trichostatin A (TSA)], cis effects dominated, which is consistent with previous reports

[1]Department of Molecular Genetics, Weizmann Institute of Science, Rehovot, Israel. [2]Department of Plant Sciences, Weizmann Institute of Science, Rehovot, Israel.

*To whom correspondence should be addressed. E-mail: avi.levy@weizmann.ac.il (A.A.L.); naama.barkai@weizmann.ac.il (N.B.)

of *Drosophila* (*6*, *7*) and mammals (*10*). However, in glycerol, on which *S. cerevisiae* grows poorly (fig. S7), the number of cis and trans effects was comparable because of an increased number of trans effects.

We compared the consistency of cis and trans effects among the conditions (Fig. 1E). Cis effects were highly correlated ($r \sim 0.85$), both in the identity of the divergent genes and the direction of the effect. Trans effects were more condition-dependent, and their number varied by approximately sixfold between conditions (Fig. 1D). Analysis of variance indicated that most (77%) of the cis effects were independent of condition, whereas most (67%) of the trans effects were condition-dependent. As a consequence of the consistency of cis effects, trans effects dominated the divergence of the transcriptional response to changing conditions (Fig. 1D), as has previously been observed for yeast strains (*3*).

Previous studies showed that the expression of certain genes diverges rapidly across different evolutionary lineages (*1*, *11*), and that this propensity for expression divergence correlates with the presence of a TATA box and with the lack of a pronounced nucleosome-free region (NFR) adjacent to transcription start sites (*12*). In our data, we found that genes with trans (but not cis) effects were enriched with TATA boxes, lacked NFRs, and displayed a high expression divergence in seven existing data sets that compared the expression program of different yeast strains or species (Fig. 2 and fig. S8). Thus, the propensity to diverge seems to mostly reflect increased sensitivity to the divergence of trans regulation and not a higher sensitivity to mutations in cis.

Trans effects could originate from functional divergence of the direct transcription and chromatin regulators ("regulator trans") or from mutations in upstream components involved in transducing environmental or internal signals to these direct regulators ("sensory trans") (Fig. 3A). The divergence (in sequence or in expression) of transcription regulators was not correlated with the trans divergence of their target genes (Fig. 3B and fig. S9). In contrast, the strength of trans divergence was strongly correlated with the variation in gene expression upon environmental changes [as estimated by a data set of hundreds of *S. cerevisiae* expression profiles (*13*)] (Fig. 3C), which suggests a dominant role of sensory trans effects.

To more rigorously distinguish between the regulator and sensory trans hypotheses, we examined pairs of genes that are controlled by different regulators but exhibit a similar response to environmental changes (Fig. 3D). If trans effects are due to regulator divergence, these pairs should diverge independently. Instead, we observed a correlated divergence for most such gene pairs (Fig. 3D), as was predicted by the sensory trans hypothesis. Similarly, divergence of most gene pairs that share a common regulator but respond differently to environmental changes was not correlated (Fig. 3D), which again is consistent with the sensory trans hypothesis. One

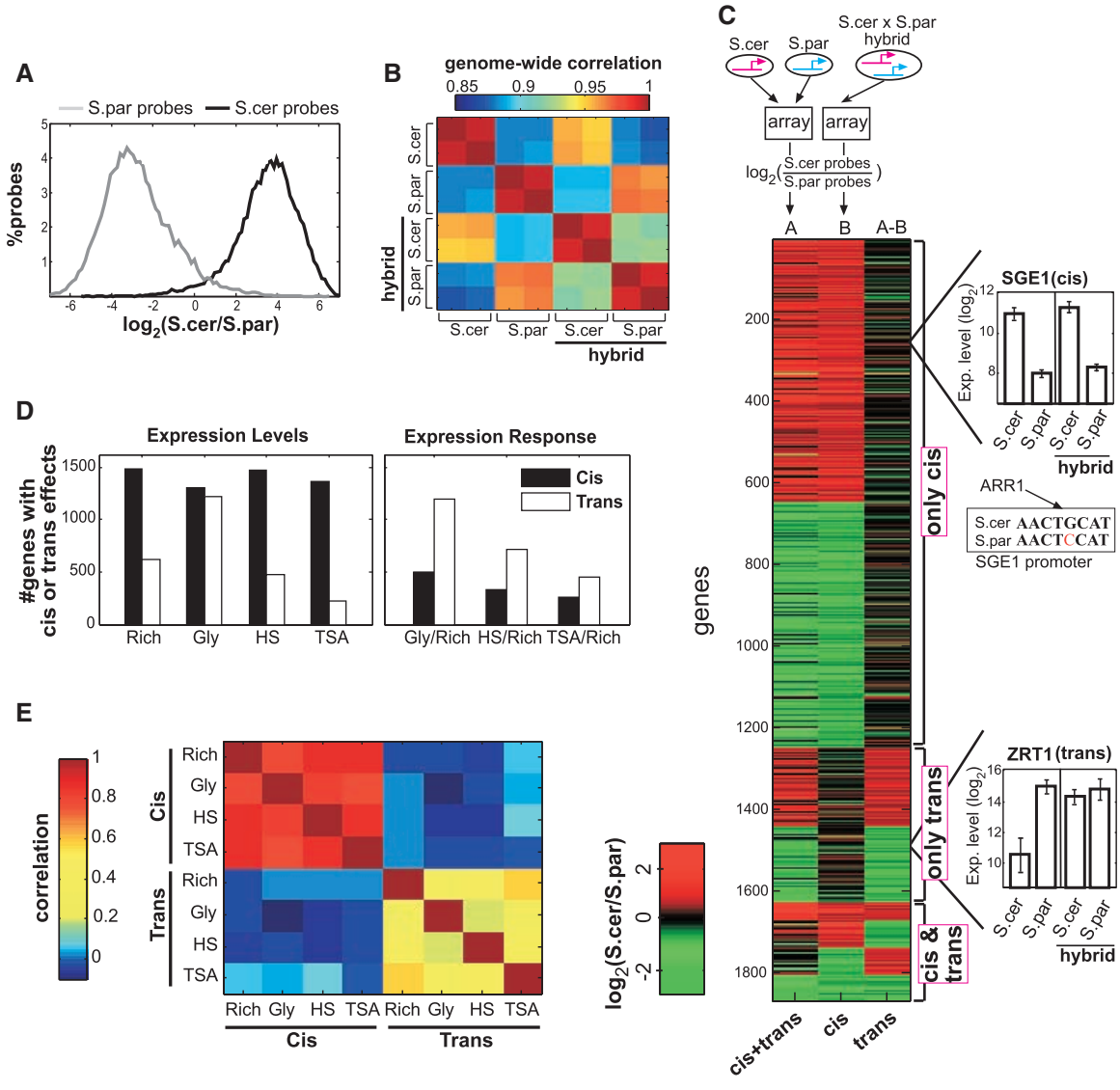

Fig. 1. Mapping cis and trans effects. (**A**) Genomic DNA of *S. cerevisiae* and *S. paradoxus* were differentially labeled and cohybridized to the array. Shown is the histogram of hybridization intensities ($\log_2$ ratio) for *S. cerevisiae* (black) or *S. paradoxus* (gray) probes. (**B**) Correlations between the genome-wide expression levels from the TSA experiment. All samples (including biological repeats) were processed in parallel (see fig. S2 for all experiments). (**C**) Clustered heat map of genes with significant cis and/or trans effects above 1.4-fold, and examples of genes with only cis [suppression of Gal11 expression 1 (SGE1)] or trans [zinc-regulated transporter 1 (ZRT1)] effects. Promoter analysis suggests a mechanistic basis for the cis effect in SGE1: an arsenicals resistance 1 (ARR1)–binding site at the *S. cerevisiae* promoter is mutated in *S. paradoxus*. (**D**) The number of genes with significant cis and trans effects above 1.4-fold in absolute expression levels (left) or in expression response (right). Rich, rich media; Gly, glycerol; HS, heat shock; TSA, TSA addition. (**E**) Genome-wide correlations between cis and trans effects across conditions.

example of the impact of differential sensing is activation of the environmental stress response (ESR). *S. cerevisiae* grows poorly on glycerol, whereas *S. paradoxus* grows poorly during heat shock. Accordingly, ESR genes were activated more strongly in *S. cerevisiae* on glycerol but more strongly in *S. paradoxus* during heat shock and were similarly expressed at the other two conditions (Fig. 3E and fig. S7). Furthermore, such patterns of growth-correlated expression differences were observed for 44% of all trans effects (as compared with less than 20% of the cis effects, as expected by chance). The idea that most trans effects reflect differences in sensory signals is supported also by previous analyses, in which variations in expression of multiple genes did not map to transcription regulators (*4*) but, in certain cases, to signal transduction genes (*3*, *4*, *14*).

Being upstream of the immediate regulators, sensory trans divergence is expected to coordinately influence a large number of genes. Mutations in cis could act to fine-tune these effects at particular genes (*15*, *16*). The interaction between cis and trans effects could increase divergence if they act in the same direction ("enhancing"; for example, both effects increasing the expression of the *S. cerevisiae* ortholog) or could decrease divergence if they act in opposite directions ("compensating") (fig. S10). Different evolutionary models make distinct predictions regarding the fraction of enhancing versus compensating interactions. Under complete neutrality, they should be equally favored. If natural selection acts to eliminate differences, compensating interactions would be favored. Finally, if expression changes are beneficial, then enhancing interactions would be preferred. We find a significant, albeit small, enrichment of compensating interactions (Fig. 4A), which suggests a role of purifying selection in the buffering of gene expression divergence. Consistent with this, both cis and trans effects are underrepresented among essential genes (fig. S11).

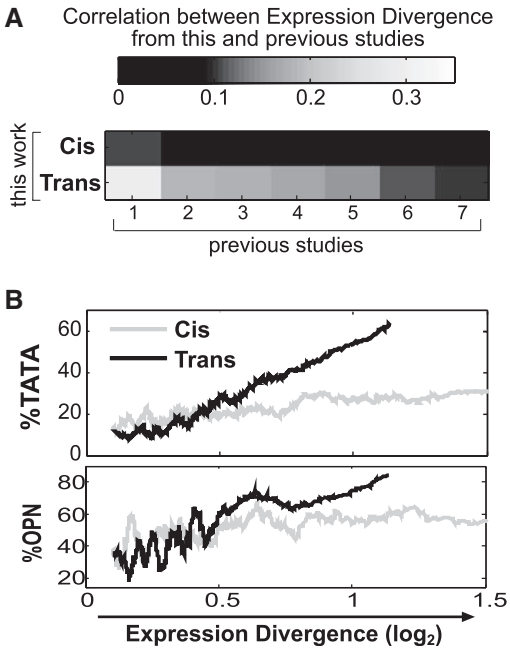

Fig. 2. Propensity for expression divergence depends on trans effects. (**A**) Correlation between the extent of cis and trans effects in our data and the expression divergence defined by seven previous studies [all trans correlations are significant at $P < 0.01$ (*20*)]. (**B**) Genes were sorted according to the extent of cis (gray) or trans (black) effects averaged over the four conditions. Shown is the proportion of promoters containing a TATA box (top) and having an occupied proximal-nucleosome (OPN) pattern (*12*) (bottom) within a sliding window of 300 genes.

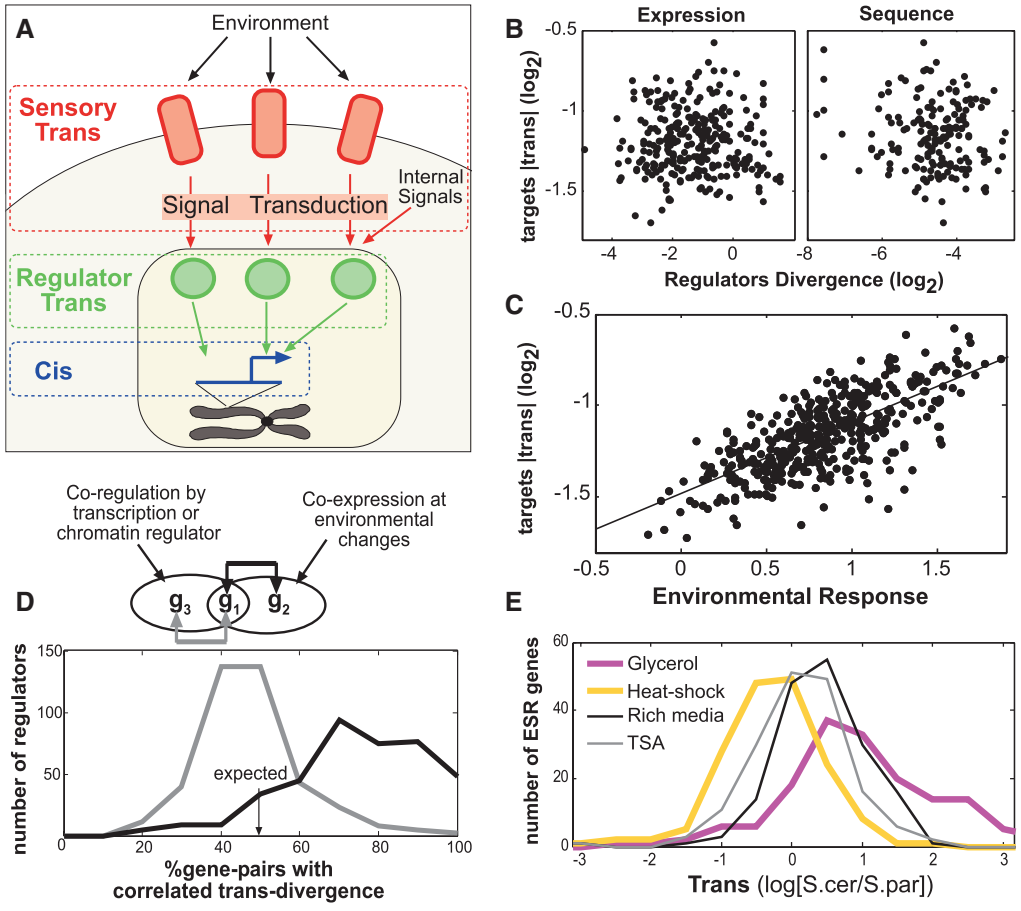

Fig. 3. Trans effects are dominated by sensory trans. (**A**) Models of sensory trans versus regulator trans. (**B**) The average magnitude of trans effects for target genes of each transcription or chromatin regulator is compared with the expression divergence (cis + trans, left) or sequence divergence [rate of nonsynonymous substitutions (Ka), right] of that regulator. (**C**) The average magnitude of trans effects was compared with the normalized response to environmental changes, as determined from a database of >1500 experiments (*13*). (**D**) Correlations between the trans effects of different genes follow the similarity in their response to environmental perturbations rather than their association with the same transcription or chromatin regulators (*20*). (**E**) Distribution of trans effects for ESR genes among the four conditions.

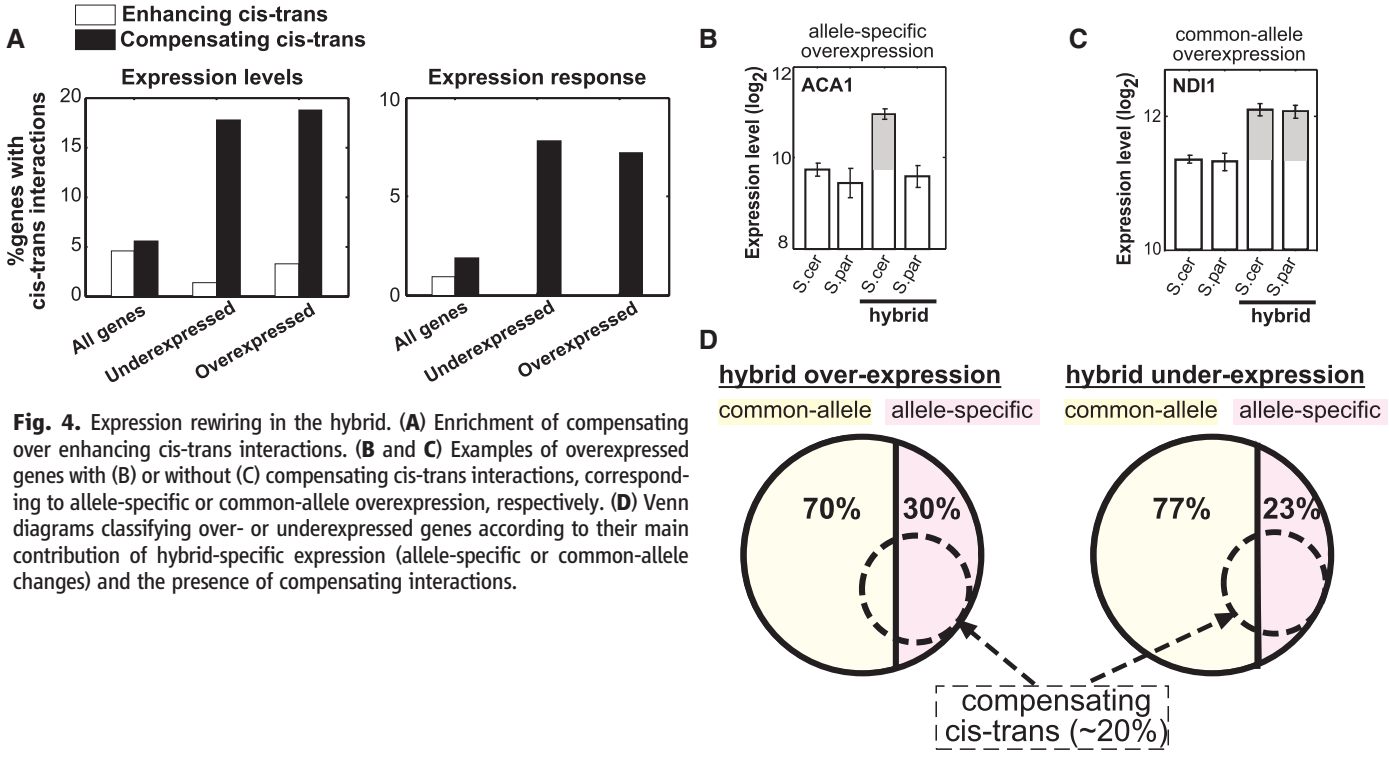

Fig. 4. Expression rewiring in the hybrid. (**A**) Enrichment of compensating over enhancing cis-trans interactions. (**B** and **C**) Examples of overexpressed genes with (B) or without (C) compensating cis-trans interactions, corresponding to allele-specific or common-allele overexpression, respectively. (**D**) Venn diagrams classifying over- or underexpressed genes according to their main contribution of hybrid-specific expression (allele-specific or common-allele changes) and the presence of compensating interactions.

Compensating cis-trans interactions can generate genetic variation that is invisible when comparing the two species but is revealed after interspecific hybridization (*16*) (fig. S10). Approximately 1 to 6% of the genes were overexpressed in the hybrid at each condition, displaying an expression that was higher than that of either parental species, and ~1 to 2% of the genes were underexpressed. Compensating cis-trans interactions were highly enriched among the genes displaying hybrid-specific expression (Fig. 4A); in most of these cases, only one of the hybrid alleles had changed in expression, whereas the other allele maintained an expression similar to that of the parental species (Fig. 4B). This is indeed expected if hybrid-specific expression results from interactions between a trans component of one genome and the respective cis element of the allele from the other genome (fig. S10) (*17*).

Although compensating cis-trans interactions were enriched in genes that displayed hybrid-specific expression, they accounted for only the minority (~20%) of such cases. More often, hybrid-specific expression was generated through a coordinated modulation of both alleles (Fig. 4, C and D), suggesting a modified trans-effect within the hybrid. These hybrid-specific trans-effects appear to be dominated by sensory trans (fig. S12), indicating that interactions between the two genomes alter the way in which the hybrid interprets its sensory signals (for example, compensating cis-trans interactions in sensory genes may propagate as hybrid-specific transeffects). Genes involved in respiration were highly enriched among the hybrid-specific trans effects (fig. S13). These genes were also subject to extensive divergence between the two parental yeasts, consistent with the idea that hybrid-specific trans-effects exaggerate differences already found between the parental species.

Taken together, our genome-wide mapping of cis and trans divergence points to three main conclusions. First, cis effects account for most of the expression divergence and are consistent across conditions, whereas trans effects are condition-specific and underlie the propensity for expression divergence. Second, trans effects are primarily attributable to differential interpretation of sensory signals and not to mutations in direct transcriptional regulators. Finally, parental genomes accumulate some compensating cis-trans effects, which is a signature of purifying selection, and their unleashing in the hybrid account for ~20% of over-dominance expression patterns. The majority of hybrid-specific expression, however, resulted from trans effects that were specific to the hybrid.

We have used the yeast hybrid as a tool, but hybridization and allopolyploidization are common in nature. Hybrids are often incompatible (*18*) but occasionally display beneficial phenotypes that are absent from the parents [hybrid vigor (*19*)]. Further studies are required to establish the possible connection between the expression rewiring described in our study and the emergence of novel hybrid phenotypes.

References and Notes

1. I. Tirosh, A. Weinberger, M. Carmi, N. Barkai, *Nat. Genet.* **38**, 830 (2006).
2. P. Khaitovich *et al.*, *Science* **309**, 1850 (2005).
3. E. N. Smith, L. Kruglyak, *PloS Biol.* **6**, e83 (2008).
4. G. Yvert *et al.*, *Nat. Genet.* **35**, 57 (2003).
5. E. Potokina *et al.*, *Plant J.* **53**, 90 (2008).
6. P. J. Wittkopp, B. K. Haerum, A. G. Clark, *Nature* **430**, 85 (2004).
7. P. J. Wittkopp, B. K. Haerum, A. G. Clark, *Nat. Genet.* **40**, 346 (2008).
8. D. Wang *et al.*, *Genome Res.* **17**, 1161 (2007).
9. N. M. Springer, R. M. Stupar, *Plant Cell* **19**, 2391 (2007).
10. M. D. Wilson *et al.*, *Science* **322**, 434 (2008).
11. C. R. Landry, B. Lemos, S. A. Rifkin, W. J. Dickinson, D. L. Hartl, *Science* **317**, 118 (2007).
12. I. Tirosh, N. Barkai, *Genome Res.* **18**, 1084 (2008).
13. J. Ihmels *et al.*, *Nat. Genet.* **31**, 370 (2002).
14. K. M. Brown, C. R. Landry, D. L. Hartl, D. Cavalieri, *Mol. Ecol.* **17**, 2985 (2008).
15. S. S. Fong, A. R. Joyce, B. O. Palsson, *Genome Res.* **15**, 1365 (2005).
16. C. R. Landry *et al.*, *Genetics* **171**, 1813 (2005).
17. Alternatively, it is possible that some of these allele-specific expression changes reflect epigenetic effects in the hybrid, although this possibility appears unlikely because cytosine methylation has not been found in budding yeast and the observed allele-specific changes are not clustered at specific chromosomal domains [as might be expected for epigenetic effects (fig. S6)].
18. C. R. Landry, D. L. Hartl, J. M. Ranz, *Heredity* **99**, 483 (2007).
19. Z. B. Lippman, D. Zamir, *Trends Genet.* **23**, 60 (2007).
20. Materials and methods are available as supporting material on *Science* Online.

21. We thank J. Berman, Y. Eshed, N. Sigal, A. Sheperberg, and members of our groups for discussions and comments. This work was supported by the Helen and Martin Kimmel Award for Innovative Investigations and grants from the Kahn Fund for Systems Biology at the Weizmann Institute of Science, the Israeli Ministry of Science, the Bi-national Science Foundation, and the European Research Council (Ideas) (to N.B). A.A.L. holds the Gilbert de Botton chair of Plant Science. Microarray data has been deposited at the Gene Expression Omnibus with accession number GSE14708.

Supporting Online Material

www.sciencemag.org/cgi/content/full/324/5927/659/DC1
Materials and Methods
Figs. S1 to S14
Table S1
References

15 December 2008; accepted 3 March 2009
10.1126/science.1169766

Shaker Powder Dispensing

Powdernium SV is a new shaker powder dispenser suitable for applications such as compound management, sample preparation, and reference standards preparation. Powdernium SV acts as a hybrid vial hopper and storage vessel that enables low-cost storage without the requirement to subdivide materials, helping to save precious resources. An important feature is a patent-pending valve cap that provides precision flow regulation and quick-access storage without cross-contamination, helping to maintain the integrity and accuracy of dispensing results. The valve cap and vial hopper are disposable, so there is no need for cleaning or worries about carryover.

Symyx Technologies
For information 408-764-2000
www.symyx.com

High Throughput Plates

The PreDictor 96-well plates for high throughput process development and parallel screening of chromatographic conditions now offer Assist software and additional prefilled 96-well plates. The extended portfolio includes Assist software for experimental setup and evaluation, MabSelect Xtra and Q and SP Sepharose Fast Flow media, anion and cation exchange chromatography (AIEX/CIEX) screening plates with multiple media in the same plate, and plates for the determination of adsorption isotherms. The Assist software guides the user through the experimental workflow and suggests an experimental design based on the type of study. PreDictor plates enable fast evaluation of up to 96 chromatography conditions per plate, reduce experiment time, and decrease sample consumption. The AIEX/CIEX screening plates provide the flexibility to screen several chromatography media in a single plate.

GE Healthcare
For information 262-501-0777
www.gelifesciences.com

Capillary Columns

Six new offerings have been added to the Onyx monolithic high-performance liquid chromatography (HPLC) column line, including a 150 x 0.05 mm ID choice for proteomics research. Optimized for the low flow rates commonly used for liquid chromatography/mass spectrometry proteomics analysis, this column delivers high sensitivity for biomarker discovery. Other new column sizes include a 0.2 mm C18 column for higher flow rates, a 150 x 0.2 mm trapping column, a 150 x 0.1 mm C8 column, and two ultrahigh-resolution C18 columns at 100 micron and 200 micron IDs. The permeable Onyx media separates viscous biological samples that clog traditional columns. These columns contain solid rods of fused silica and eliminate packing issues associated with particulate media. Run times are as much as 50 percent faster than with traditional columns.

Phenomenex
For information 310-212-0555
www.phenomenex.com

Tissue System

With the PAXgene Tissue System, researchers can perform histology, immunohistochemistry, and stabilized RNA, microRNA, and DNA extractions from one sample. The system combines tissue fixation with nucleic acid stabilization. For example, a biopsy sample can be assessed by a pathologist for morphology, then the same sample can be used for molecular analysis. The system has two components: a tissue container and tissue kits. The dual-chambered container is prefilled with two reagents: PAXgene Tissue Fix for fast penetration and fixation, and PAXgene Tissue Stabilizer for storage and transport. The fixation process features a standard histocassette with a fixative that is an alternative to formalin and is stopped by transferring the sample into the stabilizer. Tissue can then be paraffin embedded and processed in pathology workflows. After tissue has been stabilized in PAXgene tissue containers, RNA, microRNA, and DNA can be purified.

Qiagen
For information 001-240-686-7660
www.qiagen.com

Storage Tubes

The Micronic Deluxe Starter Pack contains everything needed to start using two-dimensional (2D) coded sample storage tubes: an easy-to-use electric capper, a 2D barcode rack scanner with operating software, two cases of racked 1.4-ml 2D coded tubes with caps, some manual cap removers, and a tube selector. The tubes contain a unique inside ring for secure sealing; the capper pushes caps into exactly the right depth to ensure a reliable, high-integrity seal.

Micronic
For information 724-941-6411
www.micronic.com

Pipettes

Biohit Proline Pipettes offer lightweight design, excellent accuracy and precision, and a three-year warranty. Most models are available with Safe Cone Filters. They are made following good manufacturing practices to ensure traceability. They cover a volume range from 0.1 µl to 5 ml with eight adjustable single-channel models and eight adjustable multichannel models. They are also available in fixed-volume single-channel models.

Biohit
For information 800-922-0784
www.biohit.com

Electronically submit your new product description or product literature information! Go to **www.sciencemag.org/products/newproducts.dtl** for more information.

Newly offered instrumentation, apparatus, and laboratory materials of interest to researchers in all disciplines in academic, industrial, and governmental organizations are featured in this space. Emphasis is given to purpose, chief characteristics, and availabilty of products and materials. Endorsement by *Science* or AAAS of any products or materials mentioned is not implied. Additional information may be obtained from the manufacturer or supplier.

Release The Power of Science

***Science* Careers**
Classified Advertising

For full advertising details, go to ScienceCareers.org and click For Advertisers, or call one of our representatives.

UNITED STATES & CANADA

E-mail: advertise@sciencecareers.org
Fax: 202-289-6742

Daryl Anderson
US Sales Manager
Phone: 202-326-6543

Joribah Able
Industry – US & Canada
Academic – Midwest/Canada
Phone: 202-326-6572

Alexis Fleming
Academic – East Coast
Phone: 202-326-6578

Nicholas Hintibidze
Academic – West and South Central
Phone: 202-326-6533

Tina Burks
Online Job Posting customer service
Phone: 202-326-6577

EUROPE & INTERNATIONAL

E-mail: ads@science-int.co.uk
Fax: +44 (0) 1223 326532

Tracy Holmes
Associate Director, *Science* Careers
Phone: +44 (0) 1223 326525

Alex Palmer
Phone: +44 (0) 1223 326527

Dan Pennington
Phone: +44 (0) 1223 326517

Susanne Kharraz Tavakol
Phone: +44 (0) 1223 326529

JAPAN

Mashy Yoshikawa
Phone: +81 (0) 3 3235 5961
E-mail: myoshikawa@aaas.org

To subscribe to *Science*:
In US/Canada call 202-326-6417 or 1-800-731-4939. In the rest of the world call +44 (0) 1223 326515.

Science makes every effort to screen its ads for offensive and/or discriminatory language in accordance with US and non-US law. Since we are an international journal, you may see ads from non-US countries that request applications from specific demographic groups. Since US law does not apply to other countries we try to accommodate recruiting practices of other countries. However, we encourage our readers to alert us to any ads that they feel are discriminatory or offensive.

Science Careers
From the journal *Science* AAAS

Seattle Children's
HOSPITAL · RESEARCH · FOUNDATION

Neurological Surgery
Associate Professor / Professor

The recently established Center for Neuroscience at the Seattle Children's Research Institute invites applications for a full-time faculty position, with the University of Washington School of Medicine Department of Neurological Surgery, at the rank of Associate Professor or full Professor, without tenure. Qualified applicants should be established investigators who are applying techniques of molecular, genetic or cellular biology to study mechanisms underlying hydrocephalus. The Center for Neuroscience at the Seattle Children's Research Institute's research vision is to restore children's health through a mechanistic understanding. The applicant's area of research interest should be complementary to the interests of current faculty working on various areas of neuroscience and bioengineering. Researchers interested in understanding CSF hydrodynamics, choroid plexus function, neuroendocrinology, brain metabolism, blood brain barrier function, brainstem neurobiology and proteomics research are particularly encouraged to apply. The successful candidate must have a M.D. and/or Ph.D. degree and have active nationally funded research grants. Level and salary will be based on applicant's qualifications and experience. Responsibilities of the position include development of an independent, extramurally funded research program, establishing a hydrocephalus section within the Center for Neuroscience and mentoring graduate and post-doctoral students and junior faculty investigators.

This position is open until filled. Address any inquiries to **Dr. Jan-Marino Ramirez, Center Director**, at **nino.ramirez@seattlechildrens.org**. Please send CV, a statement of current and future research interests and the names and contact information of three references to: **Wendy Kramer, Seattle Children's Research Institute, 1900 Ninth Avenue, M/S C9S-9, Seattle, WA 98101**.

For more information about Seattle Children's Research Institute, please visit:
http://research.seattlechildrens.org.

All University of Washington faculty engage in teaching, research, and service.
The University of Washington is an Equal Opportunity/Affirmative Action Employer.
Women and minorities are encouraged to apply.

UW Medicine
SCHOOL OF MEDICINE

Philadelphia College of Osteopathic Medicine (PCOM) brings to light a rich tradition of excellence in education and leadership. Work in an atmosphere and culture that is open and receptive to fresh ideas and new perspectives. Here, sparked by ideas and innovations that continue to shape the future of osteopathy, a myriad of professionals turn Ambition into Accomplishment.

Faculty Position: Anatomical Sciences

The Ga. Campus- Philadelphia College of Osteopathic Medicine, invites applications for a full-time tenure track position at the level of Assistant/Associate Professor. Teaching responsibilities will be in Medical Gross Anatomy (cadaver based) and Histology. Experience in related anatomical sciences such as embryo, neuroscience/anatomy appreciated. Applicants must have a Ph.D., D.O., M.D., or equivalent degree; post doctoral and some teaching experience preferred. Scholarly pursuit is expected.

GEORGIA CAMPUS
PCOM

Candidates should send CV and Letter of Interest to: **Philadelphia College of Osteopathic Medicine, Human Resources Department, 4190 City Avenue, Philadelphia, PA 19131, Fax 215-871-6505 or email: hr@pcom.edu** EOE **WWW.PCOM.EDU**

NOVARTIS
VACCINES

Novartis Vaccines and Diagnostics is a division of Novartis focused in the research and development of preventive vaccines. The Novartis Vaccines Research Center located in Siena (Italy) with its 225 scientists is among the most esteemed vaccine research environments worldwide and is responsible for the creation of most of the vaccines that are currently part of the Novartis pipeline. Novartis vaccines scientists pioneered the "reverse vaccinology" approach to develop several vaccine candidates including the first potentially broad coverage meningitis B vaccine currently in phase III clinical testing.

HEAD OF UNIT *IN VIVO* IMMUNOLOGY

A position is available in the Immunology Function to lead the *In vivo* Immunology team. The candidate will report directly to the Head of the Immunology function and will supervise a team composed of senior scientists, post-docs and PhD students. The *In vivo* immunology Unit is responsible for the immunological characterization of novel candidate vaccines in pre-clinical models. The successful candidate will work across a matrix environment with constant inter-actions with project leaders and other functions. The ability to manage a team and a strong background of mouse immunology are required.

Requirements:

- PhD with about 5+ years of post-doctoral experience in the field of Immunology
- Publication record in mouse immunology
- Previous experience as Lab head or Project leader
- Qualified experience in animal models of infection

Preferred qualifications:

- Previous experience in Vaccine discovery and development

Location: Siena. In addition to an attractive salary package, Novartis Vaccines & Diagnostics offers extensive relocation support. For an application please e-mail to applications.nvdit@novartis.com

Quote Job Reference: NVII003

SCIENTIST-CELLULAR IMMUNOLOGIST

A Scientist position is available in the In vitro Immunological assay Unit. The Unit is responsible for developing and running cellular assays, particularly in the area of lymphocyte and Dendritic cell biology. The successful candidate will be a laboratory scientist with a strong background in Immunology and good knowledge of Immunological methodologies. He/she will work independently within the Immunology group and across a matrix environment as part of a multidisciplinary research team focused on the discovery and development of novel vaccine candidate and adjuvants. The ability to work in a team with co-workers and outside collaborators and to present data to project teams are required. The successful candidate will be in charge of his/her own research project and, depending on his/her previous experience, may also be responsible for junior scientists/PhD students.

Requirements

- PhD degree with research focus in Immunology or related discipline
- Experience in molecular and cell biology
- In-depth understanding of immunology
- Team player with well-developed interpersonal abilities
- Excellent communication skills in English

Preferred qualifications:

- Post-doctoral experience in the area of cellular and/or molecular immunology
- A proven ability to perform flow cytometry assays of cellular activation and function (*ex-vivo* and *in-vitro*).
- Experience of designing *in-vitro* cellular assays and/or *in-vivo* experiments

Location: Siena. In addition to an attractive salary package, Novartis Vaccines & Diagnostics offers extensive relocation support. For an application please e-mail to applications.nvdit@novartis.com

Quote Job Reference: NVCI004

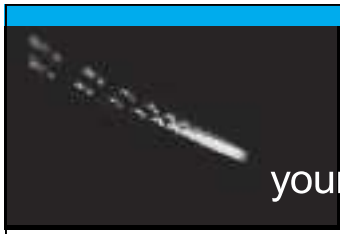

your job at **TU**Delft

CHALLENGE THE FUTURE

Junior & Senior Faculty for New Dept. of Bionanoscience

Faculty: **Applied Sciences**
Term of contract: **Tenure track or tenured**

An entirely new Department of Bionanoscience dedicated to research at the interface between nanoscience, synthetic biology, and cell biology will be established at the renowned Dutch university TU Delft. It will focus on single cells in all their complexity down to the molecular level, from both fundamental scientific and application points of view. The new activities will extend the current nanoscience research themes at the Kavli Institute of Nanoscience (www.ns.tudelft.nl) and the life sciences and biotechnology themes at the Kluyver Centre. The current biophysics core group (www.ns.tudelft.nl/mb) is very internationally oriented and has an excellent record in single-molecule nanoscience. The current faculty include Cees Dekker, Nynke Dekker, Juan Keymer Vergara and Serge Lemay. Excellent facilities are already available, and the planning for a new, state-of-the-art building for the Biotechnology, Chemistry and Bionanoscience departments is in its final stages.

We aim to attract about 15 top scientists at all levels from junior to senior faculty in a variety of disciplines. Research subjects can cover, but are not limited to, the following topics: 1) Biology and biophysics at the level of the single cell, 2) Molecular/structural biology and biochemistry, 3) Synthetic biology, 4) Theoretical biology and biophysics, 5) Single-molecule biophysics and high resolution microscopy, 6) Nanoprobes, nanomedicine, and bionanoapplications.

We look for researchers with an outstanding track record in the disciplines mentioned above, with a pioneering mentality, people who are at ease with scientific and engineering challenges and who through their research, management skills and teaching qualities can inspire co-workers and students alike. The successful candidates will be expected to establish a strong, externally funded research programme, and be committed to excellence in teaching at the undergraduate and graduate levels.

Information and application

For more information about the job and procedure you can visit our website: www.bn.tudelft.nl

www.bn.tudelft.nl

TU Delft
Delft University of Technology

Science Careers online @sciencecareers.org

ITC Faculty Position A Associate/Assistant Professor ACH 48507

The Immunotherapy Center and Department of Medicine at the Medical College of Georgia seek applicants for a faculty position primarily focused on basic research related to inflammatory processes linked to disease syndromes. The successful applicant will join an established research program dedicated to studying counter-regulatory and immune tolerance mechanisms, and using this knowledge to develop novel immunotherapies to improve clinical outcomes. Current research topics include fundamental studies on immune tolerance mechanisms, and assessing the contribution of tolerance mechanisms to chronic inflammatory diseases such as cancer, infectious and autoimmune diseases and transplant survival. Applicants should have a PhD or MD/PhD and a documented record of productivity in an area of basic or clinical immunology research that supplements or complements these research topics. Preference will be given to candidates with established research programs, although applications from exceptional younger investigators will be considered. The successful applicant will hold joint appointments in the Immunotherapy Center and the Department of Medicine, and will have access to exceptional core research facilities (listed at **http://www.mcg.edu/Core/Labs/**) and laboratory space.

For further information please contact: **Andrew Mellor, PhD, Director of the Immunotherapy Center (amellor@mcg.edu) Medical College of Georgia, Augusta, GA 30912-3220**.

The Medical College of Georgia is an EEO/AA/Equal Access Employer, and is a growing state-supported academic medical center located in a historic city with outstanding recreational and lifestyle opportunities.

ITC(IDI) faculty position B – Associate Professor/Professor – ACH 51226

The Immunotherapy Discovery Institute (IDI) at the Medical College of Georgia seeks exceptional candidates for a senior faculty position to promote translational research related to an aspect of chronic inflammatory disease syndromes. The successful applicant will have the opportunity to work with established research teams in the MCG Immunotherapy Center and clinical faculty in the Department of Medicine. An endowed chair is available for exceptionally qualified individuals with a proven track record of productivity in translational medicine related to immunotherapy in any of the following clinical areas, autoimmune, allergic and infectious diseases, transplantation, vaccine design and development. Investigators in the MCG Immunotherapy Center are studying immune counter-regulatory and tolerance mechanisms, and are developing novel immunotherapies to improve clinical outcomes such as the use of novel vaccine adjuvants to treat cancer patients. Current research topics include fundamental studies on immune tolerance mechanisms, and assessing the contribution of such mechanisms to chronic inflammatory diseases such as cancer, infectious and autoimmune diseases and tissue transplant survival. Applicants should have a MD or MD/PhD and a documented record of productivity in an area of clinical immunology research that complements these research strengths. Preference will be given to candidates with documented experience of promoting clinical research and managing early phase clinical trials. The successful applicant will hold joint appointments in the Immunotherapy Discovery Institute and the Department of Medicine, and will have access to exceptional core research facilities (listed at **http://www.mcg.edu/Core/Labs/**) and laboratory space. Generous start-up packages are available to support this recruitment.

For further information please contact: **Andrew Mellor, PhD, co-Chair Immunotherapy Discovery Institute (amellor@mcg.edu), Medical College of Georgia, Augusta, GA 30912-3220**.

The Medical College of Georgia is an EEO/AA/Equal Access Employer, and is a growing state-supported academic medical center located in a historic city with outstanding recreational and lifestyle opportunities.

Durham University

Shaped by the past, creating the future

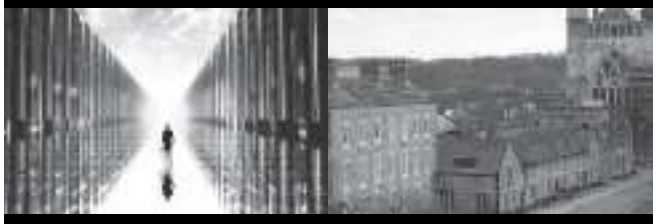

Institute of Advanced Study
2010/11 Distinguished and Fast-Track Fellowships

The IAS is an ideas-based institute launched in October 2006 as a forum for world-class multi- and interdisciplinary debate. The Institute seeks to catalyse new thinking on major annual themes through critical dialogue between gifted individuals from different professional and academic backgrounds. The theme for 2010/11 is "Futures", interpreted in its broadest sense - scientifically, symbolically, legally, philosophically, literarily, politically, economically and sociologically. Applications are now invited for up to 20 funded, three-month fellowships (October-December 2010 and January-March 2011) most, though not all, of which will be linked to the annual theme. Applicants may be scholars, writers, artists or thinkers/practitioners from any discipline and from anywhere in the world. Distinguished and fast-track fellowships are available: both include stipend, travel, accommodation, subsistence and costs associated with replacement teaching or loss of salary (where appropriate).

Further particulars are available from the IAS website www.dur.ac.uk/ias Further details of the 2010/11 Futures theme can also be found here. Informal enquiries with the Directors of the Institute can be made via Catherine Paine, the IAS administrator: Tel: +44(0)191 334 2589 or email: catherine.paine@durham.ac.uk

Closing date for applications is Sunday 14 June 2009.

NUS National University of Singapore

Appointment of Senior Research Administrator Office of the Deputy President (Research and Technology) National University of Singapore

The Office of the Deputy President (Research & Technology) at NUS (Website: http://www.nus.edu.sg/dpr/) is responsible for facilitating, regulating and developing research and technology in a wide range of disciplines and cross-disciplinary areas. We now seek to appoint a senior experienced research administrator to facilitate and simplify the functions of the Division of Research Administration (DRA). DRA administers research grants from government, industry and other bodies. DRA presently has 14 employees and in 2008 administered over 500 grants.

Responsibilities

1. To develop a strong administrative organisation that is "researcher focused", blending flexibility with accountability.
2. To lead the implementation of computerised grant handling systems that simultaneously serve the needs of researchers and the administrative requirements of NUS Senior management.
3. To take a leading role in reorientating the policies of DRA to create a strong customer focus.
4. To assist the Deputy President (Research & Technology) in engaging with supporters of NUS research.

The successful candidate will have wide experience of research management in academia, industry and/or granting bodies. Salary is commensurate with experience and qualifications.

Applications (with a full CV and names of at least three referees) and informal/confidential enquires can be sent to:

Professor Barry Halliwell
Office of the Deputy President (Research and Technology), NUS
University Hall, Lee Kong Chian Wing, UHL #05-02H
21 Lower Kent Ridge Road, Singapore 119077
Email: bchbh@nus.edu.sg

Closing date for applications: **15 June 2009**

University at Buffalo
The State University of New York

Faculty Position in Department of Exercise and Nutrition Sciences

The Department of Exercise and Nutrition Sciences, School of Public Health and Health Professions University at Buffalo, State University of New York, is seeking candidates (1-2) for 10-month tenure-track faculty positions at the Assistant Professor level. The start date is negotiable.

Qualifications: Candidates should have an earned Ph.D. or equivalent in a discipline relevant to exercise and/or nutrition sciences. Postdoctoral research experience is strongly preferred. A record of achievement in research with publications in high quality journals is expected. The candidates' research should complement existing departmental research strengths in biomechanics, exercise physiology, or nutrition. The candidates' academic goals should embrace the school's mission to improve the health of populations, communities, and individuals through disciplinary and interdisciplinary education, research, and service.

Duties

1. Develop and maintain an independent scholarly research program that will attract external funding and enhance student recruitment.
2. Teach undergraduate and/or graduate required courses consistent with the department needs and candidates' expertise.
3. Advise and mentor students at the master's and doctoral levels.
4. Perform service to the department, school, university, and profession consistent with the mission of the School of Public Health and Health Professions.

Candidates should submit 1) a letter of application, 2) a curriculum vitae, 3) a brief statement of future research plans, and 4) the names and contact information for three references to:

https://www.ubjobs.buffalo.edu Posting (#0900141)

The University at Buffalo is an Equal Opportunity/Affirmative Action Employer. The Department of Exercise and Nutrition Sciences is interested in identifying prospective minority and women candidates and professionals with disabilities. Qualified individuals with a disability may request needed reasonable accommodation to participate in the application process. No person in whatever relationship with The State University of New York shall be subject to discrimination on the basis of age, creed, color, disability, national origin, race, religion, ethnicity, gender, sexual orientation, marital or veteran status.

Medical College of Wisconsin/ Children's Hospital of Wisconsin

Pediatric Endocrinology

The Section of Endocrinology within the Department of Pediatrics at the Medical College of Wisconsin, in conjunction with the Children's Hospital of Wisconsin, Children's Research Institute is seeking candidates for faculty positions within the Max McGee National Research Center for Juvenile Diabetes. The Center is closely affiliated with the high-volume Diabetes Clinic at Children's Hospital of Wisconsin as well as the Human and Molecular Genetics Center at The Medical College of Wisconsin. We focus on using state-of-the-art analysis platforms to better understand the pathogenesis of type 1 diabetes, with a strong emphasis on translational research. Opportunities for collaborative research with clinical and basic scientists within the section, as well as with other faculty within the Medical College of Wisconsin, are excellent. Children's Hospital of Wisconsin is a large and successful freestanding children's hospital that was recently ranked #3 in the nation by *Parents* magazine. Metro-Milwaukee is a lakeshore community of 1.5 million located 90 miles north of Chicago.

Candidates should have training, experience, and active research programs within the field of immunology related to type 1 diabetes or the field of pancreatic beta cell biology. We are seeking highly productive candidates with successful track records in the procurement of extramural funding and participation in collaborative research programs. Eligible candidates are expected to hold a Ph.D. or M.D./Ph.D. (or equivalent), and proven excellence and productivity in research. Highly competitive start-up packages will be provided to facilitate program development. Please submit resumes to:

Martin J. Hessner, Ph.D., Associate Professor
Medical College of Wisconsin
Department of Pediatrics
8701 Watertown Plank Road, Milwaukee, WI 53226
e-mail: **mhessner@mcw.edu**, Fax: 414-456-4496
Or apply online: **www.mcw.edu/careers**

EEO/AA M/F/D/V

Children's Hospital and Health System™
MEDICAL COLLEGE OF WISCONSIN
Children's Specialty Group™

University of Zurich

The Faculty of Science at the University of Zurich invites applications for a

Professorship in Ecology and Evolution

We seek outstanding, innovative applicants with a record of excellence in research, who have proven their ability to develop and apply novel or interdisciplinary concepts in ecology and evolution. Areas of interest include, but are not limited to, evolution of complex traits, speciation, evolution of development, population or quantitative genetics, ecophysiology, biodiversity, or species interactions.

The successful candidate is expected to develop a strong, independent research program, attract external funding, and contribute to graduate and undergraduate teaching. The position is open rank (tenure-track assistant professor to full professor).

Zurich offers a stimulating scientific and cultural environment, including a rich spectrum of research activities in life sciences and medicine, and provides extensive opportunities for collaborations with research groups at the Faculties of Science and of Medicine of the University of Zurich, as well as teams at the nearby ETH Zurich.

The University of Zurich provides generous research support, including earmarked funds for personnel and running expenses, and competitive start-up packages.

Applications should include a curriculum vitae, a publication list, a summary of present and future research interests, and a vision statement that outlines major unsolved problems in the field and how they could be tackled by the planned research. Documents should be sent, together with names and addresses of three potential referees, to Prof. Michael Hengartner, Dean of the Faculty of Science, University of Zurich, Winterthurerstrasse 190, CH-8057 Zurich, Switzerland by June 15, 2009.
The application material should be submitted as a single PDF file to jobs@mnf.uzh.ch. For further information, please contact Prof. Lukas Keller at lukas.keller@zm.uzh.ch.

Science Careers online @sciencecareers.org

Associate/Full Professor Positions At Nanjing Medical University

Position Summary:

Nanjing Medical University is located in Nanjing, the scenic capital of Jiangsu Province, China. It is an independent set of well-known medical institution and has developed rapidly in scientific research and personnel training in recent years. In order to accelerate the development of our University, we are searching for colleagues to join our University at the associate or full professor level. Opportunities are available in all areas including Oncology, Regenerative Medicine, Reproductive Medicine, Genetics, Cell Biology, Pathogen Biology, Immunology, Pharmacology, Physiology, Forensic Science, Human Anatomy, Histology and Embryology, Pathology, Microbiology, Biochemistry and Molecular Biology, Epidemiological and Health Statistics, Occupational Medicine and Environmental Health, Public Health and Preventive Medicine, Nutrition and Food Hygiene, Pharmaceutical Chemistry, Pharmacy, Pharmaceutical Analysis and Clinical Medicine, and Nursing.

Requirements/Qualifications:

- Has been working as Assistant Professor in University abroad or has completed post-doctoral training with outstanding academic records.

For more detailed information, please visit the following website: **http://rcyj.njmu.edu.cn.**

Contact:

Mr. Hanzhan Gu
Department of Human Resouce, Nanjing Medical University
140 Hanzhong Road, Nanjing, Jiangsu Province, 210029, The People's Republic of China
Tel/Fax: 86-25-86862642 Email: **ghz@njmu.edu.cn**

INSTITUT DE PHYSIQUE DU GLOBE DE PARIS

Earth - Planets - Environnement - Natural Hazards

DIRECTOR

The Institut de Physique du Globe de Paris (IPGP) is seeking applications for the position of Director of IPGP, which will begin October 1, 2010.

The IPGP is the largest institute of Earth Sciences in France and also one of the largest in Europe. The Institute conducts research and education in geology, geophysics, geochemistry and the environmental sciences. It is in charge of monitoring the three active French volcanoes (Guadeloupe, Martinique, La Réunion) through its volcanic and seismologic observatories. It is also in charge of the magnetic observatory of Chambon-la-Foret (international INTERMAGNET network) and the global seismological network GEOSCOPE. IPGP currently employs about 300 permanent researchers and staff. There are in addition some 200 MSc and PhD students, post-docs and visitors.

The Director will be responsible for supervising the Institute's research and teaching activities, including general administrative tasks, and conducting negotiations with national and European funding agencies. The Director is also the chair of the Institute's scientific Council, whereas the IPGP Board is chaired by a scientist from outside IPGP.

Candidates are expected to be highly accomplished scientists. They will be evaluated on the basis of their academic record in research and teaching, their experience in management, and their vision for the future of IPGP. Interested candidates should submit a two-page vision statement, their Curriculum Vitae and names of three individuals who are willing to be contacted references.

Applications must be received by June 15, 2009.

Application materials should be sent to:
Lydia Zerbib - IPGP General Secretary, Institut de Physique du Globe
4 Place Jussieu, 75252 Paris Cedex 5, France
E-mail: zerbib@ipgp.fr - www.ipgp.fr

university of groningen

Faculty of Mathematics and Natural Sciences Two Tenure Track Positions in Experimental Physics

The Faculty of Mathematics and Natural Sciences of the University of Groningen is seeking applications and nominations for two tenure track positions (assistant professor) in experimental physics. The Faculty offers Bachelor, Master and Ph.D. programmes over the entire range of natural sciences. The research in the Faculty is organized in research institutes. The vacancy exists within the Zernike Institute for Advanced Materials, which unites 21 research groups in physics, chemistry, and biology. The Zernike Institute is one of six recognized National Centres of Excellence in The Netherlands. Its mission is design and functionality of novel materials, with a focus on understanding and control at the microscopic level. The Institute thrives on a strong interdisciplinary nature of its research programme and frequent collaborations between its various groups. The two open positions are:

- **Position 1: Condensed Matter Science with specialisation in ultrafast X-ray science**
- **Position 2: Surface Science with specialisation in scanning tunneling microscopy**

The complete text of the advertisements can be found on the website of the Zernike Institute for Advanced Materials at: **http://www.rug.nl/zernike/vacancies/atmsc/ocmp** (position 1) and **http://www.rug.nl/zernike/vacancies/atmsc/SurfaceScience** (position 2)

Review of applications will begin **May 31st, 2009**, and will continue until both positions are filled. Applications in hard copy should be addressed to: **Head of Personnel Department, University of Groningen, P.O. Box 72, 9700 AB Groningen, The Netherlands**; by E-mail (Word or PDF) to: **m.h.derix@rug.nl**. When applying for one of these jobs please mention the vacancy number which you can find on the websites.

VP of Stem Cell Research and Development (Asia)

This position will be based in Beijing China.

Responsibilities:

- Work closely with US Biotechnology senior management and scientific staff to establish and execute specific R&D programs and procedures.
- Manage the company's research directions in the Beijing lab, including overall technology strategies, research goals and research budgeting.
- Act as primary scientific liaison in China for communications with US research team and be responsible for bidirectional technology transfer to/from US Boston Lab.
- Establish leadership role in establishing academic collaborations with leading institutions in China involving company's stem cell technologies.
- Manage china external collaborations including selecting collaborators, setting up collaboration terms and goals.
- Conduct direct communications with granting agencies including government and private foundations to obtain support/approval for our stem cell research.
- Publish research findings in top-tier scientific/medical journals or give presentations at meetings in line with the company's confidentiality policy.

Skills and Experience:

- Independent investigator status with > 5 years of adult stem cell research.
- Evidence independent grant support.
- Strong evidence of laboratory and personnel management skills.
- Strong publication record in stem cell science with publications in international peer-reviewed journals.
- Fluent Mandarin Chinese and English, both spoken and written.
- Evidence of ability to establish quality standards for translational research and clinical activities.
- Demonstrated ability to work in a team environment. Excellent interpersonal and communication skills.

Please send cover letter and resume to **beijingcareeropportunity@gmail.com** or call **(212) 584-4181** with any questions.

Argonne NATIONAL LABORATORY

DIRECTOR, ACCELERATOR SYSTEMS DIVISION

ARGONNE NATIONAL LABORATORY

The Accelerator Systems Division (ASD) at Argonne National Laboratory is one of three divisions comprising the Advanced Photon Source (APS), the highest energy accelerator-based source of x-rays in the western hemisphere.

Argonne invites applicants for the position of Director of ASD to provide technical and scientific leadership for effective operations and future development of APS accelerator systems. ASD is responsible for the reliable and high performance operation of the APS accelerator complex, and ensuring that the APS remains at the forefront of hard x-ray science in both the near and long term.

A primary responsibility of the division is the day-to-day operation of the APS accelerator. ASD has approximately 100 people in groups responsible for the operations, maintenance and development of diagnostics, power supply systems, rf systems and undulator systems. The division also has the APS Accelerator Physics and Operations group which is responsible for control room operations and the analysis of operational data. In addition to these operational duties, ASD is responsible for all accelerator-based R&D at the APS, focusing on both near-term needs of the APS, and longer-term, fourth-generation facility upgrades, which could be Free Electron Laser or Energy Recovery Linac based.

This position requires an internationally recognized reputation in the field of accelerator science and technology, a relevant Ph.D., and 15+ years of relevant experience in research and management roles. The successful candidate should have demonstrated leadership and management abilities, and a proven track record in a combination of design, construction and operation of accelerator-based facilities. The candidate should also have a basic knowledge of beam dynamics and accelerator systems including diagnostics, power systems, rf and superconducting rf, and possess the ability to articulate a vision for accelerator R&D at the APS.

Argonne offers an excellent compensation and benefits package. Interested candidates should send curriculum vitae, list of publications and patents, professional references, and salary history to **asdsearch@anl.gov**.

Argonne National Laboratory is a multi-program laboratory managed by UChicago Argonne, LLC for the U.S. Department of Energy's Office of Science. Argonne's site is located about 25 miles southwest of Chicago on a beautiful 1,500-acre campus. For additional information, please refer to Argonne's home page at **www.anl.gov**.

Argonne is an equal opportunity employer, and we value diversity in our workplace.

FIU FLORIDA INTERNATIONAL UNIVERSITY

TENURE TRACK POSITION
ASSISTANT AND/OR ASSOCIATE/FULL PROFESSOR
ROBERT STEMPEL COLLEGE OF PUBLIC HEALTH AND SOCIAL WORK

Florida International University is ranked as a Research University in the High Research Activity category of the Carnegie Foundation's prestigious classification system. Our mission is to enhance the public's health by conducting innovative research, training future leaders and health professionals from diverse backgrounds, translating research into policy and practice, and serving our local communities as well as communities around the world, especially Latin America and the Caribbean.

Qualifications: Candidate must possess a Ph.D., M.D. or the equivalent and postdoctoral experience in environmental genomics, molecular epidemiology, human genetics, or a related area. Extensive experience in the broad field of genomics including proteomics and bioinformatics is desired. The Search Committee is especially interested in receiving applications from individuals experienced in interdisciplinary collaborative research with interests in assessment of gene-environment interactions, molecular epidemiology and toxicogenomics of human diseases. We welcome candidates with experience in evaluating intermediate biomarkers of effect and in examining the health, especially respiratory, cardiovascular, diabetes, reproductive/developmental, and cancer endpoints.

Duties and Responsibilities: The candidate will be expected to develop his/her own research program in environmental genomics, obtain competitive research funding, and engage in collaborative research with other faculty in the department as well as within the College of Public Health & Social Work and College of Medicine. Responsibilities also include teaching, advising graduate students, and serving on doctoral committees. The selected candidate will have the opportunity to participate in ongoing research with multidisciplinary researchers, and will be expected to develop and maintain an original, creative and independent research program in genetic or molecular environmental epidemiology with evidence of high quality and productivity. This requires publications in high impact peer-reviewed journals and demonstrating the potential for successful submission and management of investigator-initiated grant proposals.

Applications and Nominations: Applicants must submit the following material: letter of application that confirms applicant's interest in the position and addresses qualifications, including description of research; complete curriculum vitae; undergraduate and graduate transcripts, and documentation of the doctoral degree; representative publications, and at least three letters of recommendation.

The selection and review process will begin on April 2, 2009, and will remain open until the position is filled. To apply please visit us on-line at www.fiujobs.org and reference position #41663.

FIU is an Equal Opportunity/Equal Access Employer and Institution.

University of California – Santa Barbara
Dean of the College of Engineering and Richard A. Auhll Professor

The University of California at Santa Barbara invites nominations and applications for the position of Dean of the College of Engineering and Richard A. Auhll Professor. We seek an individual with an outstanding record of scholarly achievement who is appropriate for appointment as a full Professor and holder of an endowed chair in the UC system. We also seek an individual with vision and creative leadership abilities, demonstrated credentials in administration, and an established national and international reputation within the broader engineering community. The College of Engineering at UCSB has grown rapidly, both in the size and stature of our academic programs, and the successful applicant will be expected to provide the direction, inspiration and administrative ability to continue and expand upon these developments. In addition to the attributes mentioned above, desirable qualifications include: a broad appreciation and perspective for all fields of engineering and the physical and life sciences; experience in development; and a demonstrated ability to interface effectively with industrial, governmental and educational institutions. The University is especially interested in candidates who can contribute to the diversity and excellence of the academic community through research, teaching, or service.

The College is renowned for its high level of collaborative activity, as exemplified by the large number of interdisciplinary research centers and interactions within both the College and the rest of campus. The College contains five academic departments: Electrical and Computer Engineering, Mechanical Engineering, Chemical Engineering, Computer Science, and Materials. Of its 146 faculty members, 27 are members of the National Academy of Engineering, 8 are members of the National Academy of Sciences, 3 are Fellows of the Royal Society, 2 are Nobel Laureates, 1 is a recipient of the Millennium Technology Prize, 1 is a recipient of the National Medal of Technology, and 1 is a Fellow of the Royal Academy of Engineering. Total annual extramural funding for research in the College has grown to over $57 million in 2007-2008.

All inquiries, nominations and applications will be held in strictest confidence. Applications should include a letter of interest, curriculum vitae, and the addresses and telephone numbers of three references. Screening will begin **June 1, 2009,** and will continue until the position is filled. Inquiries, nominations, and expressions of interest should be submitted to: **Professors Linda Petzold and Edward Kramer, Co-Chairs, Search Committee for the Dean of the College of Engineering, c/o Kathy Upton, Office of Academic Personnel, Cheadle Hall 4105, University of California, Santa Barbara, Santa Barbara, CA 93106-2034.**

UCSB is an Equal Opportunity and Affirmative Action Employer and Educator.

Science Careers online @sciencecareers.org

Science Careers is the window
that displays your vision.

Visit our ENHANCED WEBSITE!

Revealing your vision to employers is our job. We're your source for connecting with top employers in industry, academia, and government. We're the experts and entry point to the latest and most relevant career information across the globe.

Our newly designed website offers a set of tools that reveal career opportunities and your personal potential. Whether you're seeking a new job, career advancement in your chosen field, or ways to stay current on industry trends, *Science* Careers is your window to a limitless future.

Improved Website Features:

- Relevant Job E-mail Alerts
- Improved Resume Uploading
- Content Specific Multimedia Section
- Facebook Profile

Job Search Functionality:

- Save and Sort Jobs
- Track Your Activity
- Search by Geography
- Enhanced Job Sorting

Your Future Awaits.

Science Careers

From the journal *Science* AAAS

ScienceCareers.org

www.mssm.edu

FACULTY OPPORTUNITY

The new Brain Institute at the Mount Sinai School of Medicine is seeking outstanding Department of Neuroscience and Department of Neurology tenure-track or tenured candidates at any rank. Brain Institute faculty interact with multidisciplinary colleagues from basic and clinical departments, to perform collaborative research with the translational goal of protecting and repairing the nervous system.

We seek outstanding candidates with active research programs preferably in the areas of: neurobiology of memory, cognitive function, synaptic plasticity, movement disorders, cerebrovascular disease, addiction, depression and schizophrenia utilizing multiphoton imaging in slices or in vivo, to address both structural and functional questions.

Applicants should send a CV, letter of application and the names of three potential referees to **Dr Susan Wearne, Brain Institute Search Committee, Department of Neuroscience, Mount Sinai School of Medicine, One Gustave L. Levy Place, Box 1065, New York. NY. 10029-6574**. An electronic copy of the CV and letter of application should be emailed to **marie.kopp@mssm.edu**. EOE

University of California, Davis
M.I.N.D. Institute
Director

The University of California, Davis, is searching for a Director of the Medical Investigation of Neurodevelopmental Disorders (M.I.N.D.) Institute. This is a tenured, ladder rank position with a state FTE. The individual selected will also hold the Tsakopoulos-Vismara Endowed Chair. The M.I.N.D. Institute is a multidisciplinary research and clinical center that focuses on the causes and treatment of neurodevelopmental disorders such as autism, Fragile-X Syndrome, ADHD, Tourette Syndrome, 22q deletion syndrome and other disorders. The M.I.N.D. Institute is located on the main medical school campus in Sacramento and consists of a state of the art basic science research building and a clinical research, assessment and education building. Approximately 32 faculty and an additional 250 staff work at the Institute.

The search committee is looking for a visionary leader who could develop and refine the direction for the M.I.N.D. Institute for the next decade. The candidate should have a background in fundraising activities and building community relationships. The candidate should also be committed to fostering diversity among faculty and staff. The successful candidate should be a prominent N.I.H.-funded investigator whose research has focused on neurodevelopmental disorders. It is preferable that the candidate be a physician who is license eligible in the State of California; however, applications from Ph.D. investigators will also be considered. The candidate should have had significant leadership and administrative experience directing a center, department or clinical service. A history of mentoring junior faculty and facilitating interdisciplinary approaches to research are also highly desirable attributes.

For more information, please review the M.I.N.D. Institute's website at **http://www.ucdmc.ucdavis.edu/mindinstitute/** or contact the search committee chair, **Robert E. Hales, M.D.** at **rehales@ucdavis.edu**. For full consideration, applications must be received by **September 30, 2009**. Position is open until filled, but no later than April 1, 2010. Interested candidates should email a curriculum vitae and letter of interest in response to Position **#AD-01R-09** to **Megan Rott** at **megan.rott@ucdmc.ucdavis.edu**.

In conformance with applicable law and University policy, the University of California, Davis, is an Equal Opportunity/Affirmative Action Employer.

SOOCHOW UNIVERSITY

Faculty Positions

The Soochow University, founded in 1900 in Suzhou, Jiangsu, is a premier university in China. The University is committed to excellence in education, science and innovation. A major expansion of its research programs is underway across a broad spectrum of areas in **mathematics, physics, chemistry, mechanical and electronic engineering, optical and energy engineering, material and computer sciences, urban planning and environmental science, textile engineering and design, life sciences, and medicine**. A complete listing of open positions is available at **http://rsc.suda.edu.cn/zpxx.asp?type=15**.

We invite the best and brightest to join us at the Associate Professor and Professor levels. Successful candidates should have an advanced degree and an outstanding record of academic achievements and high quality publications in top international journals. Established principal investigators, leading scientists, and members of Chinese Academy of Science and Engineering are encouraged to apply. We provide competitive relocation and salary packages, generous start-up funds, and state-of-the-art research facilities.

Interested individuals should send curriculum vitae, a summary of accomplishments, future research plans, and a list of three references to: **Ms. Hongmei Qi, HR Dept., Soochow University, sdrcjl@suda.edu.cn, Tel: (86) 512-67503045, Fax: (86) 512-67503248, Mail Box 428, 50 Donghuan Road, Suzhou, Jiangsu 215021, China**.

SEE YOU IN CAPE TOWN

IAS2009
cape town · south africa

5th IAS Conference on
HIV Pathogenesis,
Treatment and Prevention

19 - 22 July 2009

Register by **6 May 2009** to avoid last minute surcharge

Late Breaker Abstract Submissions
1 May – 25 May 2009

International AIDS Society
Stronger Together

www.ias2009.org

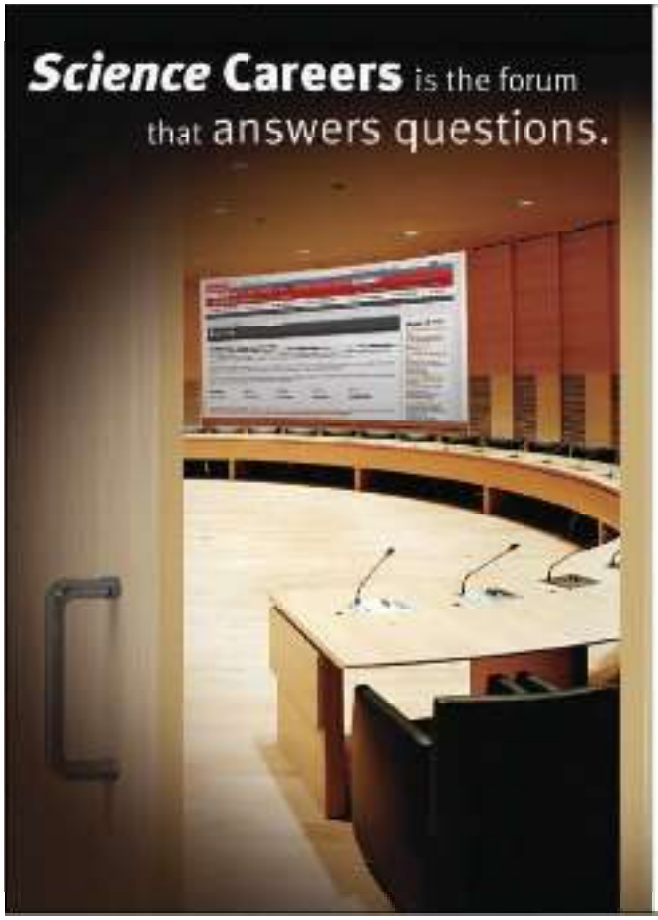

Science Careers is dedicated to opening new doors and answering questions on career topics that matter to you. With timely feedback and a community atmosphere, our careers forum allows you to connect with colleagues and experts to get the advice and guidance you seek as you pursue your career goals.

Science Careers Forum:

- Relevant Career Topics
- Timely Advice and Answers
- Community, Connections, and More!

Visit the forum and join the conversation today!

Your Future Awaits.

Science Careers
From the Journal Science AAAS

ScienceCareers.org

Science Careers online @sciencecareers.org

Your career is our cause.

Get help from the experts.

www.sciencecareers.org

- Job Postings
- Job Alerts
- Resume/CV Database
- Career Advice
- Career Forum
- Graduate Programs
- Meetings and Announcements

Science Careers
From the journal Science AAAS

POSITIONS OPEN

DEPUTY DIRECTOR NATIONAL CENTER FOR ENVIRONMENTAL ASSESSMENT CINCINNATI, OHIO

The U.S. Environmental Protection Agency, Office of Research and Development (ORD), seeks an internationally recognized risk assessment scientist to fill the position of Deputy Director, National Center for Environmental Assessment (NCEA), Cincinnati, Ohio, Division (**website: http://www.epa.gov/ncea/.**

NCEA-Cincinnati conducts assessments to characterize the toxicity and related human health effects of high priority chemicals, develops methodologies and provides guidance on the assessment of the cumulative impact of chemical mixtures, and provides tools for ecological risk and causal assessment.

The Deputy Division Director is a senior adviser on matters of science and science policy, provides recommendations, advice, and direction on risk assessment issues, and is responsible for the planning, organization, and coordination of activities within the division.

Individuals with a strong background in risk assessment are invited to apply. This is a permanent, federal appointment in Cincinnati, Ohio. *Citizenship restrictions apply.* Additional information and application instructions may be found at **website: http://www.usajobs.gov, announcement numbers RTP-DE-2009-0137 and RTP-MP-2009-0316** or by contacting **Annette Gatchett, e-mail: gatchett.annette@epa.gov.** Application deadline is June 2, 2009.

The USEPA is an Equal Opportunity Employer.

For many years, the Cleveland Clinic and Lerner Research Institute have been at the forefront of biomedical research. NIH-funded **POSTDOCTORAL POSITIONS** are available in the Department of Molecular Cardiology to investigate the molecular mechanisms of thrombosis and atherosclerosis (**Podrez et al.,** *Nature Medicine,* 2007; **Valiyaveettil et al.,** *Blood,* 2008). For more information on **Dr. Podrez's** laboratory, please visit **website: www.lerner.ccf.org/moleccard/podrez/.** Successful applicants must have a Ph.D. degree in molecular/cellular biology, biochemistry, or a related biological science. Basic experience with animal models is a plus. We emphasize motivation and productive work in a collegial environment. The institution has a history of offering outstanding benefits to its employees.

Send a cover letter, curriculum vitae, and names of three to five references to: **Eugene A. Podrez, M.D., Ph.D., The Cleveland Clinic, Department of Molecular Cardiology, 9500 Euclid Avenue, ND50, Cleveland, OH 44195** or electronically to **e-mail: podreze@ccf.org.**

Cleveland Clinic is an Equal Opportunity, Affirmative Action Employer.

POSTDOCTORAL POSITIONS
Antibody-based Therapeutics

Highly motivated individuals with a Ph.D./M.D. and a strong background in molecular and cellular biology, including fluorescence microscopy, to work on imaging studies of therapeutic antibodies. Please send curriculum vitae and details of three references to: **Dr. E. Sally Ward (e-mail: wardlab@utsouthwestern.edu), Department of Immunology, University of Texas Southwestern Medical Center, Dallas, TX 75390-9093.** *UT Southwestern is an Equal Opportunity, Affirmative Action Employer.*

UK

POSTDOCTORAL POSITIONS are available in the area of mechanism-based cancer prevention using plant-derived compounds and molecular mechanism of metal carcinogenesis in the laboratory of **Xianglin Shi,** Graduate Center for Toxicology, University of Kentucky. Send curriculum vitae to **e-mail: xianglin.shi@uky.edu.**

POSITIONS OPEN

USC

POSTDOCTORAL/RESEARCH ASSOCIATE POSITION
University of Southern California

Postdoctoral/Research Associate Position is available immediately for individual with strong molecular biology background at the Center for Craniofacial Molecular Biology, University of Southern California. This position is supported uniquely by NIH grants and collaboration with the Division of Plastic and Reconstructive Surgery of the Keck School of Medicine of USC. The successful applicant will join a large, interactive multidisciplinary team of scientists in a strong academic environment focusing on the molecular regulation of craniofacial development. For more details, please visit **website: http://www.usc.edu/hsc/dental/ccmb** (see publications under **Yang Chai**). Send resume to:

Mark Urata, M.D., D.D.S.
(E-mail: murata@chla.usc.edu)
Yang Chai, D.D.S., Ph.D.
(E-mail: ychai@usc.edu)
Center for Craniofacial Molecular Biology
University of Southern California
2250 Alcazar Street, CSA 103
Los Angeles, CA 90033
Fax: 323-442-2981

DIRECTOR, DIVISION OF ASTRONOMICAL SCIENCES
National Science Foundation, Arlington, VA

National Science Foundation's Directorate for Mathematical and Physical Sciences (MPS) seeks candidates for the position of Director, Division of Astronomical Sciences. The incumbent provides leadership and direction to the Division, which supports research in all areas of astronomy and astrophysics and related multidisciplinary studies. Information about the Division's activities can be found at **website: http://www.nsf.gov/mps/ast/about.jsp.**

Appointment to this Senior Executive Service position may be on a career basis, or on a one- to three-year limited term basis, with a salary range of $153,200 to $171,882. Alternatively, the incumbent may be assigned under Intergovernmental Personnel Act (IPA) provisions.

Announcement S20090063, with position requirements and application procedures, is posted on NSF's Home Page at **website: http://www.nsf.gov/about/career_opps/.** Applicants may also obtain the announcement by contacting the Executive Personnel Staff at **telephone: 703-292-4376** (hearing impaired individuals may call **TDD 703-292-8044**). Applications must be received by June 15, 2009.

NSF is an Equal Opportunity Employer.

MARKETPLACE

VIROGEN www.virogen.com

Detect Glutathione and Cysteine with anti-Glutathione and anti-Cysteine monoclonal antibodies

Reagents for HCV (1B and 2A) and HBV detection

617 926 9167 P | 617 926 9157 F

Immunochemical Reagents

Hapten Reporter Groups and Conjugates

Wide Selection of Conjugates: NP, DNP, TNP, PC Proteins & more!

BIOSEARCH TECHNOLOGIES Advancing Nucleic Acid Technology

+1.800.GENOME.1
www.btiimmuno.com

MILLIPORE™

FLOW CYTOMETRY

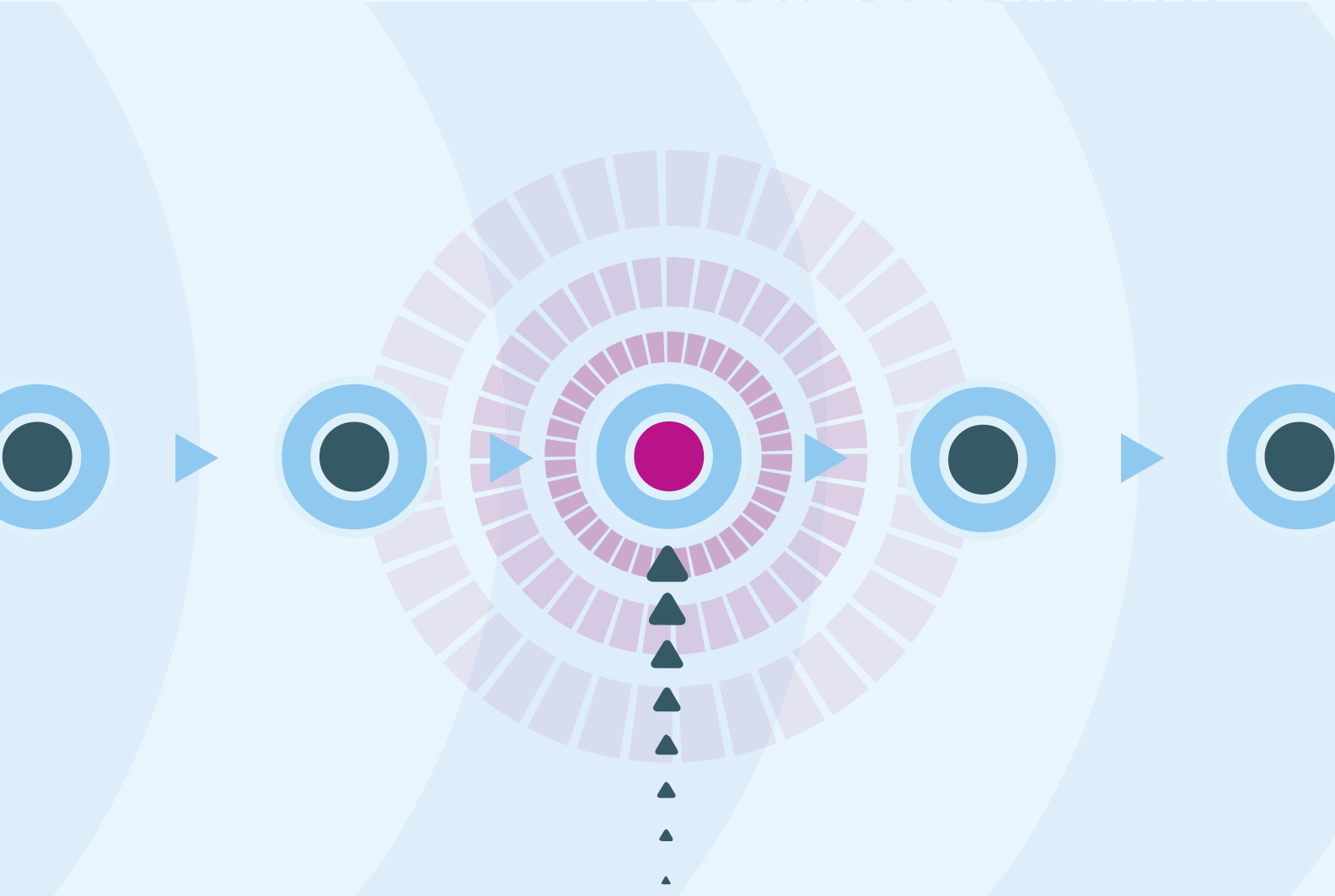

Why go with the flow when you can leap ahead?

Make a quantum leap with Millipore's breakthrough portfolio of FlowCellect™ cytometry kits optimized to monitor stem cell differentiation, GPCR expression and signaling pathways. Visit **www.millipore.com/flowcytometry** to learn how these assays combine with the Guava® system to provide turnkey solutions.

ADVANCING LIFE SCIENCE TOGETHER™
Research. Development. Production.

THE EXPERTISE OF
CHEMICON® AND UPSTATE®
IS NOW PART OF MILLIPORE

Millipore, Chemicon, and Upstate are registered trademarks of Millipore Corporation. "M" logo, "Advancing Life Science Together", and FlowCellect are trademarks of Millipore Corporation. Guava is a registered trademark of Guava Technologies, Inc.

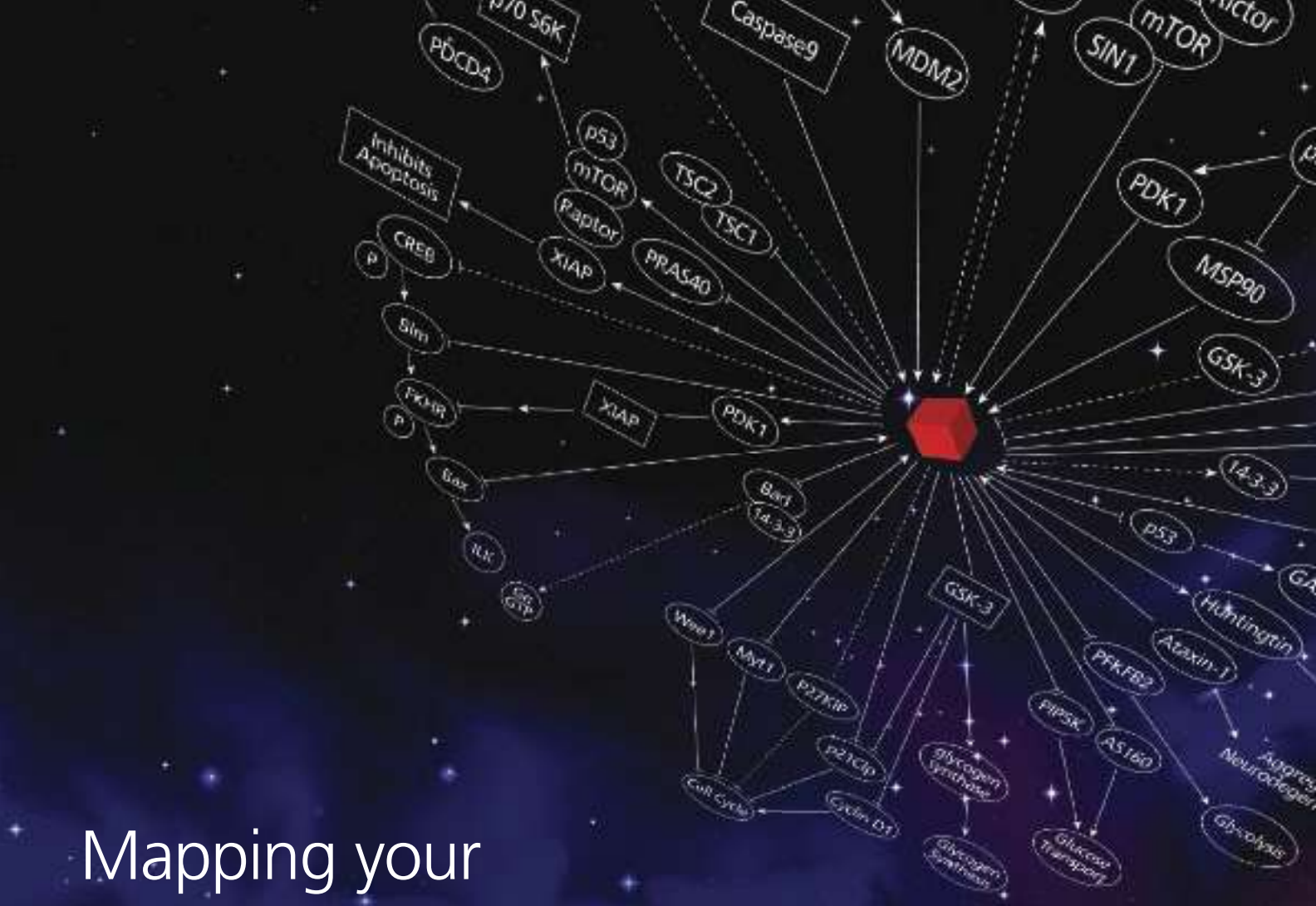

Mapping your pathway to discovery.

Move beyond the boundaries of the known. Built on the solid Sigma foundation of quality and reliability, our cell biology portfolio is backed by a universe of experience, knowledge and biological data.

- 16,000+ Antibodies
- Highly Validated Prestige Antibodies® Powered by Atlas Antibodies
- New Precisio™ Active Human Kinases
- 3,000+ Bioactive Small Molecules
- LOPAC® Libraries of Pharmacologically Active Compounds
- Navigate by Gene, Disease, Tissue or Pathway via Your Favorite Gene powered by Ingenuity

Your Favorite Gene SEARCH Powered By INGENUITY

For a closer look at cell biology content you can count on visit ***sigma.com/cellbiology***

SIGMA Life Science

Our Innovation, Your Research — Shaping the Future of Life Science

Preciso is a trademark of Sigma-Aldrich Biotechnology LP and Sigma-Aldrich Co.
LOPAC and Prestige Antibodies are registered trademarks of Sigma-Aldrich Biotechnology LP and Sigma-Aldrich Co.